Polish Academy of Sciences

Institute of Fundamental Technological Research

Archives of Mechanics

Archiwum Mechaniki Stosowanej

volume 49 issue 3

Polish Scientific Publishers PWN

Warszawa 1997

ARCHIVES OF MECHANICS IS DEVOTED TO
Theory of elasticity and plasticity • Theory of nonclassical continua • Physics of continuous media • Mechanics of discrete media • Nonlinear mechanics • Rheology • Fluid gas-mechanics • Rarefied gas • Thermodynamics

---

Printed in Poland, Editorial Office: Świętokrzyska 21,
00-049 Warszawa (Poland)

e-mail: publikac@ippt.gov.pl

Arkuszy wydawniczych 11,75. Arkuszy drukarskich 10,25.
Papier offset. kl. III 70 g. B1. Oddano do składania w kwietniu 1997 r.
Druk ukończono w czerwcu 1997 r.
Skład i łamanie: "MAT-TEX"
Druk i oprawa: Drukarnia Braci Grodzickich, Żabieniec ul. Przelotowa 7

Arch. Mech., 49, 3, p. 451, Warszawa 1997

Preface

The Editorial Committee of *Archives of Mechanics* invited the Scientific Committee of the XXXI Polish Solid Mechanics Conference – SolMec'96 organized in Mierki, September 9-14, 1996, by the Institute of Fundamental Technological Research and Committee of Mechanics of the Polish Academy of Sciences, to encourage all authors of oral and poster presentations at the SolMec'96 Conference to publish their contributions in special issues of the *Archives of Mechanics* and *Engineering Transactions*.

The present issue of *Archives of Mechanics* is the second special issue of the Journal (the first one has appeared in the previous month, i.e. Vol. 49, No 2) and contains the submitted and reviewed contributions of a more basic orientation.

The first special issue of the other journal, namely *Engineering Transactions* has been printed simultaneously and it contains the contributions of a more engineering character.

Warszawa, April 1997

Witold Kosiński
Conference Chairman

Arch. Mech., 49, 3, pp. 453–460, Warszawa 1997

Duality based solution of contact problem with Coulomb friction

Z. DOSTÁL and V. VONDRÁK (OSTRAVA)

NUMERICAL SOLUTION of quasi-variational inequalities that describe the equilibrium of elastic bodies in contact with friction is presented. The problem is first reduced to a sequence of well conditioned problems with given friction that are reformulated by means of duality as quadratic programming problems with box constraints. Then the algorithm for the solution of quadratic programming problems with proportioning and projections is applied to the solution of the resulting contact problem with Coulomb friction. The characteristic feature of this active set-based algorithm is that it accepts approximate solutions of auxiliary problems and that it is able to drop and add many constraints whenever the active set is changed. The results of our numerical experiments indicate that the algorithms presented are efficient. The algorithm may prove to be useful in parallel implementation.

1. Introduction

THE DUAL SCHUR complement domain decomposition method introduced recently by FARHAT and ROUX [5] turned out to be an efficient algorithm for parallel solution of self-adjoint elliptic partial differential equations. Recently, we have combined this method with our results [2] on quadratic programming with simple bounds, in order to develop an efficient algorithm for the solution of variational inequalities that describe the conditions of equilibrium of a system of elastic bodies in frictionless contact [3]. The results of [2] turned out to be closely related to the results of FRIEDLANDER and MARTÍNEZ [7] and were further extended in [4].

In this paper, we extend this approach to the solution of unilateral contact problems of linear elasticity with Coulomb friction. The main feature of our new algorithm for the solution of coercive problems is that it accepts approximate solutions of auxiliary minimization problems, that it is able to drop and add many constraints whenever the active set is changed, and that it treats the bodies independently of each other, so that parallel implementation is possible. The application of the duality theory to a discrete problem may be considered as an implementation of the reciprocal formulation of [8]. The performance of the algorithm is demonstrated on the solution of a model problem.

2. Discretized contact problem with given friction

We shall start our exposition from the discretized contact problem. Suppose that $\mathbf{K}$ is the stiffness matrix of the order n resulting from the finite element

discretization of a system of elastic bodies $\Omega_1, \ldots, \Omega_p$ with enhanced bilateral boundary conditions. With suitable numbering of nodes, we can achieve that $\mathbf{K} = \operatorname{diag}(\mathbf{K}_1, \ldots, \mathbf{K}_p)$, where each $\mathbf{K}_i$ denotes a band matrix which may be identified with the stiffness matrix of the body Ω_i. We assume that $\mathbf{K}$ is positive definite.

Let m denote the number of nodes in contact. The linearized conditions of contact with given friction are supposed to be defined by the $m \times n$ matrices $\mathbf{N} = (n_{ij})$, $\mathbf{T} = (t_{ij})$, by the $m \times m$ non-negative diagonal matrix $\mathbf{\Gamma} = \operatorname{diag}(\gamma_i)$, and by the m-vector $\mathbf{c} = (c_i)$. The rows $\mathbf{n}_{i*}$ of $\mathbf{N}$ are vectors defined by unit outer normals that enable us to evaluate the change of the normal distance $c_i \geq 0$ between two potential contact surfaces. The formula for the displacement $\mathbf{x}$ is $\mathbf{n}_{i*}\mathbf{x}$. The matrix $\mathbf{N}$ is sparse as non-zero entries of $\mathbf{n}_{i*}$ may be only in positions of nodal variables which correspond to the nodes involved in some constraint. The diagonal entries γ_i of the diagonal matrix $\mathbf{\Gamma}$ define what we can call nodal given friction that corresponds to a couple of points in contact. In analogy to $\mathbf{n}_{i*}$, the row vectors t_{i*} of the matrix $\mathbf{T}$ are defined by the tangential vectors in these contact points. The matrix $\mathbf{T}$ is also sparse. We shall use $\mathbf{T}$ for evaluation of the tangential part of the relative displacement of the contact surfaces.

With these notations, solution of the discretized contact problem with given friction amounts to the solution of the problem

$$\min_{\mathbf{x}\in C} \max_{\mu\in M} f(\mathbf{x}, \mu), \tag{2.1}$$

where

$$f(\mathbf{x}, \mu) = \frac{1}{2}\mathbf{x}^T\mathbf{K}\mathbf{x} - \mathbf{b}^T\mathbf{x} + \mu^T\mathbf{\Gamma}\mathbf{T}\mathbf{x}, \quad M = \left\{\mu \,\middle|\, |\mu| \leq 1\right\} \quad \text{and} \quad C = \left\{\mathbf{x} \,\middle|\, \mathbf{N}\mathbf{x} \leq \mathbf{c}\right\}.$$

In the last equation and in what follows, all the vector inequalities should be read pointwise. Similarly, $|\mu|$ denotes a vector with entries μ_i. More details about formulation and discretization of contact problems with friction may be found in Refs. [8, 9].

3. Reciprocal formulation

First observe that

$$\min_{\mathbf{x}\in C} \max_{\mu\in M} f(\mathbf{x}, \mu) = \min_{\mathbf{x}} \max_{\mu\in M} \max_{\lambda\geq 0} L(\mathbf{x}, \mu, \lambda), \tag{3.1}$$

where

$$\begin{aligned} L(\mathbf{x}, \mu, \lambda) &= f(\mathbf{x}, \mu) + \lambda^T(\mathbf{N}\mathbf{x} - \mathbf{c}) \\ &= \frac{1}{2}\mathbf{x}^T\mathbf{K}\mathbf{x} - \mathbf{b}^T\mathbf{x} + \mu^T\mathbf{\Gamma}\mathbf{T}\mathbf{x} + \lambda^T(\mathbf{N}\mathbf{x} - \mathbf{c}). \end{aligned} \tag{3.2}$$

For fixed μ and λ, the Lagrange function (3.2) is strictly convex in the first variable, and the gradient argument shows that any minimizer of $L(\cdot, \mu, \lambda)$ satisfies

$$\mathbf{K}\mathbf{x} - \mathbf{b} + \mathbf{T}^T\mathbf{\Gamma}^T\mu + \mathbf{N}^T\lambda = \mathbf{o}. \tag{3.3}$$

This equation has a solution for any $\mathbf{b}$, $\mathbf{T}$, $\mathbf{\Gamma}$, μ, $\mathbf{N}$, λ because the matrix $\mathbf{K}$ is positive definite. Simple computation shows that (3.3) is equivalent to

$$\mathbf{x} = \mathbf{K}^{-1}\left(\mathbf{b} - \mathbf{T}^T\mathbf{\Gamma}^T\mu - \mathbf{N}^T\lambda\right). \tag{3.4}$$

After substituting (3.4) into the Lagrange function (3.2) and after some simplifications that exploit the structure of the matrices, we get for fixed μ and λ the problem to find

$$\min_{\substack{\lambda \geq 0 \\ |\mu| \leq 1}} \frac{1}{2}\left(\lambda^T, \mu^T\right)\begin{pmatrix}\mathbf{N}\\ \mathbf{\Gamma T}\end{pmatrix}\mathbf{K}^{-1}\left(\mathbf{N}^T, \mathbf{T}^T\mathbf{\Gamma}^T\right)\begin{pmatrix}\lambda\\ \mu\end{pmatrix} - \left(\lambda^T, \mu^T\right)\begin{pmatrix}\mathbf{N}\mathbf{K}^{-1}\mathbf{b} - \mathbf{c}\\ \mathbf{\Gamma T}\mathbf{K}^{-1}\mathbf{b}\end{pmatrix}. \tag{3.5}$$

The latter is the quadratic programming problem

$$\min_{\mathbf{z} \in S} F(\mathbf{z}), \tag{3.6}$$

where

$$F(\mathbf{z}) = \frac{1}{2}\mathbf{z}^T\mathbf{Q}\mathbf{z} - \mathbf{z}^T\mathbf{h}, \quad \mathbf{z} = \begin{pmatrix}\lambda\\ \mu\end{pmatrix}, \quad \mathbf{Q} = \begin{pmatrix}\mathbf{N}\\ \mathbf{\Gamma T}\end{pmatrix}\mathbf{K}^{-1}\left(\mathbf{N}^T, \mathbf{T}^T\mathbf{\Gamma}^T\right),$$
$$\mathbf{h} = \begin{pmatrix}\mathbf{N}\mathbf{K}^{-1}\mathbf{b} - \mathbf{c}\\ \mathbf{\Gamma T}\mathbf{K}^{-1}\mathbf{b}\end{pmatrix} \quad \text{and} \quad S = \left\{\mathbf{z} = \begin{pmatrix}\lambda\\ \mu\end{pmatrix} \,\middle|\, \lambda \geq 0, \ |\mu| \leq 1\right\}. \tag{3.7}$$

4. Proportioning

We shall consider here the problem (3.6) with a general choice of $S = \{\mathbf{z} |\, \mathbf{l} \leq \mathbf{z} \leq \mathbf{u}\}$. The only solution $\mathbf{z}$ of this problem satisfies the Kuhn-Tucker contact conditions

$$\begin{aligned} r_i &= 0 \quad \text{for} \quad l_i < z_i < u_i, \\ r_i^- &= 0 \quad \text{for} \quad z_i = l_i, \\ r_i^+ &= 0 \quad \text{for} \quad z_i = u_i, \end{aligned} \tag{4.1}$$

where $\mathbf{r} = \mathbf{Q}\mathbf{z} - \mathbf{h}$, $r_i^- = \min\{r_i, 0\}$ and $r_i^+ = \max\{r_i, 0\}$. Let us recall that the *active set* $\mathbf{A}(\mathbf{z}) = \{i |\, z_i = l_i \vee z_i = u_i\}$ and the *free set* $\mathbf{F}(\mathbf{z}) = \{i |\, l_i < z_i < u_i\}$. The *chopped gradient* $\beta(\mathbf{z})$ and *reduced gradient* $\varphi(\mathbf{z})$ are defined by

$$\begin{gathered} \varphi_i(\mathbf{z}) = r_i(\mathbf{z}) \quad \text{for} \quad i \in \mathbf{F}(\mathbf{z}) \qquad \text{and} \qquad \varphi_i(\mathbf{z}) = 0 \quad \text{for} \quad i \in \mathbf{A}(\mathbf{z}), \\ \beta_i(\mathbf{z}) = 0 \quad \text{for} \quad i \in \mathbf{F}(\mathbf{z}), \\ \beta_i(\mathbf{z}) = r_i^- \quad \text{for} \quad z_i = l_i \quad \text{and} \quad \beta_i(\mathbf{z}) = r_i^+ \quad \text{for} \quad z_i = u_i. \end{gathered} \tag{4.2}$$

Hence the conditions (4.1) are equivalent to $\varphi(\mathbf{z}) = \beta(\mathbf{z}) = \mathbf{o}$, so that $\mathbf{z}$ is the solution of our problem iff the *projected gradient* $\nu(\mathbf{z}) = \beta(\mathbf{z}) + \varphi(\mathbf{z}) = \mathbf{o}$.

The algorithm that we proposed in [2] is a modification of the Polyak algorithm that controls the precision of the solution of auxiliary problems by the norm of violation of the Kuhn-Tucker contact condition in each iteration. If for $G > 0$ the inequality $\|\beta(\mathbf{z}^i)\|_\infty \leq G\|\varphi(\mathbf{z}^i)\|_2$ holds, we shall call $\mathbf{z}^i$ *proportional*. The algorithm explores the face $W_I = \left\{\mathbf{y}|\ y_i = l_i \text{ or } y_i = u_i \text{ for } i \in I\right\}$ with a given active set I as long as the iterations are proportional. If $\mathbf{z}^i$ is not proportional, we generate $\mathbf{z}^{i+1}$ by means of decrease direction $\mathbf{d}^i = -\beta(\mathbf{z}^i)$ in a process that we call *proportioning* and we continue by exploring the new face defined by $I = \mathbf{A}(\mathbf{z}^{i+1})$. The class of algorithms driven by proportioning may be defined as follows.

ALGORITHM GPS (General proportioning scheme).

Let $\mathbf{z}^0 \in S$ and $G > 0$ be given. For $k > 0$, choose $\mathbf{z}^{k+1}$ by the following rules:

(i) If $\mathbf{z}^i$ is not proportional, define $\mathbf{z}^{i+1}$ by proportioning.

(ii) If $\mathbf{z}^i$ is proportional, choose feasible $\mathbf{z}^{i+1}$ so that $F(\mathbf{z}^{k+1}) \leq F(\mathbf{z}^k)$ and $\mathbf{z}^{i+1}$ satisfies at least one of the conditions $\mathbf{A}(\mathbf{z}^k) \subset \mathbf{A}(\mathbf{z}^{k+1})$, $\mathbf{z}^{i+1}$ is not proportional, or $\mathbf{z}^{i+1}$ minimizes $F(\xi)$ subject to $\xi \in W_I$, $I = \mathbf{A}(\mathbf{z}^k)$.

The symbol $\subset$ denotes proper subset. The basic theoretical results have been proved in [2].

THEOREM. *Let $\mathbf{z}^k$ denote an infinite sequence generated by algorithm* GPS *with given $\mathbf{z}^0$, let $S = \{\mathbf{z}|\ \mathbf{l} \leq \mathbf{z} \leq \mathbf{u}\}$, and let $F(\mathbf{z})$ denote a strictly convex quadratic function. Then the following statements are true:*

(i) *$\mathbf{z}^k$ converges to the solution $\bar{\mathbf{z}}$ of* (3.6).

(ii) *If the problem* (3.6) *is not degenerate, then there is k such that $\bar{\mathbf{z}} = \mathbf{z}^k$.*

(iii) *If $G \geq \sqrt{\kappa(\mathbf{Q})}$, where $\kappa(\mathbf{Q})$ is the spectral condition number of $\mathbf{Q}$, then there is k such that $\bar{\mathbf{z}} = \mathbf{z}^k$.*

Step (ii) of algorithm GPS may be implemented by means of the conjugate gradient method. The implementations differ in stopping rules for the solution of auxiliary problems and in application of projectors. In the following numerical experiments, we used so-called *monotone proportioning* [2] which, starting from $\mathbf{v}^0 = \mathbf{z}^k$, generates the conjugate gradient iterations for minimization of (3.6) on current face until $F(P\mathbf{v}^{i+1}) > F(P\mathbf{v}^i)$, where P denotes the projection to S. If the conjugate gradient iterations are interrupted on this condition, then a new iteration is defined by $\mathbf{z}^{k+1} = P\mathbf{v}^i$ or by some backtracking strategy. More details may be found in [2].

5. Solution of the friction problem

Now assume that the given friction γ_i is given by $\gamma_i = \Phi_i|T_i^n(\mathbf{x})|$, $i = 1, \ldots, m$, where $\Phi = (\Phi_i)$ is the vector of friction coefficients and $\mathbf{T}^n = (T_i^n(\mathbf{x}))$ is the vector

of normal stresses on the contact surface that correspond to the displacement $\mathbf{x}$. Denoting by $\mathbf{x}(\gamma)$ the solution of the contact problem (2.1) with given friction $\gamma = (\gamma_i)$ and by $\mathbf{T}^n(\mathbf{x}(\gamma))$ the corresponding normal stress, the solution of the contact problem with friction amounts to finding the fixed point of the mapping $\Psi : \gamma \mapsto \mathbf{T}^n(\mathbf{x}(\gamma))$. Existence results of the fixed point for sufficiently small friction coefficients may be found in [8, 12]. Hence we can find the solution of the contact problem with friction by

$$\begin{cases} \text{initial } \gamma^0, \\ \gamma^{n+1} = \Psi(\gamma^n). \end{cases} \tag{5.1}$$

Notice that λ corresponds to the normal stress $\mathbf{T}^n$ and the vector $\mathbf{\Gamma}\mu$ corresponds to the tangential stress $\mathbf{T}^t$ on the contact interface.

6. Numerical experiments

We have tested our algorithm on a problem of contact of two bodies of Fig. 1 that was discretized by a grid with 169 nodes, so that the discretized problem had 338 primal and 42 dual unknowns, respectively. The problem was solved for two

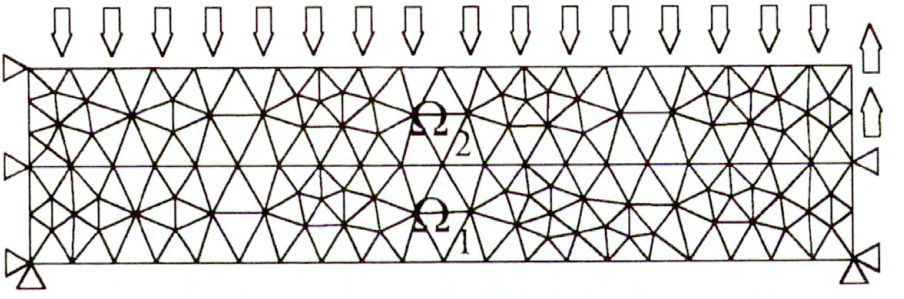

FIG. 1. Test problem.

combinations of elastic constants with the friction coefficient $\Phi = 0.3$. We used the value $G = 1$, so that we interrupted the conjugate gradient iterations when the chopped gradient began to dominate the reduced gradient. Relative precision of the solution was 10^{-3}. The solution turned out to be quite sensitive to the relative precision ε of the solution of the inner problems with given friction. The performance of the algorithm for various ε is given in Table 1 (Fig. 2, 3). The number of the conjugate gradient iterations seems to be relatively low, which also indicates that the distribution of the spectrum of the Hessian of $F(\mathbf{z})$ is favourable. Indeed, Fig. 4 shows that there are very few eigenvalues in both ends of the spectrum. This observations extend the experimental results reported by F.-X. ROUX [14] for the dual Schur complement. All numerical experiments were carried out in Mathworks Matlab with PDE Toolbox.

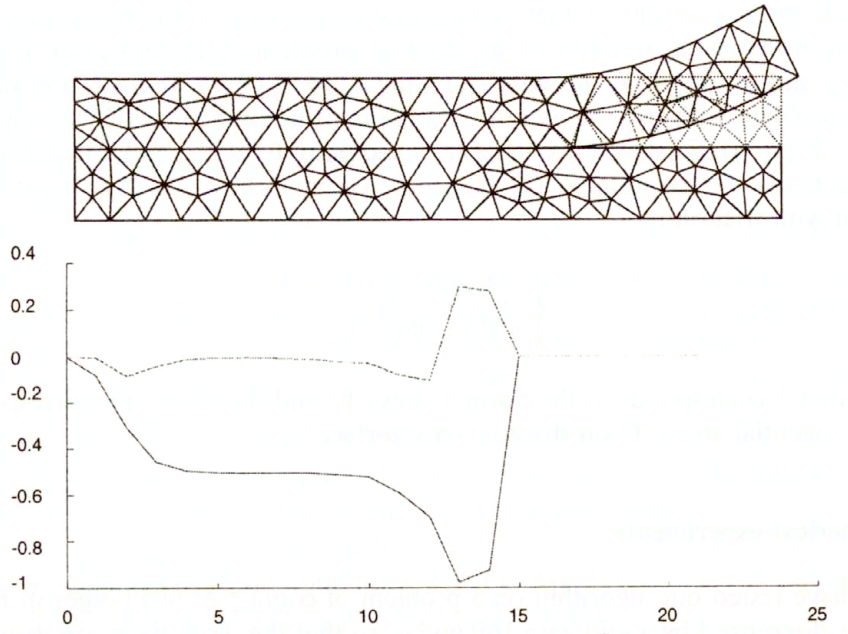

FIG. 2. Distribution of contact stresses for problem 1 ($\varepsilon = 10^{-7}$). Solid line – normal contact stress, dashed line – tangential contact stress.

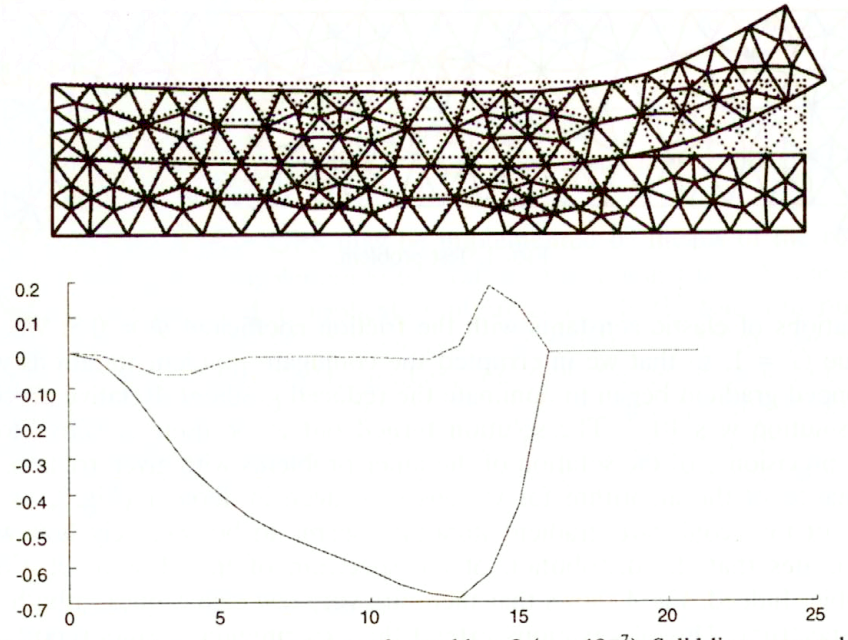

FIG. 3. Displacement and contact stresses for problem 2 ($\varepsilon = 10^{-7}$). Solid line – normal contact stress, dashed line – tangential contact stress.

Table 1. Performance of the algorithm.

Problem 1 ($E_1 = 10^6$ MPa, $E_2 = 10^3$ MPa)				Problem 1 ($E_1 = 10^2$ MPa, $E_2 = 10^3$ MPa)			
iterations				iterations			
number of outer	number of inner (cg steps)			number of outer	number of inner (cg steps)		
	$\varepsilon = 1e-5$	$\varepsilon = 1e-6$	$\varepsilon = 1e-7$		$\varepsilon = 1e-5$	$\varepsilon = 1e-6$	$\varepsilon = 1e-7$
1	28	29	38	1	58	67	75
2	28	36	55	2	84	108	142
3	4	10	15	3	2	9	13
4	3	1	6				
	63	76	114		144	184	230

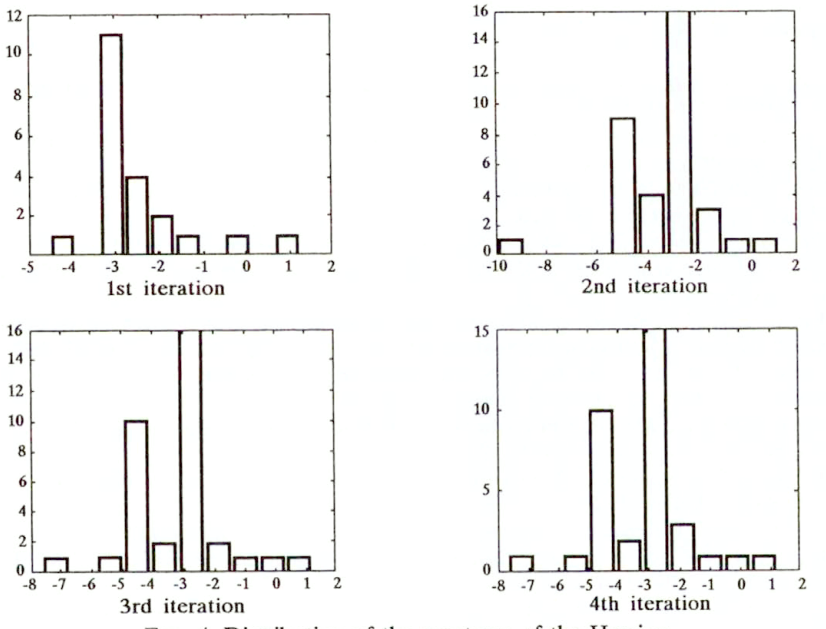

FIG. 4. Distribution of the spectrum of the Hessian.

7. Comments and conclusions

We applied a variant of our new algorithm [2] for the solution of quadratic programming problems with simple bounds to the solution of static coercive contact problem of elasticity with Coulomb friction in reciprocal formulation. A new feature of the presented algorithm is the adaptive precision control of the solution of auxiliary problems and application of projections, so that both the contact and slip interfaces may be identified in a small number of iterations. Theoretical

results are reported that grant the convergence of the algorithm. The algorithm also demonstrates the usefulness of the duality theory for practical computation.

Both theoretical results and results of numerical experiments indicate that there are problems which may be solved very efficiently by the algorithm presented. If applied to the solution of a contact problem that involves several bodies, then the algorithm may be considered as Neumann - Neumann type domain decomposition algorithm which may be useful in parallel environment. Using the results [4], the algorithm may be extended to the solution of semicoercive problems.

Acknowledgment

The research has been supported by grants No. 101/94/1853 and 105/95/1273 of the Czech Grant Agency (GAČR).

References

1. Z. DOSTÁL, *The Schur complement algorithm for the solution of contact problems*, Contemporary Mathematics, **157**, pp. 441–446, 1994.
2. Z. DOSTÁL, *Box constrained quadratic programming with proportioning and projections* [to appear in SIAM J. Opt., 7, 2, 1997].
3. Z. DOSTÁL, *Duality based domain decomposition with inexact subproblem solver for contact problems*, Contact Mechanics II, Comp. Mech. Publications, pp. 461–467, Southampton 1995.
4. Z. DOSTÁL, A. FRIEDLANDER and S.A. SANTOS, *Augmented Lagrangians with adaptive precision control for quadratic programming with simple bounds and equality constraints*, Res. report IMECC-UNICAMP, University of Campinas, 1996.
5. C. FARHAT and F.-X. ROUX, *An unconventional domain decomposition method for an efficient parallel solution of large-scale finite element systems*, SIAM J. Sci. Stat. Comput., **13**, pp. 379–396, 1992.
6. C. FARHAT, P. CHEN and F.-X. ROUX, *The dual Schur complement method with well posed local Neumann problems*, SIAM J. Sci. Stat. Comput., **4**, pp. 752–759, 1993.
7. A. FRIEDLANDER and J.M. MARTINEZ, *On the maximization of a concave quadratic function with box constraints*, SIAM J. Opt., **4**, pp. 177–192, 1994.
8. I. HLAVÁČEK, J. HASLINGER, J. NEČAS and J. LOVÍŠEK, *Solution of variational inequalities in mechanics*, Springer-Verlag, Berlin 1988.
9. N. KIKUCHI and J.-T. ODEN, *Contact problems in elasticity*, SIAM, Philadelphia 1988.
10. A. KLARBRING, *On discrete and discretized non-linear elastic structures in unilateral contact*, Int. J. Solids Structures, **24**, pp. 459–479, 1988.
11. M. KOČVARA and J.-V. OUTRATA, *On a class of quasi-variational inequalities* [submitted to Opt. Math. and Software].
12. J. NEČAS, J. JARUŠEK and J. HASLINGER, *On the solution of the variational inequality to the Signorini problem with small friction*, Boll. Unione Mat. Ital. (5), **17-B**, pp. 796–811, 1980.
13. B.-N. PSCHENICNY and Yu.-M. DANILIN, *Numerical methods in extremal problems*, Mir, Moscow 1982.
14. F.-X. ROUX, *Spectral analysis of interface operator*, [in:] DDM/91, pp. 73–90, 5th Int. Symp. on Domain Decomposition Meth. for Partial Differential Equations, D.E. KEYES *et al.* [Eds.], SIAM, Philadelphia 1992.

DEPARTMENT OF APPLIED MATHEMATICS,
TECHNICAL UNIVERSITY IN OSTRAVA, OSTRAVA-PORUBA, CZECH REPUBLIC
e-mail: zdenek.dostal@vsb.cz
e-mail: vit.vondrak@vsb.cz

Received October 28, 1996.

Arch. Mech., 49, 3, pp. 461–475, Warszawa 1997

On the convexity of the Goldenblat–Kopnov yield condition

A. GANCZARSKI and J. LENCZOWSKI (KRAKÓW)

THE PRESENT PAPER is aimed at the formulation of sufficient conditions of convexity for the Goldenblat–Kopnov yield condition. The essence of the proposed approach consists in the transposition of convexity of hypersurface from the six-dimensional stress space to the three-dimensional space of the principal stresses, and in the presentation of a surface in the Haigh–Westergaard stress space.

1. Introduction

WHEN THE CLASSICAL FLOW THEORY of plasticity is used, the yield surface is often assumed to have the form of a potential representation, from which the strain rates are derived. The second Drucker stability postulate implies that the constitutive equations are always of the Green (hyperelastic) type. Hence, the strain energy and the complementary energy functions are always positive definite, whereas the corresponding surfaces defined in strain and stress spaces, respectively, are convex (see CHEN and HAN [3], also ŻYCZKOWSKI [21]). For perfectly plastic materials, yielding itself implies failure, so the yield stress is also the limit strength. Therefore, for the failure surfaces a similar problem of convexity exists.

Obviously, the above requirements are also imposed on the flow theory of plastic anisotropic materials, as well as the anisotropic failure conditions.

2. The Goldenblat–Kopnov yield condition

Certain generalization of the Burzyński yield condition to the case of anisotropy has been proposed by GOLDENBLAT and KOPNOV [5]:

$$(\Pi_{ij}\sigma_{ij})^{\alpha} + (\Pi_{ijkl}\sigma_{ij}\sigma_{kl})^{\beta} + (\Pi_{ijklmn}\sigma_{ij}\sigma_{kl}\sigma_{mn})^{\gamma} + \ldots = 1, \tag{2.1}$$

where α, β, γ are arbitrary numbers; nevertheless, only few combinations of them have a practical sense. When the most frequent case of $\alpha = \beta = 1$, $\gamma = 0$ is assumed, the yield condition (2.1) reduces to the Burzyński paraboloid yield condition (see ŻYCZKOWSKI [21]):

$$\Pi_{ijkl}\sigma_{ij}\sigma_{kl} + \Pi_{ij}\sigma_{ij} = 1, \tag{2.2}$$

where the fourth-order tensor as well as the second-order tensor of plastic moduli satisfy the symmetry conditions $\Pi_{ijkl} = \Pi_{klij} = \Pi_{jikl} = \Pi_{ijlk}$, and $\Pi_{ij} = \Pi_{ji}$,

respectively. Consequently, 21+6 of such components are independent. In case of the orthogonal anisotropy (called orthotropy), a further reduction of the number of independent moduli is possible. Choosing the reference coordinate frame coinciding with the principal axes of orthotropy, the fourth-order tensor becomes independent of the mean stress and simultaneously, the second-order tensor becomes independent of the shear stresses (see THEOCARIS [19]). Moreover, 9 terms associated with normal and shear stress products, as well as products of two shear stresses of different indices vanish, and the following 9+3 terms remain:

$$\begin{aligned}(2.3)\qquad &\Pi_{1111}\sigma_{11}^2 + \Pi_{2222}\sigma_{22}^2 + \Pi_{3333}\sigma_{33}^2 + 4\Pi_{1212}\sigma_{12}^2 + 4\Pi_{2323}\sigma_{23}^2 \\ &+ 4\Pi_{3131}\sigma_{13}^2 + 2\Pi_{1122}\sigma_{11}\sigma_{22} + 2\Pi_{2233}\sigma_{22}\sigma_{33} + 2\Pi_{3311}\sigma_{33}\sigma_{11} \\ &+ \Pi_{11}\sigma_{11} + \Pi_{22}\sigma_{22} + \Pi_{33}\sigma_{33} = 1.\end{aligned}$$

The material under consideration requires 9+3 tests: simple tension T_i, simple compression C_i along each axis of orthotropy, and simple shear Y_{ij} along each plane of orthotropy ($i, j = 1, 2, 3$); for orthotropic materials when the coordinate system coincides with the material symmetry directions, plastic shear stresses along reverse directions on the same plane do not differ: $Y_{ij}^+ = Y_{ij}^- = Y_{ij}$ (see THEOCARIS [19]). Replacing the index notation by the engineering notation, Eq. (2.3) takes more friendly form:

$$\begin{aligned}(2.4)\qquad &a_1(\sigma_y - \sigma_z)^2 + a_2(\sigma_z - \sigma_x)^2 + a_3(\sigma_x - \sigma_y)^2 + a_4\tau_{yz}^2 + a_5\tau_{zx}^2 \\ &+ a_6\tau_{xy}^2 + a_7\sigma_x + a_8\sigma_y + a_9\sigma_z = 1,\end{aligned}$$

where the new plastic moduli are defined as follows (see SOCHA and SZCZEPIŃSKI [18]):

$$\begin{aligned}(2.5)\qquad &a_1 = \frac{1}{2}\left(\frac{1}{T_yC_y} + \frac{1}{T_zC_z} - \frac{1}{T_xC_x}\right), \quad a_2 = \frac{1}{2}\left(\frac{1}{T_zC_z} + \frac{1}{T_xC_x} - \frac{1}{T_yC_y}\right), \\ &a_3 = \frac{1}{2}\left(\frac{1}{T_xC_x} + \frac{1}{T_yC_y} - \frac{1}{T_zC_z}\right), \quad a_4 = \frac{1}{Y_{yz}^2}, \quad a_5 = \frac{1}{Y_{zx}^2}, \\ &a_6 = \frac{1}{Y_{xy}^2}, \quad a_7 = \frac{1}{T_x} - \frac{1}{C_x}, \quad a_8 = \frac{1}{T_y} - \frac{1}{C_y}, \quad a_9 = \frac{1}{T_z} - \frac{1}{C_z}.\end{aligned}$$

The plastic moduli $a_1, a_2, \ldots, a_9$ are linear combinations of the components of fourth-order tensor Π_{ijkl} (see LEMAITRE and CHABOCHE [12], also MALININ and RŻYSKO [14]) and second-order tensor Π_{ij}:

$$\begin{aligned}(2.6)\qquad &\Pi_{1111} = a_1 + a_3, \quad \Pi_{2222} = a_1 + a_2, \quad \Pi_{3333} = a_2 + a_3, \\ &\Pi_{1122} = -a_1, \quad \Pi_{2233} = -a_2, \quad \Pi_{3311} = -a_3, \\ &\Pi_{1212} = a_4/4, \quad \Pi_{2323} = a_5/4, \quad \Pi_{3131} = a_6/4, \\ &\Pi_{11} = a_8, \quad \Pi_{22} = a_9, \quad \Pi_{33} = a_7.\end{aligned}$$

The function (2.4), being a special case of the yield condition presented by PARISEAU [15], can describe materials with different tensile and compressive strengths. RALSTON [16] employed Eq. (2.4) to crushing failure analysis of column-grained ice which exhibits orthotropy and sensitivity to hydrostatic pressure. However, if the yield stresses in tension are equal to that in compression (isosensitive material), $T_x = C_x = X$, $T_y = C_y = Y$, $T_z = C_z = Z$, the coefficients a_7, a_8, a_9 vanish, so the linear terms in Eq. (2.4) disappear:

$$a_1(\sigma_y - \sigma_z)^2 + a_2(\sigma_z - \sigma_x)^2 + a_3(\sigma_x - \sigma_y)^2 + a_4\tau_{yz}^2 + a_5\tau_{zx}^2 + a_6\tau_{xy}^2 = 1, \tag{2.7}$$

whereas the coefficients a_1, a_2, a_3 take the classical form of Hill's yield condition (see HILL [6] also JACKSON *et al.* [9]):

$$a_1 = \frac{1}{2}\left(\frac{1}{Y^2} + \frac{1}{Z^2} - \frac{1}{X^2}\right), \qquad a_2 = \frac{1}{2}\left(\frac{1}{Z^2} + \frac{1}{X^2} - \frac{1}{Y_2}\right),$$
$$a_3 = \frac{1}{2}\left(\frac{1}{X^2} + \frac{1}{Y^2} - \frac{1}{Z^2}\right). \tag{2.8}$$

The classical Hill yield condition (2.7), consisting of the quadratic stress functions, that generalizes the Huber - Mises yield condition, has failed to account for the so-called "anomalous behaviour" of some commercial aluminum alloy and steel sheets. Therefore, a special case of the Hill generalized yield conditions has been developed (see HILL [7]):

$$a_1|\sigma_y - \sigma_z|^m + a_2|\sigma_z - \sigma_x|^m + a_3|\sigma_x - \sigma_y|^m + a_4|\tau_{yz}|^m + a_5|\tau_{zx}|^m + a_6|\tau_{xy}|^m = 1, \tag{2.9}$$

where the exponent m is equal to 6 or 8. The yield condition (2.9) is a generalization of the Hersey - Davis yield condition for $m = 2$ (and for $m = 4$), or the Tresca - Guest yield condition in the limiting case $m \to \infty$.

3. Convexity conditions

Although the yield function defined by Eq. (2.9) has been mathematically verified, and its convexity has been proved in case of the planar anisotropy in the principal stress space if and only if $m \geq 1$ and $a_1, a_2, a_3, \ldots$ are positive constant coefficients (see BARLAT and LIAN [1], also CHU [4]), in case of the general orthogonal anisotropy in the six-dimensional stress space and in the presence of terms associated with hydrostatic pressure, convexity of the yield surface (2.4) is not obvious.

Let us try to formulate convexity conditions for the yield functions (2.4) and (2.9). The yield condition (2.4) is defined in the six-dimensional stress space, and

if we can transform it to the three-dimensional space of the principal stresses, we will get rid of terms associated with second power of the shear stresses. However, it should be noted that for anisotropic materials, the yield condition is established in a certain reference coordinate system which is fixed with respect to the orientation of the material anisotropy. We cannot change the reference coordinate without changing the form of the yield condition. Moreover, the coefficients $a_1, a_2, a_3, \ldots, a_9$ are not components of any tensor so they are not subjected to transformation rules of tensors. To avoid these inconveniences, first, we have to recover a tensor form of the yield condition expressing the coefficients $a_1, a_2, a_3, \ldots, a_9$ by components of the fourth-order tensor Π_{ijkl} and components of the second-order tensor Π_{ij} of Eq. (2.6). Next, appropriate transformations from the directions of material orthotropy to the directions of principal stresses are done:

$$\Pi'_{ijkl} = \Pi_{mnrp} n_{im} n_{jn} n_{kr} n_{lp}, \qquad \Pi'_{ij} = \Pi_{mn} n_{im} n_{jn}, \tag{3.1}$$

where n_{ij} are direction cosines of the transformation.

Such a transformation is strictly associated with an important problem of the transposition of convexity from one space to another. SAYIR [17] proved such a transposition from the nine-dimensional stress space (in particular case, from the six-dimensional stress space) to the three-dimensional space of principal stresses, whereas LIPPMANN [13] from the three-dimensional space to the six-dimensional space.

When the new transformed coefficients $a'_1, a'_2, a'_3, \ldots, a'_9$ are calculated from Π'_{ijkl} and Π'_{ij} by means of Eq. (2.6), the yield condition (2.4) referring to the principal stress axes takes a simplified form:

$$a'_1(\sigma_1 - \sigma_2)^2 + a'_2(\sigma_2 - \sigma_3)^2 + a'_3(\sigma_3 - \sigma_1)^2 + a'_7\sigma_3 + a'_8\sigma_2 + a'_9\sigma_1 = 1. \tag{3.2}$$

Last step is the geometric representation of the surface (3.2) in the Haigh–Westergaard stress space, where the three principal stresses $(\sigma_1, \sigma_2, \sigma_3)$ are replaced by the Haigh–Westergaard coordinates (ξ, ϱ, θ) (see Appendix B):

$$\begin{Bmatrix} \sigma_1 \\ \sigma_2 \\ \sigma_3 \end{Bmatrix} = \frac{1}{\sqrt{3}} \begin{Bmatrix} \xi \\ \xi \\ \xi \end{Bmatrix} + \sqrt{\frac{2}{3}}\varrho \begin{Bmatrix} \cos\theta \\ \cos(\theta - 2\pi/3) \\ \cos(\theta + 2\pi/3) \end{Bmatrix}. \tag{3.3}$$

Substitution of (3.3) into (3.2) when the classical trigonometric identities are used, provides the formula for the surface radius:

$$\varrho(\theta, \xi) = \sqrt{\frac{2}{3}} \frac{\sqrt{B^2 + 12AC} - B}{4A}, \tag{3.4}$$

where

$$
\begin{aligned}
A &= a'_1 \sin^2\theta + a'_2 \sin^2(\theta + \pi/3) + a'_3 \sin^2(\theta - \pi/3), \\
B &= a'_7 \cos\theta + a'_8 \cos(\theta - 2\pi/3) + a'_9 \cos(\theta + 2\pi/3), \\
C &= 1 - \frac{\xi}{\sqrt{3}}(a'_7 + a'_8 + a'_9)\,.
\end{aligned} \tag{3.5}
$$

In case of independence of the hydrostatic pressure of the generalized Hill yield condition (2.9) when $m \neq 2$, we have to set $A = \hat{A}$, $B = 0$, $C = 1$, and instead of Eq. (3.4), the surface radius is found from the formula

$$
\begin{aligned}
\varrho(\theta) &= \frac{1}{\sqrt{2}} \frac{1}{\sqrt[m]{\hat{A}}} \\
&= \frac{1}{\sqrt{2}} \frac{1}{\sqrt[m]{a'_1 \sin^m\theta + a'_2 \sin^m(\theta + \pi/3) + a'_3 \sin^m(\theta - \pi/3)}}\,.
\end{aligned} \tag{3.6}
$$

In case when the material isotropy ($a'_1 = a'_2 = a'_3 = 1/2\sigma_0^2$) and $m = 2$ are assumed, Eq. (3.6) reduces to the classical Huber – Mises yield condition:

$$
\varrho = \sqrt{\frac{2}{3}}\sigma_0 = \text{const.} \tag{3.7}
$$

Quadratic form containing linear terms of the yield condition (3.2) represents an *elliptic paraboloid* with a symmetry axis parallel to the hydrostatic axis, whereas the open end of the paraboloid is usually oriented towards the direction of hydrostatic compression (see THEOCARIS [19]). It is clear that only one of the coefficients a_1, a_2, a_3 in Eqs. (2.5) can be negative (see HILL [6]). Therefore, the loss of convexity consists in that an elliptic paraboloid may become at most an imaginary elliptic paraboloid, or in other words, a hyperbolic paraboloid. Consequently, the conditions of convexity of the yield surface are formulated as follows: the radius $\varrho(\theta, \xi)$ must be a real and positive number; Eqs. (3.4), (3.5) yield

$$
\varrho(\theta, \xi) > 0 \qquad \forall\ \theta, \xi, \tag{3.8}
$$

and

$$
\operatorname{Im}\varrho = 0 \qquad \Longleftrightarrow \qquad \xi \leq \frac{\sqrt{3}}{a'_7 + a'_8 + a'_9}\left(1 + \frac{B^2}{12A}\right). \tag{3.9}
$$

In case of the generalized Hill yield surface, Eq. (3.6) represents an elliptical cylinder or at most a hyperbolic cylinder for which both conditions (3.8) and (3.9) ($\varrho(\theta) > 0 \quad \forall\ \theta$, and $\operatorname{Im}\varrho = 0$) are equivalent to each other, and lead to the following inequality:

$$
\hat{A} = a'_1 \sin^m\theta + a'_2 \sin^m(\theta + \pi/3) + a'_3 \sin^m(\theta - \pi/3) > 0, \qquad \forall\ \theta. \tag{3.10}
$$

4. Examples

4.1. Convexity of Hill's yield surfaces for the brass sheet L22

Most of anisotropic materials used in practice fulfil the convexity conditions (3.8) through (3.10), however there are few of them which do not.

Let us check convexity of the yield conditions which are independent of the hydrostatic pressure, namely (2.7) and its generalized form (2.9). MALININ and RŻYSKO in [14] give plastic properties for a brass sheet of Russian commercial symbol L22, 0.8 mm thick: $\sigma_{0x} = X = 120\,\text{MPa}$, $\sigma_{0y} = Y = 105\,\text{MPa}$, $\sigma_{0z} = Z = 950\,\text{MPa}$. Authors do not mention the shear yield stresses.

The difficulty in experimental defining the off-diagonal components of the fourth-order tensor resulted in a series of publications. Complicated tests were suggested, nevertheless they did not give the explicit form of the respective yield criterion. Therefore, several researchers used the simplifying assumption, when the small off-diagonal components (when compared to the diagonal ones) may be disregarded. This prediction, however, satisfactorily fits the experimental data only for two-dimensional loading models. On the other hand, off-axis biaxial tests indicate that vanishing of the off-diagonal components of the fourth-order tensor may lead to unreliable results.

Hence, the following *ad hoc* extensions of the classical definitions are introduced in the present paper: $\tau_{0ij} = Y_{ij} = \sqrt{\sigma_{0i}\sigma_{0j}/3}$ for $m = 2$, and $\tau_{0ij} = Y_{ij} = \sqrt{\sigma_{0i}\sigma_{0j}}/2$ for $m = 6, 8$. In case of material isotropy $\sigma_{0i} = \sigma_{0j} = \sigma_0$ we get values $\tau_0 = \sigma_0/\sqrt{3}$ (Huber - Mises) or $\tau_0 = \sigma_0/2$ (Tresca - Guest), respectively. Eventually, the complete material data are shown in Table 1.

Table 1. Yield stresses of brass L22 [14].

m	X [MPa]	Y [MPa]	Z [MPa]	Y_{zy} [MPa]	Y_{zx} [MPa]	Y_{xy} [MPa]
2	120	105	950	182	194	64.8
6 or 8	120	105	950	157	168	56.1

The Hill's yield condition (2.7) applied to the brass L22 represents an elliptic cylinder in the Haigh - Westergaard stress space. It turns out that semi-axes of the ellipse strongly depend on the direction cosines of the transformation Eq. (3.1). It has been seen from Table 1 that the direction of dominant material orthotropy is oriented parallel to the z axis of the coordinate system, whereas the plane xy exhibits slight orthotropy. Hence, the material is nearly transversely isotropic. Moreover, the material exhibits the group of symmetry which satisfies periodicity of at least one octant. Both coordinate systems associated with the directions of material orthotropy and the directions of principal stresses were linked, for convenience, by the Euler angles $(\varphi, \vartheta, \psi)$ (see Appendix A). The complete analysis

requires to check the yield condition versus all Euler angles in one octant, however it takes a lot of CPU time and memory. To avoid this inconvenience, the authors suggest to take advantage of the plane orthotropy mentioned above, and to check the yield condition for the pair of angles φ, ϑ; the third angle ψ is not essential, and may be disregarded within the following range: $0 \leq \varphi \leq 90°$ and $0 \leq \vartheta \leq 90°$.

Let us follow the evolution of the yield condition in a simple case, when only one of the Euler angles, say ϑ, is subject to change, whereas two other are kept constant. When $\vartheta = 45°$ we get the ellipse of moderate semi-axes ratio, about 1:3, each change of ϑ, either decrease or increase, increases this ratio. Consequently, the ellipse is subjected to rotation and, simultaneously, becomes, step by step, longer and more oblate. Finally, for $\vartheta = 0°$ or $\vartheta = 90°$, one of the semi-axes goes to infinity and the yield condition presents a hyperbolic cylinder (Fig. 1). As it was mentioned before, it is convenient to map the convexity of yield condition versus the pair of Euler angles: $0 \leq \varphi \leq 90°$ and $0 \leq \vartheta \leq 90°$, taken as a two-dimensional domain. The obtained map (Fig. 2) confirms the assumed group of the material symmetry; moreover, the higher-order symmetry of 45° versus angle φ is observed. The yield condition is convex in almost whole domain except for narrow zones around its corners.

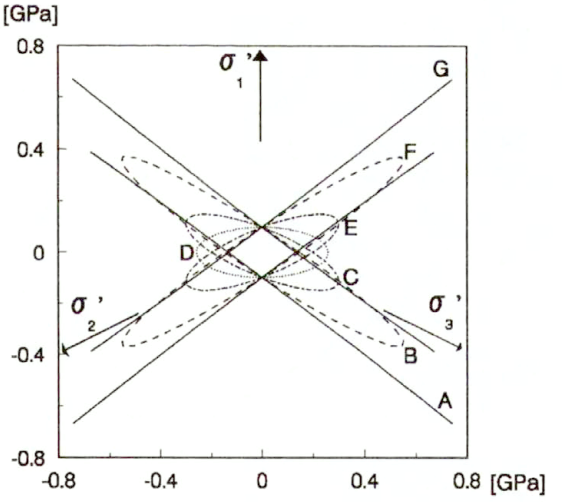

FIG. 1. Evolution of Hill's yield surface versus ϑ-Euler angle: $A - 0°$, $B - 15°$, $C - 30°$, $D - 45°$, $E - 60°$, $F - 75°$ and $G - 90°$, for brass L22 [14].

In case of the generalized Hill yield condition (2.9) describing plastic behaviour of the brass L22, the yield surface ($m = 8$) is a prism of the semi-hexagonal cross-section with oval corners (Fig. 3). The loss of convexity resembles the previous case, each decrease or increase of ϑ versus the value 22° makes the hexagon more deformed until it becomes open.

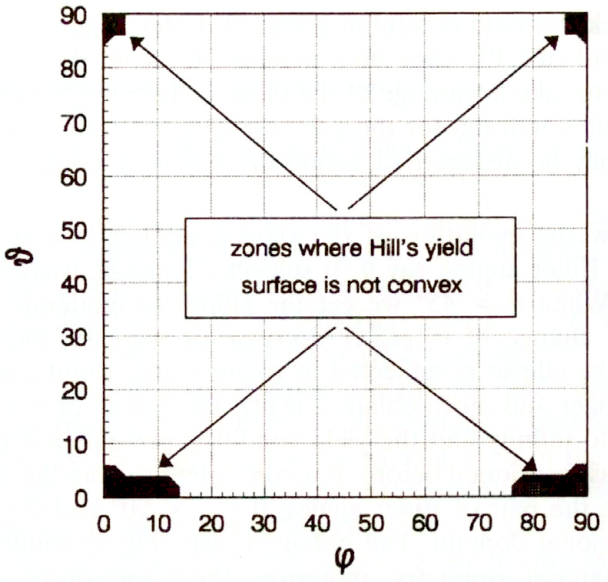

FIG. 2. Convexity map of Hill's yield surface versus φ, ϑ Euler angles for brass L22 [14].

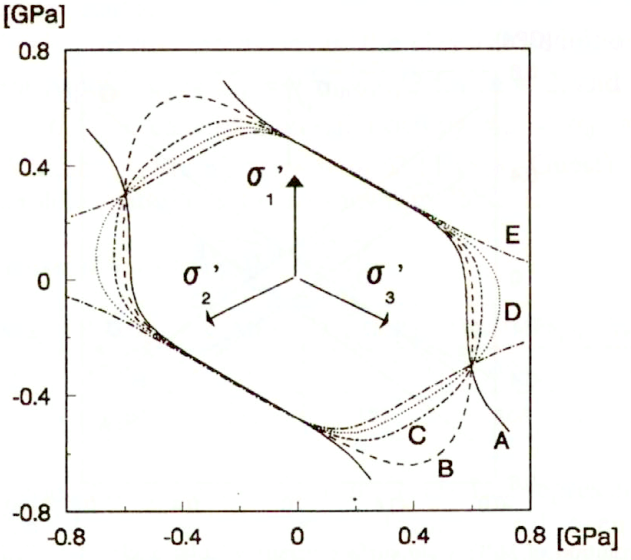

FIG. 3. Evolution of generalized Hill's yield surface ($m = 8$) versus ϑ-Euler angle: $A - 18°$, $B - 20°$, $C - 22°$, $D - 24°$ and $E - 26°$, for brass L22 [14].

The convexity map is shown in Fig. 4. The area where the yield condition is convex has been significantly decreased when compared with the case $m = 2$ (see Fig. 2). Zones neighbouring the corners where the yield condition is not convex have increased significantly: two of them which refer to the angle $\vartheta = 0°$ lie

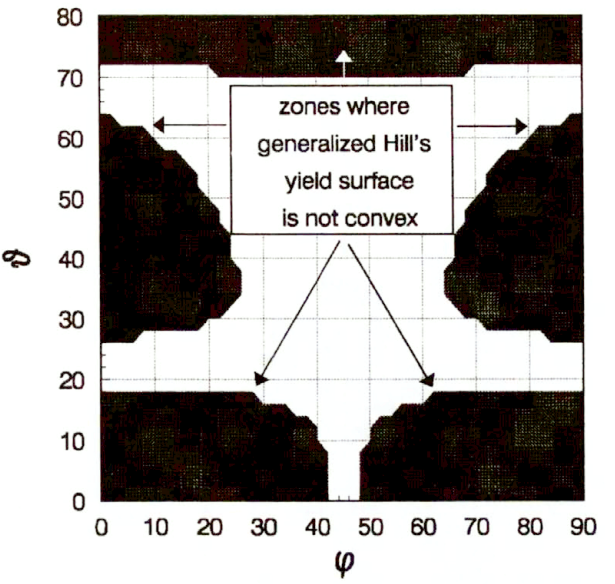

FIG. 4. Convexity map of generalized Hill's yield surface versus φ, ϑ Euler angles for brass L22 [14].

around the axis of symmetry $\varphi = 45°$ and consequently, only a very narrow zone remains convex; moreover, two zones referring to the angle $\vartheta = 90°$ have joined together and the yield condition has lost convexity in the whole range of φ. Two additional zones of nonconvexity, each of them oval in shape, have appeared for moderate values of $\vartheta = 45°$.

4.2. Convexity of the Goldenblat–Kopnov yield surface (2.4) applied as failure criterion for the carbon woven roving-epoxy resin composite

Next example deals with checking the convexity of the function containing terms associated with the hydrostatic pressure (2.4), applied as the anisotropic failure condition of a composite. THEOCARIS [19] and WU [20] cite the experimental data for the composite with the reinforcement of a carbon *woven roving*, for which the material data are presented in Table 2 ([1]).

Table 2. Anisotropic failure stresses of the carbon woven roving-epoxy resin composite [19, 20].

Failure stresses [MPa]								
T_x	C_x	T_y	C_y	T_z	C_z	Y_{yz}	Y_{zx}	Y_{xy}
1065.93	615.01	1065.93	615.01	42.40	143.20	21.20	21.20	532.96

([1]) HOA [8] recommends to take Y_{ij} for woven roving as 0.5 of T_i. This value coincides with the tensile strength of woven roving tested at 45°.

The failure condition (2.4) used for the carbon woven roving-epoxy resin composite, for the Euler angles $\varphi = 45°$, $\vartheta = 45°$ forms an elliptic paraboloid, the axis of which coincides with the direction of the hydrostatic compression (Fig. 5). If we change φ or ϑ, the previously mentioned rotation of the ellipses and simultaneous loss of convexity of the surface is observed.

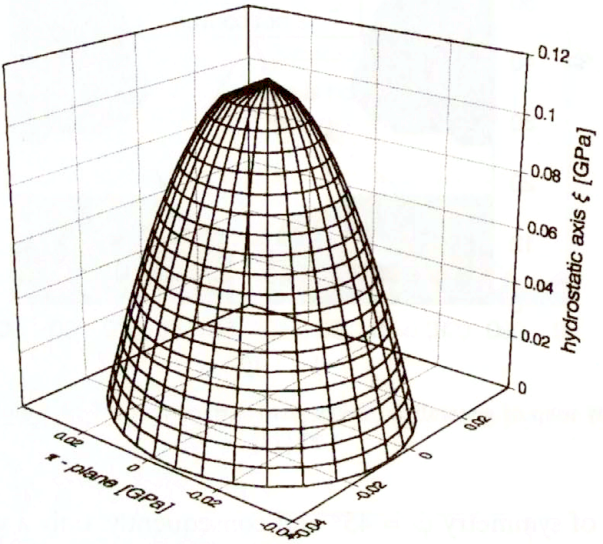

FIG. 5. The Goldenblat–Kopnov failure surface (Euler angles $\varphi = 45°$, $\vartheta = 45°$) for carbon woven roving-epoxy resin composite [19, 20].

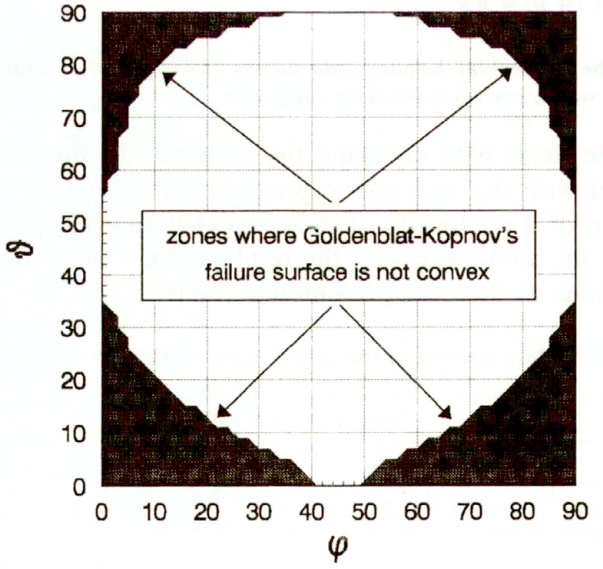

FIG. 6. Convexity map of Goldenblat–Kopnov failure surface versus φ, ϑ Euler angles for carbon woven roving-epoxy resin composite [19, 20].

Analyzing the map of convexity in Fig. 6, further reduction of area of convexity, due to anisotropy of the carbon woven roving-epoxy resin composite stronger than the brass L22, is observed. Zones of nonconvexity, around corners, have increased, and now reach almost $\vartheta = 35°$ or $\vartheta = 55°$, respectively. However, the central zone of oval shape guarantees convexity of the failure condition for all angles $\varphi \in < 10°, 50° >$, $\vartheta \in < 10°, 50° >$.

5. Conclusion

In the present paper, the convexity of the Goldenblat - Kopnov yield/failure criterion is analyzed. To illustrate the yield/failure surface in the Haigh - Westergaard stress space, the fourth-order Π_{ijkl} and the second-order Π_{ij} tensors of plastic moduli are transformed from the principal directions of material orthotropy to the principal stress directions. As examples of non-convex yield/failure conditions, included or not included hydrostatic pressure effect, a commercial brass sheet and a woven roving reinforced composite are chosen. A case of special interest is the dependence of convexity of a yield/failure surface on the direction cosines of transformation.

Appendix

A. Transformation of constitutive tensors to a new coordinate system

A tensor of rank four is subjected to the following rule of transformation:

$$T'_{ijkl} = T_{mnrp} l_{im} l_{jn} l_{kr} l_{lp} , \tag{A.1}$$

whereas a tensor of rank two fulfills the appropriate transformation rule:

$$T'_{ij} = T_{mn} l_{im} l_{jn} , \tag{A.2}$$

where for given i, j, k, l, the indices m, n, r, p are to be summed from 1 to 3. The formula (A.1) transforms the components of a tensor of rank four to new axes according to transformation rule, however an equivalent transformation is more convenient:

$$\widehat{T}'_{ij} = \widehat{T}_{mn} q_{im} q_{jn} , \tag{A.3}$$

where actually indices m and n are to be summed from 1 to 6. In this way, a transformation of the fourth rank tensor T_{mnrp} is replaced by transformation of its representation matrix $\widehat{T}_{mn}$, where symbols q_{ij} are taken from Table 3 (see LEKHNITSKII [11], also BATHE [2]).

Let us consider a convenient parametrization when a new coordinate system is obtained from the old one by rotation through Euler's angles. The following

Table 3. Symbols q_{ij} in transformation formulas.

i/j	1	2	3	4	5	6
1	l_{11}^2	l_{12}^2	l_{13}^2	$l_{12}l_{13}$	$l_{13}l_{11}$	$l_{12}l_{11}$
2	l_{21}^2	l_{22}^2	l_{23}^2	$l_{23}l_{22}$	$l_{23}l_{21}$	$l_{22}l_{21}$
3	l_{31}^2	l_{32}^2	l_{33}^2	$l_{33}l_{32}$	$l_{33}l_{31}$	$l_{32}l_{31}$
4	$2l_{31}l_{21}$	$2l_{32}l_{22}$	$2l_{33}l_{23}$	$l_{33}l_{22} + l_{32}l_{23}$	$l_{33}l_{21} + l_{31}l_{23}$	$l_{31}l_{22} + l_{32}l_{21}$
5	$2l_{31}l_{11}$	$2l_{32}l_{12}$	$2l_{33}l_{13}$	$l_{33}l_{12} + l_{32}l_{13}$	$l_{33}l_{11} + l_{31}l_{13}$	$l_{31}l_{12} + l_{32}l_{11}$
6	$2l_{21}l_{11}$	$2l_{12}l_{22}$	$2l_{13}l_{23}$	$l_{13}l_{22} + l_{12}l_{23}$	$l_{13}l_{21} + l_{11}l_{23}$	$l_{11}l_{22} + l_{12}l_{21}$

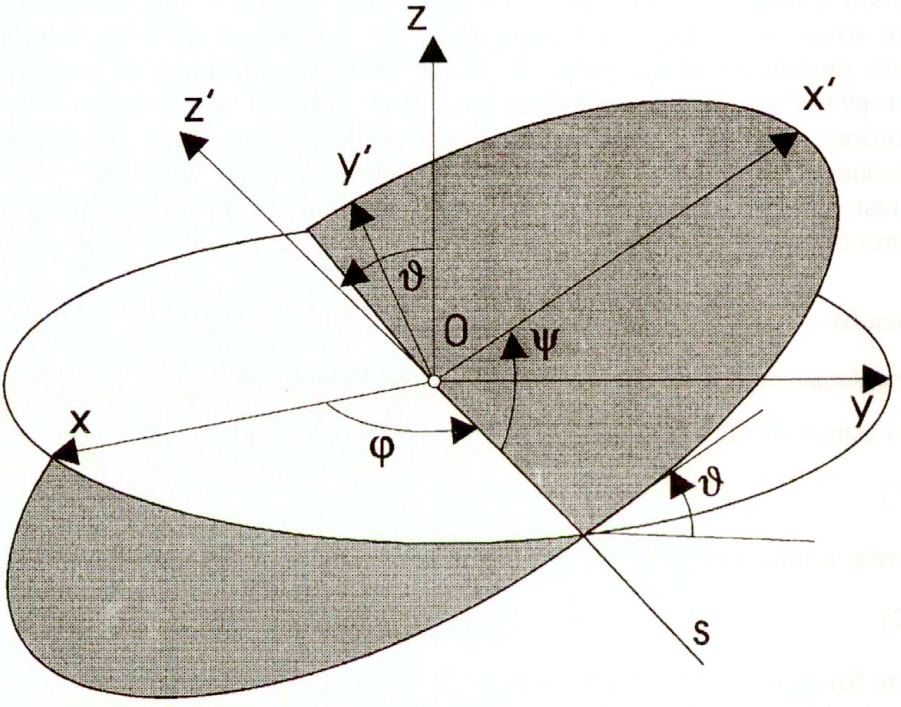

FIG. 7. The Euler angles.

sequence of rotations is taken into account (see Fig. 7); first rotation of the initial coordinate frame around z axis through precession angle ($0 \leq \varphi < 2\pi$), then rotation around the nodal line s through nutation angle ($0 \leq \vartheta \leq \pi$), and finally rotation around z' axis through angle ($0 \leq \psi < 2\pi$), for which the corresponding transformation matrices are as follows (see KARAŚKIEWICZ [10]):

$$\mathcal{A} = \begin{pmatrix} \cos\varphi & \sin\varphi & 0 \\ -\sin\varphi & \cos\varphi & 0 \\ 0 & 0 & 1 \end{pmatrix}, \tag{A.4}$$

(A.4) [cont.]

$$\mathcal{B} = \begin{pmatrix} 1 & 0 & 0 \\ 0 & \cos\vartheta & \sin\vartheta \\ 0 & -\sin\vartheta & \cos\vartheta \end{pmatrix},$$

$$\mathcal{C} = \begin{pmatrix} \cos\psi & \sin\psi & 0 \\ -\sin\psi & \cos\psi & 0 \\ 0 & 0 & 1 \end{pmatrix}.$$

Hence, the matrix of direction cosines takes the form:

$$l_{ij} = \mathcal{C}\mathcal{B}\mathcal{A}. \tag{A.5}$$

In general case angles φ, ϑ, ψ are variable, but there are three basic cases. Namely, if angles φ and ϑ are constant, but angle ψ is variable, then the coordinate frame is subjected to rotation around the fixed axis z'. If angles ψ and ϑ are constant, but angle φ is variable, then the nodal line s is subjected to rotation around the axis z on plane xy, and simultaneously axis z' describes a cone around the z axis. If angles φ and ψ are constant, but angle ϑ is variable, then the nodal line s is fixed and plane $x'y'$ changes its inclination versus plane xy.

B. Haigh–Westergaard stress space

A very convenient representation of the stress state is the Haigh – Westergaard stress space which consists of the three principal stresses as coordinates.

Consider the straight line passing through the origin and equally inclined to the coordinate axes (see Fig. 8). Then for every point on this line, the state of stress fulfills the equality $\sigma_1 = \sigma_2 = \sigma_3$. In other words, every point on this line corresponds to a hydrostatic state of stress, this line is therefore named the hydrostatic axis. Furthermore, any plane perpendicular to the hydrostatic axis is called the deviatoric plane. Such a plane has the form:

$$\sigma_1 + \sigma_2 + \sigma_3 = \sqrt{3}\xi, \tag{B.1}$$

where ξ is the distance from the origin to the plane measured along the hydrostatic axis. The particular plane passing through the origin (for $\xi = 0$) is called the π-plane or the Meldahl plane.

An arbitrary state of stresses at a given point is decomposed into the hydrostatic and the deviatoric components, respectively:

$$(\sigma_1, \sigma_2, \sigma_3) = (1, 1, 1)\mathrm{Tr}\sigma/3 + (s_1, s_2, s_3). \tag{B.2}$$

The vector representing the hydrostatic component $\xi = \mathrm{Tr}\sigma/\sqrt{3}$ lies on the hydrostatic axis, whereas the vector representing the deviatoric component of length $\varrho = \sqrt{s_1 s_2 + s_2 s_3 + s_3 s_1}$ lies on the deviatoric plane.

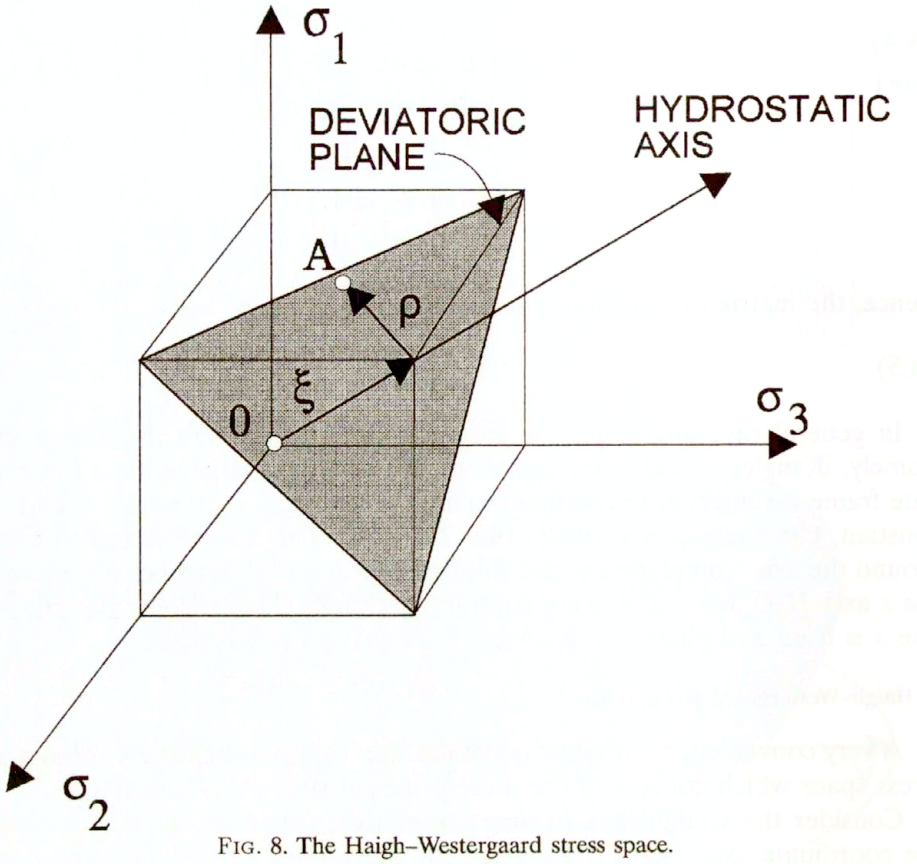

FIG. 8. The Haigh–Westergaard stress space.

Let us consider projections of both the deviatoric component and the coordinate axes on the π-plane (new and old unit vectors form the direction cosines equal to $\sqrt{2/3}$, hence new coordinates expressed in terms of the old ones are equal to $\sigma_i' = \sqrt{2/3}\sigma_i$):

$$
\begin{aligned}
s_1 &= \sqrt{\frac{2}{3}}\varrho\cos\theta, \qquad s_2 = \sqrt{\frac{2}{3}}\varrho\cos(2\pi/3-\theta),\\
s_3 &= \sqrt{\frac{2}{3}}\varrho\cos(2\pi/3+\theta),
\end{aligned}
\tag{B.3}
$$

where $0 \geq \theta \geq \pi/3$; then the state of stress $(\sigma_1, \sigma_2, \sigma_3)$ can be expressed by (ξ, ϱ, θ) called the Haigh - Westergaard coordinates:

$$
\begin{Bmatrix}\sigma_1\\ \sigma_2\\ \sigma_3\end{Bmatrix} = \frac{1}{\sqrt{3}}\begin{Bmatrix}\xi\\ \xi\\ \xi\end{Bmatrix} + \sqrt{\frac{2}{3}}\varrho\begin{Bmatrix}\cos\theta\\ \cos(\theta-2\pi/3)\\ \cos(\theta+2\pi/3)\end{Bmatrix}. \tag{B.4}
$$

References

1. F. BARLAT and J. LIAN, *Plastic behavior and stretchability of sheet metals*, Int. J. Plasticity, **5**, 1, 51, 1989.
2. K.J. BATHE, *Finite element procedures in engineering analysis*, Prentice-Hall, Chapter 5, 258–259, 1982.
3. W.F. CHEN and D.J. HAN, *Plasticity for structural engineers*, Springer-Verlag, Chapter 2, 66–86, Chapter 3, 163–173, 1988.
4. E. CHU, *Generalization of Hill's 1979 anisotropic yield criteria*, Proc. NUMISHEET'89, 199–208, 1989.
5. I.I. GOLDENBLAT and V.A. KOPNOV, *A generalized theory of plastic flow of anisotropic metals* [in Russian], Stroitelnaya Mekhanika, 307–319, 1966.
6. R. HILL, *A theory of the yielding and plastic flow of anisotropic metals*, Proc. Roy. Soc., London, **A 193**, 281–297, 1948.
7. R. HILL, *Theoretical plasticity of textured aggregates*, Proc. Camb. Phil. Soc., **85**, 179, 1979.
8. S.V. HOA, *Analysis for design of fiber-reinforced plastic vessels and pipings*, Techomic Publishing Co., Lancaster-Basel, Chapter 2, 48, 1991.
9. L.R. JACKSON, K.F. SMITH and W.T. LANKFORD, *Plastic flow in anisotropic sheet steel*, Metals Technology Techn. Publ., 2440, 1–15, 1948.
10. E. KARAŚKIEWICZ, *Introduction to theory of vectors and tensors* [in Polish], PWN, Chapter 1, 57–61, 1971.
11. S.G. LEKHNITSKII, *Theory of elasticity of an anisotropic body* [English transl.], Mir Publishers, Moscow, Chapter 1, 36–42, 1981.
12. J. LEMAITRE and J.L. CHABOCHE, *Méchanique des máteriaux solides*, Bordas, Chapter 5, 184–187, 1985.
13. H. LIPPMANN, *Matrixungleichungen und die Konvexität der Fließfläche*, ZAMM, **50**, 1-4, 134–137, 1970.
14. N.N. MALININ and J. RŻYSKO, *Mechanics of materials* [in Polish], PWN, Chapter 3, 119–155, 1981.
15. W.G. PARISEAU, *Plasticity theory for anisotropic rocks and solids*, Proc. 10th Symp. Rock Mech., Austin, Chapter 10, 1968.
16. T.D. RALSTON, *Yield and plastic deformation in ice crushing failure*, ICSI/AIDJEX Symp. Sea Ice-Processes and Models, Washington 1977.
17. M. SAYIR, *Zur Fließbedingungen der Plastizitätstheorie*, Ingenieur-Archiv., **39**, 6, 414–432, 1970.
18. G. SOCHA and W. SZCZEPIŃSKI, *On experimental determination of the coefficients of plastic anisotropy in sheet metals*, Arch. Mech., **46**, 177–190, 1994.
19. P.S. THEOCARIS, *Weighing failure tensor polynomial criteria for composites*, Int. J. Damage Mech., **1**, 4–46, 1992.
20. E.M. WU, *Mechanics of composite materials*, G.P. SENDECKYI [Ed.], Academic Press Publ., Chapter 9, 2, 353–431, 1979.
21. M. ŻYCZKOWSKI, *Combined loadings in the theory of plasticity*, PWN, Chapter 3, 94–126, 1981.

CRACOW UNIVERSITY OF TECHNOLOGY, KRAKÓW.
e-mail: artur@cut1.pk.edu.pl

Received November 8, 1996.

Arch. Mech., 49, 3, pp. 477–511, Warszawa 1997

Viscoplastic shells
Theory and numerical analysis (1)

Dedicated to Professor Franz Ziegler
on the occasion of His 60th birthday

F.G. KOLLMANN and C. SANSOUR (DARMSTADT)

THE PAPER is intended as a review of the work carried out at the institute to which the authors belong, regarding the theory of viscoplastic shells in both versions of small and finite strains. Within the first version, the kinematics incorporated is assumed to be linear allowing for an additive decomposition of the strain rate. For the axisymmetric case, a hybrid strain-based functional is presented. Contrasting this, in the finite strain case, the shell kinematics is considered as geometrically exact. Here, the shell theory itself is seven-parametric and allows for the application of a three-dimensional constitutive law. The constitutive law used is that of Bodner & Partom which falls within the class of unified constitutive models. The multiplicative decomposition of the deformation gradient is employed, but no use is made of the so-called intermediate configuration. The elastic constitutive law is of a logarithmic type. An enhanced strain finite element formulation is developed and several examples of finite deformations of various shell geometries are presented.

1. Introduction

MANY TECHNICALLY important structures can be modelled as shells, i.e. as curved bodies where one dimension, which is called the thickness, is much smaller than its other dimensions. In some applications, the material behaviour of metallic shells can be modelled by viscoplastic constitutive equations which describe rate-dependent deformation behaviour. Despite their technical importance, not so many publications deal with viscoplastic shells. In this paper we will present an overview on the work carried out at the institute to which the authors belong with regard to viscoplastic shells and their numerical analysis.

The paper will be split into two parts. In the first part we will briefly discuss a general, but geometrically linear theory of viscoplastic shells. The viscoplastic deformation behaviour can be governed by any of the more recently published so-called unified models with internal variables. Furthermore, we will demonstrate the application of the shell theory to the formulation of a family of mixed axisymmetric Finite Shell Elements (FSE). In the second, larger part we first will extend the constitutive viscoplastic theory to finite deformation. Then we will present a recently developed shell theory with 7 parameters. We will address the topics of its numerical implementation leading to very efficient FSEs. We

(1) Invited paper presented at the 31st Polish Solid Mechanics Conference in Mierki, Poland.

will present some instructive numerical examples and give an outlook on further research directions in this field.

There exits an almost unlimited literature on elastic shells. For reference purposes, let us cite the papers by NAGHDI [1], VALID [2] and BERNADOU [3]. There also exists a comprehensive literature on rate-independent elastoplastic shells which we will not address here. However, relatively few publications deal with viscoplastic shells. CORMEAU [4] investigates thick elastoplastic shells using a von Mises-type viscoplastic flow rule. He uses general linear shell kinematics and formulates an isoparametric shell element. HUGHES and LIU [5, 6] develop a geometrically nonlinear degenerate shell element. They use a quite general anisotropic viscoplastic constitutive model and solve an impressive number of examples. PARISCH [7] starts as Hughes and Liu from three-dimensional nonlinear continuum mechanics. To account for the nonlinear distribution of the stress components across the shell thickness, he develops a layered model with piecewise linear distributions through the shell thickness. Effectively, his formulation comes close to a fully three-dimensional Finite Element Method (FEM).

KOLLMANN and MUKHERJEE [8] have developed a very general geometrically linear viscoplastic shell theory. They give their entire formulation in rate form and start from a two-field variational principle [9] which for the purely elastic case has been published by ODEN and REDDY [10]. Their shell theory has been used for the formulation of an axisymmetric hybrid strain element by KOLLMANN and BERGMANN [11]. Using the same shell theory, a family of mixed axisymmetric shell elements has been formulated by KOLLMANN *et al.* [12]. KLEIBER and KOLLMANN [13] have extended the shell theory to damage, proposing a generalization of the damage model by GURSON [14]. An and KOLLMANN [15] have suggested a theory of finitely deformed viscoplastic shells.

Finally we will address the formulation of viscoplastic constitutive models. Here we will consider only the so-called *unified models* with internal variables. In such models it is assumed that in the material, inelastic strain rates evolve at any stress level. However, for small stresses these inelastic strain rates are so small that no macroscopically visible inelastic strain is accumulated. Considering this feature, most of such unified models are formulated typically without the notion of a yield surface. Almost all known viscoplastic models are formulated in the context of small strains. Therefore, the total strain rate tensor is decomposed additively into an elastic and an inelastic part. The mathematical model comprises evolution equations for the inelastic strain rates. As arguments of the constitutive functions, not only the stresses appear but also a set of suitably defined internal variables. It is clear that in addition to the evolution of the inelastic strain rates, also evolution equations for these internal variables have to be specified.

A very early model is due to PERZYNA [16]. Further models have been formulated by BODNER and PARTOM [17], CHABOCHE [18], KREMPL and coworkers [19] and STECK [20]. Only very few attempts have been made to generalize viscoplastic constitutive models to finite deformation. RUBIN [21] has extended the model by

Bodner and Partom to finite strains. Following NAGHDI and TRAPP [22], he uses a formulation in strain space. His primary variables are the right Cauchy–Green deformation tensor and its plastic part. Therefore, Rubin gives a formulation on the reference configuration. A formulation on the current configuration has been proposed by NISHIGUCHI *et al.* [23]. They assume *a priori* an additive decomposition of Almansi's strain tensor into an elastic and an inelastic part. The elastic part of the deformation is governed by a hypoplastic constitutive equation. The inelastic constitutive equations are formulated with an unusual objective rate which is an extension of the Jaumann rate. A finite element implementation and numerical examples are presented in [24].

An important issue in finite inelasticity is the time integration of the inelastic constitutive model. Specific considerations have to be taken to fulfill the constraint of inelastic incompressibility. ETEROVIC and BATHE [25] and WEBER and ANAND [26] use the exponential map for this purpose. Further, ETEROVIC and BATHE [25] and MIEHE and STEIN [27] use a logarithmic strain measure. SIMO [28] has systematically exploited the geometric structure of the elastoplastic problem and thus derived compact and closed forms of the tangent operator in the continuous and discrete cases.

2. Theory and numerical analysis of geometrically linear viscoplastic shells

In this section we first describe the essential features of the general inelastic shell theory by KOLLMANN and MUKHERJEE [8]. Then we show the implementation of a family of mixed axisymmetric shell elements. Next, we present the inelastic constitutive model by BODNER and PARTOM [17]. Finally, we give some numerical results.

2.1. Geometrically linear inelastic shell theory

In this section we give a very brief description of the underlying inelastic shell theory [8]. A shell $\mathcal{B}$ is the Cartesian product of a two-dimensional surface $\mathcal{S} \subset \mathbb{R}^3$ with a closed interval $[-h/2, h/2] \subset \mathbb{R}$, i.e.

$$\mathcal{B} := \mathcal{S} \times [-h/2, h/2] \subset \mathbb{R}^3. \tag{2.1}$$

The two-dimensional surface $\mathcal{S}$ is denoted as the shell midsurface (SMS). The quantity h is called the shell thickness. Since in this section a geometrically linear theory is considered, there is no distinction between the actual configuration $\mathcal{B}_t$, $t \in \mathbb{R}$ and the reference configuration $\mathcal{B}_0$ ($\mathcal{B}_0 = \mathcal{B}_t = \mathcal{B}$). We introduce curvilinear coordinates θ^α on $\mathcal{S}$, where Greek indices range from 1 to 2 and Latin ones from 1 to 3. For simplicity it is assumed that the shell thickness is constant on $\mathcal{S}$.

On the SMS covariant and contravariant base vectors $\boldsymbol{A}_\alpha$ and $\boldsymbol{A}^\alpha$ are introduced in a standard manner. The first and second fundamental tensor on the

SMS are denoted by **A** and **B**, respectively. The determinant of the tensor **B** is denoted as B. Next, the normal unit vector A_3 on $\mathcal{S}$ and a normal coordinate z are introduced. The covariant base vectors of the shell space $\mathcal{B}$ are given as

$$G_\alpha = \mathbf{M} A_\alpha , \tag{2.2}$$

$$G_3 = A_3 , \tag{2.3}$$

where

$$\mathbf{M} := \mathbf{I} - z\mathbf{B} \tag{2.4}$$

is the shifter tensor and **I** denotes the unit tensor on $\mathcal{S}$. The determinant of the shifter tensor is given by

$$M = 1 - z\,\mathrm{tr}\,\mathbf{B} + z^2 B, \tag{2.5}$$

where tr denotes the trace operator.

The displacement vector u^* (quantities with a star (as e.g. u^*) are referred to the shell space $\mathcal{B}$ while all unstarred quantities (as e.g. u) are defined on the SMS $\mathcal{B}$) of any point in the shell space has a representation

$$u^* = u + z\,w , \tag{2.6}$$

where u is the displacement vector of $\mathcal{S}$ and w is the difference vector. In the present paper it is presupposed that the difference vector w is independent of the displacement vector u of the SMS.

The following component representations for the strain tensor ε in the shell space $\mathcal{B}$ are available [8]

$$\begin{aligned} M\,\varepsilon_{\alpha\beta} &= e_{\alpha\beta} + z\,\kappa_{\alpha\beta} , \\ M\,\varepsilon_{\alpha 3} &= \psi_\alpha + z\,\varrho_\alpha , \\ \varepsilon_{33} &= e_{33} . \end{aligned} \tag{2.7}$$

The quantities $e_{\alpha\beta}$, $\kappa_{\alpha\beta}$, ψ_α and ϱ_α are components of tensor and vector fields, respectively, which are defined on $\mathcal{S}$. Note that the kinematic assumption (2.6) leads to transverse shear strains, which are linear in the normal coordinate z, and to a transverse normal strain which is constant over the shell thickness. We mention that completely analogous relations exist between the velocity field and the strain rate field.

Next a general frame of the inelastic constitutive equations with internal variables is presented. Only such materials are considered which are isotropic and homogeneous. A fundamental constitutive assumption presupposes that the total strain rate tensor $\dot{\varepsilon}$ can be decomposed additively into an elastic and inelastic part

$$\dot{\varepsilon} = \dot{\varepsilon}^{\mathrm{e}} + \dot{\varepsilon}^{\mathrm{n}} . \tag{2.8}$$

The tensor $\dot{\boldsymbol{\varepsilon}}^{\mathrm{e}}$ of the elastic strains is related to the stress rate tensor $\dot{\boldsymbol{\sigma}}$ by Hooke's generalized law

$$\dot{\boldsymbol{\sigma}} = 2G\,\dot{\boldsymbol{\varepsilon}}^{\mathrm{e}} + \lambda(\operatorname{tr}\dot{\boldsymbol{\varepsilon}}^{\mathrm{e}})\,\mathbf{I}\,. \tag{2.9}$$

Here G and λ are the Lamé constants. The inelastic strain rate tensor $\dot{\boldsymbol{\varepsilon}}^{\mathrm{n}}$ obeys in the isothermal case an evolution equation of the following form

$$\dot{\boldsymbol{\varepsilon}}^{\mathrm{n}} = f(\boldsymbol{\sigma}, \boldsymbol{q}^{(k)}), \qquad k = 1, 2, \ldots n\,. \tag{2.10}$$

Here f is a tensor-valued function of the current values of the stress tensor $\boldsymbol{\sigma}$ and a set $\boldsymbol{q}^{(k)}$, $k = 1, 2, \ldots n$ of suitably selected internal variables. The internal variables are either scalars or second order tensors. For these otherwise unspecified internal variables also evolution equations exist

$$\dot{\boldsymbol{q}}^{(k)} = g^{(k)}(\boldsymbol{\sigma}, \boldsymbol{q}^{(r)}), \qquad k, r = 1, 2, \ldots n\,. \tag{2.11}$$

Here again $\boldsymbol{g}^{(k)}$, $k = 1, 2, \ldots n$ denote functions which are depending on the corresponding internal variable $\boldsymbol{q}^{(k)}$ either scalar-valued or tensor-valued.

We introduce vectors (in the sense of matrix calculus) of generalized strain rates $\dot{\boldsymbol{\gamma}}$ and of generalized velocities $\dot{\boldsymbol{v}}$. The relation between the strain rates and the velocities is

$$\dot{\boldsymbol{\gamma}} = \mathbf{L}_{\gamma v}\dot{\boldsymbol{v}}\,, \tag{2.12}$$

where $\mathbf{L}_{\gamma v}$ is a generalized strain-rate velocity operator. The general representation of this operator can be found in [8].

KOLLMANN and MUKHERJEE start from a three-dimensional variational two-field principle [9] which is formulated in velocities and strain rates. Performing the integration over the shell thickness, this variational principle can be reduced to a two-dimensional form. The concise version of the variational principle reads [11]

$$\delta\left\{\int_{\mathcal{S}}\left[\frac{1}{2}\dot{\boldsymbol{\gamma}}^{T}\mathbf{D}_{\gamma\gamma}\,\dot{\boldsymbol{\gamma}} - \dot{\boldsymbol{\gamma}}^{T}\mathbf{D}_{\gamma\gamma}\,\mathbf{L}_{\gamma v}\,\dot{\boldsymbol{v}} + \dot{\boldsymbol{F}}_{L}^{\,T}\dot{\boldsymbol{v}} + \dot{\boldsymbol{f}}^{N^{T}}\mathbf{L}_{\gamma v N}\,\dot{\boldsymbol{v}}\right] dS\right\} = 0. \tag{2.13}$$

Here dS is the area element on the SMS $\mathcal{S}$. Further, $\mathbf{D}_{\gamma\gamma}$ is a generalized elasticity matrix for the shell, $\dot{\boldsymbol{F}}_{L}^{\,T}$ a generalized load rate vector, $\dot{\boldsymbol{f}}^{N^{T}}$ a generalized vector of inelastic pseudo-force rates and $\mathbf{L}_{\gamma v N}$ a linear operator. Details of these objects can be found in [8, 11, 12]. We mention that $\dot{\boldsymbol{\gamma}}$ is the assumed strain rate field while $\dot{\boldsymbol{v}}$ is the velocity field. The assumed strain rate field can be discontinuous between inter-element boundaries.

One principal advantage of the variational principle (2.13) is that it contains only strain rates and velocities but not stress rates. In inelastic shell analysis assumptions such as e.g. (2.6) concerning shell kinematics are generally made. These assumptions lead to information on the distribution of the total strain rates over the shell thickness such as e.g. (2.7). However, unlike the analysis of elastic shells, the distribution of the stresses over the shell thickness is not known *a priori* but it changes in time and space. Therefore, this distribution is a part of the unknown solution. It is not possible to conclude from the stress resultants and moments, which typically evolve from any shell theory including stresses, on the stresses in inelastic shell analysis. It has to be mentioned that KOLLMANN *et al.* [12] have shown in numerical experiments that for elastic shells, stress-like quantities such as e.g. mebrane forces and bending moments exhibit the same order of convergence (with mesh refinements) as the radial deflection of the SMS.

2.2. Implementation of mixed finite shell elements

We start with the discretization of the variational principle (2.13). KOLLMANN and BERGMANN [29] have introduced different shape functions for the generalized velocity vector $\dot{v}$ and the generalized strain rate vector $\dot{\gamma}$

$$\dot{v} = \mathbf{N}\,\hat{\dot{v}}\,, \qquad \dot{\gamma} = \overline{\mathbf{N}}\,\hat{\dot{\gamma}}\,, \tag{2.14}$$

where a hat ($\hat{}$) indicates nodal values.

Then, the mixed FE model can be derived from the variational principle (2.13) by standard procedures

$$\mathbf{K}_{\gamma\gamma}\hat{\dot{\gamma}} + \mathbf{K}_{\gamma v}\hat{\dot{v}} = \mathbf{0}\,, \qquad \mathbf{K}_{\gamma v}^{T}\hat{\dot{\gamma}} = -\dot{F}_{\mathrm{L}} - \dot{F}_{\mathrm{N}}\,, \tag{2.15}$$

where the following quantities have been defined:

$$\begin{aligned}
\mathbf{K}_{\gamma\gamma} &:= \int_{S} \overline{\mathbf{N}}^{\mathrm{T}}\mathbf{D}_{\gamma\gamma}\overline{\mathbf{N}}\,dS,\\
\mathbf{K}_{\gamma v} &:= \int_{S} \overline{\mathbf{N}}^{\mathrm{T}}\mathbf{D}_{\gamma\gamma}\mathbf{L}_{\gamma v}\mathbf{N}\,dS,\\
\dot{F}_{\mathrm{L}} &:= \int_{S} N^{\mathrm{T}}\dot{f}_{\mathrm{L}}\,dS,\\
\dot{F}_{\mathrm{N}} &:= \int_{S} \left(\mathbf{L}_{\gamma v}^{\mathrm{N}}\mathbf{N}\right)^{\mathrm{T}}\dot{f}_{\mathrm{N}}\,dS.
\end{aligned} \tag{2.16}$$

It is possible to find an implementational scheme of the mixed model which fits any FE-code based on the standard displacement formulation. Details of this implementation can be found in [12].

In the following we describe the results obtained for a conical element as originally proposed in the context of the displacement method by ZIENKIEWICZ and coworkers [30] and extended to a mixed hybrid strain formulation by KOLLMANN and BERGMANN [11]. It is important to choose approximations where the polynomial order of the approximation of the strain rate field is at least equal or higher than the approximation of the velocity field. We denote our elements by two numbers, which are separated by the capitals PSS, where PSS indicates that the shell theory is based on the assumption of plane stress and plane strain. The first number indicates the polynomial degree of the shape functions for the strain rate field, and the second one – that of the velocity field. Pursuing numerical tests for elastic cylindrical shells it could be shown that the mixed elements (1PSS1 and 2PSS2) are completely locking free down to a thickness ratio $h/R = 4 \cdot 10^{-10}$, where R is the radius of the cylinder.

2.3. Model of Bodner and Partom for infinitesimal strains

BODNER and PARTOM [17] assume an additive decomposition of the total rate of deformation tensor $\mathbf{d} = \dot{\boldsymbol{\varepsilon}}$ into an elastic and a plastic part

$$\dot{\boldsymbol{\varepsilon}} = \dot{\boldsymbol{\varepsilon}}^{\mathrm{e}} + \dot{\boldsymbol{\varepsilon}}^{\mathrm{p}} . \tag{2.17}$$

We denote the deviator of the stress tensor by $\mathrm{dev}\boldsymbol{\sigma}$. The flow rule takes the form

$$\dot{\boldsymbol{\varepsilon}}^{\mathrm{p}} = \omega \, \mathrm{dev}\boldsymbol{\sigma} . \tag{2.18}$$

HACKENBERG [31] has given the following formulation of this model which is convenient for numerical purposes. Define the following quantities:

$$\begin{aligned} \Pi &:= \sqrt{\frac{3}{2} \mathrm{dev}\boldsymbol{\sigma} : \mathrm{dev}\boldsymbol{\sigma}} = \sqrt{3 J_2} , \\ \dot{\phi} &:= \frac{2}{\sqrt{3}} \sqrt{J_2} \, \omega = \frac{2}{3} \Pi \, \omega , \\ \boldsymbol{\nu} &:= \frac{3}{2} \frac{\mathrm{dev}\boldsymbol{\sigma}}{\Pi} . \end{aligned} \tag{2.19}$$

Then (2.18) can be written as

$$\dot{\boldsymbol{\varepsilon}}^{\mathrm{p}} = \dot{\phi} \boldsymbol{\nu} . \tag{2.20}$$

REMARK 1. Note that (2.20) is the standard form for associative plasticity which is important for time integration. □

REMARK 2. We point out that in our formulation the flow function $\dot{\phi}$ is equal to the equivalent inelastic strain rate. □

The parameter ω in (2.19) is given as

$$\omega = \frac{\sqrt{3}}{\Pi} D_0 \exp\left[-\frac{1}{2}\frac{n+1}{n}\left(\frac{Z}{\Pi}\right)^{2n}\right]. \tag{2.21}$$

The function $\dot{\phi}$ takes the form

$$\dot{\phi} = \frac{2}{\sqrt{3}} D_0 \exp\left[-\frac{1}{2}\frac{n+1}{n}\left(\frac{Z}{\Pi}\right)^{2n}\right]. \tag{2.22}$$

Here Z is an internal variable which models isotropic hardening. The following evolution equation holds for this internal variable

$$\dot{Z} = \frac{m}{Z_0}(Z_1 - Z)\Pi\dot{\phi} \tag{2.23}$$

with initial condition

$$Z\big|_{t=t_0} = Z_0 . \tag{2.24}$$

The quantities D_0, n, m, Z_0 and Z_1 are material parameters which have to be determined from experiments for any material. We note that these parameters are temperature-dependent.

For our numerical work we use parameters given by BODNER and PARTOM [17] for a titanium alloy at room temperature. They are summarized in Table 1. For time integration an implicit algorithm has to be applied as shown e.g. in [32].

Table 1. Material parameters for titanium alloy.

Parameter	Value	Dimension
E	118000	MPa
ν	0.34	–
Z_0	1150	MPa
Z_1	1400	MPa
D_0^2	$1 \cdot 10^8$	s^{-2}
n	1	–
m	100	–

2.4. Numerical results of inelastic computation

As a test example we have computed a cylindrical shell made of the titanium alloy. The shell has an axial length of 1 000 mm, a radius of 250 mm and a thickness of 10 mm. It is closed at its ends. The shell has been discretized using 70 equally spaced 1PSS1 elements. The loading history of the shell is depicted in Fig. 1. The

internal pressure is increased within 1 s linearly from zero to the maximal value of 13.0 MPa. Then this pressure is held constant over the time of 9 s. Finally, the pressure drops linearly within 1 s to zero. In Fig. 2 the deflection of the shell is depicted for the following times: $t = 0.55$ s, $t = 5$ s, $t = 5.55$ s and $t = 10$ s.

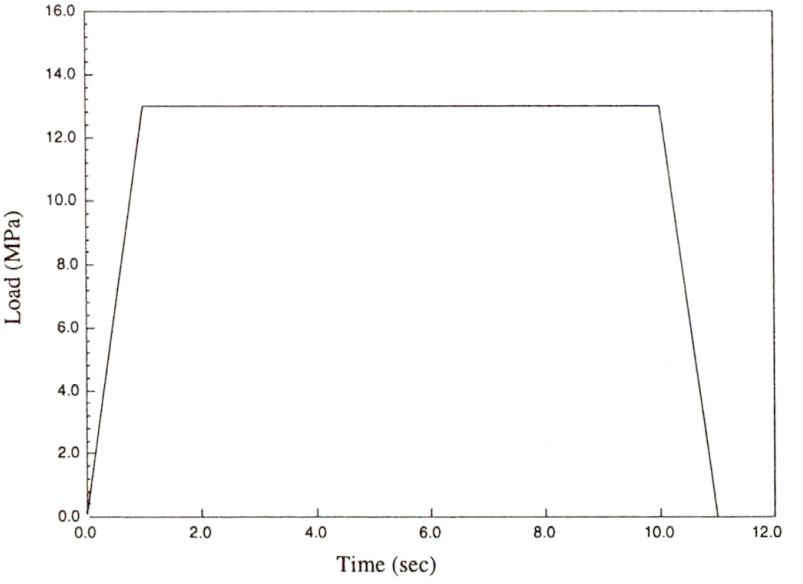

FIG. 1. Load-history for the cylindrical shell.

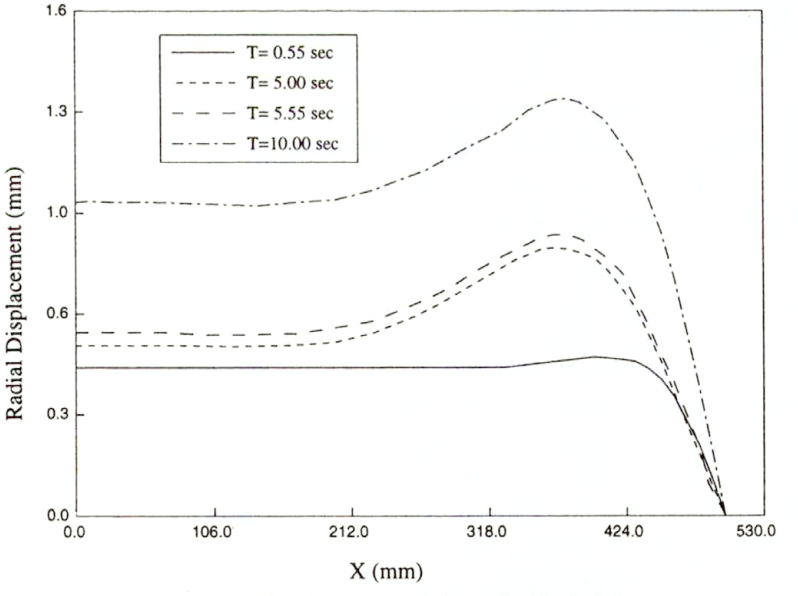

FIG. 2. Radial deflection of the cylindrical shell.

At $t = 1\,\mathrm{s}$ the loading of the shell is completed. In the middle section a pure membrane deformation prevails. Only at the edge in the region $350\,\mathrm{mm} \leq z \leq 400\,\mathrm{mm}$ bending effects can be noticed. During the hold time $1\,\mathrm{s} \leq t \leq 100\,\mathrm{s}$ considerable additional deformation due to viscoplastic effects takes place. It is remarkable that the region of noticeable bending effects spreads into the interior of the shell. During unloading ($10\,\mathrm{s} \leq t \leq 11\,\mathrm{s}$) the elastic part of the deformation is recovered. After unloading no additional inelastic deformation can be observed.

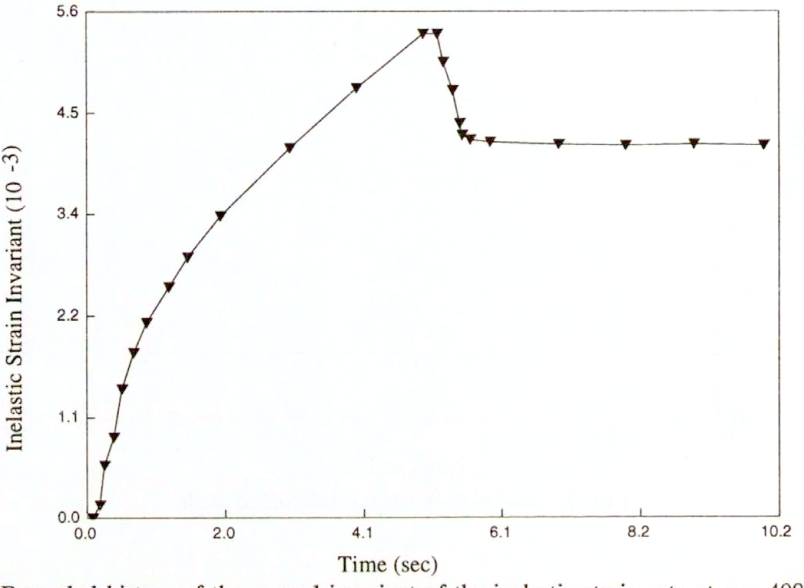

FIG. 3. Recorded history of the second invariant of the inelastic strain rate at $z = 408.948\,\mathrm{mm}$ and $r = 254.840\,\mathrm{mm}$.

Figure 3 shows the recorded history of the development of the second invariant of the inelastic strain rate tensor at a point of the shell ($z = 408.943\,\mathrm{mm}$, $r = 254.840\,\mathrm{mm}$), where bending effects dominate. The second invariant of the inelastic strain rate is defined as

$$I_2(\dot{\boldsymbol{\varepsilon}}^{\mathrm{p}}) := \sqrt{\frac{2}{3}\dot{\boldsymbol{\varepsilon}}^{\mathrm{p}} : \dot{\boldsymbol{\varepsilon}}^{\mathrm{p}}}\,. \tag{2.25}$$

During the first second of the loading history the equivalent inelastic strain rate is very small. Then it increases sharply with time. At the beginning of the hold time the second invariant of the inelastic strain rate drops continuously. With unloading it sharply drops to zero.

Finally in Fig. 4 the distribution of the axial bending stress σ_{zz} over the thickness of the shell at $z = 408.943\,\mathrm{mm}$ is given.

At $t = 0.55\,\mathrm{s}$ during the loading period the distribution of the stress is linear, i.e. the deformation is purely elastic. At the end of the loading phase $t = 1.0\,\mathrm{s}$,

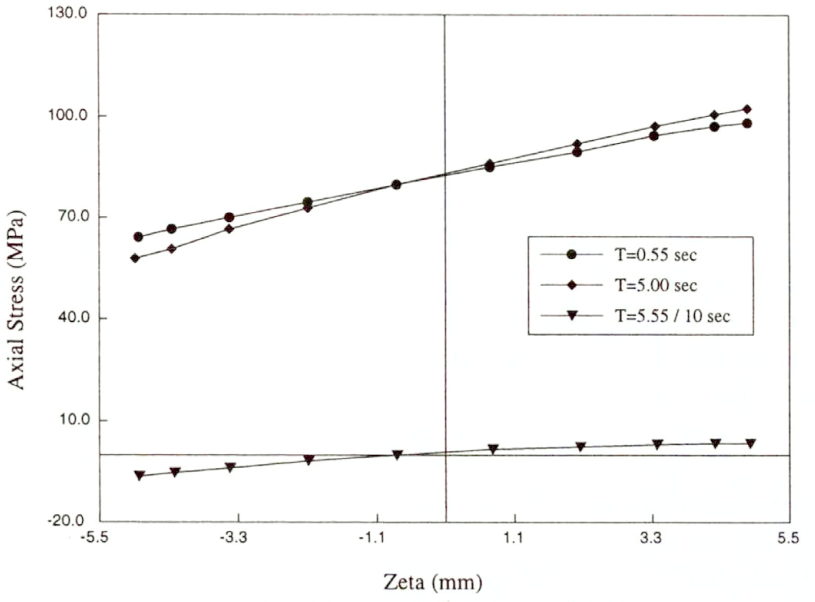

FIG. 4. Axial stress of the cylindrical shell.

a slight curvature of the stress distribution can be observed. During the hold time until $t = 10\,\mathrm{s}$, a redistribution of the bending stress occurs and the curvature of the stress distribution is increased. Finally after unloading at $t = 11\,\mathrm{s}$ the residual stress has developed. It has to be noticed that in the theory of Bodner and Partom, neither loading or unloading conditions nor a yield surface are present.

3. Finite deformation of three-dimensional viscoplastic continua

In this section we present a concise theory of a finitely deformed elasto-viscoplastic continuum. Then we apply this theory for an extension of the infinitesimal viscoplastic model by Bodner and Partom to finite deformation.

3.1. Three-dimensional elasto-viscoplastic continuum under finite deformation

After consideration of finite deformation of viscoplastic bodies we discuss in general the elastic and viscoplastic constitutive models. Then a hyperelastic model and a generalization of the model of Bodner and Partom presented in Sec. 2.3 will be given.

3.1.1. Kinematics of finitely deformed elasto-viscoplastic bodies. A motion of the body B is a one parameter mapping $\phi_t : \mathcal{B}_0 \to \mathcal{B}_t$ where $t \in \mathbb{R}$ is the time and $\mathcal{B}_t$ is the current configuration at time t. For any $X \in \mathcal{B}_0$ we have $\phi(X) = \boldsymbol{x} \in \mathcal{B}_t$. For any $X \in B$ we denote the tangent spaces of the reference and current configuration

as $T_X\mathcal{B}_0$ and $T_x\mathcal{B}_t$, respectively, and the coordinate charts, which are taken to be convected, by θ^i. The deformation gradient is defined as

$$\begin{aligned} &\mathbf{F} := T_X\mathcal{B}_0 \to T_x\mathcal{B}_t\,, \\ &\mathbf{F} = T\boldsymbol{\phi} = \boldsymbol{g}_i \otimes \boldsymbol{G}^i, \qquad i = 1,2,3, \end{aligned} \tag{3.1}$$

where we have $\boldsymbol{G}_i = \mathbf{X}_{,i}$, $\boldsymbol{g}_i = \mathbf{x}_{,i}$, $\boldsymbol{G}_i \cdot \boldsymbol{G}^j = \delta_i^j$, $\boldsymbol{g}_i \cdot \boldsymbol{g}^j = \delta_i^j$. Here, derivatives with respect to θ^i are denoted by a comma, scalar product of vectors by a dot, and δ_i^j is the Kronecker delta.

Note that the deformation gradient is a two-point tensor. Further note, that we have suppressed in (3.1) the dependence of the deformation gradient on time.

It is convenient to introduce the right Cauchy–Green deformation tensor as

$$\mathbf{C} = \mathbf{F}^T \mathbf{g}\, \mathbf{F}\,, \tag{3.2}$$

where $\mathbf{g}$ is the metric tensor in the current configuration $\mathcal{B}_t$. Speaking in geometric terms [33], the right-hand side of (3.2) can be interpreted as the pull-back of the metric tensor of the current configuration to the reference configuration, i.e. $\mathbf{C} = \phi^*(\mathbf{g})$.

Next we introduce the multiplicative decomposition [34, 35, 36] of the deformation gradient into an elastic and a plastic part

$$\mathbf{F} = \mathbf{F}_\mathrm{e}\, \mathbf{F}_\mathrm{p}\,, \tag{3.3}$$

where the assumed incompressibility of the inelastic deformations means that $\mathbf{F}_\mathrm{p} \in SL^+(3,\mathbb{R})$, $SL^+(3,\mathbb{R})$ denotes the special linear group with determinant equal one.

REMARK 3. The multiplicative decomposition (3.3) is often accepted as equivalent with the introduction of an intermediate configuration $\widehat{\mathcal{B}}$. In contrast to this understanding which has caused a lot of discussion in the literature, we define

$$\begin{aligned} &\mathbf{F}_\mathrm{p} := T_X\mathcal{B}_0 \to T_X\mathcal{B}_0\,, \\ &\mathbf{F}_\mathrm{e} := T_X\mathcal{B}_0 \to T_x\mathcal{B}_t\,. \end{aligned} \tag{3.4}$$

That is, the inelastic part of the deformation gradient is a map from $T_X\mathcal{B}_0$ onto itself. It is, accordingly, a material tensor uniquely defined by the evolution equation of an appropriately defined material plastic rate. If the constraint of plastic incompressibility is assumed, then $\det \mathbf{F}_\mathrm{p} = 1$ holds; i.e. $\mathbf{F}_\mathrm{p}$ is an unimodular tensor. □

Equation (3.3) motivates the introduction of an elastic and a plastic right Cauchy–Green deformation tensor

$$\begin{aligned} \mathbf{C}_\mathrm{e} &:= \mathbf{F}_\mathrm{e}^\mathrm{T} \mathbf{g}\, \mathbf{F}_\mathrm{e}\,, \\ \mathbf{C}_\mathrm{p} &:= \mathbf{F}_\mathrm{p}^\mathrm{T} \mathbf{F}_\mathrm{p}\,. \end{aligned} \tag{3.5}$$

The elastic right Cauchy–Green deformation tensor $\mathbf{C}_e$ can be interpreted as pull-back of the metric tensor $\mathbf{g}$ with the elastic part $\mathbf{F}_e$ of the deformation gradient.

The deformation gradient $\mathbf{F}$ is an element of the general linear group $GL^+(3,\mathbb{R})$ with positive determinant. Therefore, we can attribute to its time derivative a left and right rate

$$\begin{aligned} \dot{\mathbf{F}} &= \mathbf{l}\mathbf{F}, \\ \dot{\mathbf{F}} &= \mathbf{F}\mathbf{L}. \end{aligned} \tag{3.6}$$

Both rates are mixed tensors (contravariant-covariant). They are related by means of the equation

$$\mathbf{L} = \mathbf{F}^{-1}\mathbf{l}\mathbf{F}. \tag{3.7}$$

Geometrically Eq. (3.7) is the pull-back of the mixed velocity gradient from the current configuration to the reference configuration, i.e. $\mathbf{L} = \phi^*(\mathbf{l})$.

Since $\mathbf{F}_p \in SL^+(3,\mathbb{R})$, we can again define a right rate according to

$$\dot{\mathbf{F}}_p = \mathbf{F}_p \mathbf{L}_p \tag{3.8}$$

which proves to be more appropriate for a numerical treatment in a purely material context. If a constitutive function is specified for the right rate $\mathbf{L}_p$ of the plastic part $\mathbf{F}_p$ of the deformation gradient, then Eq. (3.8) constitutes an evolution equation for $\mathbf{F}_p$.

3.2. Elasto-viscoplastic constitutive model

We start with general considerations where we use thermodynamical arguments to formulate a general frame for the elastic part of the constitutive model. Then we modify the elastic model for the sake of numerical efficiency. Next, the infinitesimal model of Bodner and Partom presented in Sec. 2.3 is modified and generalized to finite strains.

3.2.1. General considerations. Let $\boldsymbol{\tau}$ be the Kirchhoff stress tensor. Consider the expression of the internal power

$$\mathcal{W} = \boldsymbol{\tau} : \mathbf{l}, \tag{3.9}$$

where $\mathbf{l}$ is defined in $(3.6)_1$ and the relation holds: $\mathbf{a} : \mathbf{b} = \operatorname{tr} \mathbf{a}\mathbf{b}^t$ for $\mathbf{a}$, $\mathbf{b}$ being second order tensors and tr denoting the trace operation. The expression is rewritten using material tensors as

$$\mathcal{W} = \boldsymbol{\Xi} : \mathbf{L}. \tag{3.10}$$

The comparison of (3.9) with (3.10) leads with the aid of (3.7) to the definition of the material stress tensor

$$\Xi = \phi^*(\tau) = \mathbf{F}_p^T \tau \mathbf{F}_p^{-T}. \tag{3.11}$$

The tensor Ξ is, accordingly, the mixed variant pull-back of the Kirchhoff tensor. It coincides with Noll's intrinsic stress tensor and some authors call it Mandel's stress tensor.

A common feature of unified inelastic constitutive models is the introduction of phenomenological internal variables. We denote a typical internal variable by $\mathbf{Z}$. Assuming the existence of a free energy function according to $\psi = \psi(\mathbf{C}_e, \mathbf{Z})$, the localised form of the dissipation inequality for an isothermal process takes the form

$$\begin{aligned} \mathcal{D} &= \tau : \mathbf{l} - \varrho_{ref} \dot{\psi} \\ &= \Xi : \mathbf{L} - \varrho_{ref} \dot{\psi} \geq 0, \end{aligned} \tag{3.12}$$

where ϱ_{ref} is the density at the reference configuration.

Making use of the relation

$$\dot{\mathbf{C}}_e = \mathbf{F}_p^{-T} \mathbf{L}^T \mathbf{C} \mathbf{F}_p^{-1} + \mathbf{F}_p^{-T} \mathbf{C} \mathbf{L} \mathbf{F}_p^{-1} - \mathbf{F}_p^{-T} \mathbf{L}_p^T \mathbf{C} \mathbf{F}_p^{-1} - \mathbf{F}_p^{-T} \mathbf{C} \mathbf{L}_p \mathbf{F}_p^{-1} \tag{3.13}$$

one may derive

$$\dot{\psi} = 2\mathbf{C}\mathbf{F}_p^{-1} \frac{\partial \psi}{\partial \mathbf{C}_e} \mathbf{F}_p^{-T} : (\mathbf{L} - \mathbf{L}_p) + \frac{\partial \psi}{\partial \mathbf{Z}} \cdot \dot{\mathbf{Z}}. \tag{3.14}$$

Insertion of (3.14) into (3.12) leads to

$$\begin{aligned} \mathcal{D} = \left(\Xi - 2\varrho_{ref} \mathbf{C} \mathbf{F}_p^{-1} \frac{\partial \psi(\mathbf{C}_e, \mathbf{Z})}{\partial \mathbf{C}_e} \mathbf{F}_p^{-T} \right) : \mathbf{L} \\ + 2\varrho_{ref} \mathbf{C} \mathbf{F}_p^{-1} \frac{\partial \psi(\mathbf{C}_e, \mathbf{Z})}{\partial \mathbf{C}_e} \mathbf{F}_p^{-T} : \mathbf{L}_p - \varrho_{ref} \frac{\partial \psi(\mathbf{C}_e, \mathbf{Z})}{\partial \mathbf{Z}} \cdot \mathbf{Z} \geq 0. \end{aligned} \tag{3.15}$$

By defining Y as the thermodynamical force conjugate to the internal variable $\mathbf{Z}$

$$Y := -\varrho_{ref} \frac{\partial \psi(\mathbf{C}_e, \mathbf{Z})}{\partial \mathbf{Z}}, \tag{3.16}$$

and making use of standard thermodynamical arguments, from (3.15) follows the elastic constitutive equation

$$\Xi = 2\varrho_{ref} \mathbf{C} \mathbf{F}_p^{-1} \frac{\partial \psi(\mathbf{C}_e, \mathbf{Z})}{\partial \mathbf{C}_e} \mathbf{F}_p^{-T} = 2\varrho_{ref} \mathbf{F}_p^T \mathbf{C}_e \frac{\partial \psi(\mathbf{C}_e, \mathbf{Z})}{\partial \mathbf{C}_e} \mathbf{F}_p^{-T} \tag{3.17}$$

as well as the reduced local dissipation inequality

$$\mathcal{D}_{\mathrm{p}} := \boldsymbol{\Xi} : \mathbf{L}_{\mathrm{p}} + \boldsymbol{Y} : \dot{\mathbf{Z}} \geq 0, \tag{3.18}$$

where (3.16) has been considered. $\mathcal{D}_{\mathrm{p}}$ is the plastic dissipation function. From (3.18) follows an essential result that the stress tensor $\boldsymbol{\Xi}$ and the plastic rate $\mathbf{L}_{\mathrm{p}}$ are conjugate variables. Observe that the tensor $\mathbf{L}_{\mathrm{p}}$ is defined in (3.8).

3.2.2. The elastic constitutive model. We assume that the elastic potential can be decomposed additively into one part depending only on the elastic right Cauchy–Green deformation tensor $\mathbf{C}_e$ and the other one depending only on the internal variable $\mathbf{Z}$

$$\psi = \psi_{\mathrm{e}}(\mathbf{C}_e) + \psi_{\mathrm{Z}}(\mathbf{Z}). \tag{3.19}$$

Defining the logarithmic strain measure

$$\boldsymbol{\alpha} := \ln \mathbf{C}_{\mathrm{e}}, \qquad \mathbf{C}_{\mathrm{e}} = \exp \boldsymbol{\alpha} \tag{3.20}$$

and assuming that the material is elastically isotropic, one can prove that the relation holds

$$\mathbf{C}_{\mathrm{e}} \frac{\partial \psi_{\mathrm{e}}(\mathbf{C}_{\mathrm{e}})}{\partial \mathbf{C}_{\mathrm{e}}} = \frac{\partial \psi_{\mathrm{e}}(\boldsymbol{\alpha})}{\partial \boldsymbol{\alpha}}, \tag{3.21}$$

where $\psi_{\mathrm{e}}(\alpha)$ is the potential expressed in the logarithmic strain measure $\boldsymbol{\alpha}$. The proof is given in [37]. Equation (3.17) results then in

$$\boldsymbol{\Xi} = 2\varrho_{\mathrm{ref}} \mathbf{F}_{\mathrm{p}}^{\mathrm{T}} \frac{\partial \psi_{\mathrm{e}}(\boldsymbol{\alpha})}{\partial \boldsymbol{\alpha}} \mathbf{F}_{\mathrm{p}}^{-\mathrm{T}}. \tag{3.22}$$

Note that ψ_{e} is an isotropic function of $\boldsymbol{\alpha}$. The last equation motivates the introduction of a modified logarithmic strain measure

$$\overline{\boldsymbol{\alpha}} := \mathbf{F}_{\mathrm{p}}^{-1} \boldsymbol{\alpha} \mathbf{F}_{\mathrm{p}}. \tag{3.23}$$

Since the following relation for the exponential map holds

$$\mathbf{F}_{\mathrm{p}}^{-1}(\exp \boldsymbol{\alpha}) \mathbf{F}_{\mathrm{p}} = \exp \overline{\boldsymbol{\alpha}}, \tag{3.24}$$

Eq. (3.22) takes the form

$$\boldsymbol{\Xi} = 2\varrho_{\mathrm{ref}} \frac{\partial \psi(\overline{\boldsymbol{\alpha}})}{\partial \overline{\boldsymbol{\alpha}}}. \tag{3.25}$$

REMARK 4. A comparison of (3.17) and (3.25) reveals the computational advantages of the latter formulation. For evaluation of (3.17) the inverse of the

tensor $\mathbf{F}_p^T$ has to be computed. The final expression for (3.25) contains only the derivative of the elastic potential with respect to the modified logarithmic strain tensor $\overline{\boldsymbol{\alpha}}$. □

It is interesting to note that (3.24) together with (3.20), (3.2), and $(3.5)_2$ lead to a direct definition of $\overline{\boldsymbol{\alpha}}$. The relation holds

$$\overline{\boldsymbol{\alpha}} = \ln(\mathbf{C}_p^{-1}\mathbf{C}). \tag{3.26}$$

For computational simplicity a linear relation is assumed and, therefore, the elastic constitutive model (3.25) takes its final form

$$\boldsymbol{\Xi} = K \operatorname{tr}\overline{\boldsymbol{\alpha}}^T \mathbf{1} + \mu \operatorname{dev}\overline{\boldsymbol{\alpha}}^T, \tag{3.27}$$

where

$$\overline{\boldsymbol{\alpha}}^T = \ln(\mathbf{C}\,\mathbf{C}_p^{-1}), \tag{3.28}$$

K is the bulk modulus and μ the shear modulus.

3.2.3. Extended model of Bodner and Partom. We make now use of the form of the inelastic constitutive model of BODNER and PARTOM [17]. In Sec. 3.2.1 we concluded from (3.18) that the tensors $\boldsymbol{\Xi}$ and $\mathbf{L}_p$ are conjugate. A basic issue is now to put the mentioned constitutive model into a frame which is compatible with this fact. Essentially we have to consider the stress tensor $\boldsymbol{\Xi}$ as the driving stress quantity while the plastic rate for which an evolution equation is to be formulated is taken to be $\mathbf{L}_p$. We, therefore, derive the finite formulation of Eqs. (3.19), (3.20) by the substitutions

$$\begin{aligned} \boldsymbol{\sigma} &\to \boldsymbol{\Xi}, \\ \dot{\boldsymbol{\varepsilon}}^p &\to \mathbf{L}_p^T. \end{aligned} \tag{3.29}$$

This leads to the following set of evolution equations

$$\mathbf{L}_p = \dot{\phi}\,\boldsymbol{\nu}^T; \tag{3.30}$$

$$\begin{aligned} \dot{Z} &= \frac{M}{Z_0}(Z_1 - Z)\dot{W}_p, \\ \dot{W}_p &= \Pi\dot{\phi}(\Pi, Z), \\ \Pi &= \sqrt{\frac{3}{2}\operatorname{dev}\boldsymbol{\Xi} : \operatorname{dev}\boldsymbol{\Xi}}, \\ \dot{\phi} &= \frac{2}{\sqrt{3}} D_0 \exp\left[-\frac{1}{2}\frac{N+1}{N}\left(\frac{Z}{\Pi}\right)^{2N}\right], \\ \boldsymbol{\nu} &= \frac{3}{2}\frac{\operatorname{dev}\boldsymbol{\Xi}}{\Pi}. \end{aligned} \tag{3.31}$$

Here, Z_0, Z_1, D_0, N, M are material parameters.

The choice of the transposed quantity in (3.20) is motivated by the updating formula for the stress tensor which is given in Sec. 4, Eq. (4.31). Moreover, the generalization of a flow rule of the more classical von Mises type to nonsymmetric arguments would lead to a flow rule of the form (3.30). Thus, the flow rule chosen fits the classical models of associated viscoplasticity.

Note that by its very definition in (3.11), the tensor Ξ is physically equivalent to the Kirchhoff stress tensor in the sense that both have the same invariants.

4. The nonlinear shell theory

After presenting basic features of the theory of finitely deformed shells, let us now give some details of a new shell model containing 7 parameters. Then the reduction of the three-dimensional principle of virtual work to a shell formulation will be presented.

4.1. Preliminaries of finite shell theory

We adopt the definition (2.1). However, we distinguish carefully between the reference configuration $\mathcal{B}_0$ and the current configuration $\mathcal{B}_t$. For any $X \in \mathcal{B}$ and any $x \in \mathcal{B}_t$ we recall the relations for the tangent base vectors at the reference and actual configurations

$$G_i = X_{,i}\,, \qquad g_i = x_{,i}. \tag{4.1}$$

The corresponding metrics at the actual and the reference configurations are denoted by $\mathbf{g}$ and $\mathbf{G}$, respectively. Their components are given by $G_{ij} = G_i \cdot G_j$ and $g_{ij} = g_i \cdot g_j$, respectively.

As in Sec. 2, we introduce in the reference configuration the shell midsurface as reference surface $\mathcal{M}$ where we again presuppose constant shell thicknes h. Following the standards, the coordinate ϑ^3 perpendicular to $\mathcal{M}$, will now be denoted by $z \in [-h/2, h/2]$, $h \in \mathbb{R}^+$, and the tangent vectors of $T\mathcal{M}$ in the undeformed reference configuration by A_α ($\alpha = 1, 2$) and N, with $N \cdot A_\alpha = 0$. We denote their image at an actual configuration by a_α and a_3, where in general $a_3 \cdot a_\alpha \neq 0$ and $|a_3| \neq 1$. Thus we have $A_\alpha = G_\alpha|_{z=0}$ and $a_\alpha = g_\alpha|_{z=0}$. Further, $\mathbf{A}$ refers to the metric of the reference midsurface with covariant components $A_{\alpha\beta} = A_\alpha \cdot A_\beta$, $a_{\alpha\beta}$ are then the related components at the actual configuration. Their contravariant counterparts are denoted as usual by $A^{\alpha\beta}$ and $a^{\alpha\beta}$.

In addition to the curvilinear base vectors, we consider the fixed Cartesian frame e_i and define the quantities

$$c_{\alpha i} = A_\alpha \cdot e_i\,, \qquad c_{3i} = N \cdot e_i\,, \tag{4.2}$$

to get the following relations

$$A_\alpha = c_{\alpha i} e_i\,, \qquad N = c_{3i} e_i\,, \qquad \text{and} \qquad e_i = c_{\alpha i} A^\alpha + c_{3i} N, \tag{4.3}$$

which will be of use later on.

By **B** we denote the two-dimensional curvature tensor of the undeformed reference surface with components $B_{\alpha\beta} = -A_\alpha \cdot N_{,\beta}$. We also make use of the shifter tensor **M** (see Eq. (2.4)) and its determinant M (see Eq. (2.5)). The following exact expressions hold

$$
\begin{aligned}
G_\alpha &= A_\alpha + zN_{,\alpha} = (\mathbf{I} - z\mathbf{B})A_\alpha = \mathbf{M}A_\alpha, \\
G^\alpha &= \mathbf{M}^{-1}A^\alpha, \qquad G_3 = N.
\end{aligned} \tag{4.4}
$$

4.2. Shell strain measures

The shell theory is based on the following fundamental assumption. We assume that any configuration of the shell space is determined by the equation

$$
\boldsymbol{x}(\vartheta^\alpha, z) = \boldsymbol{x}^0(\vartheta^\alpha) + (z + z^2\chi(\vartheta^\alpha))\boldsymbol{a}_3(\vartheta^\alpha), \tag{4.5}
$$

where $\boldsymbol{x}^0$ denotes the corresponding configuration of the midsurface. Then the ordered triple $(\boldsymbol{x}^0, \boldsymbol{a}_3, \chi)$ defines the configuration space of the shell.

The following basic features of the above assumption are pointed out:

1. The assumed shell kinematics belongs to a general class given by the relation $\boldsymbol{x}(\vartheta^\alpha, z) = \boldsymbol{x}^0(\vartheta^\alpha) + f(z)\boldsymbol{a}_3(\vartheta^\alpha)$ where $f(z)$ can be an arbitrary function of z. This class of kinematics differs entirely from that used e.g. by NAGHDI [1], where $\boldsymbol{x}$ is expanded into a series of z.

2. The assumed shell kinematics is the simplest possible which allows for a linear distribution of the transverse strains (shear and normal) over the shell thickness. The constant part of transverse strains over the shell thickness is described by $\mathbf{a}_3$ whereas χ determines the linearly varying part. Note that fibres perpendicular to the reference midsurface $\mathcal{M}$ remain *straight* after the deformation.

3. As a consequence, three-dimensional constitutive equations can be applied. Accordingly, the formulation is suitable for small as well as for large strain cases in elasticity or elasto-viscoplasticity.

4. The shell kinematics enables to circumvent the use of a rotation tensor. Shell formulations using a rotation tensor with 5 parameters as in [38, 39, 40] or with 6 parameters as in [41, 42, 43, 44] does not furnish directly information about the tranversal strains in thickness direction. Such an information is obtained using further constitutive assumptions such as incompressibility or plane stress assumption. Accordingly, formulations with a rotation tensor, besides being complicated due to the structure of the rotation group, seem to be less adequate for the object of this paper. In addition, as previous numerical studies show, in the present formulation the limit case of very thin shells can be achieved without loss of accuracy.

By (4.1) and (4.5) the tangent vectors become

$$
\begin{aligned}
\boldsymbol{g}_\alpha &= \frac{\partial \boldsymbol{x}^0}{\partial \vartheta^\alpha} + (z + z^2\chi)\frac{\partial \boldsymbol{a}_3}{\partial \vartheta^\alpha} + z^2\frac{\partial \chi}{\partial \vartheta^\alpha}\boldsymbol{a}_3 \\
&= \boldsymbol{a}_\alpha + (z + z^2\chi)\boldsymbol{a}_{3,\alpha} + z^2\chi_{,\alpha}\boldsymbol{a}_3\,, \qquad (4.6)\\
\boldsymbol{g}_3 &= (1 + 2z\chi)\boldsymbol{a}_3\,.
\end{aligned}
$$

For the deformation gradient defined in $(3.1)_2$ we obtain

$$
\begin{aligned}
\mathbf{F} &= \boldsymbol{g}_\alpha \otimes \boldsymbol{G}^\alpha + \boldsymbol{g}_3 \otimes \boldsymbol{N} \qquad (4.7)\\
&= \boldsymbol{a}_\alpha \otimes \boldsymbol{G}^\alpha + \left[(z + z^2\chi)\boldsymbol{a}_{3,\alpha} + z^2\chi_{,\alpha}\boldsymbol{a}_3\right] \otimes \boldsymbol{G}^\alpha + (1 + 2z\chi)\boldsymbol{a}_3 \otimes \boldsymbol{N}\,.
\end{aligned}
$$

By defining the tangent map of the midsurface $\mathbf{F}^0 := \mathbf{F}|_{z=0}$

$$
\mathbf{F}^0 := \boldsymbol{a}_\alpha \otimes \boldsymbol{A}^\alpha + \boldsymbol{a}_3 \otimes \boldsymbol{N}\,, \qquad (4.8)
$$

with $\boldsymbol{a}_\alpha = \mathbf{F}^0\boldsymbol{A}_\alpha$, $\boldsymbol{a}_3 = \mathbf{F}^0\boldsymbol{N}$ and by defining further the tensors

$$
\begin{aligned}
\mathbf{b} &= \boldsymbol{a}_{3,\alpha} \otimes \boldsymbol{A}^\alpha + 2\chi\boldsymbol{a}_3 \otimes \boldsymbol{N}, \qquad (4.9)\\
\mathbf{c} &= (\chi\boldsymbol{a}_{3,\alpha} + \chi_{,\alpha}\boldsymbol{a}_3) \otimes \boldsymbol{A}^\alpha,
\end{aligned}
$$

we arrive at the following expression for $\mathbf{F}$:

$$
\mathbf{F} = (\mathbf{F}^0 + z\mathbf{b} + z^2\mathbf{c})\mathbf{M}^{-1}. \qquad (4.10)
$$

Next, we introduce the displacement field $\boldsymbol{u}^0$ for the SMS and the difference vector $\boldsymbol{w}$ as

$$
\begin{aligned}
\boldsymbol{u}^0 &:= \boldsymbol{x}^0 - \boldsymbol{X}^0, \qquad (4.11)\\
\boldsymbol{w} &:= \boldsymbol{a}_3 - \boldsymbol{N}\,,
\end{aligned}
$$

with $\boldsymbol{X}^0$ being a point on the reference surface $\mathcal{M}$. With (4.11), it follows from (4.8) and (4.9) that

$$
\begin{aligned}
\mathbf{F}^0 &= (\boldsymbol{A}_\alpha + \boldsymbol{u}^0_{,\alpha}) \otimes \boldsymbol{A}^\alpha + (\boldsymbol{N} + \boldsymbol{w}) \otimes \boldsymbol{N}\,, \qquad (4.12)\\
\mathbf{b} &= -\mathbf{B} + \boldsymbol{w}_{,\alpha} \otimes \boldsymbol{A}^\alpha + 2\chi(\boldsymbol{N} + \boldsymbol{w}) \otimes \boldsymbol{N}\,,\\
\mathbf{c} &= -\chi\mathbf{B} + [\chi\boldsymbol{w}_{,\alpha} + \chi_{,\alpha}(\boldsymbol{N} + \boldsymbol{w})] \otimes \boldsymbol{A}^\alpha.
\end{aligned}
$$

Making use of (4.10), the right Cauchy–Green strain tensor of the shell space given in (3.2) takes the form

$$
\begin{aligned}
\mathbf{C} = \mathbf{M}^{-\mathrm{T}}\big[&\mathbf{F}^{0\mathrm{T}}\mathbf{F}^0 + z(\mathbf{F}^{0\mathrm{T}}\mathbf{b} + \mathbf{b}^{\mathrm{T}}\mathbf{F}^0) + z^2(\mathbf{b}^{\mathrm{T}}\mathbf{b} + \mathbf{F}^{0\mathrm{T}}\mathbf{c} + \mathbf{c}^{\mathrm{T}}\mathbf{F}^0) \qquad (4.13)\\
&+ z^3(\mathbf{b}^{\mathrm{T}}\mathbf{c} + \mathbf{c}^{\mathrm{T}}\mathbf{b}) + z^4\mathbf{c}^{\mathrm{T}}\mathbf{c}\big]\,\mathbf{M}^{-1}.
\end{aligned}
$$

The last expression motivates the definitions

$$\begin{aligned} \mathbf{C}^0 &:= \mathbf{F}^{0\mathrm{T}}\mathbf{F}^0, \\ \mathbf{K} &:= \mathbf{F}^{0\mathrm{T}}\mathbf{b} + \mathbf{b}^{\mathrm{T}}\mathbf{F}^0 \end{aligned} \tag{4.14}$$

with the help of which we write for (4.13)

$$\mathbf{C} = \mathbf{M}^{-\mathrm{T}}\left[\mathbf{C}^0 + z\mathbf{K} + \ldots\right]\mathbf{M}^{-1}. \tag{4.15}$$

In what follows we assume that the shell is thin in the sense that only the first two strain measures $\mathbf{C}^0$ and $\mathbf{K}$ are dominant. The inclusion of all other strain measures is of course possible but is left out for the sake of simplicity.

We consider now the following decompositions

$$\boldsymbol{u}^0 = u_i \boldsymbol{e}_i\,, \qquad \boldsymbol{w} = w_i \boldsymbol{e}_i\,. \tag{4.16}$$

Then the tensors $\mathbf{C}^0$ $(4.14)_1$ and $\mathbf{K}$ $(4.14)_2$ take the form

$$\begin{aligned} \mathbf{C}^0 &= \mathrm{C}_{\alpha\beta}\boldsymbol{A}^\beta \otimes \boldsymbol{A}^\alpha + \mathrm{C}_{3\alpha}\boldsymbol{A}^\alpha \otimes \boldsymbol{N} + \mathrm{C}_{\alpha 3}\boldsymbol{N} \otimes \boldsymbol{A}^\alpha + \mathrm{C}_{33}\boldsymbol{N} \otimes \boldsymbol{N}, \\ \mathbf{K} &:= \mathrm{K}_{\alpha\beta}\boldsymbol{A}^\beta \otimes \boldsymbol{A}^\alpha + \mathrm{K}_{3\alpha}\boldsymbol{A}^\alpha \otimes \boldsymbol{N} + \mathrm{K}_{\alpha 3}\boldsymbol{N} \otimes \boldsymbol{A}^\alpha + \mathrm{K}_{33}\boldsymbol{N} \otimes \boldsymbol{N}. \end{aligned} \tag{4.17}$$

Considering (4.16), the following representations of the components in (4.17) based on the Cartesian components (4.16) can be obtained [45]:

$$\begin{aligned} \mathrm{C}_{\alpha\beta} &= \mathrm{A}_{\alpha\beta} + \mathrm{c}_{\beta i}u_{i,\alpha} + \mathrm{c}_{\alpha i}u_{i,\beta} + u_{i,\alpha}u_{i,\beta}\,, \\ \mathrm{C}_{\alpha 3} &= \mathrm{c}_{3i}u_{i,\alpha} + \mathrm{c}_{\alpha i}w_i + u_{i,\alpha}w_i\,, \\ \mathrm{C}_{3\alpha} &= \mathrm{C}_{\alpha 3}\,, \\ \mathrm{C}_{33} &= 1 + 2\mathrm{c}_{3i}w_i + w_i w_i\,, \\ \mathrm{K}_{\alpha\beta} &= \mathrm{B}_{\alpha\beta} + \mathrm{c}_{3i,\alpha}u_{i,\beta} + \mathrm{c}_{3i,\beta}u_{i,\alpha} + \mathrm{c}_{\alpha i}w_{i,\beta} \\ &\qquad + \mathrm{c}_{\beta i}w_{i,\alpha} + u_{i,\alpha}w_{i,\beta} + u_{i,\beta}w_{i,\alpha}\,, \\ \mathrm{K}_{\alpha 3} &= (\mathrm{c}_{3i,\alpha}w_i + \mathrm{c}_{3i}w_{i,\alpha} + w_i w_{i,\alpha}) + 2\chi(\mathrm{c}_{\alpha i}w_i + \mathrm{c}_{3i}u_{i,\alpha} + w_i u_{i,\alpha}), \\ \mathrm{K}_{3\alpha} &= \mathrm{K}_{\alpha 3}\,, \\ \mathrm{K}_{33} &= 4\chi(1 + 2\mathrm{c}_{3i}w_i + w_i w_i). \end{aligned} \tag{4.18}$$

Equations (4.18) are in fact quite compact expressions, well suited for a numerical implementation.

4.3. The principle of virtual work

Let $\mathbf{S}$ be the second Piola–Kirchhoff stress tensor of the shell space.

The principle of virtual displacement in three-dimensions reads

$$\int_{\mathcal{B}} \frac{1}{2}\mathbf{S} : \delta\mathbf{C}\, dV - \int_{\mathcal{B}} \boldsymbol{f}\cdot\delta\boldsymbol{x}\, dV - \int_{\partial\mathcal{B}_t} \boldsymbol{t}\cdot\delta\boldsymbol{x}\, dS = 0, \tag{4.19}$$

where $\boldsymbol{f}$, $\boldsymbol{t}$ are the body and the surface forces, respectively, $dV = M\, d\sigma\, dz$ (see Naghdi [1]) and $d\sigma$ is a surface element of the shell midsurface given by $d\sigma = \sqrt{A}\, d\vartheta^1\, d\vartheta^2$, $A = \det(A_{\alpha\beta})$. Tractions are prescribed on the part $\partial\mathcal{B}_t$ of the boundary $\partial\mathcal{B}$ ($\partial\mathcal{B}_t \subset \partial\mathcal{B}$). We further assume that the shell midsurface $\mathcal{M}$ has a smooth curve $\partial\mathcal{M}$ as boundary with the length parameter s. The boundary of the shell consists of three parts: an upper, a lower, and a lateral surface. If we denote the upper surface by $\partial\mathcal{B}^+$, the lower one by $\partial\mathcal{B}^-$ and the lateral one by $\partial\mathcal{B}^s$ and make use of the notation $M^+ = M|_{z=h/2}$, $M^- = M|_{z=-h/2}$, and M^s for M at the lateral surface, we may write for the surface elements $dS^+ = M^+ d\sigma$, $dS^- = M^- d\sigma$ and $dS^s = M^s\, dz\, ds$.

We first consider the external virtual work.

$$\delta\mathcal{W}_{\text{ext}} := \int_{\mathcal{B}} \boldsymbol{f}\cdot\delta\boldsymbol{x}\, dV + \int_{\partial\mathcal{B}} \boldsymbol{t}\cdot\delta\boldsymbol{x}\, dS. \tag{4.20}$$

With the definitions

$$\begin{aligned}
\boldsymbol{p} &:= \int_{-h/2}^{h/2} \boldsymbol{f} M\, dz + M^+\mathbf{t}^+ + M^-\mathbf{t}^-,\\
\boldsymbol{l} &:= \int_{-h/2}^{h/2} z\boldsymbol{f} M\, dz + \frac{h}{2}M^+\boldsymbol{t}^+ - \frac{h}{2}M^-\boldsymbol{t}^-,\\
\boldsymbol{q} &:= \int_{-h/2}^{h/2} z^2\boldsymbol{f} M\, dz + \frac{h^2}{4}M^+\boldsymbol{t}^+ + \frac{h^2}{4}M^-\boldsymbol{t}^-,\\
\boldsymbol{p}^s &:= \int_{-h/2}^{h/2} \boldsymbol{t}^s M^s\, dz\,,\\
\boldsymbol{l}^s &:= \int_{-h/2}^{h/2} z\boldsymbol{t}^s M^s\, dz\,,\\
\boldsymbol{q}^s &:= \int_{-h/2}^{h/2} z^2\boldsymbol{t}^s M^s\, dz\,,
\end{aligned} \tag{4.21}$$

Equation (4.20) reduces to

$$\delta \mathcal{W}_{\text{ext}} = \int_{\mathcal{M}} \left[\boldsymbol{p} \cdot \delta \boldsymbol{x}^0 + (\boldsymbol{l} + \chi \boldsymbol{q}) \cdot \delta \boldsymbol{a}_3 + (\boldsymbol{q} \cdot \boldsymbol{a}_3) \delta \chi \right] d\sigma + \int_{\partial \mathcal{M}_t} \left[\boldsymbol{p}^s \cdot \delta \boldsymbol{x}^0 + (\boldsymbol{l}^s + \chi \boldsymbol{q}^s) \cdot \delta \boldsymbol{a}_3 + (\boldsymbol{q}^s \cdot \boldsymbol{a}_3) \delta \chi \right] ds \tag{4.22}$$

as the two-dimensional form of the external power. In (4.22) it is presupposed that on the entire upper and lower surfaces tractions are prescribed. However, we assume that only on a part $\partial \mathcal{M}_t$ of the boundary $\partial \mathcal{M}$ of the SMS tractions are prescribed.

To consider the internal virtual power we notice first that it is more appropriate to make use of the relation

$$\mathbf{S} = \mathbf{C}^{-1} \boldsymbol{\Xi} \tag{4.23}$$

since the inelastic constitutive model, as shown in Sec. 3.2.1, is formulated in terms of $\boldsymbol{\Xi}$. We define first the pull-back of $\mathbf{S}$ under $\mathbf{M}$ which gives a stress tensor defined with respect to the midsurface

$$\mathbf{S}^0 = \mathbf{M}^{-1} \mathbf{C}^{-1} \boldsymbol{\Xi} \mathbf{M}^{-\mathrm{T}}. \tag{4.24}$$

REMARK 5. Note that $\mathbf{S}^0$ still depends on the normal coordinate z. □

Equations (3.25), (4.23) and (4.24) motivate the following definitions

$$\begin{aligned} \mathbf{n} &:= \int_{-h/2}^{+h/2} \frac{1}{2} \mathbf{S}^0 N \, dz = \int_{-h/2}^{+h/2} \mathbf{M}^{-1} \mathbf{C}^{-1} \frac{\partial \psi}{\partial \overline{\boldsymbol{\alpha}}} \mathbf{M}^{-\mathrm{T}} M \, dz, \\ \mathbf{m} &:= \int_{-h/2}^{+h/2} z \mathbf{M}^{-1} \mathbf{C}^{-1} \frac{\partial \psi}{\partial \overline{\boldsymbol{\alpha}}} \mathbf{M}^{-\mathrm{T}} M \, dz \end{aligned} \tag{4.25}$$

with the help of which as well as with (4.22), the principle of virtual work given in (4.19) takes the form

$$\int_{\mathcal{M}} \left[\mathbf{n} : \delta \mathbf{C}^0 + \mathbf{m} : \delta \mathbf{K} \right] d\sigma - \int_{\mathcal{M}} \left[\boldsymbol{p} \cdot \delta \boldsymbol{x}^0 + (\boldsymbol{l} + \chi \boldsymbol{q}) \cdot \delta \boldsymbol{a}_3 + (\boldsymbol{q} \cdot \boldsymbol{a}_3) \delta \chi \right] d\sigma - \int_{\partial \mathcal{M}} \left[\boldsymbol{p}^s \cdot \delta \boldsymbol{x}^0 + (\boldsymbol{l}^s + \chi \boldsymbol{q}^s) \cdot \delta \boldsymbol{a}_3 + (\boldsymbol{q}^s \cdot \boldsymbol{a}_3) \delta \chi \right] ds = 0. \tag{4.26}$$

For given external forces, the integrals (4.21) can be expressed in almost closed form. For very thin shells the terms $\chi \boldsymbol{q} \cdot \delta \boldsymbol{a}_3$, $\boldsymbol{q} \cdot \boldsymbol{a}_3 \delta \chi$ in (4.26) can be neglected as being of higher order. However, in order to allow for the use of complex constitutive laws and path-dependent behaviour (e.g. cyclic loading), the evaluation of (4.25) is carried out in practical computations numerically. That is, the constitutive equations are considered pointwise over the shell thickness.

4.4. Numerical implementation

In this section computational issues in conjunction with a possible finite element formulation are discussed. The time integration procedure of the constitutive model at hand is outlined and necessary operations of local iterations are discussed. A closed form of the algorithmic tangent operator is presented.

4.4.1. Time integration and local iterations. We consider two consecutive times t_n and t_{n+1} with time increment $\Delta t = t_{n+1} - t_n$. Since the unimodular tensor $\mathbf{F}_p$ is an element of the Lie group $SL^+(3,\mathbb{R})$ and the tensor $\mathbf{L}_p$ is an element of the corresponding Lie algebra, the exponential map can be used for time integration. Therefore, the following update formula is considered

$$\mathbf{F}_p|_{n+1} = \mathbf{F}_p|_n \exp[\Delta t \mathbf{L}_p] \tag{4.27}$$

for some $\mathbf{L}_p$ in the interval Δt, the choice of which is defined by means of the integration procedure. This algorithm preserves the condition of plastic incompressibility exactly. From (4.27) follows directly the update formula for the elastic strain measure (3.26)

$$\mathbf{C}\,\mathbf{C}_p^{-1}|_{n+1} = \mathbf{C}|_{n+1} \exp(-\Delta t \mathbf{L}_p)\mathbf{C}_p{}^{-1}|_n \exp(-\Delta t \mathbf{L}_p^T). \tag{4.28}$$

Due to (3.30) we update the tensor $\mathbf{L}_p$ as

$$\mathbf{L}_p = \dot{\phi}\,\boldsymbol{\nu}^T. \tag{4.29}$$

Since isotropy was assumed in Sec. 3.2.2, the tensors $\boldsymbol{\Xi}$ and $\overline{\boldsymbol{\alpha}}^T$ or $\boldsymbol{\Xi}$ and $\mathbf{C}\,\mathbf{C}_p{}^{-1}$ are coaxial. Thus the single terms in (4.28) can be rearranged and the logarithms can be taken to give [45]

$$\begin{aligned} \ln(\mathbf{C}\,\mathbf{C}_p{}^{-1})_{n+1} &= \ln\left[\mathbf{C}_{n+1}\mathbf{C}_p{}^{-1}|_n \exp(-2\Delta t \mathbf{L}_p^T)\right], \\ \overline{\boldsymbol{\alpha}}_{n+1}^T &= (\overline{\boldsymbol{\alpha}}^{\,\mathrm{trial}})^T - 2\Delta t \mathbf{L}_p^T, \\ (\overline{\boldsymbol{\alpha}}^{\,\mathrm{trial}})^T &= \ln \mathbf{C}_{n+1}\mathbf{C}_p{}^{-1}|_n . \end{aligned} \tag{4.30}$$

Next, we give the update of the stress tensor as, where (3.27) is considered for the definition of the trial stress

$$\begin{aligned} \boldsymbol{\Xi}_{n+1} &= \boldsymbol{\Xi}^{\mathrm{trial}} - \mu 2\Delta t \mathbf{L}_p^T, \\ &= \boldsymbol{\Xi}^{\mathrm{trial}} - 2\Delta t \dot{\phi} \mu \boldsymbol{\nu}_{n+1}, \end{aligned} \tag{4.31}$$

$$\boldsymbol{\Xi}^{\mathrm{trial}} := K \mathrm{tr}(\overline{\boldsymbol{\alpha}}^{\,\mathrm{trial}})^T \mathbf{I} + \mu \left((\overline{\boldsymbol{\alpha}}^{\,\mathrm{trial}})^T - \frac{1}{3}\mathrm{tr}(\overline{\boldsymbol{\alpha}}^{\,\mathrm{trial}})^T \right) \tag{4.32}$$

for some $\dot{\phi}$ in the corresponding interval.

From $(3.31)_2$ and (4.31) follows

$$\Pi_{n+1} = \Pi^{\text{trial}} - 3\Delta t \mu \dot{\phi}. \tag{4.33}$$

We are now looking for the determination of $\dot{\phi}$ in accordance with (2.23) to $(2.19)_3$ as well as with (4.33). We adopt the mid-point rule according to which we have

$$\Pi = \frac{1}{2}(\Pi_{n+1} + \Pi_n) = \frac{1}{2}(\Pi^{\text{trial}} - 3\Delta t \mu \dot{\phi} + \Pi_n); \tag{4.34}$$

$$\begin{aligned} \dot{Z} &= \frac{Z_{n+1} - Z_n}{\Delta t}, \\ Z &= \frac{1}{2}(Z_{n+1} + Z_n). \end{aligned} \tag{4.35}$$

We insert Eqs. (4.35) into (2.23) and $(3.31)_2$ to obtain an explicit equation for the determination of the internal variable Z

$$Z = \frac{m\Delta t \Pi \dot{\phi} Z_1 + 2Z_0 Z_n}{m\Delta t \Pi \dot{\phi} + 2Z_0}, \tag{4.36}$$

which depends explicitly on $\dot{\phi}$. Inserting (4.36) into $(3.31)_3$ yields a nonlinear equation for the determination of $\dot{\phi}$

$$\dot{\phi} = \frac{2}{\sqrt{3}} D_0 \exp\left[-\frac{1}{2}\frac{N+1}{N}\left(\frac{Z(\Pi, \dot{\phi})}{\Pi}\right)^{2N}\right], \tag{4.37}$$

where Π is computed by means of (4.33). Equation (4.37) has to be solved iteratively by Newton's method.

4.4.2. The algorithmic tangent operator. The algorithmic tangent operator is obtained as the linearization of the update formula for the second Piola–Kirchhoff tensor $\mathbf{S}$ with respect to the right Cauchy–Green deformation tensor. With (4.31) we obtain

$$\mathbf{S} = \mathbf{C}^{-1}(\boldsymbol{\Xi}^{\text{trial}} - 2\Delta t \dot{\phi} \mu \boldsymbol{\nu}). \tag{4.38}$$

The derivative with respect to $\mathbf{C}$ gives

$$\begin{aligned} \frac{\partial \mathbf{S}}{\partial \mathbf{C}} = {} & \frac{\partial \mathbf{C}^{-1}}{\partial \mathbf{C}}(\boldsymbol{\Xi}^{\text{trial}} - 2\Delta t \dot{\phi} \mu \boldsymbol{\nu}) + \mathbf{C}^{-1} \frac{\partial \boldsymbol{\Xi}^{\text{trial}}}{\partial \mathbf{C}} \\ & - 2\Delta t \mu \frac{\partial \dot{\phi}}{\partial \Pi^{\text{trial}}} \frac{\partial \Pi^{\text{trial}}}{\partial \boldsymbol{\Xi}^{\text{trial}}} \frac{\partial \boldsymbol{\Xi}^{\text{trial}}}{\partial \mathbf{C}} \mathbf{C}^{-1} \boldsymbol{\nu} - 2\Delta t \mu \dot{\phi} \mathbf{C}^{-1} \frac{\partial \boldsymbol{\nu}}{\partial \boldsymbol{\Xi}^{\text{trial}}} \frac{\partial \boldsymbol{\Xi}^{\text{trial}}}{\partial \mathbf{C}}. \end{aligned} \tag{4.39}$$

The tedious algebra given in [45] leads to the very compact and closed form

$$\frac{\partial(\mathbf{S})_{ij}}{\partial(\mathbf{C})_{rs}} = -(\mathbf{C}^{-1})^{ir}(\mathbf{C}^{-1})^{sk}[(\Xi^{\text{trial}})_k{}^j - 2\Delta t\dot{\phi}\mu(\boldsymbol{\nu})_k{}^j] + \beta_1(\mathbf{C}^{-1})^{ij}(\mathbf{C}^{-1})^{rs} + \beta_2(\mathbf{C}^{-1})^{is}(\mathbf{C}^{-1})^{rj} + \beta_3(\mathbf{C}^{-1})^{ik}(\boldsymbol{\nu})_k{}^j(\mathbf{C}^{-1})^{rt}(\boldsymbol{\nu})_t{}^s, \tag{4.40}$$

where we have introduced the following notation

$$\beta_1 = K - \frac{1}{3}\mu + \Delta t\mu^2\frac{\dot{\phi}}{\Pi_{n+1}}, \qquad \beta_2 = \mu - 3\Delta t\mu^2\frac{\dot{\phi}}{\Pi_{n+1}}, \qquad \beta_3 = -2\Delta t\mu^2\left(\frac{\partial\dot{\phi}}{\partial\Pi^{\text{trial}}} - \frac{\dot{\phi}}{\Pi_{n+1}}\right). \tag{4.41}$$

In $(4.41)_3$

$$\frac{\partial\dot{\phi}}{\partial\Pi^{\text{trial}}} = \frac{\dfrac{\partial\dot{\phi}}{\partial\Pi}\dfrac{\partial\Pi}{\partial\Pi^{\text{trial}}} + \dfrac{\partial\dot{\phi}}{\partial Z}\dfrac{\partial Z}{\partial\Pi^{\text{trial}}}}{1 - \dfrac{\partial\dot{\phi}}{\partial\Pi}\dfrac{\partial\Pi}{\partial\dot{\phi}} - \dfrac{\partial\dot{\phi}}{\partial Z}\dfrac{\partial Z}{\partial\dot{\phi}}} \tag{4.42}$$

has to be considered.

4.5. Finite element formulation

We briefly discuss the interpolation of the shell geometry and then present an enhanced strain element.

4.5.1. Interpolation of shell geometry. The geometric quantities describing the shell surface (the fields $B_{\alpha\beta}$, $c_{\alpha i}$, c_{3i}, $\sqrt{A}$) are taken exactly at every integration point. The natural coordinates ϑ^α describing the shell surface are mapped onto the bi-unit square using bilinear interpolations.

On the other hand, the Cartesian components of the kinematical fields $\boldsymbol{u}$, $\boldsymbol{w}$ as well as χ are interpolated using the bilinear interpolation functions.

4.5.2. An enhanced strain functional. We formulate first a strain-based element. We appeal to the enhanced strain concept in the spirit of SIMO and RIFAI [46] applied by them to linear problems. Accordingly, the right Cauchy–Green deformation tensor itself is enhanced. This is in contrast with the nonlinear version of the concept given by SIMO and ARMERO [47] where the deformation gradient was enhanced. Accordingly, we consider the following functional

$$\frac{1}{2}\int_{\mathcal{B}}(\mathbf{C}+\mathbf{C}^i)^{-1}\Xi : \delta(\mathbf{C}+\mathbf{C}^i)\,dV - \int_{\mathcal{B}}\boldsymbol{f}\cdot\delta\boldsymbol{x}\,dV - \int_{\partial\mathcal{B}}\boldsymbol{f}\cdot\delta\boldsymbol{x}\,dS = 0, \tag{4.43}$$

where we have

$$\begin{aligned} \boldsymbol{\Xi} &= 2\varrho_{\text{ref}}\frac{\partial \psi}{\partial \tilde{\boldsymbol{\alpha}}} = K \operatorname{tr}\tilde{\boldsymbol{\alpha}}^{\mathrm{T}}\mathbf{I} + \mu\left(\tilde{\boldsymbol{\alpha}}^{\mathrm{T}} - \frac{1}{3}\operatorname{tr}\tilde{\boldsymbol{\alpha}}^{\mathrm{T}}\mathbf{I}\right), \\ \tilde{\boldsymbol{\alpha}} &= \ln[\mathbf{C}_{\mathrm{p}}^{-1}(\mathbf{C} + \mathbf{C}^{i})] \end{aligned} \tag{4.44}$$

and $\mathbf{C}^{i}$ is the enhanced strain field. Since $\mathbf{C}^{i}$ is assumed to be independent of the displacements, Eq. (4.43) splits into the following two equations

$$\frac{1}{2}\int_{\mathcal{B}} (\mathbf{C} + \mathbf{C}^{i})^{-1}\boldsymbol{\Xi} : \delta\mathbf{C}\, dV - \int_{\mathcal{B}} \boldsymbol{f}\cdot\delta\boldsymbol{u}\, dV - \int_{\partial\mathcal{B}_{\mathrm{t}}} \boldsymbol{t}\cdot\delta\boldsymbol{u}\, dS = 0, \tag{4.45}$$

and

$$\frac{1}{2}\int_{\mathcal{B}} (\mathbf{C} + \mathbf{C}^{i})^{-1}\boldsymbol{\Xi} : \delta\mathbf{C}^{i}\, dV = 0. \tag{4.46}$$

The choice of the interpolation functions for $\mathbf{C}^{i}$ is crucial in order to arrive at well behaving elements. Equation (4.15) motivates to restrict the incompatible deformation tensor $\mathbf{C}^{i}$ to the form $\mathbf{C}^{i} = \mathbf{M}^{-\mathrm{T}}\mathbf{C}^{0^{i}}\mathbf{M}^{-1}$ where $\mathbf{C}^{0^{i}}$ is independent of z. This is equivalent to an enhancement of the strains related to the shell midsurface alone.

Equations (4.45) and (4.46) are still defined for the three-dimensional shell body. The reduction to two dimensions is carried out in the same way as demonstrated in Sec. 4.3 (compare (4.21)). One has

$$\begin{aligned} &\int_{\mathcal{M}} (\mathbf{n} : \delta\mathbf{C}^{0} + m : \delta\mathbf{K})\, d\sigma - \int_{\mathcal{M}} \left[\boldsymbol{p}\cdot\delta\boldsymbol{x}^{0} + (\boldsymbol{l} + \chi\boldsymbol{q})\cdot\delta\mathbf{a}_3(\boldsymbol{q}\cdot\mathbf{a}_3)\delta\chi\right] d\sigma \\ &\qquad - \int_{\partial\mathcal{M}_{\mathrm{t}}} \left[\boldsymbol{p}^{\mathrm{s}}\cdot\delta\boldsymbol{x}^{0} + (\boldsymbol{l}^{\mathrm{s}} + \chi\boldsymbol{q}^{\mathrm{s}})\cdot\delta 3 + (\boldsymbol{q}^{\mathrm{s}}\cdot 3)\delta\chi\right] ds = 0, \\ &\int_{\mathcal{M}} \mathbf{n} : \delta\mathbf{C}^{0^{i}}\, d\sigma = 0. \end{aligned} \tag{4.47}$$

The contributions of the external loads are defined in (4.21) while $\mathbf{n}$, $\mathbf{m}$ are now defined according to

$$\begin{aligned} \mathbf{n} &:= \int_{-h/2}^{+h/2} \mathbf{M}^{-1}\left(\mathbf{C} + \mathbf{C}^{i}\right)^{-1}\frac{\partial \psi}{\partial \tilde{\boldsymbol{\alpha}}}\mathbf{M}^{-\mathrm{T}} M\, dz, \\ \mathbf{m} &:= \int_{-h/2}^{+h/2} z\mathbf{M}^{-1}\left(\mathbf{C} + \mathbf{C}^{i}\right)^{-1}\frac{\partial \psi}{\partial \tilde{\boldsymbol{\alpha}}}\mathbf{M}^{-\mathrm{T}} M\, dz. \end{aligned} \tag{4.48}$$

The interpolation functions for the components of the incompatible deformation $\mathbf{C}^{0^i}$ are taken to be of the form

$$
\begin{aligned}
C^{0^i}_{11}(\xi,\eta) &= C_1\xi + C_2\xi\eta\,,\\
C^{0^i}_{22}(\xi,\eta) &= C_3\eta + C_4\xi\eta\,,\\
C^{0^i}_{33}(\xi,\eta) &= C_5\xi + C_6\eta + C_7\xi\eta\,,\\
C^{0^i}_{12}(\xi,\eta) &= C_8\xi + C_9\eta + C_{10}\xi\eta\,,\\
C^{0^i}_{13}(\xi,\eta) &= C_{11}\xi + C_{12}\xi\eta\,,\\
C^{0^i}_{23}(\xi,\eta) &= C_{13}\eta + C_{14}\xi\eta\,.
\end{aligned}
\tag{4.49}
$$

The quantities ξ and η are the local coordinates at the element level. Clearly, the fields $C^{0^i}_{11}\ldots C^{0^i}_{23}$ are the components of the incompatible deformation tensor $\mathbf{C}^{0^i}$ with respect to the natural curvilinear base system G_i.

The introduction of interpolation functions of the displacement fields as well as of the enhanced strain fields in (4.47) leads to two coupled nonlinear sets of algebraic equations. The enhanced strain field is assumed to be discontinuous over elements and is eliminated at the element level.

Again (4.48) have to be linearized (compare Sec. 4.4.2). The tangent operator for the shell space given by (4.40) is a fourth order tensor which we denote by $\mathbf{H}$. The systematic linearization of (4.48) leads to the following expressions

$$
\begin{aligned}
\int_{\mathcal{M}} [\Delta\mathbf{n} : \delta\mathbf{C}^0 + \Delta\mathbf{m} : \delta\mathbf{K}]\, d\sigma = \int_{\mathcal{M}} \Big(&\mathbf{H}^0(\Delta\mathbf{C}^0 + \Delta\mathbf{C}^{0^i}) + \mathbf{H}^1\Delta\mathbf{K} : \delta\mathbf{C}^0\\
&+ [\mathbf{H}^1\Delta(\mathbf{C}^0 + \mathbf{C}^{0^i}) + \mathbf{H}^2\Delta\mathbf{K}] : \delta\mathbf{K}\Big)\, d\sigma\,,\\
\int_{\mathcal{M}} \Delta\mathbf{n} : \delta\mathbf{C}^{0^i}\, d\sigma = \int_{\mathcal{M}} \Big([\mathbf{H}^0(\Delta\mathbf{C}^0 + \Delta\mathbf{C}^{0^i}) + \mathbf{H}^1\Delta\mathbf{K}] &: \delta\mathbf{C}^{0^i}\Big)\, d\sigma\,.
\end{aligned}
\tag{4.50}
$$

The following definitions hold

$$
\begin{aligned}
(\mathbf{H}^0)^{ijkl} &:= \int_{-h/2}^{+h/2} (\mathbf{M}^{-1})^i_a (\mathbf{M}^{-\mathrm{T}})^j_b (\mathbf{H})^{abrs} (\mathbf{M}^{-1})^k_r (\mathbf{M}^{-\mathrm{T}})^l_s\, M\, dz,\\
(\mathbf{H}^1)^{ijkl} &:= \int_{-h/2}^{+h/2} z(\mathbf{M}^{-1})^i_a (\mathbf{M}^{-\mathrm{T}})^j_b (\mathbf{H})^{abrs} (\mathbf{M}^{-1})^k_r (\mathbf{M}^{-\mathrm{T}})^l_s\, M\, dz,\\
(\mathbf{H}^2)^{ijkl} &:= \int_{-h/2}^{+h/2} z^2(\mathbf{M}^{-1})^i_a (\mathbf{M}^{-\mathrm{T}})^j_b (\mathbf{H})^{abrs} (\mathbf{M}^{-1})^k_r (\mathbf{M}^{-\mathrm{T}})^l_s\, M\, dz.
\end{aligned}
\tag{4.51}
$$

The integrals in (4.51) must be evaluated numerically. Further details of the implementation are standard and hence they have been omitted.

4.6. Numerical results

4.6.1. Comparison with experiments. In the first example the verification of the model presented in the previous sections is compared with experiments.

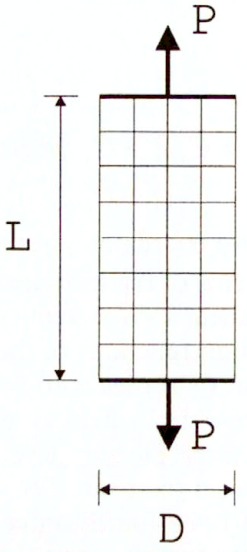

$L = 52$
$D = 8$

FIG. 5. Specimen under tension. Definition of the problem.

In [17] a specimen of pure titanium of 1 mm thickness, 8 mm width and 52 mm length (Fig. 5) was subject to different straining histories. BODNER and PARTOM used in [17] a model based on an additive decomposition of the deformation rate. The process of adjusting the calculated stress-strain curves to the experimental ones led in [17] to the following material parameters:

$$
\begin{aligned}
K &= 1.845 \times 10^5 \ \mathrm{N/mm^2}, \\
\mu &= 4.4 \times 10^4 \ \mathrm{N/mm^2}, \\
Z_0 &= 1150 \ \mathrm{N/mm^2}, \\
Z_1 &= 1400 \ \mathrm{N/mm^2}, \\
D_0 &= 10000 \ 1/\mathrm{sec}, \\
N &= 1, \\
M &= 100.
\end{aligned}
\tag{4.52}
$$

Two loading velocities corresponding to a crosshead velocity of 5 mm/min and 10 mm/min have been calculated with the model presented in this paper. It is interesting to note that a material parameter Z_1 different than that calculated by Bodner and Partom was needed to fit the experimental results.

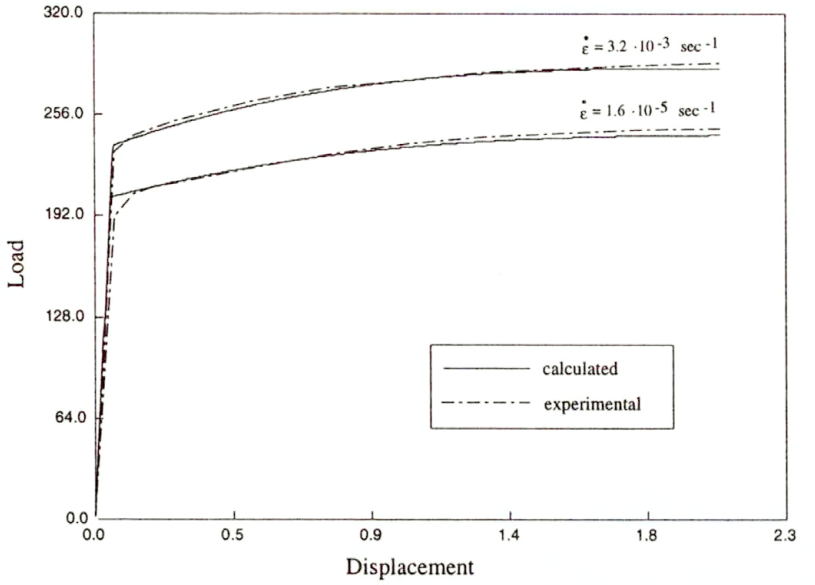

FIG. 6. Specimen under tension. Load-displacement curves.

In Fig. 6 the experimental results are compared with the calculated ones using a time step of 0.5 sec for a material parameter $Z_1 = 1540\,\mathrm{N/mm^2}$, where very good agreement can be observed.

4.6.2. Square plate under uniform loading. In all following examples the material data as formulated in (4.52) are used. A square plate is uniformly loaded as shown in Fig. 7.

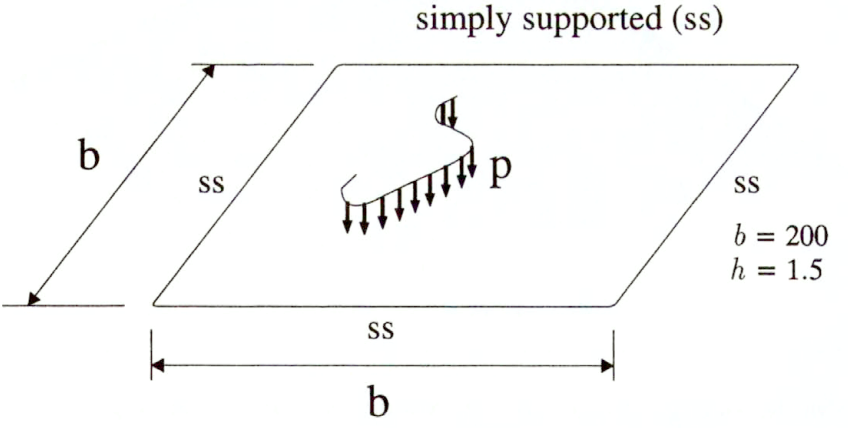

FIG. 7. Plate under dead load. Definition of the problem.

Due to symmetry conditions, only one quarter of the plate is discretized using 32×32 elements. The load is increased so as to result in a deformation velocity at

the midpoint of 1 cm/sec. Using a time step of 0.5 sec, altogether 30 time steps are calculated when the maximal loading capacity of the plate is arrived. The response of the plate is presented in Fig. 8 where the load versus the midpoint-diplacement is plotted. The maximal deformed configuration is given in Fig. 9.

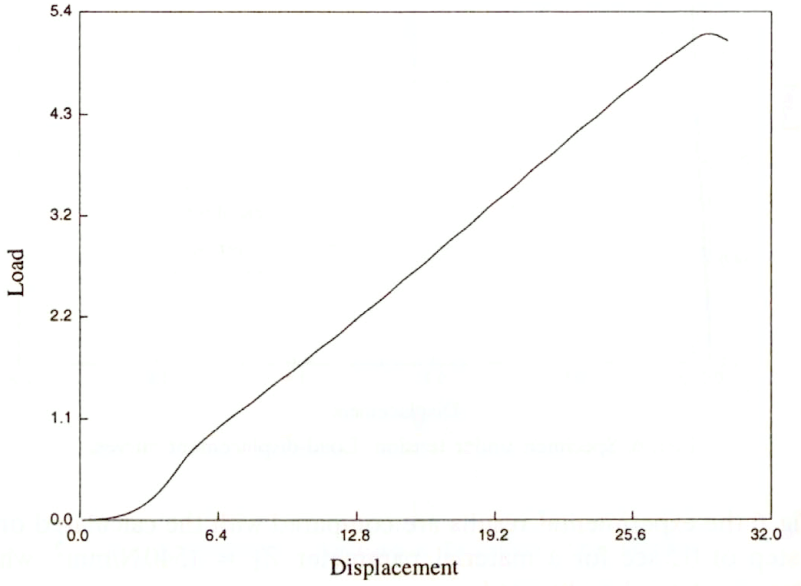

FIG. 8. Plate under dead load. Load-midpoint displacement curve.

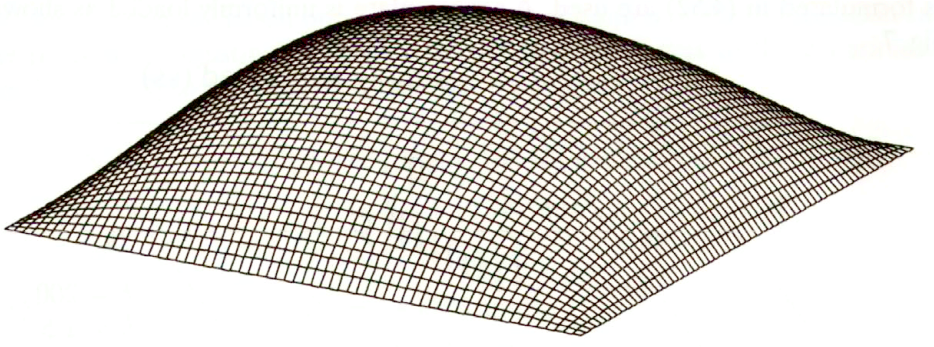

FIG. 9. Plate under dead load. Deformed configuration.

4.6.3. Cylinder with rigid diaphragms. A cylinder with rigid diaphragms is subject to a line load as described in Fig. 10. The length of the load segment is 88.35 cm. Only one eighth of the cylinder in modeled using 32×32 elements.

A loading cycle was calculated using a time step of 0.5 sec where altogether 150 time steps are considered. The loading history is chosen so as to result

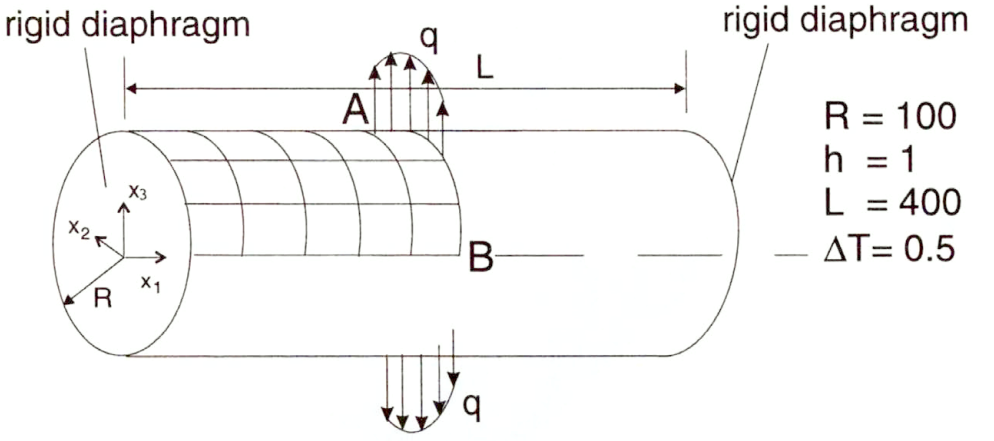

FIG. 10. Pinched cylinder with rigid diaphragm. Definition of the problem.

in a linear increase of the displacement at the top of 0.25 mm/sec. In Fig. 11 load-displacement curves are plotted for the point at the top as well as that at the side. A configuration of the cylinder at the maximal deformation is given in Fig. 12.

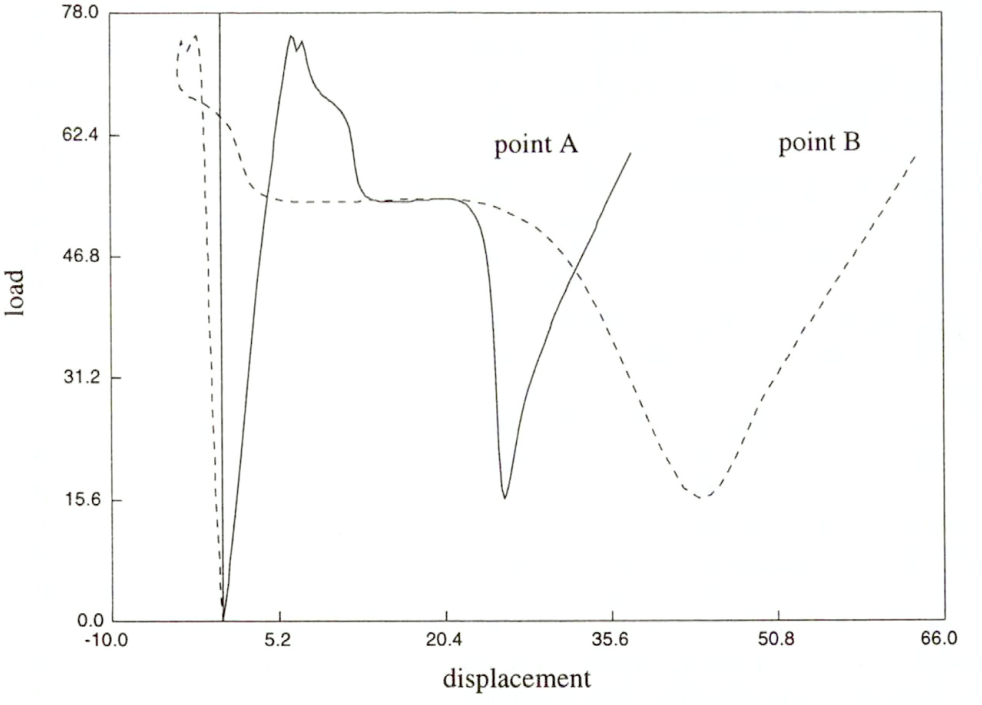

FIG. 11. Pinched cylinder with rigid diaphragm. Load-displacement curves.

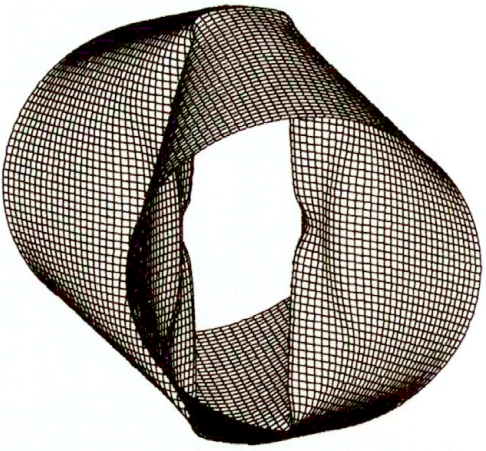

FIG. 12. Pinched cylinder with rigid diaphragm. Deformed configuration.

5. Conclusions

In this paper we give a thorough overview on the theory and numerical analysis of viscoplastic shells. In Sec. 2 we present a general theory for geometrically linear elasto-viscoplastic shells [8]. This theory is based on a two-field variational [9] principle which contains velocities and strain rates as variables to be varied independently. Families of mixed and hybrid strain elements are derived for axisymmetric shells. It is crucial to choose stable approximation schemes for the velocity and the strain rate field, respectively. Numerical experiments [12] for elastic shells demonstrate that the mixed elements are locking free and exhibit the same order of convergence for displacements and stress-like quantities such as e.g. membrane forces and bending moments. Some numerical results are presented for a cylindrical shell under internal pressure, where the viscoplastic constitutive model of BODNER and PARTOM [17] has been used.

In the major part of this paper (compare Sec. 3 and Sec. 4) we present a general theory of viscoplastic shells under finite deformation and its numerical implemetation by means of the FEM. For this purpose we first develop a general theory of finitely deformed elasto-viscoplastic three-dimensional bodies. We assume a hyperelastic model and based on the assumption of persisting isotropy, we derive a very concise representation of the elastic part of the constitutive model by introducing a logarithmic strain measure. Next, a shell theory with seven parameters is formulated, which can account for distributions of the transverse strains over the shell thickness varying linearly with the normal coordinate. Therefore, this shell model enables the use of fully three-dimensional constitutive models without using the typical "shell assumptions". Basing on the principle of virtual work, we formulate our shell equations. Furthermore, we discuss such

computional issues as time integration and the computation of the algorithmic tangent operator. Finally, an enhanced strain finite shell element is derived. Some test examples are presented.

References

1. P.M. NAGHDI, *Theory of plates and shells*, [in:] Handbuch der Physik, S. FLÜGGE and C. TRUESDELL [Eds.], Vol. VIa/2., pp. 473–479, Springer, Berlin, Heidelberg, New York 1972.
2. R. VALID, *The nonlinear theory of shells through variational principles*, John Wiley & Sons, Chichester, New York, Brisbane, Singapore 1995.
3. M. BERNADOU, *Finite element analysis for thin shells*, John Wiley & Sons, Chichester, New York, Brisbane, Singapore 1996.
4. I. CORMEAU, *Elastoplastic thick shell analysis by viscoplastic solid finite elements*, Int. J. Num. Meth. Engng., **12**, 203–227, 1978.
5. T.J.R. HUGHES and W.K. LIU, *Nonlinear finite element analysis of shells. Part 1. Three-dimensional shells*, Comp. Meth. Appl. Mech.Engng., **26**, 333–362, 1981.
6. T.J.R. HUGHES and W.K. LIU, *Nonlinear finite element analysis of shells. Part 2. Two-dimensional shells*, Comp. Meth. Appl. Mech. Engng., **27**, 167–181, 1981.
7. H. PARISCH, *Large displacements of shells including material nonlinearities*, Comp. Meth. Appl. Mech. Engng., **27**, 183–204, 1981.
8. F.G. KOLLMANN and S. MUKHERJEE, *A general, geometrically linear theory of inelastic thin shells*, Acta Mech., **57**, 41–67, 1985.
9. S. MUKHERJEE and F.G. KOLLMANN, *A new rate principle suitable for analysis of inelastic deformation of plates and shells*, J. Appl. Mech., **52**, 533–535, 1985.
10. J.T. ODEN and J.N. REDDY, *On dual complementary variational principles in mathematical physics*, Int. J. Engng. Sci., **12**, 1–29, 1974.
11. F.G. KOLLMANN and V. BERGMANN, *Numerical analysis of viscoplastic axisymmetric shells based on a hybrid strain finite element*, Comp. Mech., 7, 89–105, 1990.
12. F.G. KOLLMANN, D. CORDTS and H.-P. HACKENBERG, *Implementation and numerical tests of a family of mixed finite elements for the computation of axisymmetric viscoplastic shells*, Unpublished report MuM-Report 90/1, Technische Hochschule Darmstadt, Darmstadt, Federal Republic of Germany 1990.
13. M. KLEIBER and F.G. KOLLMANN, *A theory of viscoplastic shells including damage*, Arch. Mech., **45**, 423–437, 1993.
14. A.L. GURSON, *Continuum theory of ductile rupture by void nucleation and growth. Part 1. Yield criteria and flow rules for ductile materials*, Trans. ASME, J. Engng. Mat. Tech., **99**, 2–15, 1977.
15. Q. AN and F.G. KOLLMANN, *A general theory of finite deformation of viscoplastic thin shells*, Acta Mech., **117**, 47–70, 1996.
16. P. PERZYNA, *Fundamental problems in viscoplasticity*, [in:] Advances in Applied Mechanics, G.G. CHERNYI *et al.* [Eds], pp. 243–377, Academic Press, 1966.
17. S.R. BODNER and Y. PARTOM, *Constitutive equations for elastic-viscoplastic strain-hardening materials*, ASME, J. Appl. Mech., **42**, 385–389, 1975.
18. J.L. CHABOCHE, *Constitutive equations for cyclic plasticity and cyclic viscoplasticity*, Int. J. Plasticity, **5**, 247–302, 1989.
19. E. KREMPL, J. MCMAHON and D. YAO, *Viscoplasticity based on overstress with a differential growth law for the equilibrium stress*, Mech. of Mat., 5, 35–48, 1986.
20. E.A. STECK, *A stochastic model for the high-temperature plasticity of metals*, Int. J. Plasticity, 1, 243–258, 1985.
21. M.B. RUBIN, *A elasto-viscoplastic model for large strains*, Int. J. Engng. Sci., **24**, 1083–1095, 1986.

22. P.M. NAGHDI and J.A. TAPP, *Restrictions on constitutive equations of finitely deformed elastic-plastic materials*, Q.J. Mech. Appl. Math., **28**, 25–46, 1975.

23. I. NISHIGUCHI, T.-L. SHAM and E. KREMPL, *A finite deformation theory of viscoplasticity based on overstress. Part I. Constitutive equations*, J. Appl. Mech., **57**, 548–552, 1988.

24. I. NISHIGUCHI, T.-L. SHAM and E. KREMPL, *A finite deformation theory of viscoplasticity based on overstress. Part II. Finite element implementation and numerical experiments*, J. Appl. Mech., **57**, 553–561, 1988.

25. A.L. ETEROVIC and K.J. BATHE, *A hyperelastic-based large strain elasto-plastic constitutive formulation with combined isotropic-kinematic hardening using the logarithmic stress and strain measures*, Int. J. Num. Meth. Engng., **30**, 1099–1115, 1990.

26. G. WEBER and L. ANAND, *Finite deformation constitutive equations and a time integration procedure for isotropic hyperelastic-viscoplastic solids*, Comp. Meth. Appl. Mech. Engng., **79**, 465–477, 1990.

27. C. MIEHE and E. STEIN, *A canonical model of multiplicative elasto-plasticity: formulation and aspects of the numerical implementation*, Eur. J. Mech., A/Solids, **11**, 25–43, 1992.

28. J.C. SIMO, *A framework for finite strain elastoplasticity based on maximum dissipation. Part II. Computational aspects*, Comp. Meth. Appl. Mech. Engng., 368, 1–31, 1988.

29. F.G. KOLLMANN and V. BERGMANN, *A new finite element for geometrically linear, inelastic analysis of axisymmetric plates and shells*, Unpublished report, Cornell University, Theoret. and Appl. Mech., Ithaca, N.Y. 1986.

30. O.C. ZIENKIEWICZ, J. BAUER, K. MORGAN and E. ONATE, *A simple and efficient element for axisymmetric shells*, Int. J. Num. Meth. Engng., **11**, 1545–1558, 1977.

31. H.-P. HACKENBERG, *Über die Anwendung inelastischer Stoffgesetze auf finite Deformationen mit der Methode der Finiten Elemente*, PhD Thesis, Technische Hochschule Darmstadt, 1991.

32. D. CORDTS and F.G. KOLLMANN, *An implicit time integration scheme for inelastic constitutive equations with internal state variables*, Int. J. Num. Meth. Engng., **23**, 533–554, 1986.

33. E. MARSDEN and T.J.R. HUGHES, *Mathematical foundations of elasticity*, Prentice Hall, Englewood Cliffs, 1983.

34. J.F. BESSELING, *A thermodynamic approach to rheology*, [in:] Irreversible Aspects of Continuum Mechanics, H. PARKUS and L.I. SEDDOV [Eds], pp. 16–53, Springer, Wien 1968.

35. E. KRÖNER, *Allgemeine Kontinuumstheorie der Versetzungen und Eigenspannungen*, Arch. Rat. Mech. Anal., **4**, 4, 273–334, 1960.

36. E.H. LEE, *Elastic-plastic deformation at finite strains*, Trans. ASME, J. Appl. Mech., **36**, 1–6, 1969.

37. C. SANSOUR and F.G. KOLLMANN, *On theory and numerics of large viscoplastic deformation*, [Prep. for press 1996].

38. J.C. SIMO and D.D. FOX, *On stress resultant geometrically exact shell model. Part I. Formulation and optimal parametrization*, Comp. Meth. Appl. Mech. Engng., **72**, 267–304, 1989.

39. Y. BASAR, Y. DING and W.B. KRAETZIG, *Finite rotation shell elements via mixed formulations*, Comp. Mech., **10**, 289–306, 1992.

40. P. WRIGGERS and F. GRUTTMANN, *Thin shell with finite rotations in Biot stresses: theory and finite element formulation*, Int. J. Num. Meth. Engng., **36**, 4027–4043, 1993.

41. A. LIBAI and J.G. SIMMONDS, *Nonlinear elastic shell theory*, [in:] Advances in Applied Mechanics, HUTCHINSON and WU [Eds.], Academic Press, New York, USA 1983.

42. J. MAKOWSKI, J. CHROSCIELEWSKI and H. STUMPF, *Genuinely resultant shell finite elements accounting for geometric and material nonlinearity*, Int. J. Num. Meth. Engng., **35**, 63–94, 1992.

43. C. SANSOUR and H. BUFLER, *An exact finite rotation shell theory, its mixed variational formulation and its finite element implementation*, Int. J. Num. Meth. Engng., **34**, 73–115, 1992.

44. C. SANSOUR and H. BEDNARCZYK, *The Cosserat surface as a shell model, theory and finite-element formulation*, Comp. Meth. Appl. Mech. Engng., **120**, 1–32, 1995.

45. C. SANSOUR and F.G. KOLLMANN, *Large viscoplastic deformations of shells. Theory and finite element formulation*, [Prep. for press 1996].

46. J.C. SIMO and M.S. RIFAI, *A class of mixed assumed strain methods and the method of incompatible modes*, Int. J. Num. Meth. Engng., **29**, 1595–1638, 1992.

47. J.C. SIMO and F. AMERO, *Geometrically nonlinear enhanced strain mixed methods and the method of incompatible modes*, Int. J. Num. Meth. Engng., **33**, 1413–1449, 1992.

TECHNISCHE HOCHSCHULE DARMSTADT
FACHGEBIET MASCHINENELEMENTE UND MASCHINENAKUSTIK
Magdalenenstr. 4, 64289 Darmstadt, Germany.

Received December 8, 1996; new version March 21, 1997.

Arch. Mech., 49, 3, pp. 513–523, Warszawa 1997

On attainability of Hashin-Shtrikman bounds by iterative hexagonal layering Plane elasticity problems

T. LEWIŃSKI and A. M. OTHMAN (WARSZAWA)

THE PAPER presents a derivation of the Hashin–Shtrikman bounds for the plane elasticity problems and for the Kirchhoff problem of plates in bending. A two-dimensional counterpart of the method of FRANCFORT–MURAT [1] is applied. The method consists of three subsequent layerings along the directions of vertices of a unilateral triangle.

1. Introduction

FRANCFORT AND MURAT [1] showed how to mix in space two isotropic elastic components to obtain the stiffest possible isotropic material. The aim of the present paper is twofold. First we consider this problem in a two-dimensional setting, which means that both plane-stress and plane-strain elasticity problems are comprised. Secondly we deal with the plate bending problem of Kirchhoff.

FRANCFORT and MURAT [1] performed subsequent layerings in the directions of vertices of a regular icosahedron and arrived at an isotropic material of extremal properties. The present paper shows details of a similar but plane mixing process, using layerings in the directions of vertices of a unilateral triangle.

The Hashin - Shtrikman bounds for both the problems considered are similar due to the analogy between two-dimensional elasticity and plate bending problems. This paper shows the details of how to perform the passage between the bounds. It turns out that such a passage is feasible, but requires a change of the assumptions of ordering of the material phases, which makes it non-intuitive. Thus the independent derivations of these bounds, like that presented here for both the problems, seem indispensable, whether the analogy recalled applies here or not.

2. Plane elasticity problem. Laminate of first rank composed of two isotropic materials

Let us denote by $\mathbf{A}$ the tensor of elastic moduli for a plane-stress or plane-strain problem. We consider two isotropic materials of moduli $\mathbf{A}_\alpha$ ($\alpha = 1, 2$) and restrict our consideration to the ordered case: $\mathbf{A}_2 > \mathbf{A}_1$. These tensors are

determined by the pairs of moduli (k_α, μ_α) as follows

$$\mathbf{A}_\alpha = 2k_\alpha \mathbf{a}_1 \otimes \mathbf{a}_1 + 2\mu_\alpha(\mathbf{a}_2 \otimes \mathbf{a}_2 + \mathbf{a}_3 \otimes \mathbf{a}_3), \tag{2.1}$$

where

$$\begin{aligned} \mathbf{a}_1 &= \frac{1}{\sqrt{2}}(\mathbf{e}_1 \otimes \mathbf{e}_1 + \mathbf{e}_2 \otimes \mathbf{e}_2), \\ \mathbf{a}_2 &= \frac{1}{\sqrt{2}}(\mathbf{e}_1 \otimes \mathbf{e}_1 - \mathbf{e}_2 \otimes \mathbf{e}_2), \\ \mathbf{a}_3 &= \frac{1}{\sqrt{2}}(\mathbf{e}_1 \otimes \mathbf{e}_2 + \mathbf{e}_2 \otimes \mathbf{e}_1), \end{aligned} \tag{2.2}$$

and $(\mathbf{e}_1, \mathbf{e}_2)$ are versors of the orthogonal Cartesian coordinate system.

Let us stack both materials to make an in-plane laminate directed along versor $\mathbf{n}$ with area fractions θ_α. The tensor of effective moduli of the laminate is given by the formula of FRANCFORT and MURAT [1], truncated here to the plane problem, see also KOHN [3]

$$\theta_1(\mathbf{A}_2 - \mathbf{A}_h)^{-1} = (\mathbf{A}_2 - \mathbf{A}_1)^{-1} - \frac{\theta_2}{\mu_2}\,\boldsymbol{\Psi}^{(\mathbf{n})}, \tag{2.3}$$

where

$$\boldsymbol{\Psi}^{(\mathbf{n})} = \Psi^{\mathbf{n}}_{\alpha\beta\gamma\delta}\mathbf{e}_\alpha \otimes \mathbf{e}_\beta \otimes \mathbf{e}_\gamma \otimes \mathbf{e}_\delta\,, \tag{2.4}$$

$$\Psi^{\mathbf{n}}_{\alpha\beta\gamma\delta} = \frac{1}{4}\,(\delta_{\beta\gamma}n_\alpha n_\delta + \delta_{\beta\delta}n_\alpha n_\gamma + \delta_{\alpha\gamma}n_\beta n_\delta + \delta_{\alpha\delta}n_\beta n_\gamma) - \frac{k_2}{k_2 + \mu_2}n_\alpha n_\beta n_\delta n_\gamma \tag{2.5}$$

with $n_\alpha = \mathbf{n}\cdot\mathbf{e}_\alpha$. The formula (2.3) holds true if $\mathbf{A}_1$ is non-isotropic, which will be utilised later.

3. Layering of second rank

Let us form the subsequent laminate by stacking the layers of material 2 with the first-rank laminate constructed in Sec. 2, along direction of versor $\mathbf{m} = (m_\alpha)$ with area fractions α_2 (material 2) and α_1 (composite material of moduli $\mathbf{A}_h$). Since Eq. (2.3) holds even if the first material is anisotropic, we apply this formula to arrive at the following implicit formula for the effective stiffness tensor $\mathbf{A}_{hh}$:

$$\alpha_1(\mathbf{A}_2 - \mathbf{A}_{hh})^{-1} = (\mathbf{A}_2 - \mathbf{A}_h)^{-1} - \frac{\alpha_2}{\mu_2}\,\boldsymbol{\Psi}^{(\mathbf{m})}. \tag{3.1}$$

By combining (3.1) and (2.3) one finds

$$\alpha_1\theta_1(\mathbf{A}_2 - \mathbf{A}_{hh})^{-1} = (\mathbf{A}_2 - \mathbf{A}_1)^{-1} - \frac{\theta_2}{\mu_2}\,\boldsymbol{\Psi}^{(\mathbf{n})} - \frac{\alpha_2\theta_1}{\mu_2}\,\boldsymbol{\Psi}^{(\mathbf{m})}. \tag{3.2}$$

One can prove that $\mathbf{A}_2 > \mathbf{A}_{hh}$, hence the first term of Eq. (3.2) makes sense.

4. Laminate of third rank

Now we stack the material obtained by the second layering with material (2), in layers along versor **p**, with area fractions β_1 (material of modulus $\mathbf{A}_{hh}$) and β_2 (material of modulus $\mathbf{A}_2$) to obtain a laminate of moduli $\mathbf{A}_{hhh}$. Again $\mathbf{A}_2 > \mathbf{A}_{hhh}$ and by applying (2.3) one finds

$$\beta_1(\mathbf{A}_2 - \mathbf{A}_{hhh})^{-1} = (\mathbf{A}_2 - \mathbf{A}_{hh})^{-1} - \frac{\beta_2}{\mu_2}\boldsymbol{\Psi}^{(\mathbf{p})}. \tag{4.1}$$

On combining (4.1) and (3.2) one arrives at

$$\alpha_1\theta_1\beta_1(\mathbf{A}_2 - \mathbf{A}_{hhh})^{-1} = (\mathbf{A}_2 - \mathbf{A}_1)^{-1} - \frac{1}{\mu_2}\boldsymbol{\Psi}, \tag{4.2}$$

$$\boldsymbol{\Psi} = \theta_2\boldsymbol{\Psi}^{(\mathbf{n})} + \theta_1\alpha_2\boldsymbol{\Psi}^{(\mathbf{m})} + \beta_2\alpha_1\theta_1\boldsymbol{\Psi}^{(\mathbf{p})}. \tag{4.3}$$

5. Hexagonal lamination

Let us choose

$$\mathbf{n} = (1,0), \qquad \mathbf{m} = \left(-\frac{1}{2}, \frac{\sqrt{3}}{2}\right), \qquad \mathbf{p} = \left(-\frac{1}{2}, -\frac{\sqrt{3}}{2}\right), \tag{5.1}$$

hence end points of versors **n**, **m**, **p** are vertices of a unilateral triangle. A direct computation yields

$$\begin{gathered} \Psi^{(\mathbf{n})}_{1111} = 1 - b, \qquad \Psi^{(\mathbf{n})}_{1212} = \frac{1}{4}, \qquad \Psi^{(\mathbf{n})}_{\alpha\alpha\beta\beta} = 0, \\ \alpha = 2, \qquad \beta = 1 \text{ or } 2, \qquad b = \frac{k_2}{k_2 + \mu_2}; \end{gathered} \tag{5.2}$$

$$\begin{aligned} \Psi^{(\mathbf{m})}_{1111} &= \frac{1}{4} - \frac{b}{16}, & \Psi^{(\mathbf{m})}_{2222} &= \frac{3}{4} - \frac{9}{16}b, \\ \Psi^{(\mathbf{m})}_{1122} &= -\frac{3b}{16}, & \Psi^{(\mathbf{m})}_{1112} &= -\frac{\sqrt{3}}{4}\left(\frac{1}{2} - \frac{b}{4}\right), \\ \Psi^{(\mathbf{m})}_{2221} &= -\frac{\sqrt{3}}{4}\left(\frac{1}{2} - \frac{3b}{4}\right), & \Psi^{(\mathbf{m})}_{1212} &= \frac{1}{4} - \frac{3b}{16}; \end{aligned} \tag{5.3}$$

$$\begin{aligned} \Psi^{(\mathbf{p})}_{1111} &= \frac{1}{4} - \frac{b}{16}, & \Psi^{(\mathbf{p})}_{1212} &= \frac{1}{4} - \frac{3b}{16}, \\ \Psi^{(\mathbf{p})}_{1122} &= -\frac{3}{16}b, & \Psi^{(\mathbf{p})}_{2221} &= \frac{\sqrt{3}}{4}\left(\frac{1}{2} - \frac{3}{4}b\right), \\ \Psi^{(\mathbf{p})}_{1112} &= \frac{\sqrt{3}}{8}\left(1 - \frac{b}{2}\right), & \Psi^{(\mathbf{p})}_{2222} &= \frac{3}{4} - \frac{9}{16}b. \end{aligned} \tag{5.4}$$

Now we stipulate that Ψ given by Eq. (4.3) is isotropic. Conditions $\Psi_{2221} = 0$, $\Psi_{1112} = 0$ yield $\beta_2 = \alpha_2/\alpha_1$. The condition $\Psi_{1111} = \Psi_{2222}$ implies $\alpha_2 = \theta_2/\theta_1$. Thus we have

$$
\begin{aligned}
&\Psi_{1111} = \theta_2\left(\frac{3}{2} - \frac{9}{8}b\right), \qquad \Psi_{2222} = \Psi_{1111}, \\
&\Psi_{1212} = \theta_2\left(\frac{3}{4} - \frac{3}{8}b\right), \qquad \Psi_{1122} = -\frac{3}{8}b\theta_2
\end{aligned} \tag{5.5}
$$

and finally we conclude that Ψ can be put in the form similar to (2.1)

$$
\Psi = \frac{3}{2}\theta_2\left[(1-b)\mathbf{a}_1 \otimes \mathbf{a}_1 + \left(1 - \frac{b}{2}\right)(\mathbf{a}_2 \otimes \mathbf{a}_2 + \mathbf{a}_3 \otimes \mathbf{a}_3)\right]. \tag{5.6}
$$

Let us compute

$$
\begin{aligned}
(\mathbf{A}_2 - \mathbf{A}_1)^{-1} - \frac{1}{\mu_2}\Psi &= \left[\frac{1}{2\Delta k} - \frac{3(1-b)}{2\mu_2}\theta_2\right]\mathbf{a}_1 \otimes \mathbf{a}_1 \\
&\quad + \left[\frac{1}{2\Delta\mu} - \frac{3}{2\mu_2}\left(1 - \frac{b}{2}\right)\theta_2\right](\mathbf{a}_2 \otimes \mathbf{a}_2 + \mathbf{a}_3 \otimes \mathbf{a}_3), \\
\Delta f &= f_2 - f_1, \qquad f = k \text{ or } \mu
\end{aligned} \tag{5.7}
$$

and equate this expression to

$$
\begin{aligned}
&\alpha_1\theta_1\beta_1(\mathbf{A}_1 - \mathbf{A}_{hhh})^{-1} \\
&\quad = \frac{\alpha_1\beta_1\theta_1}{2(k_2 - \overline{k}_{hhh})}\mathbf{a}_1 \otimes \mathbf{a}_1 + \frac{\alpha_1\beta_1\theta_1}{2(\mu_2 - \overline{\mu}_{hhh})}(\mathbf{a}_2 \otimes \mathbf{a}_2 + \mathbf{a}_3 \otimes \mathbf{a}_3),
\end{aligned} \tag{5.8}
$$

where

$$
\mathbf{A}_{hhh} = 2\overline{k}_{hhh}\mathbf{a}_1 \otimes \mathbf{a}_1 + 2\overline{\mu}_{hhh}(\mathbf{a}_2 \otimes \mathbf{a}_2 + \mathbf{a}_3 \otimes \mathbf{a}_3),
$$

which gives

$$
\begin{aligned}
\frac{\theta_1\alpha_1\beta_1}{k_2 - \overline{k}_{hhh}} &= \frac{1}{\Delta k} - \frac{3\theta_2(1-b)}{\mu_2}, \\
\frac{\theta_1\alpha_1\beta_1}{\mu_2 - \overline{\mu}_{hhh}} &= \frac{1}{\Delta\mu} - \frac{3\theta_2(1-b/2)}{\mu_2}.
\end{aligned} \tag{5.9}
$$

Assume that the area fraction of the first material is fixed and equals m_1, or

$$
m_1 = \alpha_1\beta_1\theta_1. \tag{5.10}
$$

We can express θ_2, α_2, β_2 in terms of m_1 as follows

$$
\theta_2 = \frac{m_2}{3}, \qquad \alpha_2 = \frac{m_2}{3 - m_2}, \qquad \beta_2 = \frac{m_2}{3 - 2m_2} \tag{5.11}
$$

and Eqs. (5.9) assume the form

$$(5.12)_1 \qquad \begin{aligned} \frac{m_1}{k_2 - \overline{k}_{hhh}} &= \frac{1}{k_2 - k_1} - \frac{m_2}{k_2 + \mu_2}, \\ \frac{m_1}{\mu_2 - \overline{\mu}_{hhh}} &= \frac{1}{\mu_2 - \mu_1} - \frac{m_2(k_2 + 2\mu_2)}{2\mu_2(k_2 + \mu_2)}. \end{aligned}$$

The moduli $(\overline{k}_{hhh}, \overline{\mu}_{hhh})$ determined by Eq. (5.12) are just upper estimates of Hashin and Shtrikman, see CHERKAEV and GIBIANSKI [2]. Formulae (5.12) can be written as follows

$$(5.12)_2 \qquad \begin{aligned} \overline{k}_{PE} &= F(m; k_1, k_2, \mu_2), \\ \overline{\mu}_{PE} &= G_{PE}(m; \mu_1, \mu_2, k_2); \qquad m = (m_1, m_2); \end{aligned}$$

PE means "plane elasticity problem", the functions F and G_{PE} being determined by Eq. $(5.12)_1$; here $\overline{k}_{PE} = \overline{k}_{hhh}$, $\overline{\mu}_{PE} = \overline{\mu}_{hhh}$.

REMARK 1. The laminate of 3rd rank constructed by subsequent layerings discussed here is the stiffest among all isotropic composites made from two given isotropic materials with given area fractions. Let us stress that both bounds for μ and k are attained simultaneously.

REMARK 2. In a similar way one can construct the softest isotropic composite. To this end one should mix subsequent laminates with the softest material to get

$$(5.13)_1 \qquad \begin{aligned} \frac{m_2}{k_1 - \underline{k}_{hhh}} &= \frac{1}{k_1 - k_2} - \frac{m_1}{k_1 + \mu_1}, \\ \frac{m_2}{\mu_1 - \underline{\mu}_{hhh}} &= \frac{1}{\mu_1 - \mu_2} - \frac{m_1(k_1 + 2\mu_1)}{2\mu_1(k_1 + \mu_1)} \end{aligned}$$

or

$$(5.13)_2 \qquad \begin{aligned} \underline{k}_{PE} &= F(\widetilde{m}; k_2, k_1, \mu_1), \\ \underline{\mu}_{PE} &= G_{PE}(\widetilde{m}; \mu_2, \mu_1, k_1), \qquad \widetilde{m} = (m_2, m_1), \end{aligned}$$

where hhh is replaced with PE, which indicates that the plane elasticity problem is considered. We recognize that $\underline{k}_{hhh} = \underline{k}_{PE}$, $\underline{\mu}_{hhh} = \underline{\mu}_{PE}$ are lower bounds of Hashin and Shtrikman, see CHERKAEV and GIBIANSKI [2]. These lower bounds are attained simultaneously.

6. Kirchhoff bending problem. A rank-1 Kirchhoff's in-plane laminate

Let us consider now a bending problem of thin transversely symmetric plates. Given two isotropic plate materials of bending/torsion stiffness tensors $\mathbf{D}_\alpha$,

$\alpha = 1, 2$; $\mathbf{D}_2 - \mathbf{D}_1 > \mathbf{0}$, we construct an in-plane laminate (we use the term *laminate* to stress similarities with the layering construction of the previous sections; the term *ribbed plate* would be more appropriate) in the $\mathbf{n}$ direction, $\mathbf{n} = (n_1, n_2)$, with area fractions θ_α, respectively. Let $\mathbf{e}_\alpha$ be versors of Cartesian axes. Let us decompose

$$\mathbf{D}_\lambda = D_\lambda^{\alpha\beta\gamma\delta} \mathbf{e}_\alpha \otimes \mathbf{e}_\beta \otimes \mathbf{e}_\gamma \otimes \mathbf{e}_\delta , \tag{6.1}$$

$$D_\alpha^{1111} = D_\alpha^{2222} = k_\alpha + \mu_\alpha , \qquad D_\alpha^{1122} = k_\alpha - \mu_\alpha , \qquad D_\alpha^{1212} = \mu_\alpha , \tag{6.2}$$

k_α, μ_α being Kelvin and Kirchhoff moduli, respectively.

Within the Kirchhoff's framework the effective stiffness tensor $\mathbf{D}_h$ of the in-plane laminate considered is uniquely determined. The dispersed in the literature contributions by G. Duvaut, R.V. Kohn, A.V. Cherkaev, K.A. Lur'e, G. Francfort, F. Murat, G. Milton, R. Lipton and L. Tartar lead to the formula

$$\theta_1 (\mathbf{D}_2 - \mathbf{D}_h)^{-1} = (\mathbf{D}_2 - \mathbf{D}_1)^{-1} - \frac{\theta_2}{s_2} \mathbf{\Gamma}^{(\mathbf{n})}, \tag{6.3}$$

$$s_2 = k_2 + \mu_2 , \qquad \mathbf{\Gamma}^{(\mathbf{n})} = \mathbf{n} \otimes \mathbf{n} \otimes \mathbf{n} \otimes \mathbf{n}, \tag{6.4}$$

$\mathbf{D}_1$ being not necessarily isotropic. A derivation of Eq. (6.3) can be found in LIPTON [4].

7. A rank-two Kirchhoff laminate

Let us envelop the rank-1 laminate around the strongest phase (2), the area fractions of $\mathbf{D}_h$, $\mathbf{D}_2$ being α_1 and α_2, respectively. Thus we stack materials $\mathbf{D}_h$, $\mathbf{D}_2$ in layers orthogonal to a versor $\mathbf{m}$. To find effective stiffness tensor $\mathbf{D}_{hh}$ one can apply (6.3) again to find

$$\alpha_1 (\mathbf{D}_2 - \mathbf{D}_{hh})^{-1} = (\mathbf{D}_2 - \mathbf{D}_h)^{-1} - \frac{\alpha_2}{s_2} \mathbf{\Gamma}^{(\mathbf{m})}. \tag{7.1}$$

On combining (6.3) and (7.1) one finds

$$\theta_1 \alpha_1 (\mathbf{D}_2 - \mathbf{D}_{hh})^{-1} = (\mathbf{D}_2 - \mathbf{D}_1)^{-1} - \frac{\theta_2}{s_2} \mathbf{\Gamma}^{(\mathbf{n})} - \frac{\theta_1 \alpha_2}{s_2} \mathbf{\Gamma}^{(\mathbf{m})}, \tag{7.2}$$

the quantity $\theta_1 \alpha_1$ being the resulting area fraction of material (1).

8. A rank-three Kirchhoff's laminate

Let us stack the materials of stiffnesses $\mathbf{D}_{hh}$, $\mathbf{D}_2$ together thus building an in-plane laminate along versor $\mathbf{p}$, with area fractions β_1, β_2, respectively. Applying

(6.3) once again we have

$$\beta_1(\mathbf{D}_2 - \mathbf{D}_{hhh})^{-1} = (\mathbf{D}_2 - \mathbf{D}_{hh})^{-1} - \frac{\beta_2}{s_2}\boldsymbol{\Gamma}^{(\mathbf{p})}. \tag{8.1}$$

On combining (8.1) with (7.2) one finds

$$\beta_1\theta_1\alpha_1(\mathbf{D}_2 - \mathbf{D}_{hhh})^{-1} = (\mathbf{D}_2 - \mathbf{D}_1)^{-1} - \frac{1}{s_2}\boldsymbol{\Gamma}, \tag{8.2}$$

$$\boldsymbol{\Gamma} = \theta_2\boldsymbol{\Gamma}^{(\mathbf{n})} + \theta_1\alpha_2\boldsymbol{\Gamma}^{(\mathbf{m})} + \theta_1\alpha_1\beta_2\boldsymbol{\Gamma}^{(\mathbf{p})}. \tag{8.3}$$

9. Hexagonal lamination

Let us take versors $\mathbf{n}$, $\mathbf{m}$, $\mathbf{p}$ such that their vertices form an unilateral triangle. Thus

$$\begin{aligned} \mathbf{m} &= \left(-\frac{1}{2}n_1 - \frac{\sqrt{3}}{2}n_2,\ -\frac{1}{2}n_2 + \frac{\sqrt{3}}{2}n_1\right), \\ \mathbf{p} &= \left(-\frac{1}{2}n_1 + \frac{\sqrt{3}}{2}n_2,\ -\frac{1}{2}n_2 - \frac{\sqrt{3}}{2}n_1\right). \end{aligned} \tag{9.1}$$

We shall prove that the above choice of $\mathbf{m}$ and $\mathbf{p}$ implies isotropy of $\boldsymbol{\Gamma}$. Assume for simplicity that $\mathbf{n} = (1, 0)$, which is not a restriction. Let us compute

$$\begin{aligned} &\Gamma_{1111} = \theta_2 + \frac{\theta_1}{16}(\alpha_2 + \beta_2\alpha_1), && \Gamma_{2222} = \left(\frac{\sqrt{3}}{2}\right)^4\theta_1(\alpha_2 + \beta_2\alpha_1), \\ &\Gamma_{1122} = \frac{1}{4}\left(\frac{\sqrt{3}}{2}\right)^2\theta_1(\alpha_2 + \beta_2\alpha_1), && \Gamma_{1112} = \frac{\sqrt{3}}{16}\theta_1(-\alpha_2 + \beta_2\alpha_1), \\ &\Gamma_{2221} = \Gamma_{1112}, && \Gamma_{1212} = \frac{3}{16}\theta_1(\alpha_2 + \beta_2\alpha_1). \end{aligned} \tag{9.2}$$

We stipulate

$$\Gamma_{1222} = \Gamma_{1112} = 0, \qquad \Gamma_{1111} = \Gamma_{2222}, \tag{9.3}$$

hence

$$\beta_2 = \alpha_2/\alpha_1, \qquad \theta_2 = \theta_1\alpha_2, \tag{9.4}$$

and consequently make the tensor $\boldsymbol{\Gamma}$ isotropic

$$\boldsymbol{\Gamma} = \frac{3}{4}\theta_2[2\mathbf{a}_1 \otimes \mathbf{a}_1 + (\mathbf{a}_2 \otimes \mathbf{a}_2 + \mathbf{a}_3 \otimes \mathbf{a}_3)]. \tag{9.5}$$

Let us find now $\overline{k}_{hhh}$, $\overline{\mu}_{hhh}$ involved in the representation

$$\mathbf{D}_{hhh} = 2\overline{k}_{hhh}\mathbf{a}_1 \otimes \mathbf{a}_1 + 2\overline{\mu}_{hhh}(\mathbf{a}_2 \otimes \mathbf{a}_2 + \mathbf{a}_3 \otimes \mathbf{a}_3). \tag{9.6}$$

Since

$$(\mathbf{D}_2 - \mathbf{D}_{hhh})^{-1} = \frac{1}{2(k_2 - \overline{k}_{hhh})}\mathbf{a}_1 \otimes \mathbf{a}_1 + \frac{1}{2(\mu_2 - \overline{\mu}_{hhh})}(\mathbf{a}_2 \otimes \mathbf{a}_2 + \mathbf{a}_3 \otimes \mathbf{a}_3) \tag{9.7}$$

and

$$(\mathbf{D}_2 - \mathbf{D}_1)^{-1} - \frac{1}{s_2}\mathbf{\Gamma} \tag{9.8}$$

$$= \left[\frac{1}{2(k_2 - k_1)} - \frac{\frac{3}{2}\theta_2}{s_2}\right]\mathbf{a}_1 \otimes \mathbf{a}_1 + \left[\frac{1}{2(\mu_2 - \mu_1)} - \frac{\frac{3}{4}\theta_2}{s_2}\right](\mathbf{a}_2 \otimes \mathbf{a}_2 + \mathbf{a}_3 \otimes \mathbf{a}_3),$$

the formula (4.2) implies

$$\begin{aligned} \frac{\theta_1\alpha_1\beta_1}{k_2 - \overline{k}_{hhh}} &= \frac{1}{k_2 - k_1} - \frac{3\theta_2}{k_2 + \mu_2}, \\ \frac{\theta_1\alpha_1\beta_1}{\mu_2 - \overline{\mu}_{hhh}} &= \frac{1}{\mu_2 - \mu_1} - \frac{3\theta_2}{2(k_2 + \mu_2)}. \end{aligned} \tag{9.9}$$

Denote the resulting area fraction of phase 1 by m_1. Then $m_1 = \theta_1\alpha_1\beta_1$, $m_2 = 1 - m_1$. The previous results imply

$$\theta_2 = \frac{m_2}{3}, \qquad \alpha_2 = \frac{m_2}{3 - m_2}, \qquad \beta_2 = \frac{m_2}{3 - 2m_2}. \tag{9.10}$$

By (9.9), (9.10) we find finally

$$\begin{aligned} \frac{m_1}{k_2 - \overline{k}_{hhh}} &= \frac{1}{k_2 - k_1} - \frac{m_2}{k_2 + \mu_2}, \\ \frac{m_1}{\mu_2 - \overline{\mu}_{hhh}} &= \frac{1}{\mu_2 - \mu_1} - \frac{m_2}{2(k_2 + \mu_2)}. \end{aligned} \tag{9.11}$$

REMARK 3. Functions $\overline{k}_{hhh}(m_2)$, $\overline{\mu}_{hhh}(m_2)$ grow monotonically from k_1 to k_2 and from μ_1 to μ_2, respectively, if m_2 varies from 0 to 1.

REMARK 4. It turns out that the resulting isotropic plate of stiffness $\mathbf{D}_{hhh}$ given by (9.6) with $\overline{k}_{hhh}$, $\overline{\mu}_{hhh}$ given by (9.11) is just the stiffest possible plate among all plates formed from phases (1) and (2) with given area fractions m_1, m_2. Thus equations (9.11) provide the upper Hashin - Shtrikman bounds for both k and μ.

REMARK 5. To find the softest plate one should envelop the homogenized material around the softest one. In the same manner one arrives at the lower Hashin - Shtrikman estimates for k and μ.

10. Plane elasticity versus plate bending results

One can show a remarkable correspondence between Hashin - Shtrikman bounds for Kirchhoff plates and plane elasticity problems. For Kirchhoff plate model the upper Hashin - Shtrikman bounds $\overline{k}_K, \overline{\mu}_K$ are solutions to the following equations, cf. Eq. (9.11)

$$\overline{k}_K = F(m; k_1, k_2, \mu_2), \tag{10.1}$$

$$\overline{\mu}_K = G_K(m; \mu_1, \mu_2, k_2). \tag{10.2}$$

Index K refers to the Kirchhoff plate model; function G_K is determined by (9.11) and function F – defined by Eq. (5.12). Let us note that

$$\begin{aligned} F(m; k_1, k_2, \mu_2) &= \left[F\left(m; (k_1)^{-1}, (k_2)^{-1}, (\mu_2)^{-1}\right)\right]^{-1}, \\ G_K(m; \mu_1, \mu_2, k_2) &= \left[G_{PE}\left(m; (\mu_1)^{-1}, (\mu_2)^{-1}, (k_2)^{-1}\right)\right]^{-1}, \end{aligned} \tag{10.3}$$

which can be proved by algebraic manipulations. Thus the link between plane elasticity bounds

$$\begin{aligned} F(\widetilde{m}; k_2, k_1, \mu_1) \le k_{PE} \le F(m; k_1, k_2, \mu_2), \\ G_{PE}(\widetilde{m}; \mu_2, \mu_1, k_1) \le \mu_{PE} \le G_{PE}(m; \mu_1, \mu_2, k_2), \end{aligned} \tag{10.4}$$

and Kirchhoff plate bounds

$$\begin{aligned} F(\widetilde{m}; k_2, k_1, \mu_1) \le k_K \le F(m; k_1, k_2, \mu_2), \\ G_K(\widetilde{m}; \mu_2, \mu_1, k_1) \le \mu_K \le G_K(m; \mu_1, \mu_2, k_2), \end{aligned} \tag{10.5}$$

can be explained as follows.

Assume that $k_1 \ge k_2$, $\mu_1 \ge \mu_2$. Then the bounds for the plate moduli assume the form

$$\begin{aligned} F(m; k_1, k_2, \mu_2) \le k_K \le F(\widetilde{m}; k_2, k_1, \mu_1), \\ G_K(m; \mu_1, \mu_2, k_2) \le \mu_K \le G_K(\widetilde{m}; \mu_2, \mu_1, k_1), \end{aligned} \tag{10.6}$$

since $\widetilde{\widetilde{m}} = m$. Hence by (10.3) we find the bounds for the flexibilities

$$\begin{aligned} F\left(\widetilde{m}; (k_2)^{-1}, (k_1)^{-1}, (\mu_1)^{-1}\right) \le (k_K)^{-1} \le F\left(m; (k_1)^{-1}, (k_2)^{-1}, (\mu_2)^{-1}\right), \\ G_{PE}\left(\widetilde{m}; (\mu_2)^{-1}, (\mu_1)^{-1}, (k_1)^{-1}\right) \le (\mu_K)^{-1} \\ \le G_{PE}\left(m; (\mu_1)^{-1}, (\mu_2)^{-1}, (k_2)^{-1}\right), \end{aligned} \tag{10.7}$$

similar to elasticity bounds (10.4). We see the analogy

$$k_{PE} \Leftrightarrow (k_K)^{-1}, \qquad \mu_{PE} \Leftrightarrow (\mu_K)^{-1}, \qquad k_\alpha \Leftrightarrow (k_\alpha)^{-1}, \qquad \mu_\alpha \Leftrightarrow (\mu_\alpha)^{-1}. \tag{10.8}$$

Let us stress that inequalities (10.4) are valid for

$$k_2 > k_1\,, \qquad \mu_2 > \mu_1\,, \tag{10.9}$$

while inequalities (10.7) are valid if

$$(k_2)^{-1} > (k_1)^{-1}, \qquad (\mu_2)^{-1} > (\mu_1)^{-1}, \tag{10.10}$$

which is compatible with analogy (10.8).

Let us prove a correspondence between (10.4) and (10.7).

The analogy to be proved follows from the following homogenization formulae

a) the homogenized plane elasticity tensor $\mathbf{A}_h$ is given by

$$E_{\alpha\beta}A_h^{\alpha\beta\lambda\mu}E_{\lambda\mu} = \min\Big\{\Big\langle \varepsilon_{\alpha\beta}A^{\alpha\beta\lambda\mu}\varepsilon_{\lambda\mu}\Big\rangle \,|\varepsilon_{\alpha\beta} \text{ are kinematically admissible:} \tag{10.11}$$

$$\varepsilon_{11,22} + \varepsilon_{22,11} - 2\varepsilon_{12,12} = 0, \qquad Y\text{-periodic and such that } \langle\boldsymbol{\varepsilon}\rangle = \mathbf{E}\Big\}.$$

$\langle\cdot\rangle$ means averaging over periodicity cell Y; $(\,)_{,\alpha} = \partial/\partial y_\alpha$, $y = (y_1, y_2) \in Y$.

b) the homogenized tensor $\mathbf{C}_h$ of Kirchhoff's plate flexibilities is given by

$$M^{\alpha\beta}C^h_{\alpha\beta\lambda\mu}M^{\lambda\mu} = \min\Big\{\Big\langle m^{\alpha\beta}C_{\alpha\beta\lambda\mu}m^{\lambda\mu}\Big\rangle \,|m^{\alpha\beta} \text{ are statically admissible:} \tag{10.12}$$

$$m^{\alpha\beta}{}_{,\alpha\beta} = 0, \qquad Y\text{-periodic and such that } \langle\mathbf{m}\rangle = \mathbf{M}\Big\}.$$

Let us denote

$$\varepsilon_{22} = n^{11}, \qquad \varepsilon_{11} = n^{22}, \qquad \varepsilon_{12} = -n^{12}. \tag{10.13}$$

Then

$$n^{\alpha\beta}{}_{,\alpha\beta} = 0, \qquad \langle n^{\alpha\beta}\rangle = e_{\alpha\sigma}e_{\beta\gamma}E_{\sigma\gamma} = \tilde{E}_{\alpha\beta}\,, \tag{10.14}$$

where $e_{\alpha\alpha} = 0$, $e_{12} = -e_{21} = 1$. Thus formula (10.11) assumes the form

$$\tilde{E}_{\alpha\beta}\tilde{A}_h^{\alpha\beta\lambda\mu}\tilde{E}_{\lambda\mu} = \min\Big\{\Big\langle n^{\gamma\sigma}\tilde{A}_{\gamma\delta\sigma\kappa}n^{\sigma\kappa}\Big\rangle \tag{10.15}$$

$$|n^{\alpha\beta}{}_{,\alpha\beta} = 0; \quad n^{\alpha\beta} \text{ are } Y\text{-periodic; } \langle\mathbf{n}\rangle = \tilde{\mathbf{E}}\Big\},$$

where

$$\tilde{A}_{\gamma\delta\sigma\kappa} = e_{\alpha\gamma}e_{\beta\delta}e_{\lambda\sigma}e_{\mu\kappa}A^{\alpha\beta\lambda\mu}, \tag{10.16}$$

and $\tilde{\mathbf{A}}_h$ is defined similarly. Transformation (10.16) changes indices (1,2) into (2,1), which is unimportant if we estimate the energy by isotropic quadratic forms, which is the case here. Hence the upper/lower estimates for strain energy (10.15) assume the form of upper/lower estimates of complementary energy of Kirchhoff's plate, cf. Eq. (10.12). Therefore estimates (10.4) have formally the same form as estimates (10.7) for the plate flexibilities. Note, however, that the applicability ranges of both estimates are complementary.

Acknowledgment

The financial support by the State Committee for Scientific Research through the grant No. 3 P404 013 06 and through the Statutory Project No. 504/072/253/1 is gratefully acknowledged.

References

1. G.A. FRANCFORT and F. MURAT, *Homogenization and optimal bounds in linear elasticity*, Arch. Rat. Mech. Anal., **94**, 307–334, 1986.
2. A.V. CHERKAEV and L.V. GIBIANSKI, *Coupled estimates for the bulk and shear moduli of a two-dimensional isotropic elastic composite*, J. Mech. Phys. Solids, **41**, 937–980, 1993.
3. R.V. KOHN, *Recent progress in the mathematical modelling of composite materials*, [in:] Proc. of a Workshop on Composite Materials. Constitutive Relations and Damage Mechanisms, G.C. SIH, G.F. SMITH, I.H. MARSHALL, J.J. SU [Eds.], Glasgow 1987.
4. R. LIPTON, *Optimal design and relaxation for reinforced plates subject to random transverse loads*, Probab. Engng. Mech., **9**, 167–177, 1994.

CIVIL ENGINEERING FACULTY, INSTITUTE OF STRUCTURAL MECHANICS
WARSAW UNIVERSITY OF TECHNOLOGY
Al. Armii Ludowej 16, 00-637 Warszawa, Poland.

Received February 10, 1997.

Arch. Mech., 49, 3, pp. 525–545, Warszawa 1997

The influence of deformation path on adaptation process of a solid

J. SACZUK (GDAŃSK)

THE IDEA of a criterion of adaptation process of a body, accounting for the influence of deformation path on the material properties of the body, is proposed. A change of the deformation path, realized either through the change of slip systems and/or by changing external loads, is analyzed within the Finslerian description of the solid behaviour. In this continuum model no yield rule and no intermediate configuration are assumed to exist, and the transition from micro- to macroscales is natural. This approach makes possible the description of yielding, softening, hardening and localization of solids within the unified concept. A shakedown theorem, based on the Finslerian continuum model, is formulated within the theory of differential inequalities. The presented theorem, in which a definite amount of the total strain energy comes into play, has no counterparts in the available literature. It generalizes the classical approaches to the adaptation problems by including arbitrary deformations and material nonlinearities.

1. Introduction

THE COMPLEXITY of inelastic behaviour of a solid is caused primarily by the fact that its internal state is changing during the deformation process as a consequence of glide mechanisms, twinning and other shear transformations. Understanding of the overall deformation resistance of the material and the evolution of its internal structure is also important in the accurate prediction of the long-term average behaviour of structure. On the other hand, in many practical applications both the loading and the initial state of the body are not known with a sufficient accuracy. In these cases the knowledge of the whole evolution has only of limited interest. A desired theory should (i) deliver good estimations of the average behaviour of the structure and thereby correct of theoretical results compatible with experimental ones, and (ii) predict the correct asymptotic behaviour whatever are the initial conditions and the loading programme.

The answer to this question can to some degree, be obtained from the shakedown theory, since the classical theory of limit analysis can sometimes give unsafe estimates of collapse loads in certain cases (KOITER [1]). For that reason the shakedown theory provides a criterion of failure which may be considered as a more realistic basis for design than that of the limit analysis which assumes failure to occur when critical elastic stress is attained. Such an analysis is crucial for the assessment of the structural behaviour under varying loads within the range of time-independent plasticity. The problem is classically solved by analyzing possible residual stress fields in the static approach (MELAN [2], KOITER [1]) or by considering possible mechanisms of plastic deformation in the kinematic

method (KOITER [1]), under the assumptions of geometric linearity, elastic-perfectly plastic or linear and unlimited hardening material behaviour, the validity of an associated flow law, etc. The extension of classical shakedown technique to broader classes of problems including the change of temperature, (limited) hardening, the influence of geometric effects are discussed by MANDEL [3], KÖNIG [4], POLIZZOTTO [5], WEICHERT [6, 7], GROSS–WEEGE [8], SACZUK and STUMPF [9], SACZUK [10]. The second direction in the adaptation analysis, being the generalization of the post-yield analysis, is known as the inadaptation analysis (CORRADI and MAIER [11], KÖNIG and SIEMASZKO [12]).

The shakedown criterion characterized by the non-specified definite bound of the plastic work (there exists an instant beyond which no additional plastic deformations occur) has certain shortcomings. A few of them are connected with the impossibility of estimating a (safe) number of load cycles (observed in practice), to estimate lower and upper limits of the plastic work, to take into account a continuous change of material characteristics during its evolution. Different, even of a catastrophic nature, bulk properties of solid deformation, like shear bands, Lüders and Portevin–Le Chatelier bands, hardening and softening, are sensitive to a change of deformation path both at the micro- and macro-levels (cf. KORBEL [13]). On the other hand, the importance of this problem is connected with the fact that the safety problem of structure subjected to variable loads is one of the major problems of structural design. We are still at the initial stage of such analysis.

The aim of this paper is to propose a certain innovation in the assessment of the structural safety, according to the Finslerian modelling of solid behaviour. A measure of adaptation, identified with the boundedness of plastic work, is of course physically justified but is too simple in reality. It is desirable to control the amount of energy necessary to create stable thermodynamic states of the deformation process, and to know how this energy is affected by internal and external parameters. The more correct measure seems to be the definite amount of the total (strain) work. One should stress that the plastic (dissipative) work is not generally easily selected as a part of the total work created during a deformation process. In our case the "plastic" work can be identified with the vertical (internal state) component of deformation process, but not as *a priori* assumption (cf. Sec. 2). We shall try both to propose an improvement of the classical shakedown methodology within the theory of differential inequalities (SZARSKI [14], LAKSHMIKANTHAM and LEELA [15]) and to present its justification within the scope of the generally accepted technique to shakedown problems.

2. Outline of a Finslerian continuum model

The objective in this section is to present the main concepts of the Finslerian modelling of solid behaviour (SACZUK [16]) that need to be known for a thorough

understanding of the technique adapted to the shakedown analysis. A reader who whishes to get information beforehand concerning the whole Finsler geometry is asked to consult RUND [17] and MATSUMOTO [18] monographs. The mathematical preliminaries on Finslerian geometry are presented in Appendix A.

2.1. General assumptions

A continuous model of inelastic behaviour of solids modelled by means of the Finsler geometry (SACZUK [16]) is based on the following assumptions:

A.1. A material body (a continuum) $\mathcal{B}$ is assumed to be a 3-dimensional Finsler bundle F^3 whose points will be called line-elements (RUND [17]).

A.2. A motion of the body $\mathcal{B}$ is defined by the mapping:

$$\hat{\chi} : \mathcal{B} \times R \to E^3 \times E^3 \times R, \qquad (\mathbf{x}, \mathbf{y}, t) \mapsto \mathbf{X} = \hat{\chi}(\mathbf{x}, \mathbf{y}, t),$$

where E denotes an Euclidean space and R is a real number space.

A.3. A time-space of events is the product $E^3 \times E^3 \times R$.

A.4. The body $\mathcal{B}$ is under external and internal force fields.

A.5. Laws of evolution of the body $\mathcal{B}$ results from a variational principle for the first order functional describing its motion.

2.2. The motion

We sketch an approach (SACZUK [16]) which allows one to describe the irreversible deformation process of the solid taking place from the very beginning of its deformation, in conformity with its real internal nature.

In this approach the body $\mathcal{B}$, identified with the three-dimensional Finsler space F^3, is embedded into the product $E^3 \times E^3$ of Euclidean spaces and its points are called line-elements (oriented particles) (Assumptions (A.1) and (A.2)).

The position vector in an actual configuration is defined to be

$$\mathbf{X} = \hat{\chi}(\mathbf{x}, \mathbf{y}), \tag{2.1}$$

where a diffeomorphism $\hat{\chi} : E^6 \supset F^3 \to F^3 \subset E^6$ is a deformation of the body $\mathcal{B}$. The line-element $(\mathbf{x}, \mathbf{y})$ consisting of a position vector and a direction (or an internal variable) vector can be identified with an oriented particle of the body $\mathcal{B}$. The position vector $\mathbf{x}$, identified here with the material point of the configuration space with local coordinates (x^i) at the macro-level, is treated at the micro-level as a separate continuum with coordinates (y^i) at the point $\mathbf{x}$. In special cases we can consider the internal vector $\mathbf{y}$ as the micro-displacement, or the deviation from the mean displacement (KONDO [19]), or the microposition vector (WOŹNIAK [20]).

The deformation gradient is defined as the direct sum of components describing the deformation process of the body (SACZUK [16]) in the form

$$\widehat{\mathbf{F}} = \mathbf{F}^h + \mathbf{F}^v. \tag{2.2}$$

In (2.2) vertical $\mathbf{F}^v$ and horizontal $\mathbf{F}^h$ parts are respectively equal to

$$\mathbf{F}^v = \nabla^v \mathbf{X} = {}_vX^i_k \partial_i \otimes Dl^k, \qquad \mathbf{F}^h = \nabla^h \mathbf{X} = {}_hX^i_k \partial_i \otimes dx^k, \tag{2.3}$$

where $l^k = y^k/L(\mathbf{x},\mathbf{y})$ are components of the unit tangent vector, $L(\mathbf{x},\mathbf{y})$ is the fundamental function identified with the energy stored in dislocations and induced by the deformation process, ∂_i is the unit vector in the current configuration of the body and $\otimes$ denotes the tensor product. We shall denote further horizontal and vertical components of any tensor $\mathbf{T}$ by ${}_hT^{i\cdots}_{j\cdots}$ and ${}_vT^{i\cdots}_{j\cdots}$, respectively. The h-derivatives and v-derivatives of the position vector $\mathbf{X} = \mathbf{X}(\mathbf{x},\mathbf{y})$ are defined as follows (MATSUMOTO [18], RUND [17])

$$(\mathbf{F}^h)^i_k \equiv {}_hX^i_k = \partial_k X^i - \dot\partial_l X^i \dot\partial_k G^l + \Gamma^{\star i}_{lk} X^l, \tag{2.4}$$

$$(\mathbf{F}^v)^i_k \equiv {}_vX^i_k = L\dot\partial_k X^i + A^i_{lk} X^l, \tag{2.5}$$

where $\partial_i \equiv \partial/\partial x^i$, $\dot\partial_i \equiv \partial/\partial y^i$ and the remaining unknowns in (2.4), (2.5) are defined by means of components of the metric tensor

$$g_{ij}(\mathbf{x},\mathbf{y}) = \frac{1}{2}\frac{\partial^2 L^2(\mathbf{x},\mathbf{y})}{\partial y^i \partial y^j} \tag{2.6}$$

according to

$$\Gamma^\star_{ijk} = \Gamma_{ijk} - C_{jkl}\frac{\partial G^l}{\partial y^i} = \gamma_{ijk} - C_{kjl}\frac{\partial G^l}{\partial y^i} - C_{ijl}\frac{\partial G^l}{\partial y^k} + C_{ikl}\frac{\partial G^l}{\partial y^j}, \tag{2.7}$$

$$\Gamma^\star_{ijk} = g_{jl}\Gamma^{\star l}_{ik}, \qquad \Gamma_{ijk} = g_{jl}\Gamma^l_{ik}, \qquad 2G^l = \gamma^l_{jk} y^j y^k, \tag{2.8}$$

$$\begin{aligned} N^l_k &= \dot\partial_k G^l = \frac{\partial G^l}{\partial y^k} = \Gamma^l_{jk} y^j = \Gamma^{\star l}_{jk} y^j, \\ \gamma_{ijk} &= \frac{1}{2}\left(\frac{\partial g_{ij}}{\partial x^k} + \frac{\partial g_{jk}}{\partial x^i} - \frac{\partial g_{ki}}{\partial x^j}\right), \end{aligned} \tag{2.9}$$

$$\begin{aligned} C_{ijk} &= \frac{1}{2}\frac{\partial g_{ij}}{\partial y^k}, \qquad C_{ijk}y^k = C_{ijk}y^j = C_{ijk}y^i = 0, \\ C_{ijk} &= g_{jl}C^l_{ik}, \qquad A^i_{jk} = LC^i_{jk}, \end{aligned} \tag{2.10}$$

$$Dl^i = dl^i + N^i_k dx^k. \tag{2.11}$$

2.3. Strain measures

For an orientation-preserving deformation $\hat{\chi}$ ($\hat{J} = \det \hat{\mathbf{F}} > 0$), the Lagrangian strain tensor is defined by

$$\hat{\mathbf{E}} = \frac{1}{2}(\hat{\mathbf{C}} - \mathbf{1}), \tag{2.12}$$

where $\hat{\mathbf{C}} = \hat{\mathbf{F}}^T \hat{\mathbf{F}}$ is the right Cauchy–Green deformation tensor. In the representation of the direct sum the relation (2.12), after using (2.2), is equivalent to

$$\hat{\mathbf{E}} = \begin{pmatrix} \mathbf{E}^h & \mathbf{0} \\ \mathbf{0} & \mathbf{E}^v \end{pmatrix} = \frac{1}{2} \begin{pmatrix} \mathbf{C}^h - \mathbf{1} & \mathbf{0} \\ \mathbf{0} & \mathbf{C}^v - \mathbf{1} \end{pmatrix}.$$

Using (2.4) and (2.5), the horizontal and vertical parts of the Cauchy–Green strain tensor are then respectively equal to

$$\begin{aligned} \mathbf{C}^h = \big(&\partial_h X^i \partial_l X^j + \dot{\partial}_m X^j \dot{\partial}_l G^m \dot{\partial}_k X^i \dot{\partial}_h G^k + \Gamma^{\star j}_{nl} \Gamma^{\star i}_{kh} X^n X^k \\ &- \partial_{(l} X^{(j} \dot{\partial}_{|k|} X^{i)} \dot{\partial}_{h)} G^k - \dot{\partial}_m X^{(j} \dot{\partial}_{(l} G^{|m|} \Gamma^{\star i)}_{|k|h)} X^k \\ &+ \partial_{(l} X^{(j} \Gamma^{\star i)}_{|k|h)} X^k \big) \bar{g}_{ij}\, dx^l \otimes dx^h, \end{aligned} \tag{2.13}$$

$$\begin{aligned} \mathbf{C}^v = L^2 \big(&\dot{\partial}_h X^i \dot{\partial}_l X^j + \dot{\partial}_{(l} X^{(j} C^{i)}_{|k|h)} X^k \\ &+ C^i_{kh} C^j_{ml} X^k X^m \big) \bar{g}_{ij}\, Dl^l \otimes Dl^h, \end{aligned} \tag{2.14}$$

where ( ) means the symmetric part with respect to the enclosed indices, the sign | | enclosing the index is used to exclude it from the symmetrization operation, and $\bar{g}_{ij}$ are components of the metric tensor in the actual configuration. The interrelated pair of measures of any deformation process (2.13) and (2.14) is defined in the invariant way.

In the case when the internal state is neglected, i.e. $\mathbf{y} = \mathbf{0}$, we obtain

$$\mathbf{C}^h = \big(\partial_h X^i \partial_l X^j + \Gamma^{\star j}_{nl} \Gamma^{\star i}_{kh} X^n X^k\big) \bar{g}_{ij}\, dx^l \otimes dx^h, \tag{2.15}$$

$\mathbf{C}^v$ is identically equal zero, and $\mathbf{X}$ and $\mathbf{g}$ are functions of position $\mathbf{x}$ only. The case $\mathbf{y} = \mathbf{y}_r$ with $\mathbf{y}_r$ being a residual or imperfection vector leads to non-singular $\mathbf{C}^h$ and $\mathbf{C}^v$. To specify the connection coefficients C^i_{jk}, G^i_j and $\Gamma^{\star i}_{jk}$ we first have to estimate the local internal (dislocation) structure of the solid under consideration defining its fundamental function L (square root of the internal energy stored in dislocations and induced by the deformation process) or its metric tensor $\mathbf{g}$.

2.4. Equilibrium equations

The equilibrium equations and boundary conditions are obtained from the variation of the action integral (cf. SACZUK [16])

$$I = \int_G \mathcal{L}(\mathbf{x}, \mathbf{y}, \mathbf{X}, \mathbf{F}^h, \mathbf{F}^v)\, dV, \tag{2.16}$$

where G denotes a fixed, closed and simply-connected region in the 6-dimensional space of $(\mathbf{x}, \mathbf{y})$, bounded by a surface ∂G, and

$$dV = \sqrt{\hat{g}}\, dx^1 dx^2 dx^3 dy^1 dy^2 dy^3 = \sqrt{\hat{g}}\, d\mathbf{x} d\mathbf{y}$$

with $\hat{g} = \det(g_{ij} \oplus g_{ij})$ being the volume element. The variational derivative of the action integral I can be written in the form

$$\delta I = \int_G \Big[\mathcal{L}(D_k \delta x^k + \dot{D}_k \delta y^k) + \mathcal{L}_{|i} \delta x^i + L^{-1} \mathcal{L}|_i\, \delta y^i + \frac{\partial \mathcal{L}}{\partial X^k} \delta X^k + \frac{\partial \mathcal{L}}{\partial_h X_i^k} \delta_h X_i^k + \frac{\partial \mathcal{L}}{\partial_v X_i^k} \delta_v X_i^k \Big] dV, \tag{2.17}$$

where

$$D_i(\cdot) = \partial_i(\cdot) + \frac{\partial(\cdot)}{\partial X^n} \partial_i X^n, \qquad \dot{D}_i(\cdot) = \dot{\partial}_i(\cdot) + \frac{\partial(\cdot)}{\partial X^n} \dot{\partial}_i X^n \tag{2.18}$$

are the total partial derivatives with respect to x^i and y^i, and

$$\mathcal{L}_{|i} = \partial_i \mathcal{L} - \dot{\partial}_k \mathcal{L} \dot{\partial}_i G^k - \mathcal{L} \Gamma^{\star k}_{ik}, \qquad \mathcal{L}|_i = L \dot{\partial}_i \mathcal{L} - \mathcal{L} A^k_{ik} \tag{2.19}$$

are h- and v-derivatives of the density function $\mathcal{L}$, respectively.

The components of generalized body forces are defined by

$${}_h f_k \equiv (\mathbf{f}^h)_k = \frac{\partial \mathcal{L}}{\partial (\mathbf{X}^h)^k}, \qquad {}_v f_k \equiv (\mathbf{f}^v)_k = \frac{\partial \mathcal{L}}{\partial (\mathbf{X}^v)^k}, \tag{2.20}$$

where $\mathbf{f}^h$ is identified with the external body force and $\mathbf{f}^v$ can be identified with the internal source of the exchange of momentum between dislocated states (cf. AIFANTIS [21]).

When variations of the independent variables in δI are neglected, i.e. $\delta \mathbf{x} = \mathbf{0}$ and $\delta \mathbf{y} = \mathbf{0}$, then

$$\delta I = \int_G \left[(\mathbf{f}^h + \mathrm{Div}^h \mathbf{T}) \cdot \delta \mathbf{X}^h + (\mathbf{f}^v + \mathrm{Div}^v \mathbf{T}) \cdot \delta \mathbf{X}^v \right] dV - \int_{\partial G} \left[\delta \mathbf{X}^h \cdot (\mathbf{T}^h \mathbf{n} - \mathbf{T}^h \dot{\partial}_{\mathbf{G}} \mathbf{m}) + \delta \mathbf{X}^v \cdot L \mathbf{T}^v \mathbf{m} \right] dS, \tag{2.21}$$

where

$$
\begin{aligned}
(\mathrm{Div}^h\,\mathbf{T})_k &= D_i({}_hT^i_k) - \dot{\partial}_i G^j \dot{D}_j({}_hT^i_k) - {}_hT^i_j \Gamma^{\star j}_{ki}\,, \\
(\mathrm{Div}^v\,\mathbf{T})_k &= L\dot{D}_i({}_vT^i_k) - {}_vT^i_j A^j_{ki}
\end{aligned}
\tag{2.22}
$$

are h-divergence and v-divergence of $\mathbf{T}$, and n_i, m_i are the components with respect to x^i and y^i of the unit vectors normal to the boundary ∂G, respectively.

One should point out that according to the connections Γ^h and Γ^v, one can distinguish the base space approach and the fibre space approach, respectively (cf. TAKANO [22]). The fundamental lemma of the calculus of variations applied to (2.21) gives the field equations

$$
{}_hf_k + (\mathrm{Div}^h\,\mathbf{T})_k = 0, \qquad {}_vf_k + (\mathrm{Div}^v\,\mathbf{T})_k = 0,
\tag{2.23}
$$

for all variations of $\delta\mathbf{X}^h$ and $\delta\mathbf{X}^v$, or in the component forms

$$
\begin{aligned}
{}_hf_k + \frac{\partial T^i_k}{\partial x^i} - \frac{\partial G^j}{\partial y^i}\frac{\partial T^i_k}{\partial y^j} - T^i_j\Gamma^{\star j}_{ki} &= 0, \\
{}_vf_k + L\frac{\partial T^i_k}{\partial y^i} - T^i_j A^j_{ki} &= 0,
\end{aligned}
$$

which should be satisfied in the interior of the inelastic body. The field equations (2.23), interrelated at the micro-level, form the equilibrium equations for both h- and v-ingredients of the inelastic behaviour of solids.

3. Ideas of a new criterion of adaptation

The classical shakedown criterion which defines the necessary condition of structural safety in the case of variable repeated loads is formulated as follows:

A certain domain of load variations is given and the question arises whether will a given structure will shake down in an arbitrary sequence of the loads contained within this domain.

One of the drawbacks of the classical shakedown theory is that a definite bound of the plastic work is not specified in the shakedown criterion (KÖNIG [23]). A definite amount of this work is at any rate of fundamental value for an adaptation and can be used, among others, to establish a safe number of load cycles for the structure's life. For that reason modifications in the classical criterion of adaptation seem to be necessary.

3.1. Motivation

A more realistic assessment of structural safety demands to change the way of estimation of the energy function used in the shakedown theorem, according to the methodology of Finslerian description of solid behaviour. The source of our idea comes from the proof of shakedown theorem (cf. GROSS–WEEGE [8], SACZUK and STUMPF [9]). In this proof we have to estimate the time-dependent energy function Π in the form

$$\Pi(t) = \frac{1}{2}\int_V \mathbf{T}\cdot\mathbf{F}\, dV,$$

where $\mathbf{T}$ is the first Piola – Kirchhoff stress tensor and $\mathbf{F}$ is the deformation gradient tensor. We analyze the time derivative of Π by decomposing its right-hand side according to the following scheme:

$$\partial_t\Pi = -\int_V (\check{\mathbf{S}} - \bar{\mathbf{S}})\cdot\partial_t\check{\mathbf{E}}^p dV + \int_V (\check{\mathbf{T}} - \bar{\mathbf{T}})\cdot\partial_t\check{\mathbf{H}}\mathbf{F} dV$$

$$\downarrow \qquad\qquad \downarrow$$

the convexity conditions — equilibrium conditions

$$\downarrow \qquad\qquad \downarrow$$

decreases when $\check{\mathbf{E}}^p \neq \mathbf{0}$ — $\mathbf{0}$

where $\check{\mathbf{S}}$ is the actual residual (second Piola – Kirchhoff) stress tensor, $\bar{\mathbf{S}}$ is a (fictitious) shakedown stress tensor, $\check{\mathbf{E}}^p$ is the residual plastic strain tensor obtained from the multiplicative decomposition of the deformation gradient tensor, and $\check{\mathbf{H}}$ is the residual displacement gradient.

The above estimation of $\partial_t\Pi$ we replace by

$$\partial_t\Pi(t, \hat{\mathbf{C}}) \leq \beta \parallel \partial_{\hat{\mathbf{C}}}\Pi(t, \hat{\mathbf{C}}) \parallel + \psi(t, \Pi(t, \hat{\mathbf{C}})), \tag{3.1}$$

where $\hat{\mathbf{C}}$ is the Cauchy – Green strain tensor, β is a constant connected with a safe domain of admissible strains and ψ is a comparison function being a maximal solution of a comparison differential problem used to estimate Π. The basic problem here is how to define the comparison function. Before that we will introduce the notion of the maximal solution of a differential problem and the comparison differential theorem within the theory of differential inequalities (LAKSHMIKANTHAM and LEELA [15], SZARSKI [14]). Let us note that differential inequalities are extremely important and constitute a very helpful technique in the differential problems to formulate the uniqueness conditions for their solutions and to make their certain estimations.

Assume that $I = [t_0, T) \subset R$, $0 < t_0 < T$ is a time-interval, $G \subset R^2$ is an open set in R^2.

DEFINITION 1. *Let r be a solution of a differential problem*

$$u' = \psi(t,u), \qquad u(t_0) = u_0, \qquad t \in I \tag{3.2}$$

and $\psi \in C(G,R)$. Then r is said to be a maximal solution of (3.2) *if*

$$u(t) \leq r(t), \qquad t \in I \tag{3.3}$$

for every solution u of (3.2) *in I.*

COMPARISON THEOREM (LAKSHMIKANTHAM and LEELA [15], Vol. I)
Suppose:
1. *$\psi \in C(G,R)$ and r is the maximal solution of* (3.2).
2. *$m \in C(I,R)$, $(t,m(t)) \in G$ for $t \in I$, $m(t_0) \leq u_0$, and*

$$Dm(t) \leq \psi(t,m(t)), \qquad t \in I \backslash S \tag{3.4}$$

with D being a fixed Dini derivative and S at most a countable subset of I. Then

$$m(t) \leq r(t) \qquad \text{in} \quad I. \tag{3.5}$$

3.2. A comparison problem

A comparison function ψ in (3.1) is identically equal zero in the classical case. This takes place when the microstructure-independent equilibrium conditions for $\check{\mathbf{T}}$ and $\bar{\mathbf{T}}$ are satisfied *a priori*. Therefore, the equilibrium conditions, or more strictly the equations of motion, will be used to define the comparison function ψ.

Our comparison problem will be defined by differential equations, deduced from the equations of motion in the continuum with microstructure (cf. Eqs. (2.23))

$$\rho_0 \, {}_h\dot{v}_k = {}_hf_k + \frac{\partial T^i_k}{\partial x^i} - \frac{\partial G^j}{\partial y^i}\frac{\partial T^i_k}{\partial y^j} - T^i_j \Gamma^{\star j}_{ki}, \tag{3.6}$$

$$\rho_0 \, {}_v\dot{v}_k = {}_vf_k + L\frac{\partial T^i_k}{\partial y^i} - T^i_j A^j_{ki}, \tag{3.7}$$

where ${}_hv_k$ and ${}_vv_k$ are components of macro- and micro-velocity. The remaining unknowns were defined in Sec. 2. The first equation describes the macro-motion of the body (in the configuration space), while the second one its micro-motion (in the internal state space), or briefly h-motion and v-motion.

For clarity, the above partial differential equations are reduced to the scalar differential equations of the form

$$\dot{v}^h = \psi^h(t,v^h), \tag{3.8}$$

$$\dot{v}^v = \psi^v(t,v^v) \tag{3.9}$$

using an Euclidean norm $\| \mathbf{a} \| = \sqrt{(\mathbf{a} \cdot \mathbf{a})}$ under the following assumptions. If body forces $\mathbf{f}^h$ and $\mathbf{f}^v$ are neglected and classical equilibrium conditions $\partial_i T_k^i = 0$ and $\dot{\partial}_i T_k^i = 0$ are satisfied inside the body, then the right-hand sides in (3.6) and (3.7) lead to the following identifications:

$$\mathbf{\Gamma}^\star \propto \frac{1}{x} \frac{y^1}{y}, \qquad \mathbf{A} \propto \frac{1}{y}, \tag{3.10}$$

where $y = \sqrt{(y^1)^2 + (y^2)^2 + (y^3)^2}$ is the Euclidean distance in the internal state space. The identification used in (3.10) is due to the following form of L:

$$L^2(\mathbf{x}, \mathbf{y}) = g_{ij}(\mathbf{x}, \mathbf{y}) y^i y^j = \frac{2x^1 y^1}{y} (y^1)^2 + 2x^2 (y^2)^2 + 2x^3 (y^3)^2.$$

This assumed relation, identified here with the internal energy stored in dislocations, is proportional to the square of the microposition vector.

According to equations (3.8) and (3.9) one can write the admissible functions in the form

$$\psi^h = \frac{v^h}{x} \frac{y^1}{y}, \qquad \psi^v = \frac{v^v}{y}$$

and, then, their solutions under homogeneous initial conditions are respectively equal

$$v^h = \exp\left(\frac{y^1}{xy} t\right), \qquad v^v = \exp\left(\frac{t}{y}\right). \tag{3.11}$$

3.3. Method of solution

The language of the theory of differential inequalities (LAKSHMIKANTHAM and LEELA [15], SZARSKI [14]) is used to provide a general definition of "adaptation" of structures. Within this methodology it is sufficient to assume:

1. There exist (experimental or other) time-dependent comparison functions ψ^h and ψ^v defined in a certain domain Ω of the strain-time space.

2. The estimation (3.1) takes place at any instant of time t.

Then, according to the comparison theorem (cf. SZARSKI [14], Chap. 7, LAKSHMIKANTHAM and LEELA [15], Chap. 9) one can make the following estimations

$$\Pi^h(t, \mathbf{C}^h) \leq r^h(t), \tag{3.12}$$

$$\Pi^v(t, \mathbf{C}^v) \leq r^v(t), \tag{3.13}$$

where r^h and r^v are the maximal solutions (see Definition 1) of the differential problems induced by ψ^h and ψ^v, respectively, i.e. at the given time interval the

energy function is estimated by known *a priori* time-dependent functions. In this case we have to find the time-dependent comparison functions ψ^h and ψ^v, instead of a time-independent residual stress field postulated by the classical shakedown criterion (MELAN [2], KOITER [1]). The condition (3.1) is the asymptotic estimation of the rate of energy function. Moreover, the energy function $\Pi = \Pi^h + \Pi^v$ is the position-direction dependent function. It should be emphasized that the variable t can here mean either the time or a monotonically-increasing loading parameter. The presented explanation allows us to propose

DEFINITION 2. *It is said that the structure will shake down over any programme of loading if the total energy created during its deformation satisfies* (3.12) *and* (3.13) *at any time interval of that programme.*

Note that the classical shakedown demands only boundedness of the total plastic work in the limit as the time approaches infinity. To define the plastic energy for defining a criterion of adaptation, one has to decompose the total strain tensor into elastic and plastic parts. In the classical approach it is generally realized within the multiplicative decomposition of the deformation gradient using the unstressed intermediate configuration concept, while in the Finslerian one the additive decomposition is given by definition. The shortcoming of such the additive decomposition lies in that a common sense of elastic and plastic part of the deformation is slightly changed. It is due to the fact that any deformation process cannot be strictly decomposed into elastic and plastic parts [16]. For simplicity, one can consider the state of strain in the structure that does not vary with position in it. Then the deformation gradient $\widehat{\mathbf{F}}$ is a function of the microposition vector $\mathbf{y}$. Summarizing the quoted explanations we assume:

1. The total (strain) energy is defined as a time-dependent energy function

$$\Pi(t, \widehat{\mathbf{C}}) = \int_V (\mathbf{T}^h \cdot \mathbf{C}^h + \mathbf{T}^v \cdot \mathbf{C}^v)\, dV,$$

where the Cauchy–Green strain tensors $\mathbf{C}^h$ and $\mathbf{C}^v$ are defined by (2.13) and (2.14), and appropriate stress tensors from (2.23), for given $\mathbf{f}^h$ and $\mathbf{f}^v$, respectively.

2. We also establish by calculation or using experimental results the safe domain Ω, required to any individual shakedown problem, and the comparison functions ψ^h and ψ^v.

3.4. Algorithm

The above explanation can be arranged in the following algorithm.

For $i = 1, n$

$(i, 1)$ Calculate the strain state of the body for a given loading programme and an assumed internal state, or basing on experimental data connected with internal state of its material;

$(i,2)$ Define the strain energy function;

$(i,3)$ Define the function of a comparison problem;

$(i,4)$ Find the maximal solution of the comparison problem;

$(i,5)$ Verify the conditions of adaptation (see Shakedown Theorem).

The steps from (i,2) to (i,5) are changed according to a demand. The index i can symbolize a number of states which are relevant for a prediction of the safe domain in the space of admissible strains. In general, an optimization technique is necessary to define the safe domain of adaptation for the given structure.

4. A proposition of the shakedown theorem

Under the preparation of Sec. 3 we come to the following theorem

SHAKEDOWN THEOREM:

(i) *Suppose that* $r^h(t,t_0,v_0^h)$ *and* $r^v(t,t_0,v_0^v)$ *are the maximal solutions of the scalar differential problems*

$$\dot{v}^h = \psi^h(t,v^h) \equiv \frac{1}{\rho_0} \parallel \mathrm{Div}^h \mathbf{T} + \mathbf{f}^h \parallel, \qquad v^h(t_0) = v_0^h \equiv \parallel \mathbf{C}_0^h \parallel, \tag{4.1}$$

$$\dot{v}^h = \psi^v(t,v^v) \equiv \frac{1}{\rho_0} \parallel \mathrm{Div}^v \mathbf{T} + \mathbf{f}^v \parallel, \qquad v^v(t_0) = v_0^v \equiv \parallel \mathbf{C}_0^v \parallel . \tag{4.2}$$

(ii) *Suppose that the energy function* $\Pi(t,\widehat{\mathbf{C}}) = \Pi^h + \Pi^v$ *possesses continuous partial derivatives* $\partial_t\Pi$ *and* $\partial_C\Pi$ *on*

$$\Omega = \Big\{(t,C):\ t_0 \le t \le t_0 + a, \quad C = \parallel \widehat{\mathbf{C}} \parallel \le \alpha - \beta(t-t_0)\Big\}. \tag{4.3}$$

(iii) *The following inequalities are satisfied on* Ω*:*

$$\partial_t\Pi^h \le \beta \parallel \partial_{\mathbf{C}^h}\Pi^h(t,\mathbf{C}^h) \parallel + \psi^h(t,\Pi^h(t,\mathbf{C}^h)), \tag{4.4}$$

$$\partial_t\Pi^v \le \beta \parallel \partial_{\mathbf{C}^v}\Pi^v(t,\mathbf{C}^v) \parallel + \psi^v(t,\Pi^v(t,\mathbf{C}^v)). \tag{4.5}$$

Then,

$$\Pi^h(t_0,\mathbf{C}^h) \le v_0^h, \tag{4.6}$$

$$\Pi^v(t_0,\mathbf{C}^v) \le v_0^v \tag{4.7}$$

for $C \le \beta$ *implies*

$$\Pi^h(t,\mathbf{C}^h) \le r^h(t,t_0,v_0^h), \tag{4.8}$$

$$\Pi^v(t,\mathbf{C}^v) \le r^v(t,t_0,v_0^v), \tag{4.9}$$

i.e. the body shakes down under the given loading programme.

REMARK 1. The inequalities (4.6) and (4.7) define initial conditions for the strain state. In fact, they can be neglected as in the classical shakedown theorem, if we shall remember that strains in reality are not arbitrary quantities, but have always definite values. These conditions mean simply that an analyzed initial strain state is inside the domain Ω.

Proof of the Shakedown Theorem is analogous to the proof of Theorem 9.2.1 in LAKSHMIKANTHAM and LEELA [15]. In this proof, in the spirit of the Comparison Theorem, we have to estimate the function

$$m(t) = \max_{\|\widehat{\mathbf{C}}\| \leq \alpha - \beta(t-t_0)} \Pi(t, \widehat{\mathbf{C}}), \tag{4.10}$$

which satisfies the differential inequality (3.4), using the extremal solutions $r^h(\cdot, t_0, \| \mathbf{C}_0^h \|)$ and $r^v(\cdot, t_0, \| \mathbf{C}_0^v \|)$ of the corresponding differential equations (4.1) and (4.2) under conditions (4.6) and (4.7), respectively.

There are two observations which we would like to make with respect to the presented technique. In the first place, the presented idea of new criterion of adaptation can be treated as an example, and its extension to more complicated cases is also possible (cf. LAKSHMIKANTHAM and LEELA [15]). For a more detailed and rigorous discussion of the generalized cases the reader is referred to the cited literature. The second observation is that the fundamental conditions used in Shakedown Theorem depend on a particular internal strain distribution. This information is of fundamental importance since the mechanical response of the solid like softening, hardening, localization is only changed by the history of deformation and the applied load system (BASINSKI and JACKSON [24]).

5. Conclusions

The importance of shakedown theorems depends on proving that if the structure shakes down under some particular programme of loading, it will shake down under any loading programme. The proposed shakedown theorem can be used to predict the behaviour of structures based on the properties of the energy function and its internal energy distribution. As final conclusions one may cite:

1. It generalizes the classical approaches (MELAN [2], KOITER [1], CORRADI and MAIER [11], KÖNIG and SIEMASZKO [12]) by including arbitrary deformations and material nonlinearities.

2. It is based on the consistent continuum theory of solid behaviour which allows one to describe, among others, the specific internal structure of the material, the influence of initial deformations or imperfections of the deformation process within the unified concept.

3. It can be used to estimate a safe number of load cycles for the real or predicted structure's life.

4. It can be used to estimate lower and upper limits of the total (or plastic under certain conditions) work in the given time interval.

A. Appendix. Basic notions in Finslerian geometry

In this appendix we give the mathematical preliminaries on Finslerian geometry (RUND [17], MATSUMOTO [18]), especially on the definitions of connections, absolute differential and covariant derivatives.

A Finslerian (generalized metric) geometry is a natural generalization of a Riemannian one and of which a metric tensor depends both on the position and on the direction. Following BUSEMANN [25] the Finsler space is a metric, finitely compact (i.e. every bounded, infinite sequence of points in a metric space contains a converging subsequence) and locally Minkowskian space. The anisotropic character (the Minkowskian metric is not symmetric in general) of this geometry is expressed completely by the physically useful concept of indicatrix. Therefore, common inelastic solid behaviours like anisotropy and hysteresis loop are modelled easily within this geometry. The major obstacle encountered in the practical application of this geometry is caused by its complexity and a difficulty of using its concepts to define mechanical counterparts.

The subject is described in the monographs of RUND [17], ASANOV [26], MATSUMOTO [18], ABATE and PATRIZIO [27], ANTONELLI and MIRON [28] where additional bibliography can be found. In this appendix we shall use the notation employed mainly in [18] and [17] without further comments.

A.1. Basic concepts

We consider an n-dimensional differentiable manifold M (cf. CHOQUET–BRUHAT *et al.* [29, Ch. III], WESTENHOLTZ [30, Parts II and V]) as the space for modelling of a solid behaviour. Let T_xM be the tangent space of M at a point $\mathbf{x}$, and $T(M)$ be the set of all tangent vectors parameterized by M. The mapping (projection) $\pi_T : T(M) \to M$ is defined by $\pi_T(\mathbf{y}) = \mathbf{x}$ for $\mathbf{y} \in T_xM$. Let $L(M)$ be the linear frame bundle of the manifold M. The projection $\pi_L : L(M) \to M$ is given by $(\mathbf{x}, \mathbf{z}) \to \mathbf{z}$, where a frame $\mathbf{z}$ at a point $\mathbf{x}$ of M is by definition a base $\mathbf{z} = \{z_i\}_{1,\ldots,n}$ of the tangent vector space T_xM.

The Finsler bundle $F(M)$ of M is, by definition [18], the principal bundle $\pi_T^{-1}L(M)$ over $T(M)$ induced from the frame bundle $L(M)$ by the projection π_T of the tangent bundle $T(M)$. This construction is represented by the following commutative diagram

$$\begin{array}{ccccc} (\mathbf{y}, \mathbf{z}) \in F(M) & \xrightarrow{\pi_2} & L(M) & \ni & (\mathbf{x}, \mathbf{z}) \\ \pi_1 \downarrow & & \downarrow \pi_L & & \\ (\mathbf{x}, \mathbf{y}) \in T(M) & \xrightarrow{\pi_T} & M & \ni & (\mathbf{x}) \end{array}$$

where π_T, π_L and π_1, π_2 are projections.

To introduce a Finsler connection $F\Gamma$ it is worth reminding that a (nonlinear) connection N on M is a distribution $\mathbf{y} \in T(M) \mapsto N_y$ in the $T(M)$ satisfying $T_y = N_y \oplus T_y^v$, namely, the tangent space T_y at every point $\mathbf{y}$ of $T(M)$ is the direct sum of N_y and the vertical subspace T_y^v.

A vertical connection Γ^v is a distribution $u \in F(M) \mapsto \Gamma_u^v$ in the $F(M)$ such that the restriction $\Gamma^v|_{F(x)}$ of Γ^v of the subbundle $F(x)$ of $F(M)$ over the fibre $\pi_\tau^{-1}(x)$ over every point $\mathbf{x} \in M$ is an ordinary connection in $F(x)$. In turn, the horizontal connection Γ^h is a distribution $u \in F(M) \mapsto \Gamma_u^h$ in $F(M)$ satisfying

$$T_u F(M) = \Gamma_u^h \oplus \Gamma_u^v \oplus T_u F(M)^v, \tag{A.1}$$

$$\tau_g' \Gamma_u^h = \Gamma_{ug}^h, \tag{A.2}$$

where $T_u F(M)^v$ is the vertical subspace of the tangent space $T_u F(M)$ and τ_g is a right translation of $F(M)$ by $g \in GL(n, R)$. Other equivalent ways leading to the Finsler connection have been discussed by MATSUMOTO [18].

The h-part Γ^h of the Finsler connection $F\Gamma = (\Gamma^h, \Gamma^v)$ is spanned by the h-basic vector field $\mathbf{B}^h(\mathbf{v})$, $\mathbf{v} \in V$, V – a vector space, of the form (MATSUMOTO [31])

$$\mathbf{B}^h(\mathbf{v}) = z_a^i v^a \left(\frac{\partial}{\partial x^i} - N_i^j \frac{\partial}{\partial y^j} - z_b^k F_{ki}^j \frac{\partial}{\partial z_b^j} \right), \tag{A.3}$$

at a point $u = (x^i, y^i, z_a^i)$ and for $\mathbf{v} = (v^a)$, where (x^i, y^i, z_a^i) are local coordinates on $F(M)$ induced from local coordinates (x^i) on M. The connection coefficients F_{ki}^j are defined by $F_{ki}^j = \Gamma_{ki}^j - C_{kr}^j N_i^r$; following RUND [17] they will be denoted by Γ_{ki}^{*j}.

The v-part Γ^v of the Finsler connection $F\Gamma = (\Gamma^h, \Gamma^v)$ is spanned by the v-basic vector field $\mathbf{B}^v(\mathbf{v})$, $\mathbf{v} \in V$, of the form (MATSUMOTO [31])

$$\mathbf{B}^v(\mathbf{v}) = z_a^i v^a \left(\frac{\partial}{\partial y^i} - z_b^i C_{ki}^j \frac{\partial}{\partial z_b^j} \right), \tag{A.4}$$

where functions $C_{ki}^j(\mathbf{x}, \mathbf{y})$ are connection parameters of the vertical connection Γ^v.

The h- and v-covariant derivatives of an arbitrary Finsler tensor field K [18] are defined, within the bundle theory, by

$$\nabla^h K(\mathbf{v}) = \mathbf{B}^h(\mathbf{v}) \cdot K, \tag{A.5}$$

$$\nabla^v K(\mathbf{v}) = \mathbf{B}^v(\mathbf{v}) \cdot K, \tag{A.6}$$

for any $\mathbf{v} \in V$. The components of $\nabla^h(\,)$ and $\nabla^v(\,)$ are usually distinguished by "$|$" and "$\mid$", respectively (cf. (A.17) and (A.18)).

The torsion tensor fields $\mathbf{T}^1$, $\mathbf{R}^1$, $\mathbf{C}^1$, $\mathbf{P}^1$, $\mathbf{S}^1$ ($\mathbf{T}^1$ and $\mathbf{C}^1$ are often denoted by $\mathbf{T}$ and $\mathbf{C}$, respectively, cf. RUND [17]) and the curvature tensor fields $\mathbf{R}^2$, $\mathbf{P}^2$, $\mathbf{S}^2$ of a Finsler connection $F\Gamma$ are introduced by the structure equations

$$
\begin{aligned}
[\mathbf{B}^h(1), \mathbf{B}^h(2)] &= \mathbf{B}^h(\mathbf{T}^1(1,2)) + \mathbf{B}^v(\mathbf{R}^1(1,2)) + \mathbf{Z}(\mathbf{R}^2(1,2)),\\
[\mathbf{B}^h(1), \mathbf{B}^v(2)] &= \mathbf{B}^h(\mathbf{C}^1(1,2)) + \mathbf{B}^v(\mathbf{P}^1(1,2)) + \mathbf{Z}(\mathbf{P}^2(1,2)),\\
[\mathbf{B}^v(1), \mathbf{B}^v(2)] &= \mathbf{B}^v(\mathbf{S}^1(1,2)) + \mathbf{Z}(\mathbf{S}^2(1,2)),
\end{aligned}
\tag{A.7}
$$

where $\mathbf{v}_1$, $\mathbf{v}_2 \in V$ are present by their indices 1, 2 only. Here $\mathbf{Z}(A)$ is the fundamental vector field on $F(M)$ corresponding to the element A of the Lie algebra of $GL(n, R)$.

The torsion and curvature tensors are called as follows:

$\mathbf{T}^1$ is $(h)h$-torsion,	$\mathbf{R}^1$ is $(v)h$-torsion,	$\mathbf{R}^2$ is h-curvature,
$\mathbf{C}^1$ is $(h)hv$-torsion,	$\mathbf{P}^1$ is $(v)hv$-torsion,	$\mathbf{P}^2$ is hv-curvature,
$\mathbf{S}^1$ is $(v)v$-torsion,	$\mathbf{S}^2$ is v-curvature.	

DEFINITION A.1. *A Finsler connection $F\Gamma$ of a Finsler space $F(M)$ with a fundamental function L is the Cartan connection if*:

(i) $\nabla^h \mathbf{g} = \mathbf{0}$ *and* $\mathbf{T}^1 \equiv \mathbf{0}$;

(ii) $\nabla^v \mathbf{g} = \mathbf{0}$ *and* $\mathbf{S}^1 \equiv \mathbf{0}$;

(iii) *The deflection tensor field* $\mathbf{D} = \nabla^h \mathbf{y}$ *is given.*

In practice $\mathbf{D} \equiv \mathbf{0}$. This condition means that nonlinear connection coefficients N^i_j are defined by horizontal connection coefficients $\Gamma^{\star i}_{rj}$ as $N^i_j = \Gamma^{\star i}_{rj} y^r$.

The triplet $F\Gamma = (F^i_{jk}, N^i_k, C^i_{jk})$ is known as the Finsler connection. Before determining the Finsler connection $F\Gamma$ one has to introduce the Finsler metric. In this geometry the differentiable manifold M is equipped with a line element $ds = L(\mathbf{x}, d\mathbf{x})$, where the function L, homogeneous of degree one in $d\mathbf{x}$, is called the fundamental function of the Finsler space. Its geometric significance results from the fact that in each tangent space $T_x M$ of M the function $L(\mathbf{x}, \mathbf{y})$ defines the $(n-1)$-dimensional hypersurface,

$$L(\mathbf{x}, \mathbf{y}) = 1, \tag{A.8}$$

called the indicatrix, where $\mathbf{x}$ is assumed to be fixed. The concept of the indicatrix (YASUDA [32], MATSUMOTO [33], WATANABE [34]), as developed by modern geometry, provides a precise explanation of the main geometric properties of a given manifold. The definition (A.8) represents a sphere in the Riemannian case.

Physically, one can construct the fundamental function L using a relation

$$L(\mathbf{x}, \mathbf{y}) = \sqrt{W(\mathbf{x}, \mathbf{y})}, \tag{A.9}$$

where the function W, homogeneous of the second degree with respect to $\mathbf{y}$, can be interpreted as a stored energy in dislocations and induced by the deformation process. One should stress that the geometric structure of a yield surface in elasto-plasticity falls under the general concept of indicatrix of the Finsler space. The most evident analogy between the indicatrix and the classical yield surface is that they both are closed convex hypersurfaces in the 6-dimensional spaces. The first one is in the 6-dimensional (x, y)-space of the Finsler bundle, the second one is in the 6-dimensional x-space of symmetric stress or strain tensors (the stress or strain space). The further analogies are not so evident due to their different geometro-physical meanings. For example, the indicatrix can represent an abstract model of internal structure of the given solid, while the yield surface has a sense of the surface separating an elastic region from a plastic one. In other words, the indicatrix is the fundamental geometric object of underlying (physical) space for any solid, while the yield surface is a certain auxiliary notion of criterion type used to distinguish between loading and unloading criteria. In Finslerian approach such a distinction can be superfluous.

The function $L = L(\mathbf{x}, \mathbf{y})$ satisfies, by assumptions, the following two conditions:

(i) The function L is at least of class C^3 with respect to $\mathbf{x}$;

(ii) The function L is positive homogeneous of degree one with respect to $\mathbf{y}$.

The homogeneity condition (ii) plays an important role in the Finsler geometry. The application of the Euler theorem on homogeneous functions to L^2 gives

$$L^2(\mathbf{x}, \mathbf{y}) = g_{ij}(\mathbf{x}, \mathbf{y}) y^i y^j, \tag{A.10}$$

where

$$g_{ij}(\mathbf{x}, \mathbf{y}) = \frac{1}{2} \dot{\partial}_i \dot{\partial}_j L^2(\mathbf{x}, \mathbf{y}) \tag{A.11}$$

is the Finslerian metric tensor.

For example, the Riemannian space as a special case of the Finsler space demands

$$ds^2 = g_{ij}(x) dx^i dx^j \equiv L^2(\mathbf{x}, d\mathbf{x}),$$

where the metric tensor is defined by

$$g_{ij}(\mathbf{x}) = \frac{1}{2} \frac{\partial^2 L^2}{\partial dx^i \partial dx^j}. \tag{A.12}$$

Using the relation $y_i = g_{ij}(\mathbf{x}, \mathbf{y}) y^j$, from (A.10) we obtain $y_i = L \dot{\partial}_i L$. Then the unit tangent vector

$$l_i = \frac{y_i}{L(\mathbf{x}, \mathbf{y})} = \dot{\partial}_i L(\mathbf{x}, \mathbf{y}) = g_{ij}(\mathbf{x}, \mathbf{y}) l^j. \tag{A.13}$$

The definition (A.11) (cf. Definition A.1) allows us to define, among others, connection coefficients (A.20)–(A.23) as functions of L only. For example, the so-called Cartan torsion tensor is then defined from

$$C_{ijk}(\mathbf{x},\mathbf{y}) = \frac{1}{4}\dot{\partial}_i\dot{\partial}_j\dot{\partial}_k L^2(\mathbf{x},\mathbf{y}). \tag{A.14}$$

The remaining torsion tensors, curvature tensors, Cartan structure equations are discussed by RUND [17], MATSUMOTO [18].

A.2. Covariant derivatives

The definitions of covariant derivatives (A.5) and (A.6) restricted to the Cartan connection (Definition A.1) can be introduced as follows. Consider an $(\mathbf{x},\mathbf{y})$-dependent tensor $\mathbf{T} = \mathbf{T}(\mathbf{x},\mathbf{y})$, then the absolute differential and covariant derivatives are defined by

$$DT^j_k = T^j_{k|i}dx^i + T^j_k|_i\, Dl^i, \tag{A.15}$$

or, in the absolute tensor notation, by

$$D\mathbf{T} = \nabla^h_i\mathbf{T}\otimes dx^i + \nabla^v_i\mathbf{T}\otimes Dl^i, \tag{A.16}$$

where

$$T^j_{k|i} = \partial_i T^j_k - \dot{\partial}_i G^l \dot{\partial}_l T^j_k + \Gamma^{\star j}_{lk}T^l_i - \Gamma^{\star l}_{ik}T^j_l\,, \tag{A.17}$$

$$T^j_k|_i = L\dot{\partial}_i T^j_k + A^j_{il}T^l_k - A^l_{ik}T^j_l \tag{A.18}$$

are h-derivative and v-derivative, respectively, and

$$Dl^i = dl^i + \Gamma^i_{jk}y^k dy^j \tag{A.19}$$

is the absolute differential of the unit tangent vector (A.13). To define the remaining quantities in (A.17) and (A.18) one has to use Definition A.1 (RUND [17], MATSUMOTO [18]). In this case they are given as follows:

$$\Gamma^\star_{ijk} = \Gamma_{ijk} - C_{jkl}\frac{\partial G^l}{\partial y^i} = \gamma_{ijk} - C_{kjl}\frac{\partial G^l}{\partial y^i} - C_{ijl}\frac{\partial G^l}{\partial y^k} + C_{ikl}\frac{\partial G^l}{\partial y^j}\,, \tag{A.20}$$

$$\Gamma^\star_{ijk} = g_{jl}\Gamma^{\star l}_{ik}\,, \qquad \Gamma_{ijk} = g_{jl}\Gamma^l_{ik}y^j, \qquad 2G^l = \gamma^l_{jk}y^j y^k, \tag{A.21}$$

$$\dot{\partial}_k G^l = \frac{\partial G^l}{\partial y^k} = \Gamma^l_{jk}y^j = \Gamma^{\star l}_{jk}y^j, \qquad \gamma_{ijk} = \frac{1}{2}\left(\frac{\partial g_{ij}}{\partial x^k} + \frac{\partial g_{jk}}{\partial x^i} - \frac{\partial g_{ki}}{\partial x^j}\right), \tag{A.22}$$

$$\begin{aligned} &C_{ijk} = \frac{1}{2}\frac{\partial g_{ij}}{\partial y^k}\,, \qquad C_{ijk}y^k = C_{ijk}y^j = C_{ijk}y^i = 0,\\ &C_{ijk} = g_{jl}C^l_{ik}\,, \qquad A^i_{jk} = LC^i_{jk}\,. \end{aligned} \tag{A.23}$$

In particular,

$$X^k_{|j} = \partial_j X^k - \dot\partial_j G^n \dot\partial_n X^k + \Gamma^{*k}_{nj} X^n, \tag{A.24}$$

$$X^k|_j = L\dot\partial_j X^k + A^k_{ij} X^i \tag{A.25}$$

for a contravariant vector field $\mathbf{X} = \mathbf{X}(\mathbf{x}, \mathbf{y})$, and

$$f_{|j} = \partial_j f - \dot\partial_j G^k \dot\partial_k f, \tag{A.26}$$

$$f|_j = L\dot\partial_j f \tag{A.27}$$

for a scalar field $f = f(\mathbf{x}, \mathbf{y})$.

Instead of using (A.5) and (A.6) to define the absolute differential and covariant derivatives, one can apply the linear mapping

$$\nabla_{\mathbf{X}} : TF(M) \to TF(M), \qquad \mathbf{Y} \mapsto \nabla_{\mathbf{X}}\mathbf{Y} \tag{A.28}$$

for any $\mathbf{X}, \mathbf{Y} \in TF(M)$. To obtain a desirable result we can proceed as follows.

In Finsler spaces all quantities are depend both on the position vector ($\mathbf{x}$) and the direction vector ($\mathbf{y}$). If we define coordinate transformations by

$$\bar x^a = f^a(x), \qquad \bar y^a = \frac{\partial \bar x^a}{\partial x^j} y^j, \qquad \operatorname{rank}\left[\frac{\partial \bar x^a}{\partial x^j}\right] = n \tag{A.29}$$

and, if there exist the quantities $N^a_j(\mathbf{x}, \mathbf{y})$ which transform under (A.29) according to the rule

$$\frac{\partial^2 \bar x^a}{\partial x^j \partial x^k} y^k = \frac{\partial \bar x^a}{\partial x^k} N^k_j - \frac{\partial \bar x^b}{\partial x^j} \bar N^a_b,$$

then one can define the covariant differential operator by

$$\frac{\delta}{\delta x^k} = \frac{\partial}{\partial x^k} - N^i_k \frac{\partial}{\partial y^i} \qquad \text{or} \qquad \delta_k = \partial_k - N^i_k \dot\partial_i . \tag{A.30}$$

The quantities N^i_k in the light of Definition A.1 are equal to $\dot\partial_k G^i$. It is important to note that the basis $(\partial_i, \dot\partial_i)$, with respect to the coordinate transformation (A.29), does not transform as a vector, while the basis $(\delta_i, \dot\partial_i)$ has the desired property (cf. ČOMIĆ [35]). The dual basis to $(\delta_i, \dot\partial_i)$ is denoted by (dx^i, Dy^i), where

$$Dy^i = dy^i + N^i_k dx^k.$$

Any vector field $\mathbf{X}$ in $TF(M)$ can be represented in the basis $(\delta_i, \dot\partial_i)$ in the following form

$$\mathbf{X} = \mathbf{X}^h + \mathbf{X}^v = X^i \delta_i + X^a \dot\partial_a , \tag{A.31}$$

where we call $\mathbf{X}^h = X^i \delta_i$ the horizontal vector field, and $\mathbf{X}^v = X^a \dot{\partial}_a$ the vertical vector field. Generalization to more complex geometric object is straightforward.

Under this preparation, if we take $X^i = dx^i$ and $X^a = Dy^a$ in $D\mathbf{T} = \nabla_{\mathbf{X}}\mathbf{T}$, the relation (A.16) can be alternatively written as

$$D\mathbf{T} = \nabla_{\delta_i}\mathbf{T} \otimes dx^i + \nabla_{\dot{\partial}_i}\mathbf{T} \otimes Dy^i.$$

Analogously to the Riemannian geometry, the Cartan covariant derivatives are defined to be metric, i.e.

(A.32) $$g_{ik|j} = 0, \qquad g_{ik}\,|_j = 0.$$

In addition

(A.33) $$l^k_{|j} = y^k_{|j} = L_{|j} = 0, \qquad L\,|_j = y_j\,, \qquad y^i|_j = L\delta^i_j\,, \qquad y_i|_j = Lg_{ij}\,.$$

The identities (A.32) and (A.33) show that the metric tensor g_{ik}, the metric function L, and the tangent vectors y^i and l^i can be treated as constants for the h-derivative. In the case of v-derivative this is true only for the metric tensor g_{ik}.

References

1. W.T. KOITER, *General theorems for elastic-plastic solids*, [in:] Progress in Solid Mechanics, pp. 165– 221, J.N. SNEDDON and R. HILL [Eds.], North–Holland, Amsterdam 1960.
2. E. MELAN, *Theorie statisch unbestimmter Systeme aus ideal-plastischem Baustoff*, Sitzungsbericht der Akad. D. Wiss. (Wien), Akt. IIa, **145**, 195–218, 1936.
3. J. MANDEL, *Adaptation d'une structure plastique écrouissable et approximations*, Mech. Res. Comm., **3**, 483–488, 1976.
4. J.A. KÖNIG, *On stability of the incremental collapse process*, Arch. Inż. Ląd., **26**, 219–229, 1980.
5. C. POLIZZOTTO, *A unified treatment of shakedown theory and related bounding techniques*, SM Arch., **7**, 19–75, 1982.
6. D. WEICHERT, *On the influence of geometrical nonlinearities on the shakedown of elastic-plastic structures*, Int. J. Plast., **2**, 135–148, 1986.
7. D. WEICHERT, *Advances in the geometrically nonlinear shakedown theory*, [in:] Inelastic Solids and Structures, pp. 489–502, M. KLEIBER and J.A. KÖNIG [Eds.], Pineridge Press, Swansea 1990.
8. J. GROSS–WEEGE, *A unified formulation of statical shakedown criteria for geometrically nonlinear problems*, Int. J. Plast., **6**, 433–447, 1990.
9. J. SACZUK and H. STUMPF, *On statical shakedown theorems for non-linear problems*, Mitt. Inst. für Mech., Ruhr–Univ. Bochum, **74**, 1990.
10. J. SACZUK, *On theorems of adaptation of elastic-plastic structures*, [in:] Inelastic Behaviour of Structures under Variable Loads, pp. 203–218, Z. MRÓZ, D. WEICHERT and S. DOROSZ [Eds.], Kluwer Academic Press, Dordrecht 1995.
11. L. CORRADI and G. MAIER, *Inadaptation theorems in the dynamics of elastic-workhardening structures*, Ing.–Archiv, **43**, 44–57, 1973.
12. J.A. KÖNIG and A. SIEMASZKO, *Strainhardening effects in shakedown process*, Ing.–Archiv, **58**, 58–66, 1988.

13. A. KORBEL, *Mechanical instability of metal substructure – catastrophic plastic flow in single and polycrystals*, [in:] Advances in Crystal Plasticity, pp. 43–86, D.S. WILKINSON and J.B. EMBURY [Eds.], Canadian Institute of Mining, Metallurgy and Petroleum, Montreal 1992.

14. J. SZARSKI, *Differential inequalities*, 6th edn., PWN, Polish Scientific Publishers, Warszawa 1967.

15. V. LAKSHMIKANTHAM and S. LEELA, *Differential and integral inequalities*, Vol. I and II, Academic Press, New York 1969.

16. J. SACZUK, *On variational aspects of a generalized continuum*, Rend. di Matematica, **16**, 315–327, 1996.

17. H. RUND, *The differential geometry of Finsler spaces*, Springer–Verlag, Berlin 1959.

18. M. MATSUMOTO, *Foundations of Finsler geometry and special Finsler spaces*, Kaiseisha Press, Saikawa, Ōtsu 1986.

19. K. KONDO, *On the fundamental equations of the macroscopic mechanical behaviour of microscopically nonuniform materials*, RAAG Mem., **D–II**, 470–483, 1955.

20. Cz. WOŹNIAK, *Continuous media with microstructure*, [in:] Geometric Methods in Physics and Engineering, pp. 295–311 [in Polish], PWN, Warszawa 1968.

21. E.C. AIFANTIS, *The physics of plastic deformation*, Int. J. Plast., **3**, 211–247, 1987.

22. Y. TAKANO, *Variational principle in Finsler spaces*, Lett. Nuovo Cimento, **11**, 486–490, 1974.

23. J.A. KÖNIG, *Shakedown of elastic-plastic structures*, PWN Polish Scientific Publishers, Warszawa 1987.

24. Z.S. BASINSKI and P.J. JACKSON, *The effect of extraneous deformation on strain hardening in Cu single crystals*, Appl. Phys. Lett., **6**, 148–150, 1965.

25. H. BUSEMANN, *Metric methods in Finsler space and in the foundations of geometry*, Ann. Math. Studies No. 8, Princeton University Press, Princeton 1942.

26. G.S. ASANOV, *Finsler geometry, relativity and gauge theories*, D. Reidel, Dordrecht 1985.

27. M. ABATE and G. PATRIZIO, *Finsler metrics – A global approach*, Springer Verlag, Berlin 1994.

28. P.L. ANTONELLI and R. MIRON, *Lagrange and Finsler geometry*, Kluwer Academic Publishers, Dordrecht 1996.

29. Y. CHOQUET-BRUHAT, C. DE WITT-MORETTE and M. DILLARD-BLEICK, *Analysis, manifolds and physics*, North–Holland, Amsterdam, New York, Oxford 1977.

30. C. VON WESTENHOLTZ, *Differential forms in mathematical physics*, North–Holland, Amsterdam, New York, Oxford 1981.

31. M. MATSUMOTO, *Affine transformations of Finsler spaces*, J. Math. Kyoto Univ., **3**, 2, 1–35, 1963.

32. H. YASUDA, *On the indicatrices of a Finsler space*, Tensor, N.S., **33**, 213–221, 1979.

33. M. MATSUMOTO, *On the indicatrices of a Finsler space*, Period. Math. Hung., **8**, 185–191, 1977.

34. S. WATANABE, *On indicatrices of a Finsler space*, Tensor, N.S., **27**, 135–137, 1973.

35. I. ČOMIĆ, *A generalization of d-connection*, Tensor, N.S., **48**, 199–208, 1989.

INSTITUTE OF FLUID-FLOW MACHINERY
POLISH ACADEMY OF SCIENCES
e-mail: jsa@imppan.imp.pg.gda.pl

Received November 4, 1996.

Arch. Mech., 49, 3, pp. 547–572, Warszawa 1997

Transformation thermomechanics of R-phase in TiNi shape memory alloys (*)

K. TANAKA, F. NISHIMURA, H. KATO (HINO/TOKYO)
and S. MIYAZAKI (TSUKUBA)

THERMOMECHANICAL BEHAVIOUR in TiNi shape memory alloys after the R-phase transformation is formulated from the continuum mechanical point of view based on two metallurgical processes progressing simultaneously: the lattice distortion in the R-phase and the variants reorientation of the twinned R-phase variants. The start and evolution of both processes are assumed to be governed by conditions similar to the yield condition and the associated consistency condition in plasticity. The evolution equations are derived by solving a conditional extremum problem derived from the dissipation inequality. Uniaxial behaviour is discussed under several thermomechanical load conditions. The simulation of the recovery stress induced during constraint heating presents a clear coupled effect of the two metallurgical processes.

1. Introduction

THE R-PHASE TRANSFORMATION occurs in TiNi shape memory alloys in a certain temperature range just prior to the martensitic transformation [1–4]. The rhombohedral phase is produced from the parent B2 phase during the transformation. The stress-strain curve changes its form from apparent plasticity to pseudoelasticity depending on the test temperature; the former is the shape memory effect exhibiting the recoverable deformation, whereas in the latter, the stress-induced pseudoelasticity is associated with the stress-induced forward and reverse transformations. In almost all cases, the pseudoelasticity is observed in a relatively narrow temperature range without showing any large hysteresis. This is the reason why the R-phase transformation is preferably used in shape memory devices requiring a sensitive response to the input.

Metallurgy tells us that the R-phase transformation starts during thermomechanical loading when a transformation start condition is satisfied, and finishes when a transformation finish condition is fulfilled, forming the twin-related R-phase variants. The twinned structure is self-accommodated under the stress-free state and is preferred by the applied stress, as in the case of the martensitic transformation. The lattice distortion in the R-phase and/or the variants reorientation of the twinned variants then follow in the subsequent thermomechanical loading. The transformation start/finish condition was determined on

(*) Part of the paper has been reported at the 31st Polish Solid Mechanics Conference: SolMec 96 (Mierki, July 10–14, 1996).

the stress-temperature plane, both in the R-phase forward and reverse transformations. The shift and change in the stress-strain or strain-temperature hysteresis loop have rarely been observed during cyclic mechanical or thermal loading because the strain induced by the R-phase transformation is small, less than one tenth of that induced by the martensitic transformation.

Investigations should be carried out from the continuum mechanical point of view to predict as rigorously as possible the elongation and force induced in the shape memory devices during the actual operations. In fact a few studies have been carried out according to the models of R-phase transformation. So far the models employed are all taken from the study of martensitic transformations, meaning that the volume fraction of the R-phase is regarded as an internal variable to measure the extent of R-phase transformation, and the transformation kinetics is characterized as an evolution equation [5–8]. It should, however, be clearly noted that the case is true only during the R-phase transformation. When the thermomechanical load path crosses the R-phase transformation finish line in the stress-temperature space, the strain observed in the subsequent loading is attributed to the temperature-dependence of the lattice constants of the R-phase; in other words, to the lattice distortion in the R-phase and the variants reorientation of the R-phase twinned variants formed in the progress of the preceding R-phase transformation [2, 3]. MIYAZAKI *et al.* [4] measured in the sputter-deposited Ti-Ni thin films that, in the cooling process under constant applied stress, about two times larger amount of strain is further induced after the R-phase transformation, and proved that the strain is due both to the lattice distortion in the R-phase and the variants reorientation of the twinned R-phase variants. The growth of the strain is misunderstood in the Refs. [5–8] to be the response in the R-phase transformation. Theoretical descriptions carried out so far on the thermomechanical behaviour of the R-phase are, therefore (although some qualitative/quantitative coincidence is observed between the prediction and the experimental observations), not acceptable. A new theoretical framework should be established fully based on the results of metallurgical study.

In this paper, the thermomechanical behaviour of the R-phase in TiNi shape memory alloys is discussed from the macroscopic point of view, not during the R-phase transformation but after it, in order to emphasize that the alloy response after the R-phase transformation plays an important role in the design of the shape memory alloy devices. The two types of the microscopic structural changes, the lattice distortion in the R-phase and the variants reorientation of the twinned R-phase variants, are regarded to be responsible for the macroscopic thermomechanical behaviour of the alloys. A unified macroscopic theory is constructed by solving a conditional extremum problem subject to the conditions of these microscopic fundamental processes. Constitutive equations, thermomechanical and calorimetric, are derived together with the evolution equations for the lattice distortion in the R-phase and the variants reorientation. The uniaxial case is discussed numerically referring to the experimental observations.

2. Metallurgy in R-phase transformation and subsequent thermomechanical process

The metallurgical study [1–3, 9, 10] has clearly revealed that the unit cell of the R-phase is created from the parent B2 cell by elongating the lattice along any one of the <111> directions, as shown in Fig. 1 a. The length of the three axes remains unchanged during this R-phase transformation while the rhombohedral angle α (cf. Fig. 1 b) changes. Upon cooling under constant applied stress, the nucleation of the R-phase starts at a critical temperature which strongly depends on the applied stress. In a narrow temperature region, of the order of less than 10 K, the R-phase transformation progresses, inducing the transformation strain. The rhombohedral angle α decreases sharply.

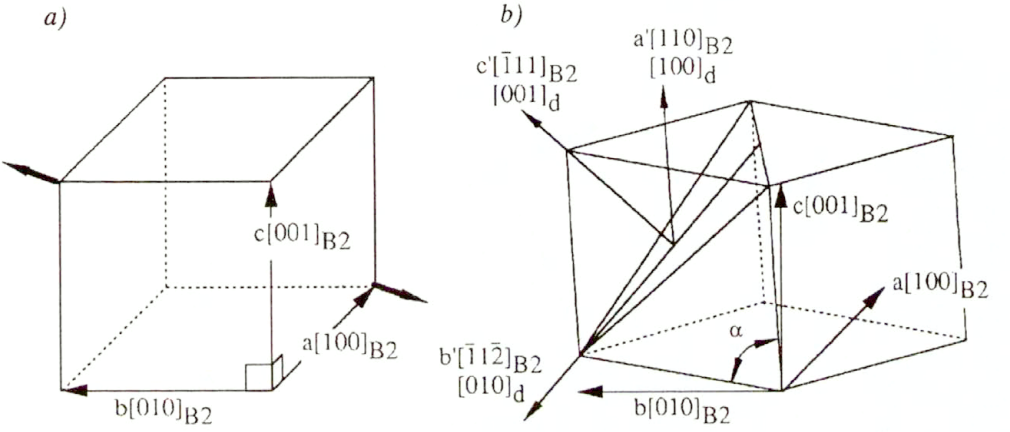

FIG. 1. R-phase transformation in unit cell.

Then the lattice distortion follows in the R-phase. Its extent can be measured by means of the rhombohedral angle α, which depends solely on the temperature T in the TiNi alloy [3, 4, 11, 12];

$$\alpha = \alpha(T). \tag{2.1}$$

Some macroscopic deformation may also be induced due directly to the change in α. The main source of the macroscopic deformation is, however, the variants reorientation occurring in the self-accommodated twinned variants through the migration of the twin boundaries [2]. In the coalescence process, the thermally-induced R-phase variants convert to the stress-preferred variants by twinning deformation process, leading finally to a single variant crystal. This variants reorientation process results in a macroscopic deformation till the value of the strain reaches a maximum recoverable strain which has been "stored" in the alloy during the self-accommodation process [2].

The R-phase formed in the alloy during cooling transforms back to the original parent phase in the subsequent heating process just after the lattice constants

of the R-phase become close to those of the parent B2 phase. The reverse transformation takes place by being associated with a very small strain change as the first-order transformation [13], as in the case of the forward transformation, at the reverse transformation temperature which also depends on the applied stress. Thus, the R-phase transformation has a hysteresis although it is very small corresponding to the small strain change, meaning that Eq. (2.1) has different functional forms on cooling and heating, respectively. However, again the major part of the recovery strain upon heating appears as a function of temperature in the second-order transformation manner until the reverse transformation takes place in the first-order transformation manner.

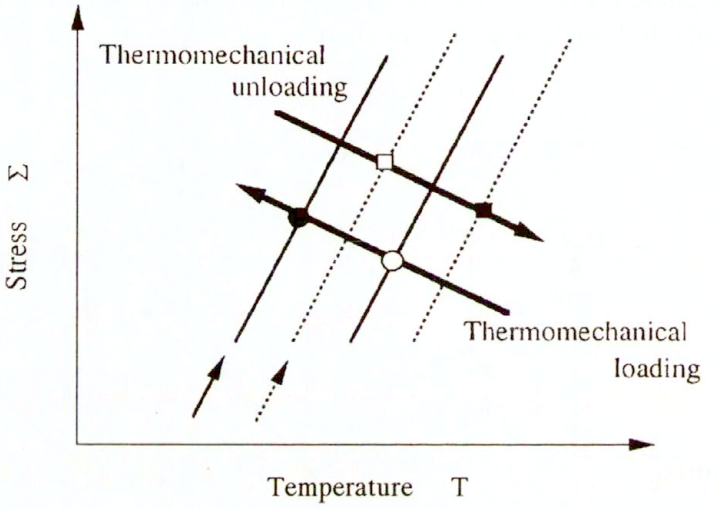

FIG. 2. R-phase forward and reverse transformation lines (schematic).

Explaining the situation in the stress (Σ) – temperature (T) plane in Fig. 2, the R-phase transformation starts when the thermomechanical loading path meets the transformation start line at the hollow circle in the figure, and finishes on the transformation finish line at the solid circle. The R-phase transformation zone bounded by the transformation start/finish (solid) lines is narrow. The lattice distortion and the variants reorientation processes go on in the R-phase in the subsequent thermomechanical loading. During thermomechanical unloading, the R-phase reverse transformation starts on the R-phase reverse transformation line at the hollow box in the figure, and finishes on the R-phase reverse transformation line at the solid box. The R-phase reverse transformation zone, bounded by the reverse transformation start/finish (broken) lines, is also narrow. The present discussion takes notice of the alloy behaviour when the load state (Σ, T) is on the left side of either the R-phase finish line (solid arrow) in the loading process or the R-phase reverse transformation start line (broken arrow) in the unloading process. The width of these two lines was measured to be very narrow, less

than 5 K, corresponding to the small strain change associated with the R-phase transformation. The lines are called in the following discussion the R-phase transformation line and the R-phase reverse transformation line, respectively.

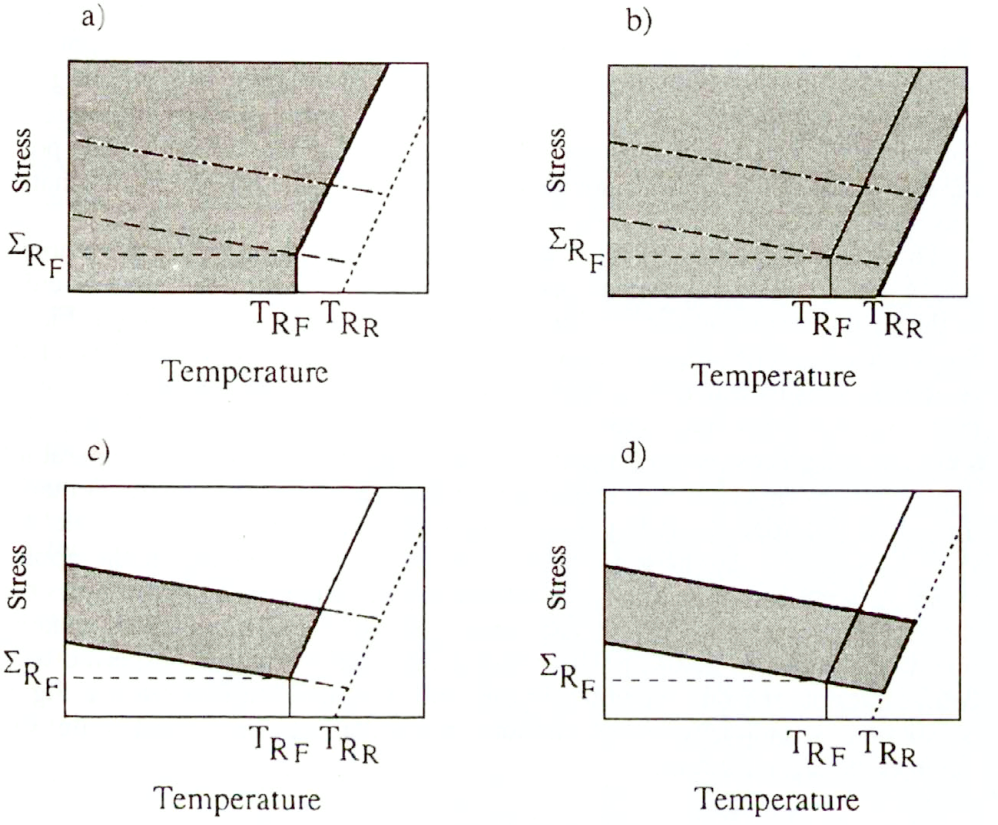

FIG. 3. Transformation lines (schematic).

A series of extensive experimental study on the R-phase transformation in TiNi shape memory alloys [1–4] has revealed the conditions of the lattice distortion in the R-phase and of the variants reorientation of the R-phase variants to undergo the uniaxial thermomechanical loading. The results are summarized schematically in Fig. 3 on the applied stress-temperature plane (see BARRETT [14] and BRINSON *et al.* [15] for similar sketch for the martensitic transformation). The R-phase transformation finishes when the thermomechanical load state (T, Σ) reaches the R-phase transformation line, the thick straight lines starting from the point (T_{R_F}, Σ_{R_F}) in Fig. 3 a. The lattice distortion in the R-phase progresses when the thermomechanical load point is inside the shaded region shown in Fig. 3 a and moves with $\dot{T} < 0$. The upper section of the R-phase transformation line has a very high value in slope c, of nearly $c \approx 10\,\text{MPa/K}$, whereas the lower section is temperature-independent. The reverse lattice distortion, on the other hand,

occurs in the shaded region sketched in Fig. 3 b when the load state moves with $\dot{T} > 0$. Another straight line intersecting the horizontal axis at $(T_{R_R}, 0)$, almost parallel to the upper section of the R-phase transformation line, is the R-phase reverse transformation line at which the reverse transformation starts with an associated small strain recovery. The R-phase reverse transformation line might have a critical stress as in the case of the R-phase transformation line, meaning that the section of the line below the critical stress might be temperature-independent. Since no definite experimental data is available so far with respect to this point, the straight line in Fig. 3 b is employed here as the R-phase reverse transformation line.

The variants reorientation of the R-phase variants progresses by twinning only when the R-phase variants exist in the alloy and the load state is either in the shaded region in Fig. 3 c during cooling or in the shaded region in Fig. 3 d during heating. The variants reorientation start line, the lower boundary of the region, exhibits a clear temperature-dependence since, firstly, the mobility of the twin boundaries becomes lower with the decreasing strain due to twinning, and secondly, the process is essentially a thermal activation process. The temperature-dependence is almost linear. The process completes on the variants reorientation finish line, the upper boundary of the region, which is almost parallel to the start line. A preferred variant is formed inside the alloy depending on the applied stress. A comment: there exists no definite experimental proof which shows that the variants reorientation start line intersects with the R-phase transformation line at the point (T_{R_F}, Σ_{R_F}). The point of intersection is in fact expected to be below, but not far from, the point. In this study the situation illustrated in Fig. 3 c is assumed for simplicity with the understanding that the sketch must be not very far from the actual situation.

3. State variables during lattice distortion and variants reorientation

Let us consider the thermomechanical behaviour in a shape memory alloy which, after having finished the R-phase transformation, is in the process of both the lattice distortion in the R-phase and the crystal reorientation under thermal and/or mechanical loading.

The extent of the lattice distortion in the R-phase can, as explained in the preceding section, be described in an appropriate representative volume of the alloy by means of a value α of the rhombohedral angle defined in Eq. (2.1) [4]. A twinned structure is produced in the variants as a result of the R-phase transformation. In most cases the deformation associated with the R-phase transformation is averaged to be null from the macroscopic point of view since the self-accommodation process goes on during the R-phase transformation. The internal twinned structure is formed during the process so that a certain amount of strain, the recoverable strain, is induced in the subsequent variants reorientation

process. In this study, the self-accommodation is understood to be a phenomenon in which the possibility to produce a certain amount of recoverable strain, $\boldsymbol{\Omega}^*$, say, is stored in the variants. The strain is induced as a macroscopic deformation during the subsequent thermomechanical loading. Under the presence of load, however, the self-accommodation is not realized but a different crystallographic structure is attained depending on the stress state to minimize the free energy of the alloy. The same amount of recoverable strain is, nevertheless, "stored" in the alloy to be induced macroscopically in the subsequent thermomechanical processes. The recoverable strain $\boldsymbol{\Omega}^*$ is assumed to be simply governed by the equation

$$\dot{\boldsymbol{\Omega}}^* = \boldsymbol{\Omega}^*_\alpha \dot{\alpha}, \tag{3.1}$$

where the material coefficient tensor $\boldsymbol{\Omega}^*_\alpha$ is determined by means of the thermomechanical state at the instant of R-phase transformation.

Upon loading, the twinned structure in the alloy changes through the variants reorientation, inducing a macroscopic deformation [2]. The extent of the process on the microscopic structural level can be characterized by a set of scalar variables which represent the volume fractions of the pairs of martensite twin and of one variant comprising a twin pair [16–19].

By averaging these variables over a representative volume in the alloy, one can introduce the macroscopic variables $(\zeta_1, \zeta_2, \ldots)$, say, which represent the microscopic alloy structure. The evolution equations of these internal variables estimate the change in the microscopic alloy structure.

In the present study, for the sake of simplicity, two internal variables (α, ζ) are chosen to characterize the lattice distortion in the R-phase and the variants reorientation processes, leaving a generalization of the theory for the next study. LECLERCQ and LEXCELLENT [19] have developed a generalized theory of shape memory alloys by introducing the volume fractions of the thermal-induced martensite and of the oriented martensite variants which corresponds to the present ζ, and suggested that the theory could be applied to transformation thermomechanics of the R-phase, too. It can be applied if the lattice distortion is taken into account in addition.

It should be noted that hereafter, for the sake of theoretical convenience, the internal variable α is understood to be the angle $\pi/2 - \alpha$ with the rhombohedral angle α illustrated in Fig. 1 b. It takes, therefore, a value in $[0, (\pi/2))$, whereas the variable ζ is normalized to have a value in [0,1].

When the lattice distortion and/or the crystal reorientation take place, a macroscopic irreversible strain tensor $\mathbf{E}^*$ is induced, which is also employed here as another internal variable.

Let us propose that the Green strain tensor $\mathbf{E}$ can be additively decomposed in the rate form,

$$\dot{\mathbf{E}} = \dot{\mathbf{E}}^e + \dot{\mathbf{E}}^*, \tag{3.2}$$

where $\dot{\mathbf{E}}^e$ stands for the elastic component while $\dot{\mathbf{E}}^*$ is the irreversible component due to the lattice distortion in the R-phase and the variants reorientation [19]. For the irreversible strain $\mathbf{E}^*$, the following kinematical relation is assumed:

$$\dot{\mathbf{E}}^* = \mathbf{E}^*_\alpha(\alpha, \zeta; \boldsymbol{\Sigma}, T)\dot{\alpha} + \boldsymbol{\Omega}^*\dot{\zeta}\,, \tag{3.3}$$

representing an additive decomposition into the terms due to the lattice distortion in the R-phase and to the variants reorientation, where $\boldsymbol{\Sigma}$ and T denote the stress tensor and the temperature, respectively. The second term on the right-hand side clearly states that, assuming $\boldsymbol{\Omega}^*$ be constant during the process, $\boldsymbol{\Omega}^*$ can be read as the macroscopic strain at the completion of the variants reorientation process. This is the reason why $\boldsymbol{\Omega}^*$ is called the recoverable strain. The first term covers the case in which the lattice distortion process might directly produce a macroscopic deformation, very likely under the stressed state.

4. Unified thermomechanical theory of lattice distortion in R-phase and variants reorientation

In order to construct a unified theory of the lattice distortion in the R-phase and variants reorientation in shape memory alloys, let us start from the energy balance and the Clausius–Duhem inequality [20, 21];

$$\varrho\dot{U} - \boldsymbol{\sigma} : \mathbf{L} + \operatorname{div}\mathbf{q} - \varrho\sigma = 0, \qquad \varrho\dot{\eta} - \frac{\sigma}{T} + \operatorname{div}\left(\frac{\mathbf{q}}{T}\right) \geq 0, \tag{4.1}$$

where, here and henceforth, the variables have the following physical significance: ϱ, ϱ_0 – densities in the current and reference configurations, respectively, U – internal energy density, $\boldsymbol{\sigma}$ – Cauchy stress tensor, $\mathbf{L} = \dot{\mathbf{F}}\cdot\dot{\mathbf{F}}^{-1}$ – velocity gradient with $\mathbf{F}$ being the deformation gradient, $\mathbf{q}$ – heat flux, σ – heat production term, η – entropy density.

Throughout this study the notation div stands for the divergence with respect to the Eulerian coordinate, while Grad is the gradient with respect to the Lagrangean coordinate, respectively.

Following standard continuum thermodynamics, one can reach the relations

$$\begin{aligned} &\mathbf{E}^e = -\varrho_0\frac{\partial\Psi}{\partial\boldsymbol{\Sigma}}, \qquad \eta = -\frac{\partial\Psi}{\partial T}, \\ &\mathcal{D} = K_1\dot{\alpha} + K_2\dot{\zeta} - \frac{1}{T}\mathbf{Q}\cdot\operatorname{Grad}T \geq 0, \end{aligned} \tag{4.2}$$

where

$$\Psi = \Psi(\boldsymbol{\Sigma}, T; \alpha, \zeta, \mathbf{E}^*) = U - \eta T - \frac{1}{\varrho_0}\boldsymbol{\Sigma} : \mathbf{E}^e \tag{4.3}$$

represents the Gibbs free energy, and the second Piola – Kirchhoff stress tensor $\boldsymbol{\Sigma}$, the material heat flux $\mathbf{Q}$ and the thermodynamic forces K_1 and K_2 are defined by

$$\boldsymbol{\Sigma} = \frac{\varrho_0}{\varrho}\mathbf{F}^{-1}\cdot\boldsymbol{\sigma}\cdot\mathbf{F}^{-T}, \qquad \mathbf{Q} = \frac{\varrho_0}{\varrho}\mathbf{F}^{-1}\cdot\mathbf{q},$$

$$K_1 = -\varrho_0\frac{\partial\Psi}{\partial\alpha} + \left(\boldsymbol{\Sigma} - \varrho_0\frac{\partial\Psi}{\partial\mathbf{E}^*}\right) : \mathbf{E}^*_\alpha, \tag{4.4}$$

$$K_2 = -\varrho_0\frac{\partial\Psi}{\partial\zeta} + \left(\boldsymbol{\Sigma} - \varrho_0\frac{\partial\Psi}{\partial\mathbf{E}^*}\right) : \boldsymbol{\Omega}^*.$$

Equations $(4.2)_{1,2}$ govern the reversible thermomechanical process of the material, from which one can derive the thermomechanical and calorimetric constitutive equations in rate form if the elastic process is reasonably assumed to be not influenced by the irreversible processes [20, 22]:

$$\dot{\mathbf{E}}^e = \mathbf{S} : \dot{\boldsymbol{\Sigma}} + \boldsymbol{\Theta}\dot{T}, \qquad \dot{\eta} = \frac{\boldsymbol{\Theta}}{\varrho_0} : \dot{\boldsymbol{\Sigma}} + Tc\dot{T},$$

$$\mathbf{S} = -\varrho_0\frac{\partial^2\Psi}{\partial\boldsymbol{\Sigma}\partial\boldsymbol{\Sigma}}, \qquad \boldsymbol{\Theta} = -\varrho_0\frac{\partial^2\Psi}{\partial\boldsymbol{\Sigma}\partial T}, \qquad c = -\frac{\varrho_0}{T}\frac{\partial^2\Psi}{\partial T^2}, \tag{4.5}$$

where $\mathbf{S}$ stands for the elastic compliance tensor while $\boldsymbol{\Theta}$ and c correspond to the thermoelastic tensor and the specific heat, respectively.

Later consideration is limited to the case of the processes in which the following dissipation inequality holds:

$$\mathcal{D} = K_1\dot{\alpha} + K_2\dot{\zeta} \geq 0, \tag{4.6}$$

and the thermomechanical constitutive equation is solely discussed.

5. Evolution equations in irreversible processes

The thermomechanical study on the R-phase transformation carried out so far in metallurgy [1–3] allows one to assume that, as in plasticity with the yield condition, the lattice distortion in the R-phase occurs only under a thermomechanical restriction

$$f = f(\boldsymbol{\Sigma}, T; K_1, K_2; \alpha, \zeta) = 0 \qquad \text{and} \qquad \dot{f} = 0. \tag{5.1}$$

Figures 3 a and b actually provide a uniaxial picture of this condition in TiNi shape memory alloy. It is worthwhile to note that the time t is included in Eq. (5.1) as an implicit parameter through the state variables, which reflects the fact that the lattice distortion process is diffusionless.

The variants reorientation is activated under the condition that a twinned structure has already been formed in the alloy, being independent of whether the

lattice distortion in the R-phase progresses or not, and produces a corresponding macroscopic deformation [2, 3]. It is natural to assume that the process is governed by a thermomechanical condition

$$g = g(\boldsymbol{\Sigma}, T; K_1, K_2; \alpha, \zeta) = 0 \qquad \text{and} \qquad \dot{g} = 0, \tag{5.2}$$

which is a mathematical rephrase of the actual situation illustrated in Figs. 3 c, d.

The transformation start condition and the associated consistency condition during the process of transformation have been discussed in the Refs. [17–19, 21] in the case of martensitic transformations. PATOOR *et al.* [18] have pointed out, from the micromechanical point of view, that the transformation condition should include the third invariant of the deviatoric stress tensor as one of the variables, in addition to the von Mises-type second variant of the deviatoric stress tensor. The shift of the transformation lines, which represents the consistency conditions, have experimentally been investigated in an Fe-based shape memory alloy [23, 24].

The requirement of the second law of thermodynamics (4.6) can be re-read as a conditional extremum problem of

$$\overline{\mathcal{D}} = \mathcal{D} - \dot{\lambda} f - \dot{\mu} g = K_1 \dot{\alpha} + K_2 \dot{\zeta} - \dot{\lambda} f - \dot{\mu} g \tag{5.3}$$

with the Lagrange multipliers $\dot{\lambda}$ and $\dot{\mu}$ [25–27]. The usual procedure yields the final formulae

$$\dot{\alpha} = \dot{\lambda} \frac{\partial f}{\partial K_1} + \dot{\mu} \frac{\partial g}{\partial K_1}, \qquad \dot{\zeta} = \dot{\lambda} \frac{\partial f}{\partial K_2} + \dot{\mu} \frac{\partial g}{\partial K_2}, \tag{5.4}$$

which represent the evolution equations for the internal variables α and ζ.

For the sake of compact presentation of the theory, the generalized thermodynamic force $\mathbf{K} = (K_1, K_2)$ is introduced, and an appropriate inner product $*$ is defined for the quantities relating to $\mathbf{K}$, i.e., for example,

$$\frac{\partial f}{\partial \mathbf{K}} * \frac{\partial \mathbf{K}}{\partial \alpha} = \frac{\partial f}{\partial K_1} \frac{\partial K_1}{\partial \alpha} + \frac{\partial f}{\partial K_2} \frac{\partial K_2}{\partial \alpha}.$$

The Lagrange multipliers introduced in Eq. (5.3) can be determined from the consistency conditions, Eqs. $(5.1)_2$ and $(5.2)_2$:

$$\begin{aligned}
\dot{f} &= \left(\frac{\partial f}{\partial \boldsymbol{\Sigma}} + \frac{\partial f}{\partial \mathbf{K}} * \frac{\partial \mathbf{K}}{\partial \boldsymbol{\Sigma}} \right) : \dot{\boldsymbol{\Sigma}} + \left(\frac{\partial f}{\partial T} + \frac{\partial f}{\partial \mathbf{K}} * \frac{\partial \mathbf{K}}{\partial T} \right) \dot{T} \\
&\quad + \left(\frac{\partial f}{\partial \alpha} + \frac{\partial f}{\partial \mathbf{K}} * \frac{\partial \mathbf{K}}{\partial \alpha} \right) \dot{\alpha} + \left(\frac{\partial f}{\partial \zeta} + \frac{\partial f}{\partial \mathbf{K}} * \frac{\partial \mathbf{K}}{\partial \zeta} \right) \dot{\zeta} = 0, \\
\dot{g} &= \left(\frac{\partial g}{\partial \boldsymbol{\Sigma}} + \frac{\partial g}{\partial \mathbf{K}} * \frac{\partial \mathbf{K}}{\partial \boldsymbol{\Sigma}} \right) : \dot{\boldsymbol{\Sigma}} + \left(\frac{\partial g}{\partial T} + \frac{\partial g}{\partial \mathbf{K}} * \frac{\partial \mathbf{K}}{\partial T} \right) \dot{T} \\
&\quad + \left(\frac{\partial g}{\partial \alpha} + \frac{\partial g}{\partial \mathbf{K}} * \frac{\partial \mathbf{K}}{\partial \alpha} \right) \dot{\alpha} + \left(\frac{\partial g}{\partial \zeta} + \frac{\partial g}{\partial \mathbf{K}} * \frac{\partial \mathbf{K}}{\partial \zeta} \right) \dot{\zeta} = 0.
\end{aligned} \tag{5.5}$$

The result reads as

$$
\begin{aligned}
\dot{\lambda} &= \overline{\Delta}\left(-\frac{\partial g}{\partial K_1}\mathbf{Z}_{\Sigma} + \frac{\partial g}{\partial K_2}\mathbf{A}_{\Sigma}\right) : \dot{\mathbf{\Sigma}} + \overline{\Delta}\left(-\frac{\partial g}{\partial K_1}Z_T + \frac{\partial g}{\partial K_2}A_T\right)\dot{T}, \\
\dot{\mu} &= \overline{\Delta}\left(\frac{\partial f}{\partial K_1}\mathbf{Z}_{\Sigma} - \frac{\partial f}{\partial K_2}\mathbf{A}_{\Sigma}\right) : \dot{\mathbf{\Sigma}} + \overline{\Delta}\left(\frac{\partial f}{\partial K_1}Z_T - \frac{\partial f}{\partial K_2}A_T\right)\dot{T}, \\
\mathbf{A}_{\Sigma} &= \Delta\,(-g_{\zeta} f_{\Sigma} + f_{\zeta} g_{\Sigma}), \qquad A_T = \Delta\,(-g_{\zeta} f_T + f_{\zeta} g_T), \\
\mathbf{Z}_{\Sigma} &= \Delta\,(g_{\alpha} f_{\Sigma} - f_{\alpha} g_{\Sigma}), \qquad Z_T = \Delta\,(g_{\alpha} f_T - f_{\alpha} g_T), \\
f_{\Sigma} &= \frac{\partial f}{\partial \mathbf{K}} * \frac{\partial \mathbf{K}}{\partial \mathbf{\Sigma}} + \frac{\partial f}{\partial \mathbf{\Sigma}}, \qquad f_T = \frac{\partial f}{\partial T} + \frac{\partial f}{\partial \mathbf{K}} * \frac{\partial \mathbf{K}}{\partial T}, \\
g_{\Sigma} &= \frac{\partial g}{\partial \mathbf{\Sigma}} + \frac{\partial g}{\partial \mathbf{K}} * \frac{\partial \mathbf{K}}{\partial \mathbf{\Sigma}}, \qquad g_T = \frac{\partial g}{\partial T} + \frac{\partial g}{\partial \mathbf{K}} * \frac{\partial \mathbf{K}}{\partial T}, \\
f_{\alpha} &= \frac{\partial f}{\partial \mathbf{K}} * \frac{\partial \mathbf{K}}{\partial \alpha} + \frac{\partial f}{\partial \alpha}, \qquad f_{\zeta} = \frac{\partial f}{\partial \mathbf{K}} * \frac{\partial \mathbf{K}}{\partial \zeta} + \frac{\partial f}{\partial \zeta}, \\
g_{\alpha} &= \frac{\partial g}{\partial \mathbf{K}} * \frac{\partial \mathbf{K}}{\partial \alpha} + \frac{\partial g}{\partial \alpha}, \qquad g_{\zeta} = \frac{\partial g}{\partial \mathbf{K}} * \frac{\partial \mathbf{K}}{\partial \zeta} + \frac{\partial g}{\partial \zeta}, \\
\Delta^{-1} &= f_{\alpha} g_{\zeta} - f_{\zeta} g_{\alpha}, \qquad \overline{\Delta}^{-1} = \frac{\partial f}{\partial K_1}\frac{\partial g}{\partial K_2} - \frac{\partial f}{\partial K_2}\frac{\partial g}{\partial K_1},
\end{aligned}
\tag{5.6}
$$

and the evolution equations of the internal variables α and ζ are given by

$$
\dot{\alpha} = \mathbf{A}_{\Sigma} : \dot{\mathbf{\Sigma}} + A_T \dot{T}, \qquad \dot{\zeta} = \mathbf{Z}_{\Sigma} : \dot{\mathbf{\Sigma}} + Z_T \dot{T}. \tag{5.7}
$$

Equation $(5.7)_1$ governs the progress of the lattice distortion in the R-phase, whereas Eq. $(5.7)_2$ – the progress of variants reorientation. Equation (5.7) state that both processes are rate-independent, or diffusionless according to the terminology in metallurgy.

The irreversible strain rate $\dot{\mathbf{E}}^*$ due to the lattice distortion and the variants reorientation can be obtained from Eqs. (5.7) and (3.4) to be

$$
\dot{\mathbf{E}}^* = (\mathbf{E}^*_{\alpha} \otimes \mathbf{A}_{\Sigma} + \mathbf{\Omega}^* \otimes \mathbf{Z}_{\Sigma}) : \dot{\mathbf{\Sigma}} + (\mathbf{E}^*_{\alpha} A_T + \mathbf{\Omega}^* Z_T)\,\dot{T}, \tag{5.8}
$$

which, together with Eqs. (3.2) and $(4.5)_1$, finally leads to the following thermomechanical constitutive equation in rate form:

$$
\dot{\mathbf{E}} = (\mathbf{S} + \mathbf{E}^*_{\alpha} \otimes \mathbf{A}_{\Sigma} + \mathbf{\Omega}^* \otimes \mathbf{Z}_{\Sigma}) : \dot{\mathbf{\Sigma}} + (\mathbf{\Theta} + \mathbf{E}^*_{\alpha} A_T + \mathbf{\Omega}^* Z_T)\,\dot{T}. \tag{5.9}
$$

The dissipation inequality (4.6) delivers

$$
\mathcal{D} = \dot{\lambda}\left(\mathbf{K} * \frac{\partial f}{\partial \mathbf{K}}\right) + \dot{\mu}\left(\mathbf{K} * \frac{\partial g}{\partial \mathbf{K}}\right) \geq 0, \tag{5.10}
$$

which states that the lattice distortion in the R-phase and the variants reorientation progress when

$$\dot{\lambda} > 0 \qquad \text{and} \qquad \dot{\mu} > 0 \tag{5.11}$$

hold, respectively, under the situation in which the conditions

$$\mathbf{K} * \frac{\partial f}{\partial \mathbf{K}} \geq 0, \qquad \mathbf{K} * \frac{\partial g}{\partial \mathbf{K}} \geq 0 \tag{5.12}$$

always hold. The condition (5.11) can be used, like the loading condition in conventional plasticity, to judge whether the process starts, continues or stops during an applied thermomechanical loading $(\dot{T}, \dot{\boldsymbol{\Sigma}})$.

6. Analysis of uniaxial behaviour

6.1. Fundamental uniaxial relations

Although the experimental results shown in Fig. 3 could be summarized to give an explicit form of the functions f and g introduced in Eqs. (5.1) and (5.2), here in this study the uniaxial analysis on the behaviour in TiNi shape memory alloy is carried out starting directly from Fig. 3, leaving the construction of a fully closed description of the phenomena to the next study. The uniaxial version of the relations developed so far and the additional assumptions are as follows: The progress of the lattice distortion in the R-phase is independent of the applied stress Σ and is governed by

$$\dot{\alpha} = A_T \dot{T} \qquad \text{with} \qquad A_T = a_c(A_{T0} - \alpha), \tag{6.1}$$

where a_c and A_{T0} are the constant material parameters. The evolution equation (6.1) is solved to give a direct form

$$\alpha = A_{T0}\left[1 - \exp a_c(T^*_{R_F} - T)\right], \tag{6.2}$$

where $T^*_{R_F}$ is the temperature on the R-phase transformation start line (see the experimental observation by MIYAZAKI *et al.* [4]). When $\Sigma < \Sigma_{R_F}$, $T^*_{R_F} = T_{R_F}$ as is seen in Fig. 3 a.

The variants reorientation, characterized uniaxially by

$$\dot{\zeta} = Z_\Sigma \dot{\Sigma} + Z_T \dot{T}, \tag{6.3}$$

is assumed, following the experimental observation [3], to have an explicit form

$$\dot{\zeta} = (1 - \zeta)\overline{Z}_\Sigma \left(\dot{\Sigma} + b\dot{T}\right), \tag{6.4}$$

where $b > 0$ and $\overline{Z}_\Sigma$ denote the constant material parameters. Integrating Eq. (6.4) and taking into account the fact that the point (T_{R_F}, Σ_{R_F}) is on the start line ($\zeta = 0$), one has

$$\zeta = 1 - \exp \overline{Z}_\Sigma [b(T_{R_F} - T) + (\Sigma_{R_F} - \Sigma)] . \tag{6.5}$$

The variants reorientation start line in Fig. 3c is given by inserting $\zeta = 0$ into Eq. (6.6) as

$$\Sigma = \Sigma_{R_F} - b(T - T_{R_F}), \tag{6.6}$$

which reveals that $-b$ stands for the slope of the variants reorientation start line in the $\Sigma - T$ plane. On the contrary, if $\zeta = 0.99$ is assumed to be the completion of the variants reorientation, the variants reorientation finish line is expressed by

$$\Sigma = \Sigma_{R_F} - b(T - T_{R_F}) + (\ln 100)/\overline{Z}_\Sigma . \tag{6.7}$$

The iso-ζ lines are parallel to the variants reorientation start/finish lines, and to each other.

In order that ζ can move in the interval $[0, 1]$ when the thermomechanical load is in the shaded region in Fig. 3c, the conditions

$$(\ln 100)/\overline{Z}_\Sigma \geq \Sigma - \Sigma_{R_F} + b(T - T_{R_F}) \geq 0 \qquad \text{and} \qquad \overline{Z}_\Sigma > 0, \tag{6.8}$$

must be satisfied. The forward process, $\dot{\zeta} > 0$, occurs only when

$$\dot{\Sigma} + b\dot{T} > 0 \tag{6.9}$$

holds. The relation well explains the experimental observation that no variants reorientation progresses in the isostatic cooling processes ($\dot{\Sigma} = 0$ and $\dot{T} < 0$).

The recoverable strain Ω^* in the variants is assumed to be formed during the lattice distortion process according to

$$\dot{\Omega}^* = \Omega^*_\alpha \dot{\alpha} , \tag{6.10}$$

where Ω^*_α is a constant material parameter. Equation (6.10) states, therefore, nothing other than a linear relation

$$\Omega^* = \Omega^*_\alpha \alpha . \tag{6.11}$$

The uniaxial macroscopic strain due both to the lattice distortion in the R-phase and the crystal reorientation is given by

$$\dot{E}^* = E^*_\alpha \dot{\alpha} + \Omega^* \dot{\zeta} , \tag{6.12}$$

where the material parameter E^*_α is proposed to be expressed as

$$E^*_\alpha = E^*_{\alpha 0}\,\zeta^*_s \tag{6.13}$$

with a constant material parameter $E^*_{\alpha 0}$, and ζ^*_s denotes the value of the extent of variants reorientation at the point where the thermomechanical loading path crosses the R-phase transformation line. The final expression for $\dot{E}^*$ in Eq. (6.12) is now given by

$$\dot{E}^* = E^*_{\alpha 0}\,\zeta^*_s\,\dot{\alpha} + \Omega^*_\alpha\,\alpha\,\dot{\zeta}\,. \tag{6.14}$$

It should be noted that $\dot{\alpha}$ and $\dot{\zeta}$ in Eq. (6.14) are linearly connected to $\dot{\Sigma}$ and $\dot{T}$ as can be understood from Eqs. (6.1) and (6.4). So is $\dot{E}^*$, too.

The uniaxial constitutive equation is now obtained from Eqs. (3.3), $(4.5)_1$ and (6.14) in rate form as

$$\dot{E} = S\,\dot{\Sigma} + \Theta\,\dot{T} + \dot{E}^*. \tag{6.15}$$

6.2. Cooling under free stress followed by isothermal loading

On the first cooling run down to T_t under $\Sigma = 0$, the lattice distortion in the R-phase starts at T_{R_F} in Fig. 3 a. The angle α has a value determined from Eq. (6.3) at T_t, and the recovery strain "stored" in the alloy is estimated by

$$\Omega^* = \Omega^*_\alpha\,\alpha = \Omega^*_\alpha\,A_{T0}\left[1 - \exp a_c(T^*_{R_F} - T_t)\right]. \tag{6.16}$$

Since no variants reorientation progresses during this constant stress loading below Σ_{R_F} (cf. Fig. 3 c), it means, since $\zeta^*_s = 0$, that no macroscopic strain is induced in the process;

$$E^*_{\text{isostatic}} = 0. \tag{6.17}$$

In the subsequent isothermal loading the variants reorientation progresses from the start line on. The strain can, therefore, be calculated by means of Eqs. (6.5), (6.12) and (6.16) as

$$E^* = \int_0^\zeta \Omega^*_\alpha\,\alpha\,d\zeta = \Omega^*_\alpha\,\alpha \int_{\Sigma_{ts}}^{\Sigma} \overline{Z}_\Sigma \exp \overline{Z}_\Sigma\,[b(T_{R_F} - T_t) + (\Sigma_{R_F} - \Sigma)]\,d\Sigma, \tag{6.18}$$

where in the first equation the upper limit ζ is given by Eq. (6.5) with $T = T_t$, whereas in the second equation Σ_{ts} denotes the variants reorientation start stress at T_t; i.e.,

$$\Sigma_{ts} = \Sigma_{R_F} - b(T_t - T_{R_F}). \tag{6.19}$$

When the specimen is loaded up to a stress value higher than the variants reorientation finish line (cf. Fig. 3 c), the macroscopic strain observed after the second isothermal run reads from Eq. (6.18) as

$$E^*_{\text{isothermal}} = \Omega^*_\alpha \alpha \,. \tag{6.20}$$

The total strain observed after the whole process is, therefore, estimated by

$$E^*_{\max} = E^*_{\text{isostatic}} + E^*_{\text{isothermal}} = \Omega^*_\alpha A_{T0}[1 - \exp a_c(T_{R_F} - T)]\,, \tag{6.21}$$

which is measured as the residual strain after the full elastic unloading. The temperature-dependence of $E^*_{\max}$ given in Eq. (6.21) (cf. Fig. 4) explains well the experimental observations [2].

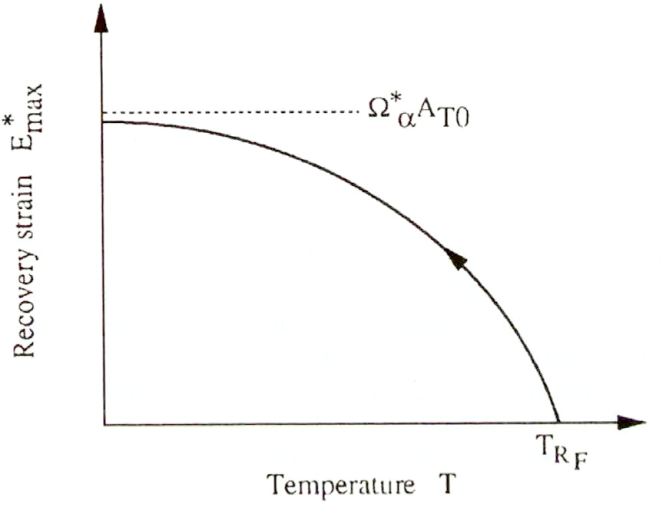

FIG. 4. Temperature dependence of recovery strain (schematic).

6.3. Cooling under constant applied stress

The isostatic cooling under a constant applied stress Σ^* does, as explained above in relation to Eq. (6.17), not drive the variants reorientation in the thermally-induced R-phase twinned structure. The macroscopic strain observed at the end of the cooling down to T is, therefore, calculated from Eq. (6.14) by

$$\begin{aligned} E^* &= E^*_{\alpha 0}\, \zeta^*_s\, \alpha \\ &= E^*_{\alpha 0} A_{T0} \left[1 - \exp \overline{Z}_\Sigma \left(\frac{b}{c} - 1\right)(\Sigma^* - \Sigma_{R_F})\right] \left[1 - \exp a_c \left(T^*_{R_F} - T\right)\right], \end{aligned} \tag{6.22}$$

when the upper section of the R-phase transformation line is expressed by

$$\Sigma = \Sigma_{R_F} + c(T - T_{R_F}) \tag{6.23}$$

with the slope $c > 0$ of the line, therefore, when

$$T^*_{R_F} = T_{R_F} + (\Sigma^* - \Sigma_{R_F})/c. \tag{6.24}$$

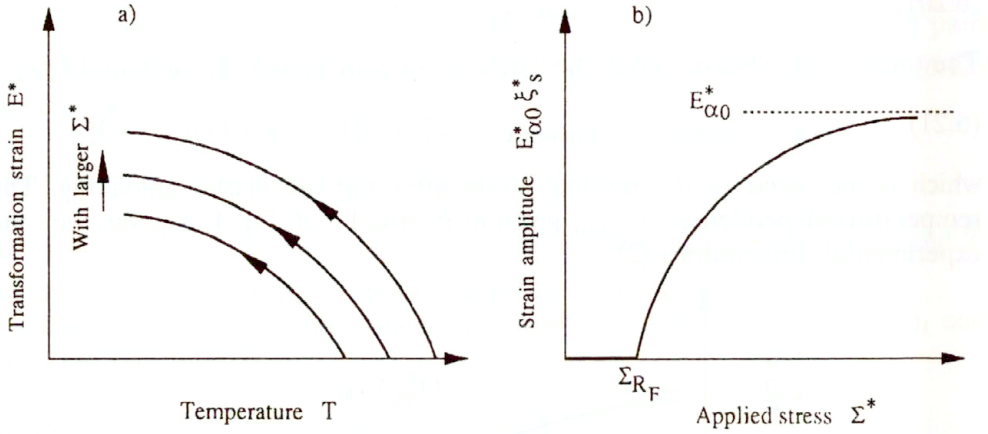

FIG. 5. Transformation strain during cooling (schematic).

Figure 5a shows a schematic plot of the transformation strain E^* vs. the temperature T with the applied stress Σ^* as a parameter. The curve shifts to the higher strain and higher temperature sides with the larger applied stress. The later shift stems simply from the positive slope of the R-phase transformation line, while the former shift comes from the stress-dependence of the amplitude $E^*_{\alpha 0}\zeta^*_s$ in Eq. (6.22). The amplitude gradually tends to a limit value with Σ^* as illustrated in Fig. 5b. So does the strain-temperature curve.

6.4. Cooling/heating under constant applied stress

Suppose the cooling stops at a lower limit temperature T_l and a heating process follows, always under a constant stress Σ^*. In order to take into account the hysteretic behaviour in α during the process, the reverse lattice distortion in the R-phase is assumed to be governed not by Eq. (6.1) but by

$$\dot{\alpha} = a_h(A_{T0} - \alpha)\dot{T}, \tag{6.25}$$

with a different material parameter a_h. Equation (6.25) is solved to give

$$\alpha = \alpha_l + (A_{T0} - \alpha_l)[1 - \exp a_h(T_l - T)] \tag{6.26}$$

with α_l, the value of α at T_l. Since the R-phase inverse transformation finishes at the thermomechanical load state $(T^*_{R_R}, \Sigma^*)$ on the R-phase reverse transformation line (cf. Fig. 3b) expressed by

$$\Sigma = c(T - T_{R_R}), \qquad T^*_{R_R} = T_{R_R} + \Sigma^*/c, \tag{6.27}$$

the parameter a_h introduced in Eq. (6.25) can be estimated from a set of the material parameters by

$$a_h = \frac{1}{T_l - T^*_{R_R}} \ln \frac{A_{T0}}{A_{T0} - \alpha_l}. \tag{6.28}$$

The macroscopic strain observed in the heating process is, by taking Eq. (6.14) into account, given by

$$E^* = E^*_{\alpha 0}\, \zeta^*_s \alpha + \int_{\alpha_l}^{\alpha} E^*_{\alpha 0}\, \zeta^*_s \, d\alpha + \int_{\zeta^*_s}^{\zeta} \Omega^*_\alpha \alpha \, d\zeta \,, \tag{6.29}$$

where the first term stands for the strain at the start of heating, cf. Eq. (6.22), while the second integral with respect to ζ works only at the temperature range between the R-phase transformation line and the R-phase reverse transformation line, i.e., between $T^*_{R_F}$ and $T^*_{R_R}$, in which the forward reorientation occurs.

The total macroscopic strain after a cycle of thermal loading under constant applied stress, $T^*_{R_F} \to T_l \to T^*_{R_R}$, is calculated to be

$$E^*_{\text{total}} = \Omega^*_\alpha \int_{T^*_{R_F}}^{T^*_{R_R}} \{\alpha_l + (A_{T0} - \alpha_l)[1 - \exp a_h(T_l - T)]\} \times (1 - \zeta^*_s)\overline{Z}_\Sigma b \exp\left[\overline{Z}_\Sigma b(T_l - T)\right] dT, \tag{6.30}$$

which is expected to be a small value since according to the experiments, the width of the R-phase transformation line and the R-phase reverse transformation line is narrow; $T^*_{R_R} - T^*_{R_F} \approx 5\,\text{K}$.

6.5. Thermomechanical process

Let us estimate the macroscopic strain developed during a thermomechanical loading sketched in Fig. 6 by the points 1 to 6, which is composed of the consecutive processes; cooling down to T_l under stress-free state ($1 \to 2$), isothermal loading up to Σ^* at T_l ($2 \to 3$), isostatic cooling down to T_l under Σ^* ($3 \to 4$) and isostatic heating up to $T^*_{R_R}$ under Σ^* ($4 \to 3 \to 5 \to 6$). The macroscopic strain induced in each of the processes is already calculated;

The cooling process ($1 \to 2$): No strain observed.

The isothermal loading up to Σ^* ($2 \to 3$): Eq. (6.20).

The process of cooling down to T_l ($3 \to 4$) under constant applied stress: Eq. (6.22).

The process of heating up to $T^*_{R_R}$ ($4 \to 3 \to 5 \to 6$) under constant applied stress: Eq. (6.30).

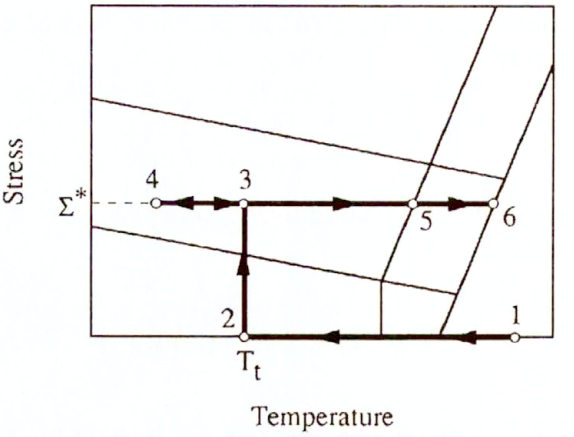

FIG. 6. Thermomechanical processes.

6.6. Recovery stress during heating

The simulation in the preceding subsections shows that a shrinkage strain is observed during heating along any kind of thermomechanical path. A tensile stress is, therefore, induced in the specimen when the strain is constrained during heating. The stress is called the recovery stress and plays an important role of the driving force in the shape memory devices. Change in stress under the condition of the constrained strain is incrementally governed by

$$0 = S\,d\Sigma + \Theta\,dT + dE^*, \tag{6.31}$$

which is derived from Eq. (6.15). The essential thing is, therefore, to calculate the increment of transformation strain dE^* along a prescribed thermomechanical loading path, which is already performed by means of Eq. (6.14) together with Eqs. (6.4) and (6.25). If the result is combined with Eq. (6.31), one obtains

$$\begin{aligned} d\Sigma = &- \left[S + \delta_\zeta \overline{Z}_\Sigma \Omega^*_\alpha \alpha(1-\zeta)\right]^{-1} \\ &\times \left[\Theta + \delta_\alpha E^*_{\alpha 0} \zeta^*_s a_h (A_{T0} - \alpha) + \delta_\zeta b\, \overline{Z}_\Sigma \Omega^*_\alpha \alpha(1-\zeta)\right] dT, \end{aligned} \tag{6.32}$$

which determines the stress increment $d\Sigma$ due to prescribed temperature increment dT. The indicators δ_ζ and δ_α have the following meaning:

$$\delta_\zeta = \begin{cases} 1 & \text{when the crystal reorientation progresses,} \\ 0 & \text{otherwise,} \end{cases}$$

$$\delta_\alpha = \begin{cases} 1 & \text{when the reverse lattice distortion in the R-phase progresses,} \\ 0 & \text{otherwise.} \end{cases}$$

From the practical point of view, the recovery stress induced during heating after the following two thermomechanical paths is important to be investigated: the process in which the residual strain is constrained at the point 2 in Fig. 6 after the successive thermomechanical preloading of the cooling ($1 \rightarrow 2$), loading ($2 \rightarrow 3$) and unloading ($3 \rightarrow 2$); and the process in which the total strain is constrained at the point 3 after the successive thermomechanical preloading of the cooling ($1 \rightarrow 2$) and loading ($2 \rightarrow 3$). The simulated results will be given in the next section.

7. Numerical illustrations

Uniaxial behaviours explained in Sec. 6 are simulated in this section with the use of the value of the material parameters tabulated in Table 1, which are partly determined from the data of a TiNi alloy [2], the transformation lines of which are illustrated in Fig. 7. The thermal strain is neglected in the following simulation.

Table 1. Material parameters.

S	a_c	b	c	$\overline{Z}_\Sigma$	T_{R_F}	T_{R_R}	Σ_{R_F}	A_{T0}	$\Omega^*_{\alpha_0}$	$E^*_{\alpha_0}$
1/MPa	1/K	MPa/K	MPa/K	1/MPa	K	K	MPa			
5×10^{-5}	−0.026	0.163	12	0.0132	300	310	10	1.2	0.01	0.01

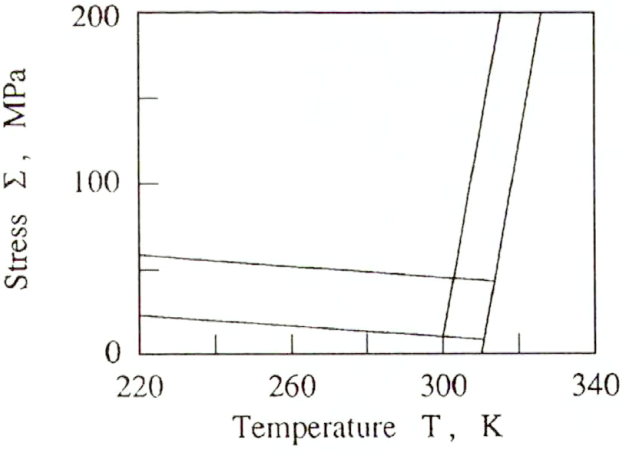

FIG. 7. Transformation lines.

Figure 8 shows the stress-strain curves observed during each isothermal loading and unloading at T_t in the successive cooling-loading-unloading processes ($1 \rightarrow 2 \rightarrow 3 \rightarrow 2$ in Fig. 6). It should be noted that the strain induced in this process is due only to the variants reorientation (cf. Sec. 6.2). The ferroelastic curves exhibit, under the temperature range of $T_t \leq T_{R_F} = 300\,\text{K}$, the same response as

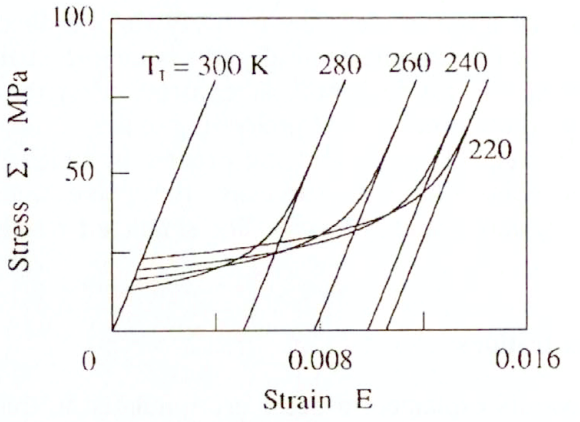

FIG. 8. Stress-strain curves.

the shape memory effect in the martensitic transformation. The strain amplitude, the recovery strain E^*_{max}, at each temperature is plotted in Fig. 9, which corresponds to the schematic illustration in Fig. 4 and represents well the experimental observation [2]. Figure 10 is a plot of the transformation strain E^* observed when the applied stress at the state 3 in Fig. 6 is Σ^*. The results show firstly that, for the higher stress and higher temperature, the transformation strain converges at the earlier stage to a limit curve which corresponds to the curve in Fig. 9. It is a rephrase of the fact that the variants reorientation finishes when the generic point reaches the variants reorientation finish line in Fig. 3 c, d. Secondly, the lower intersection of the iso-Σ^* curve with the horizontal line represents the point on the variants reorientation start line in Fig. 3 c, d at which the variants reorientation starts and the transformation strain starts being induced.

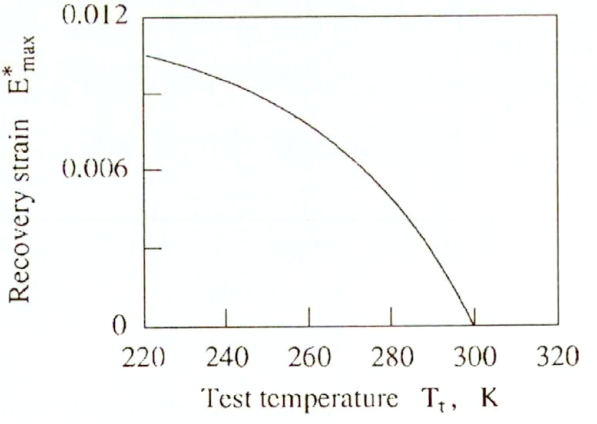

FIG. 9. Temperature dependence of recovery strain.

Figure 11 illustrates the development of the transformation strain E^* in the isostatic cooling processes ($6 \rightarrow 5 \rightarrow 3 \rightarrow 4$ in Fig. 6) down to $T_l = 220\,\mathrm{K}$ under

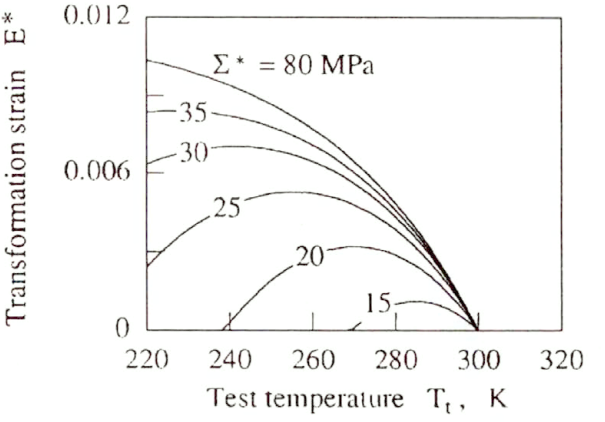

FIG. 10. Stress and temperature dependence of recovery strain.

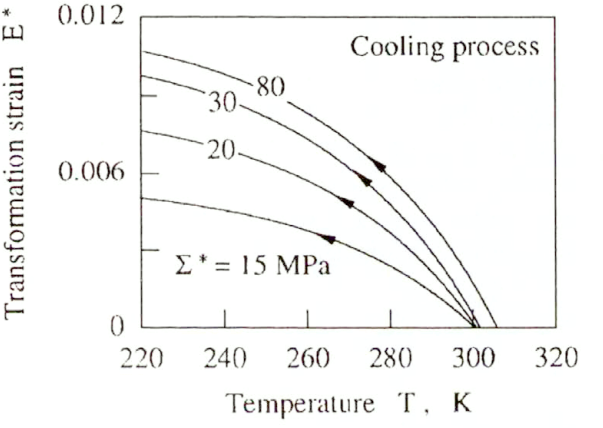

FIG. 11. Change in transformation strain during cooling under constant applied stress.

a constant applied stress Σ^*. As explained in Sec. 6.3, the strain is induced only by the forward lattice distortion in the R-phase. Two points have to be noted: the transformation strain increases with Σ^* and converges to a limit curve at each temperature level. Secondly, the temperature of the strain to start being induced increases with the applied stress, which is due to nothing other than the fact that the R-phase transformation line has a positive inclination as shown in Fig. 3 a.

Under the cooling/heating processes ($6 \rightarrow 5 \rightarrow 3 \rightarrow 4 \rightarrow 3 \rightarrow 5 \rightarrow 6$ in Fig. 6) down to $T_l = 220\,\mathrm{K}$ under a constant applied stress Σ^*, the strain induced in the cooling process, which has already been calculated above, fully recovers in the subsequent heating process as given in Fig. 12. The strain vanishes on the R-phase reverse transformation line (cf. Fig. 3 b), meaning at different temperatures. The change in transformation strain stems from the reverse lattice distortion process in the R-phase. The variants reorientation progresses in the heating process only

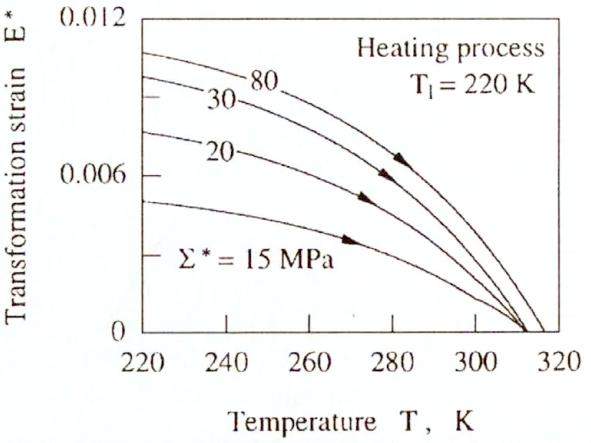

FIG. 12. Change in transformation strain during heating under constant applied stress.

in a narrow region between the R-phase transformation line and the R-phase reverse transformation line, which has no notable effect on the results. The change in transformation strain during the whole cooling/heating process is plotted in Fig. 13 in the case of T_l = 220 K under Σ^* = 20 MPa. The transformation strain increases in the cooling process and recovers fully in the subsequent heating process. A hysteresis is observed due to the fact that the R-phase transformation line and the R-phase reverse transformation line are different.

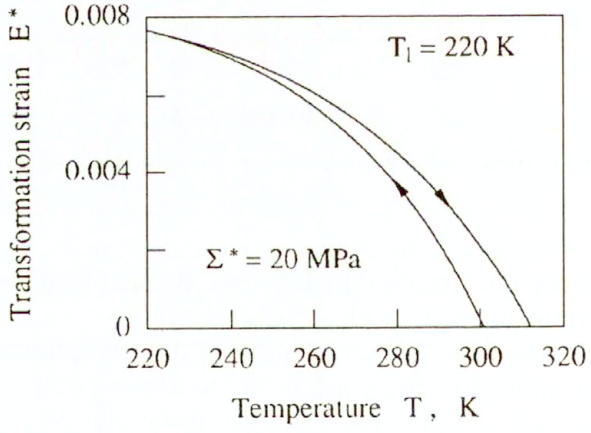

FIG. 13. Strain hysteresis during cooling/heating under constant applied stress.

When the specimen is heated after a cooling-loading-unloading process ($1 \rightarrow 2 \rightarrow 3 \rightarrow 2$ in Fig. 6), with the residual strain at the state 2 constrained, a positive recovery stress is induced, which is plotted in Fig. 14 for the cases of the isothermal loading to Σ^* at T_t = 220 K. The variants reorientation progresses up to an extent ζ^* when Σ^* is in the variants reorientation zone in Fig. 3 c dur-

ing isothermal loading. During heating, a negative increase of the transformation strain first progresses due to the reverse lattice distortion in the R-phase. A positive increase of the recovery stress is, therefore, observed at this stage as shown in the figure. When the generic point (T, Σ_R) reaches the ζ^* line, the variants reorientation starts progressing from the extent ζ^* on. The process induces a positive strain increase, resulting in a decrease of the stress. From this moment on, two metallurgical progresses occur simultaneously. The reverse lattice distortion in the R-phase increases the recovery stress, whereas the variatns reorientation decreases the recovery stress. The case is typically observed in the figure for the cases of Σ^* = 25, 30 and 35 MPa. When Σ^* is large, the variants reorientation almost finishes during the first isothermal loading. No decrease in recovery stress is, therefore, observed in the subsequent heating process (cf. the case of Σ^* = 80 MPa). When Σ^* is lower than the variants reorientation start line, neither the residual strain nor the recovery stress is produced.

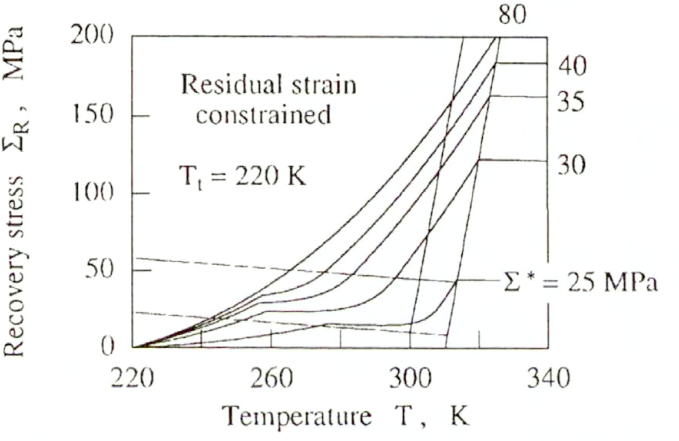

FIG. 14. Recovery stress under residual strain constrained.

The maximum recovery stress $\Sigma_{R\,\max}$ is reached on the R-phase reverse transformation line, which is plotted in Fig. 15 versus the test temperature T_t with the applied stress Σ^* as a parameter. The intersections of the iso-Σ^* curves and the horizontal axis are on the variants reorientation start line.

When the specimen is heated after a cooling-loading process ($1 \rightarrow 2 \rightarrow 3$ in Fig. 6), with the total strain constrained at the state 3 (T_t, Σ^*), the recovery stress starts increasing from the initial value Σ^* as given in Fig. 16. The two metallurgical processes occur simultaneously when the start point is in the variants reorientation zone, as in the case of the constrained residual strain (Fig. 14). The variants reorientation process finishes when the generic point reaches the finish line on each iso-Σ^* curve. The remaining process progresses only due to the reverse lattice distortion in the R-phase. A slower increase in the strain for the lower value of Σ^* is a point to be noted when comparing the simulated results with the experimental data.

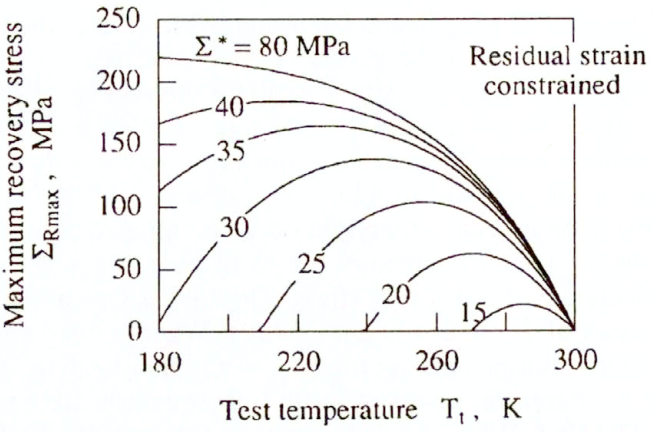

FIG. 15. Maximum recovery stress under residual strain constrained.

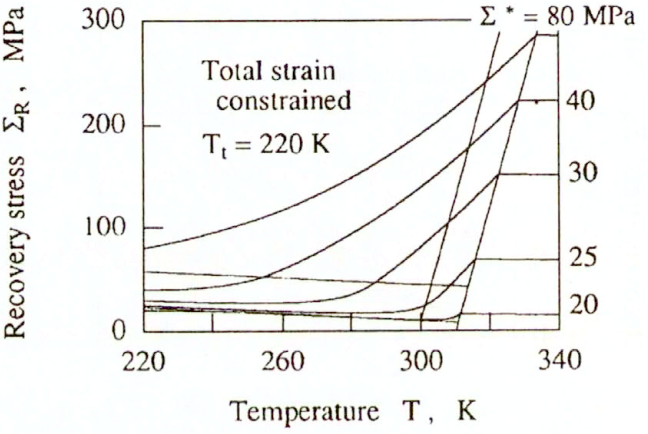

FIG. 16. Recovery stress under total strain constrained.

8. Concluding remarks

The metallurgical observations have clearly revealed in the TiNi shape memory alloys that the R-phase transformation starts on a R-phase transformation start line in the stress-temperature plane and finishes on the other line, the R-phase transformation finish line. The same is true for the R-phase reverse transformation being represented by the R-phase reverse transformation start/finish lines. The processes which have mistakenly been understood as the R-phase transformation in the mechanical formulations carried out so far, include the processes "after" the R-phase transformation, the lattice distortion in the R-phase variants and the variants reorientation of the R-phase variants by twinning.

The theoretical framework established in this paper on the thermomechanics of R-phase transformation is based on this metallurgical understanding. The

uniaxial governing equations are reduced from the general formulation in order to simulate the alloy behaviour under several thermomechanical load processes. The validity of the theory can be well proved by carrying out the experiments on the recovery stress explained in Figs. 14 and 15, which show a clear coupled effect of the lattice distortion in the R-phase and the variants reorientation. This is a task of the next study.

Acknowledgments

Part of this work was financially supported by the Special Research Fund/Tokyo Metropolitan Government as well as by the Grant-in-Aid for Scientific Research (No. 08611507) through the Ministry of Education, Science and Culture, Japan.

References

1. S. MIYAZAKI and K. OTSUKA, *Deformation and transition behavior associated with the R-phase in Ti-Ni alloys*, Metall. Trans. A, **17A**, 53–63, 1986.
2. S. MIYAZAKI and C.M. WAYMAN, *The R-phase transition and associated shape memory mechanism in TiNi single crystals*, Acta Metall., **36**, 181–192, 1988.
3. S. MIYAZAKI, S. KIMURA and K. OTSUKA, *Shape-memory effect and pseudoelasticity associated with the R-phase transition in Ti-50.5 at. % Ni single crystals*, Phil. Mag. A, **57**, 467–478, 1988.
4. S. MIYAZAKI, K. NOMURA and A. ISHIDA, *Shape memory effects associated with the martensitic and R-phase transformations in sputter-deposited Ti-Ni thin films*, J. Physique IV, Coll. C8, suppl. J. Phys. III, vol. 5, C8/677-C8/682, 1995.
5. T. SAWADA, H. TOBUSHI, K. KIMURA, T. HATTORI, K. TANAKA and P.H. LIN, *Stress-strain-temperature relationship associated with the R-phase transformation in TiNi shape memory alloy (Influence of shape memory processing temperature)*, JSME Int. J., Ser. A, **36**, 395–401, 1993.
6. P.H. LIN, H. TOBUSHI, Y. HATTORI, K. TANAKA and CH. LEXCELLENT, *Recovery stress associated with the R-phase transformation in TiNi shape memory alloy*, [in:] Proc. First ASIA-Oceania Int. Symp. on Plasticity, WANG TZUCHIANG and XU BINGYE [Eds.], Peking University Press, Beijing, 72–79, 1994.
7. P.H. LIN, H. TOBUSHI, A. IKAI and K. TANAKA, *Deformation properties associated with the martensitic and R-phase transformations in TiNi shape memory alloy*, [in:] Shape Memory Materials 94, CHU YOUYI and TU HAILING [Eds.], International Academic Publishers, 530–534, 1994.
8. S. LECLERCQ, CH. LEXCELLENT, H. TOBUSHI and P.H. LIN, *Thermodynamical modelling of recovery stress associated with R-phase transformation in TiNi shape memory alloys*, Mater. Trans., JIM, **35**, 325–331, 1994.
9. C.M. HWANG, M.E. MEICHLE, M.B. SALAMON and C.M. WAYMAN, *Transformation behavior of a $Ti_{50}Ni_{47}Fe_3$ alloy*, II. *Subsequent premartensitic behavior and the commensurate phase*, Phil. Mag. A, **47**, 31–62, 1983.
10. M.B. SALAMON, M.E. MEICHLE and C.M. WAYMAN, *Premartensitic phases of $Ti_{50}Ni_{47}Fe_3$*, Phys. Rev., **B31**, 7306–7315, 1985.
11. H.C. LING and R. KAPLOW, *Phase transitions and shape memory in NiTi*, Metall. Trans. A, **11A**, 77–83, 1980.
12. H.C. LING and R. KAPLOW, *Stress-induced shape changes and shape memory in the R and martensite transformations in equiatomic NiTi*, Metall. Trans. A, **12A**, 2101–2111, 1981.
13. H.B. CALLEN, *Thermodynamics*, John Wiley & Sons, New York 1960.
14. D.J. BARRETT, *A three-dimensional phase transformation model for shape memory alloys*, J. Intell. Material Syst. Struct., **6**, 831–840, 1995.

15. L.C. BRINSON, A. BEKKER and S. HWANG, *Deformation of shape memory alloys due to thermo-induced transformation*, J. Intell. Material Syst. Struct., 7, 97–107, 1996.

16. L.C. BRINSON, *One-dimensional constitutive behavior of shape memory alloys: Thermomechanical derivation with non-constant material functions and redefined martensite internal variable*, J. Intell. Material Syst. Struct., **4**, 229–242, 1993.

17. Q.P. SUN and K.C. HWANG, *Micromechanics modelling for the constitutive behavior of polycrystalline shape memory alloys. I. Derivation of general relations*, J. Mech. Phys. Solids, **41**, 1–17, 1993.

18. E. PATOOR, A. EBERHARDT and M. BERVEILLER, *Micromechanical modelling of the shape memory behavior*, [in:] Mechanics of Phase Transformations and Shape Memory Alloys, L.C. BRINSON and B. MORAN [Eds.], ASME, New York, 23–37, 1994.

19. S. LECLERCQ, CH. LEXCELLENT, *A general macroscopic description of the thermomechanical behavior of shape memory alloys*, J. Mech. Phys. Solids, **44**, 953–980, 1996.

20. K. TANAKA, S. KOBAYASHI and Y. SATO, *Thermomechanics of transformation pseudoelasticity and shape memory effect in alloys*, Int. J. Plasticity, **2**, 59–72, 1986.

21. K. TANAKA, E.R. OBERAIGNER and F.D. FISCHER, *A unified theory on thermomechanical mesoscopic behavior of alloy materials in the process of martensitic transformation*, [in:] Mechanics of Phase Transformations and Shape Memory Alloys, L.C. BRINSON and B. MORAN [Eds.], ASME, New York, 151–157, 1994.

22. B. RANIECKI and A. SAWCZUK, *Thermal effect in plasticity. Part I. Coupled theory*, ZAMM, **55**, 333–341, 1975.

23. K. TANAKA, F. NISHIMURA, H. TOBUSHI, E.R. OBERAIGNER and F.D. FISCHER, *Thermomechanical behavior of an Fe-based shape memory alloy: Transformation conditions and hystereses*, [in:] Proc. ICOMAT 95, J. Physique IV, Coll. C8, Suppl. J. Phys. III, Vol. 5, R. GOTTHARDT and J. VAN HUMBEECK [Eds.], Les Editions De Physique, Les Ulis, C8/463-C8/468, 1995.

24. F. NISHIMURA, N. WATANABE and K. TANAKA, *Transformation lines in an Fe-based shape memory alloy under tensile and compressive stress states*, Materials Sci. Engng. A, **221**, 134–142, 1996.

25. D.G.B. EDELEN, *Primitive thermodynamics: A new look at the Clausius-Duhem inequality*, Int. J. Engng. Sci., **12**, 121–141, 1974.

26. A.C. ERINGEN, *Thermodynamics of continua*, [in:] Continuum Physics, A.C. ERINGEN [Ed.], Vol. II, Part I-3, Academic Press, New York, 89–127, 1975.

27. D. PERIC, *On a class of constitutive equations in viscoplasticity: formulation and computational issues*, Int. J. Num. Methods Engng., **36**, 1365–1393, 1993.

DEPARTMENT OF AEROSPACE ENGINEERING,
TOKYO METROPOLITAN INSTITUTE OF TECHNOLOGY, HINO/TOKYO
e-mail: kikitana@astan1.tmit.ac.jp

and

INSTITUTE OF MATERIALS SCIENCE
UNIVERSITY OF TSUKUBA, TSUKUBA, J-305 IBARAKI, JAPAN

Received April 17, 1996; new version December 12, 1996.

Arch. Mech., 49, 3, pp. 573–584, Warszawa 1997

A new method of finding strong approximation to solutions to some IBVPs

Z. TUREK (WARSZAWA)

IT HAS BEEN PROVED that every solution to a 1D initial boundary value problem (IBVP) represented by a uniformly convergent series in some domain can be approximated by a Fourier cosine series. The new series is also uniformly convergent in that domain. The strong approximation to the heat-conduction problem subject to any boundary conditions with the application of the *Fourier cosine series* is found. It is the Fourier cosine series approximation to the exact solution to the problem under consideration. Its coefficients form an infinite set of ordinary differential equations (ISODE). Numerical results presented for heat conduction problems show – in comparison with solutions derived by the method of seperation of variables – that relatively small number of terms of the Cosine Series approximate very well the exact solutions.

1. Introduction

IN [6] A NEW METHOD of finding approximate solutions to the heat conduction equation in one dimension subject to mixed boundary conditions has been presented. From the results obtained we could see that the solution to the problem derived by the *Fourier cosine series* approximated well the solution to the same problem derived by the method of seperation of variables. The boundary conditions for the problem were not satisfied. Paper [7], however, applies the new method to a certain class of partial differential equations of engineering and physics subject to non-Dirichlet boundary conditions, considering the problem of boundary conditions as well. In that paper we solved two initial boundary-value problems with non-Dirichlet boundary conditions without solving the eigenvalue problems. The new approach was applied to the equation describing the heat conduction subject to non-Dirichlet boundary conditions and the vibrations of a rod also subject to non-Dirichlet boundary conditions. The numerical results showed that the new solutions also approximated well the solutions derived by the method of seperation of variables. For the heat equation, however, even the boundary conditions at the initial instant of time were satisfied. Analysing the boundary conditions of the vibrating rod for a given initial displacement of the rod we came to the conditions on the Fourier cosine coefficients at $t = 0$. They were expressed as convergent series of the Fourier cosine coefficients mentioned above. They did not tend to zero which meant that the new method solution did not satisfy the prescribed boundary conditions even at $t = 0$. The classical method of solution did not satisfy the prescribed boundary conditions either since the initial condition for the problem did not satisfy the given boundary conditions.

The aim of the present paper is to give mathematical grounds to the new method. So it has first been proved that every solution to a one-dimensional IBVP represented by a uniformly convergent series in $[0, L] \times [0, t_e)$ can be approximated by the Fourier cosine series which is uniformly convergent in that domain. It has been proved that the Fourier cosine series is a strong approximation to the problem under consideration, which is a solution to the so-called integro-differential-boundary equations (IDBE) [6, 7]. It has been found out that solutions to the corresponding ISODE form the Fourier cosine coefficients for the strong solution (*satisfying given equations and conditions*) of the heat-conduction problem (*this is why we call our approximation strong approximation*). In the paper we present the new approach to the heat conduction problem for all kinds of homogeneous boundary conditions. But the method can be applied to other boundary-value problems as well [5].

2. Fourier cosine series representation for a certain function of two variables

In this section we are going to show a Fourier cosine series representation for a function of two variables which is a sum of a uniformly convergent series. To this end we need some results concerning a Fourier cosine representation for a function of one variable.

LEMMA 1 [4]. Every function X, continuous in the interval $[0, L]$ whose derivative X' is piecewise continuous in that interval can be expressed by a uniformly convergent series

$$X(x) = \frac{\gamma_0}{2} + \sum_{n=1}^{\infty} \gamma_n \cos \frac{n \pi x}{L},$$

in that interval, where

$$\gamma_n = \frac{2}{L} \int_0^L \cos \frac{n \pi x}{L} X(x)\, dx, \qquad n = 0, 1, 2, \ldots . \tag{2.1}$$

P r o o f. Let $\overline{X}$ be an even extension of X. Then $\overline{X}$ is an even cortinuous function whose derivative $\overline{X}'$ is piecewise continuous on $[-L, L]$. The Fourier coefficients for $\overline{X}$ are

$$c_n = \frac{1}{L} \int_{-L}^{L} \overline{X}(x) \cos \frac{n \pi x}{L} dx = \frac{1}{\pi n} \left[\overline{X}(x) \sin \frac{n \pi}{L} x \right]_{-L}^{L} \tag{2.2}$$

$$- \frac{1}{\pi n} \int_{-L}^{L} \overline{X}'(x) \sin \frac{n \pi}{L} x\, dx = - \frac{1}{\pi n} \int_{-L}^{L} \overline{X}'(x) \sin \left(\frac{n \pi}{L} x \right) dx =: - \frac{L}{\pi n} \beta_n$$

and

$$b_n = \frac{1}{L}\int_{-L}^{L} \overline{X}(x)\sin\frac{n\pi x}{L}dx = 0,$$

as the function $\overline{X}$ is even. The Fourier Coefficients β_n for the derivative $\overline{X}'$ of the function $\overline{X}$ exist since $\overline{X}'$ is piecewise continuous and the series

$$\sum_{n=1}^{\infty} \beta_n^2 \tag{2.3}$$

is convergent. Let us now consider the formula

$$\left(|\beta_n| - \frac{L}{n\pi}\right)^2 = \beta_n^2 - \frac{2L|\beta_n|}{n\pi} + \left(\frac{L}{n\pi}\right)^2 \geq 0,$$

from which we have

$$\frac{L|\beta_n|}{n\pi} \leq \frac{1}{2}\beta_n^2 + \frac{1}{2}\left(\frac{L}{n\pi}\right)^2 \qquad (n = 1, 2, \ldots).$$

The right-hand side of the above inequality consists of the elements of a convergent series. Then the series

$$\sum_{n=1}^{\infty} \frac{L|\beta_n|}{n\pi}$$

is convergent and so is the series

$$\sum_{n=1}^{\infty} |c_n| . \tag{2.4}$$

As the series in (2.4) is convergent, then the series

$$\frac{c_0}{2} + \sum_{n=1}^{\infty} c_n \cos\frac{n\pi x}{L}$$

is absolutely and uniformly convergent and its sum is $\overline{X}(x)$ [1]. But the function $\overline{X}$ is an even extension of X and coincides with X in the fundamental interval, then

$$c_n = \frac{1}{L}\int_{-L}^{L} \overline{X}(x)\cos\frac{n\pi x}{L}dx = \frac{2}{L}\int_{0}^{L} X(x)\cos\frac{n\pi x}{L}dx = \gamma_n .$$

So the Lemma has been proved. □

Now we will use a known result [1] concerning the uniform convergence of an infinite series whose terms are products of functions of a certain class. This results in verifying formal solutions to boundary value problems represented in the following form:

$$S(x,t) = \sum_{i=1}^{\infty} X_i(x) T_i(t). \tag{2.5}$$

Abel's test for uniform convergence [1]

The series (2.5) converges uniformly with respect to the two variables x and t together in a region D of the $x - t$ plane provided that

a) the series

$$\sum_{i=1}^{\infty} X_i(x)$$

converges uniformly with respect to x for all x such that (x,t) is in D, and

b) the functions T_i are uniformly bounded and monotonic with respect to i $(i = 1, 2, ...)$ for all t such that (x,t) is in D. □

In establishing the way for the Fourier cosine series representation of the series in (2.5) we will mostly depend on the important fact stated in the following lemma which is an extension of Lemma 1 for a function with a parameter t.

LEMMA 2. Any continuous function

$$u(\cdot, t) : [0, L] \to \mathcal{R}$$

piecewise C^1 in $[0, L]$ for every $t \in [0, t_e)$ can be represented by the Fourier cosine series

$$\frac{c_0(t)}{2} + \sum_{n=1}^{\infty} c_n(t) \cos \frac{n \pi x}{L}, \tag{2.6}$$

that is uniformly convergent in $[0, L]$ for all $t \in [0, t_e)$ with coefficients

$$c_n(t) = \frac{2}{L} \int_0^L u(x,t) \cos \frac{n \pi x}{L} dx. \tag{2.7}$$

The proof of this fact is exactly the same as that of Lemma 1. □

The fundamental fact leading to the Fourier cosine representation for the series (2.5) is expressed by the following theorem.

THEOREM 1. *Let X_i satisfy, for each $i = 0, 1, 2, \ldots$ the conditions stated in Lemma 1 and additionally let X_i and T_i satisfy for each $i = 0, 1, 2, \ldots$ the conditions of the Abel's test for uniform convergence.*

If the sum $S(x,t)$ *of the series* (2.5) *satisfies the conditions stated in Lemma* 2 *in* $D := [0,L] \times [0,t_e)$, *then the series*

$$\frac{c_0(t)}{2} + \sum_{n=1}^{\infty} c_n(t) \cos \frac{n\pi x}{L}, \tag{2.8}$$

with the coefficients

$$c_n(t) = \sum_{i=1}^{\infty} \gamma_{ni} T_i(t) \qquad n = 0,1,2..., \tag{2.9}$$

where γ_{ni} *are defined by* (2.1) *for* $X \equiv X_i$, *converges uniformly to the sum* $S(x,t)$ *of the series* (2.5) *in D.*

P r o o f. Notice that

$$c_n(t) = \sum_{i=1}^{\infty} \gamma_{ni} T_i(t) = \frac{2}{L} \sum_{i=1}^{\infty} \int_0^L \cos \frac{n\pi x}{L} X_i(x) T_i(t)\, dx.$$

Using the theorem on integration term by term [2] we come to

$$c_n(t) = \frac{2}{L} \int_0^L \cos \frac{n\pi x}{L} \sum_{i=1}^{\infty} X_i(x) T_i(t)\, dx = \frac{2}{L} \int_0^L \cos \frac{n\pi x}{L} S(x,t)\, dx,$$

for $n = 0,1,2,.....$ These coefficients are Fourier cosine series coefficients for the sum $S(x,t)$ of the series (2.5). So the series (2.8) is the Fourier cosine series for the sum $S(x,t)$ which satisfies the conditions of Lemma 2, and that ends the proof of the theorem. □

3. A new approach to strong approximation to a solution to the heat conduction equation

From Theorem 1 we know that every series $\sum_{i=1}^{\infty} X_i(x) T_i(t)$ uniformly convergent in $[0,L] \times [0,t_e)$ whose sum $S(x,t)$ satisfies the conditions of Lemma 2, can be represented by a Fourier cosine series that is uniformly convergent in that domain. This means that every solution $u(x,t)$ to an IBVP represented by a series satisfying the conditions mentioned above can be expanded in the cosine series

$$u(x,t) = \frac{c_0(t)}{2} + \sum_{n=1}^{\infty} c_n(t) \cos \frac{n\pi x}{L} \tag{3.1}$$

with

$$c_n(t) = \sum_{i=1}^{\infty} \gamma_{ni} T_i(t), \tag{3.2}$$

where

$$\gamma_{ni} = \frac{2}{L} \int_0^L X_i(x) \cos \frac{n \pi x}{L} dx$$

with $X_i(x)$ being eigenfunctions of the problem under consideration and $T_i(t)$ satisfying the corresponding uncoupled infinite set of ordinary differential equations.

The above representation will have a practical application if we find a method of calculating Fourier coefficients other than those presented by (3.2). Such a method exists, however, and has been described in [5, 6, 7]. The method leads first to the IDBE and then to the ISODE for the problem. The corresponding IDBE and ISODE are derived for each boundary-value problem separately. In the present paper we are going to demonstrate the approach for the heat conduction problem.

3.1. IDBE and ISODE for the heat conduction problem with non-Dirichlet boundary conditions

Let us consider the equation

$$\frac{\partial U}{\partial t} - \frac{\partial^2 U}{\partial x^2} = 0 \qquad \text{for} \quad (x, t) \in (0, L) \times (0, t_e), \tag{3.3}$$

subject to the boundary conditions

$$\begin{aligned} \frac{\partial U}{\partial x} - h U &= 0 \qquad \text{for} \quad x = 0, \\ \frac{\partial U}{\partial x} + g U &= 0 \qquad \text{for} \quad x = L, \end{aligned} \tag{3.4}$$

for all $t \in [0, t_e]$, and the initial condition

$$U(x, 0) = U_0(x), \tag{3.5}$$

for all $x \in [0, L]$, where h and g are constants. The IDBE for the problem is the following one [6, 7]:

$$\begin{aligned} &\frac{d}{dt} \int_0^L U(x, t) \cos \frac{n \pi x}{L} dx + \alpha_n^2 \int_0^L U(x, t) \cos \frac{n \pi x}{L} dx = F_n, \\ &F_n = -h U(0, t) - g U(L, t)(-1)^n, \qquad \alpha_n = \pi n / L, \quad n = 0, 1, 2, \ldots. \end{aligned} \tag{3.6}$$

Before we find the ISODE let us introduce a notion

DEFINITION. *A function*

$$U(\cdot,\cdot):[0,L]\times[0,t_e)\to\mathcal{R}$$

is a strong approximation to a solution to the initial boundary-value problem (3.3) – (3.5) *if it satisfies the IDBE in* (3.6), *i.e.* U *satisfies almost everywhere the following infinite set of integro-differential boundary equations*

$$\frac{d}{dt}\int_0^L U(x,t)\cos\frac{n\pi x}{L}dx+\alpha_n^2\int_0^L U(x,t)\cos\frac{n\pi x}{L}dx=F_n\,,$$
$$F_n=-hU(0,t)-gU(L,t)(-1)^n \tag{3.7}$$

for $n=0,1,2,\ldots$. □

The corresponding ISODE for the problem in (3.3)–(3.5) appears in the following lemma which we give without a proof.

LEMMA 3. Any function $U(\cdot,\cdot):[0,L]\times[0,t_e)\to\mathcal{R}$ satisfying the conditions stated in Lemma 2 is a strong approximation to a solution to the IBV problem (3.3)–(3.5) and can be represented by the series

$$U(x,t)=\frac{c_0(t)}{2}+\sum_{n=1}^{\infty}c_n(t)\cos\frac{n\pi x}{L} \tag{3.8}$$

with c_n computed from the so-called ISODE for the problem (3.3)–(3.5) in the following form

$$\dot{c}_n+\alpha_n^2c_n=\frac{2}{L}G_n\,,$$
$$G_n:=-\frac{c_0}{2}[h+g(-1)^n]-\sum_{k=1}^{\infty}c_k[h+g(-1)^{k+n}], \tag{3.9}$$
$$c_n(0)=\frac{2}{L}\int_0^L U_0(x)\cos\frac{n\pi x}{L}dx,$$

for $n=0,1,2,\ldots$ and G_n were derived from F_n using the boundary conditions in (3.4) □

Solutions to the ISODE in (3.9) follow from the following theorem.

THEOREM 2. *If the series*

$$U(x,t)=\sum_{i=1}^{\infty}X_i(x)T_i(t) \tag{3.10}$$

is a solution to (3.3) – (3.5) *derived by the method of seperation of variables, then*

$$c_n(t) = \sum_{i=1}^{\infty} \gamma_{ni} T_i(t), \qquad n = 0, 1, 2, \ldots \tag{3.11}$$

with

$$\gamma_{ni} = \frac{2}{L} \int_0^L \cos \frac{n \pi x}{L} X_i(x) dx$$

being solutions to the ISODE (3.9).

P r o o f. We have to consider two cases; $n \neq 0$ and $n = 0$.

In the first case (for $n \neq 0$) let us consider the second term at the left-hand side of $(3.9)_1$

$$\alpha_n^2 c_n = \alpha_n^2 \sum_{i=1}^{\infty} \gamma_{ni} T_i = \sum_{i=1}^{\infty} \alpha_n^2 \gamma_{ni} T_i \,. \tag{3.12}$$

Using now the expression for γ_{ni} and integrating twice by parts we get for each term in (3.12) the following expression

$$\alpha_n^2 \gamma_{ni} T_i = T_i \alpha_n^2 \frac{2}{L} \int_0^L \cos \frac{n \pi x}{L} X_i(x) dx \tag{3.13}$$

$$= -\frac{2}{L} [g X_i(L) T_i (-1)^n + h X_i(0) T_i] - \dot{T}_i \gamma_{ni} \,.$$

In the above formula we have used the boundary conditions (3.4) and the fact that $X_i'' + \omega_i^2 X_i = 0$ and $\dot{T}_i + \omega_i^2 T_i = 0$, where ω_i is the i-th eigenvalue for the problem (3.3) – (3.5).

As the terms of (3.13) contain terms of the series (3.10), we can add up both sides of (3.13), to get

$$\alpha_n^2 \sum_{i=1}^{\infty} \gamma_{ni} T_i = -\frac{2}{L} \left[g(-1)^n \sum_{i=1}^{\infty} X_i(L) T_i + h \sum_{i=1}^{\infty} X_i(0) T_i \right] - \sum_{i=1}^{\infty} \dot{T}_i \gamma_{ni} \,,$$

or using the fact that

$$\sum_{i=1}^{\infty} X_i(L) T_i(t) = U(L, t), \qquad \sum_{i=1}^{\infty} X_i(0) T_i(t) = U(0, t), \qquad \sum_{i=1}^{\infty} \dot{T}_i(t) \gamma_{ni} = \dot{c}_n$$

we have

$$\alpha_n^2 \sum_{i=1}^{\infty} \gamma_{ni} T_i = -\frac{2}{L} [g U(L, t)(-1)^n + h U(0, t)] - \dot{c}_n \,.$$

Now we can exploit the above formula at the left-hand side of $(3.9)_1$

$$\dot{c}_n + \alpha_n^2 c_n = \dot{c}_n + \alpha_n^2 \sum_{i=1}^{\infty} \gamma_{ni} T_i = \dot{c}_n - \frac{2}{L}[gU(L,t)(-1)^n + hU(0,t)] - \dot{c}_n$$

$$= -\frac{2}{L}[gU(L,t)(-1)^n + hU(0,t)] = \frac{2}{L} G_n$$

and that ends the proof for $n \neq 0$.

In the second case (for $n = 0$), Eq. $(3.9)_1$ has the form

$$\dot{c}_0 = \frac{2}{L} G_0 .$$

Consider the left-hand side of the above equation. Proceeding in the same way as for $n \neq 0$ we get

$$\mathcal{L} \equiv \dot{c}_0 = \sum_{i=1}^{\infty} \gamma_{0i} \dot{T}_i = -\frac{2}{L} \sum_{i=1}^{\infty} T_i(t) \int_0^L \omega_i^2 X_i(x)\, dx$$

$$= \frac{2}{L} \sum_{i=1}^{\infty} T_i(t) \int_0^L X_i''(x)\, dx = -\frac{2}{L} \sum_{i=1}^{\infty} T_i(t)[gX_i(L) + hX_i(0)]$$

$$= -\frac{2}{L}[gU(L,t) + hU(0,t)] = \frac{2}{L} G_0$$

and that ends the proof for $n = 0$.

We also have to prove the initial condition $(3.9)_3$ to be true. Consider Eq. (3.11) for $t = 0$. Then

$$c_n(0) = \frac{2}{L} \sum_{i=1}^{\infty} \int_0^L \cos \frac{n\pi x}{L} X_i(x) T_i(0)\, dx$$

$$= \frac{2}{L} \int_0^L \cos \frac{n\pi x}{L} \sum_{i=1}^{\infty} X_i(x) T_i(0)\, dx = \frac{2}{L} \int_0^L U_0(x) \cos \frac{n\pi x}{L} dx$$

which agrees with $(3.9)_3$. □

3.2. ISODE for the heat conduction problem with any boundary conditions

This time we consider the heat conduction equation

$$\frac{\partial U}{\partial t} - \frac{\partial^2 U}{\partial x^2} = 0 \qquad \text{for} \quad (x,t) \in (0,L) \times (0,t_e), \tag{3.14}$$

subject to the boundary conditions

$$\begin{aligned} \beta\frac{\partial U}{\partial x} + \alpha U &= 0 \qquad \text{for} \quad x = 0, \\ \delta\frac{\partial U}{\partial x} + \gamma U &= 0 \qquad \text{for} \quad x = L, \end{aligned} \tag{3.15}$$

for all $t \in [0, t_e]$, and the initial condition

$$U(x, 0) = U_0(x), \tag{3.16}$$

for all $x \in [0, L]$ where $\alpha, \beta, \gamma, \delta$ are constants satisfying the conditions

$$\alpha^2 + \beta^2 \neq 0, \qquad \gamma^2 + \delta^2 \neq 0.$$

This time the boundary conditions in (3.15) describe also the Dirichlet boundary conditions for the heat equation (3.14).

The IDBE for the heat conduction equation with these boundary conditions are the following:

$$\begin{aligned} &\frac{d}{dt}\int_0^L U(x,t)\cos\frac{n\pi x}{L}dx + \alpha_n^2\int_0^L U(x,t)\cos\frac{n\pi x}{L}dx = Z_n, \\ &Z_n := \frac{\partial U}{\partial x}(x,t)\cos\frac{n\pi x}{L}\Big|_0^L, \qquad n = 0, 1, 2, \ldots. \end{aligned} \tag{3.17}$$

Although the functions Z_n in (3.17) are defined by the boundary values of spatial derivative of the function $U(x, t)$ and, in general, case cannot be expressed by the given boundary conditions, we can also find an infinite set of ordinary differential equations for the coefficients c_n. In this case the ISODE is in the form

$$\begin{aligned} &\dot{c}_n + \alpha_n^2 c_n = \frac{2}{L}H_n(t), \\ &c_n(0) = \frac{2}{L}\int_0^L U_0(x)\cos\frac{n\pi x}{L}dx, \qquad n = 0, 1, 2, \ldots, \end{aligned} \tag{3.18}$$

where after exploiting the cosine series representation for the first derivative [5] in the function Z_n, we get H_n instead of Z_n

$$H_n(t) = \frac{c_0^{(1)}}{2}\left[(-1)^n - 1\right] + \sum_{k=1}^{\infty} c_k^{(1)}(t)\left[(-1)^{k+n} - 1\right] \tag{3.19}$$

with

$$
\begin{aligned}
c_k^{(1)}(t) &= \frac{2}{L}\sum_{j=1}^{\infty} c_j(t)\left[(-1)^{j+k} - \eta_{jk} - 1\right], \\
\eta_{jk} &= -\alpha_k \int_0^L \cos\frac{j\pi x}{L}\sin\frac{k\pi x}{L}dx.
\end{aligned} \tag{3.20}
$$

We can also prove that c_n are Fourier cosine coefficients for the function U which is the Fourier cosine approximation to a strong solution to (3.14), (3.15). Theorem 2 is also valid for this case.

4. Some applications of the new approach

In [6] we have solved the heat conduction problem for mixed boundary conditions (3.4). In [7] we have solved two IBVPs with non-Dirichlet type boundary conditions for the heat equation and for the wave equation. Now we solve the heat conduction problem for other boundary conditions (*including also Dirichlet ones*) using the new method. Generally we solve

$$
\frac{\partial U}{\partial t} - \frac{\partial^2 U}{\partial x^2} = 0 \qquad \text{for} \quad (x,t) \in (0,L)\times(0,t_e), \tag{4.1}
$$

subject to the boundary conditions

$$
\begin{aligned}
\beta\frac{\partial U}{\partial x} + \alpha U &= 0 \qquad \text{for} \quad x = 0, \\
\delta\frac{\partial U}{\partial x} + \gamma U &= 0 \qquad \text{for} \quad x = L,
\end{aligned} \tag{4.2}
$$

for all $t \in [0, t_e]$ and initial condition

$$
U(x,0) = U_0(x), \tag{4.3}
$$

for all $x \in [0, L]$ where

$$
\alpha^2 + \beta^2 \neq 0, \qquad \gamma^2 + \delta^2 \neq 0.
$$

In further calculations $U_0(x) = 1 + \sin[2\pi(x - L/4)/L]$, $L = 1$ for all the examples and Bi = 0.185. The corresponding approximate solutions

$$
U_a(x,t) = \frac{c_0(t)}{2} + \sum_{k=1}^{N_a} c_k(t)\cos\frac{k\pi x}{L} \tag{4.4}
$$

for N_a terms of the series (4.4) we compare to the corresponding classical solutions of the problem (4.1)–(4.3),

$$U_c(x,t) = \sum_{k=1}^{\infty} a_k \exp(-\omega_k^2 t)\psi_k(x), \tag{4.5}$$

for N_c terms of the series (4.5), where

$$a_k := \int_0^L U_0(x)\psi_k(x)\,dx / \|\psi_k(x)\|^2;$$

$\psi_k(x)$ and ω_k are eigenfunctions and eigenvalues, respectively, calculated from a corresponding IBVP. We compute the corresponding ISODE using the Runge–Kutta method.

The form of the ISODE depends on the type of boundary conditions involved. In the case of *non-Dirichlet boundary conditons* (i.e. $\beta\delta \neq 0$), the function Z_n (3.17) can be expressed by the boundary values of the function U itself (e.g. (3.6)) and consequently, by a single series in terms of the coefficients of U (e.g. (3.9)). The simplest case in this class is when $\alpha^2 + \gamma^2 = 0$ where the new method solution agrees with the classical one. In this case the functions $\cos[(n\pi x)/L]$ are eigenfunctions of the heat equation and the ISODE reduces to the infinite uncoupled set of ordinary differential equations for the time components of the Fourier series known from the method of seperation of variables. Other examples are presented in Figs. 1–2.

$$\frac{\partial U}{\partial x} - \mathrm{Bi}\,U = 0 \quad \text{for} \quad x = 0, \qquad \frac{\partial U}{\partial x} = 0 \quad \text{for} \quad x = L.$$

$$\frac{\partial U}{\partial x} = 0 \quad \text{for} \quad x = 0, \qquad \frac{\partial U}{\partial x} + \mathrm{Bi}\,U = 0 \quad \text{for} \quad x = L.$$

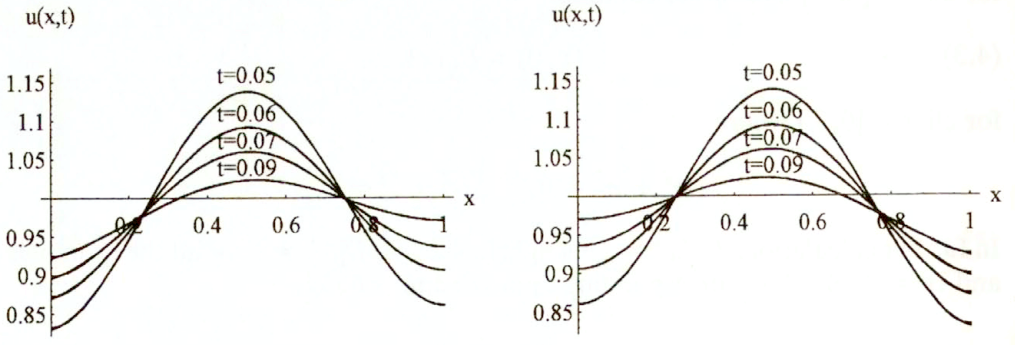

FIG. 1. Temperature field for some values of t for $N_a = 10$ due to the new solution and for $N_c = 5$ due to the classical solution (they cannot be distnguished).

$$\frac{\partial U}{\partial x} - \mathrm{Bi}\, U = 0 \quad \text{for} \quad x = 0,$$
$$\frac{\partial U}{\partial x} + \mathrm{Bi}\, U = 0 \quad \text{for} \quad x = L.$$

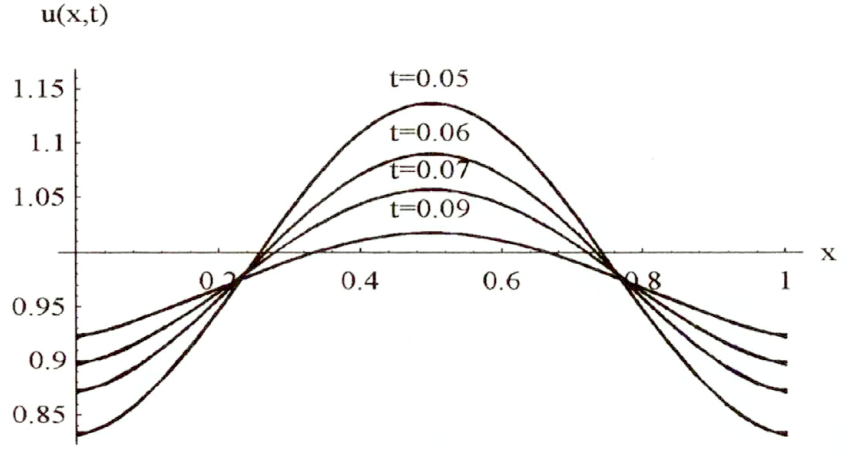

FIG. 2. Temperature field for some values of t for $N_a = 10$ due to the new solution and for $N_c = 5$ due to the classical solution (they cannot be distnguished).

$$U = 0 \quad \text{for} \quad x = 0,$$
$$\frac{\partial U}{\partial x} + \mathrm{Bi}\, U = 0 \quad \text{for} \quad x = L.$$

$$\frac{\partial U}{\partial x} - \mathrm{Bi}\, U = 0 \quad \text{for} \quad x = 0,$$
$$U = 0 \quad \text{for} \quad x = L.$$

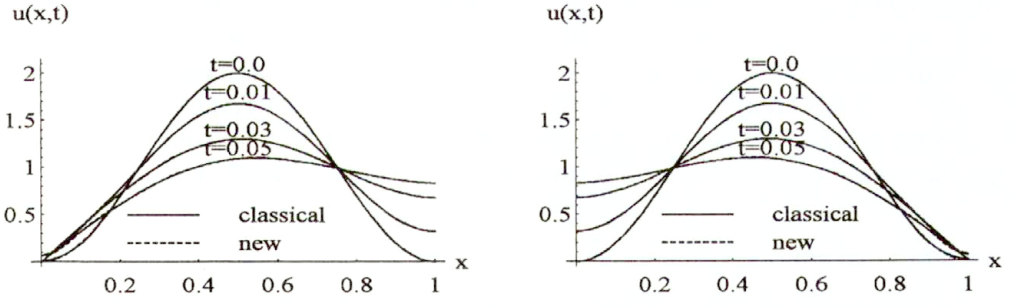

FIG. 3. Temperature field for some values of t for $N_a = 15$ due to the new solution and for $N_c = 10$ due to the classical solution.

For *Dirichlet-type boundary conditions* (i.e. $\beta\delta = 0$), the function Z_n in (3.17) is expressed by a double series (3.19). In this class we consider three examples of boundary conditions. For each IBVP we solve the corresponding ISODE and numerical results are drawn in Figs. 3–4.

From the figures presented it will be seen how closely the new solutions approach the classical solutions right through the interval.

$$U = 0 \quad \text{for} \quad x = 0,$$
$$U = L \quad \text{for} \quad x = L.$$

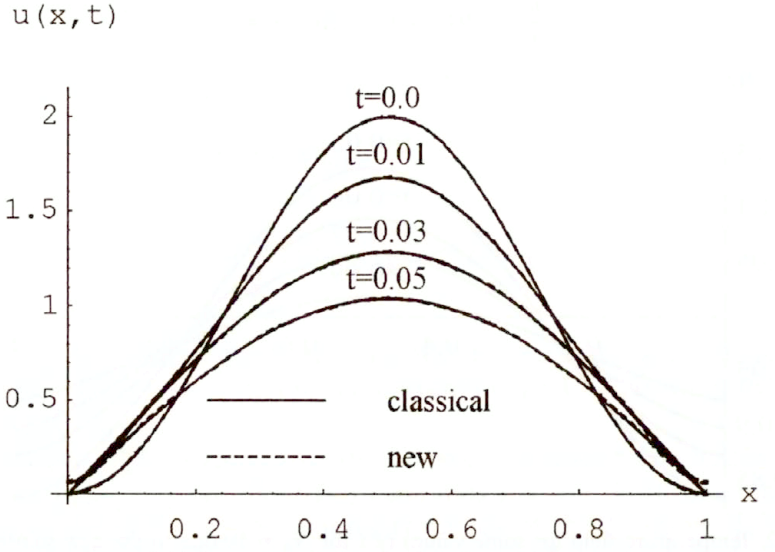

FIG. 4. Temperature field for some values of t for $N_a = 15$ due to the new solution and for $N_c = 10$ due to the classical solution.

5. Conclusions

From the mathematical considerations presented in the paper we conclude that the Fourier cosine series can be applied to many initial-boundary value problems without solving eigen-value problems. Computing relatively small number of terms of the cosine series, the new solutions called strong approximations approach very closely the exact solutions right through the interval. Since the new solutions are Fourier cosine series approximations to the exact solutions of such problems, the boundary conditions in general cannot be satisfied.

Acknowledgment

The author thanks the anonymous reviewer for valuable comments which resulted in improving the final version of the paper. The author also thanks Prof. W. KOSIŃSKI for helpful discussion and time spent for correcting the final version of the paper.

References

1. R.V. CHURCHILL and J.W. BROWN, *Fourier series and boundary value problems*, McGraw-Hill Book Company, New Jork 1978.
2. J.M. HYSLOP, *Infinite series*, Interscience Publishers INC, Edinburgh and London 1947.

3. K. KNOPP, *Theory and application of infinite series*, Hafner Publishing Company, New York 1947.

4. G.P. TOLSTOV, *Fourier series*, [in Russian], Moscow 1960.

5. Z. TUREK, *Application of the Fourier Cosine Series for the solution of differential equations* [in Polish], ZTUREK Research-Scientific Institute, Warszawa 1996.

6. Z. TUREK, *A new method of finding approximate solutions of the heat conduction equation*, Engng. Trans., **44**, 2, 295–301, 1996.

7. Z. TUREK, *Application of the Fourier Cosine Series to the approximation of solutions to initial non-Dirichlet boundary-value problems* [accepted for publication in Arch. Mech.].

ZTUREK RESEARCH-SCIENTIFIC INSTITUTE

02-352 Warszawa, Szczęśliwicka 2/26.

Received June 14, 1996; new version March 3, 1997.

Arch. Mech., 49, 3, pp. 589–609, Warszawa 1997

A gradient theory of finite viscoelasticity

K.C. VALANIS (VANCOUVER)

IN THIS PAPER we present a *gradient* theory of finite viscoelasticity. The theory is founded on the concept of internal fields, in conjunction with a variational principle and the dissipation inequality. The internal variables, which in local theories obey *local* evolution equations, have been replaced by internal fields *and their gradients*, which arise from physical processes that involve non-affine deformation. At variance with the local theory, these fields obey "internal" field equations and appropriate boundary and initial conditions. As a result, *uniform* boundary tractions give rise to inhomogeneous strain fields. This phenomenon is illustrated in one dimension, where it is shown that the creep function, normally a function of time only, is a function of space as well as time, even though the material domain is phenomenologically homogeneous.

1. Introduction

WE BEGIN with the experimental observation that macroscopically *uniform* material domains, under *uniform* surface tractions, develop localized, i.e., non-uniform deformation fields – contrary to predictions of "local" theories. There are other issues such as "regularization" whereby ill-posed boundary and/or initial value problems are rectified by the introduction of gradients in the constitutive parameters. Such issues are less clear and are often due to the inadequacy of the constitutive theories, rather than the material behaviour itself.

Phenomenological theories with higher gradients in mass density began with the work of Van der Waal. More recently we have witnessed the development of elasticity (hyperelasticity) theories with higher deformation gradients. We mention the papers of TOUPIN [1, 2], MINDLIN [3, 4] and GREEN and RIVLIN [5] as characteristic of that era. It is not our purpose to discuss these theories in detail except to say that a more precise formulation of the constitutive response of an elastic material was sought, in the light of the perceived long-range interaction effects, particularly when strong spatial variations in the boundary tractions and/or displacements were present.

In the present paper, the phenomenon of localization of macroscopic deformation was a motivating force for the development of continuum theories with (higher) gradients in the constitutive variables. Their recent advocacy, AIFANTIS [6–8], is due mainly to finer and more convincing experiments, pointing to the need for including gradients of these variables in a constitutive equation.

Other contributions in this area were forthcoming. We note the work of VARDOULAKIS and AIFANTIS [9] and VARDOULAKIS and FRANTZISKONIS [10] in the area of plasticity, where higher order plastic deformation gradients were introduced. The field is still in its infancy with a large scope for development.

Our object, in this paper, is to develop a *gradient theory of* viscoelasticity using the notion of *internal fields under isothermal conditions*. The condition of uniform temperature allows for the developmemt of the theory in a strictly *mechanical setting* without a need for entropy arguments, even though such arguments have been used before, successfully, in the context of local theories. See VALANIS [11–13] and COLEMAN and GURTIN [14].

2. Physical foundations

The basic premise of continuum mechanics is that the deformation of a material region is given mathematically by a one-to-one and on-to mapping:

$$x \to y \tag{2.1}$$

in the usual notation. Both frames x and y are Euclidean or reducible to Euclidean by a coordinate transformation. More importantly, the deformation of a neighbourhood in x, this being a "sphere" of radius $\|dx\| \leq \delta$, where parallel bars denote the Euclidean norm and δ is a suitably small number, is given by Eq. (2.1):

$$dy_i = F_{i\alpha}\, dx^{\alpha}, \tag{2.2}$$

where the deformation gradient $F_{i\alpha}$ $(\partial y_i/\partial x^{\alpha})$ is non-singular and constant within the neighbourhood. More precisely, no matter how heterogeneous the deformation is, a sufficiently small δ can be found such that $\|F_{i\alpha}dx^{\alpha}\|$ is of order δ. A fundamental topological consequence of the above assertions, in terms of the motion of discrete particles within a neighbourhood, is that the order of disposition of the particles is invariant under deformation. Thus, a material line contains always the same particles and in an order that remains unchanged with deformation.

Furthermore, neighbourhoods that are disjoint sets of particles before deformation, remain disjoint after deformation, i.e., no particle "diffusion" is allowed and particle membership of the initial material neighbourhood is conserved in the course of deformation. In short, the deformation of a neighbourhood given by Eq. (2.2) is affine. However, the basic physical characteristic of inelastic deformation is the non-affine motion of the particles either through the mechanism of slip, dislocation motion or particle migration.

2.1. Non-affine deformation

We consider a neighbourhood N undergoing non-affine deformation. In this case, at least one particle which, before deformation, occupied a position P in N, now occupies a position P' *not* in N. Note that this position P' cannot be described by Eq. (2.2). If a sufficiently large number of particles leave their original neighbourhoods, one may regard these as constituting a "migratory phase",

ideally a continuous material sub-domain of particles whose material coordinates are no longer x^α but $p^K(x^\alpha, t)$. The functions p^K are posited to be continuous and differentiable in x^α and t; furthermore $\mathrm{Det}(\partial p^K/\partial x^\alpha) \neq 0$. We call $p^K(x^\alpha)$, or $p(x)$ for short, the "migration map".

To avoid repetition, lower Latin suffixes will denote vector (tensor) components in the y-frame, upper Latin suffixes in the p-frame and upper Greek – those in the x-frame. Furthermore any such suffixes following a comma, will denote partial differentiation with respect to the corresponding coordinate.

Consider now the deformation of a domain whose particles *initially* at x^α, occupy points y_i in a Euclidean spatial frame. Further, let a subset of these particles, previously referred to as the migratory phase, occupy positions $p^K(x^\alpha, t)$ in the material reference frame. The deformation gradient of the affine phase, i.e. the phase of particles that have *not* migrated, is $\partial y_i/\partial x^\alpha$, symbolically y_x, the suffix x denoting differentiation, while the deformation gradient of the migratory phase is $\partial y_i/\partial p^K$ or y_p. In a more general setting, n migratory phases could exist, each with a different migration map $p^r(x)$.

REMARK. The particles that constitute the affine as well as the other phases, are *indistinguishable* in the deformed configuration y. Their only signature lies in the description of their motion relative to the x-frame. The motion of the ones that deform affinely is given by the map $x \to y$, while the motion of those in a migratory phase is given by the map $p^r \to y$. Thus the position y in the deformed configurations pertains to *all* particles, irrespective of phase, and similarly the traction on the surface of the deformed domain bears on all the particles of a neighbourhood of the deformed surface. The same argument applies in the case of body forces (inertia forces included).

2.2. The free energy density

The physics that underlies the migration process is very complex. Here we shall consider two simple, yet realistic models of this process with a view to obtaining equations that are reasonably tractable. Because viscoelasticity applies most naturally to polymeric materials, we shall consider models that pertain to such materials.

MODEL (i). This is an assembly of polymer networks that are not *elastically* interactive with each other. However they impede each other's motion in a resistive sense, so that they are *viscously* interactive. Initially, particles of the networks are identified by the material coordinate x^α. In the course of deformation however, the networks drift relative to each other, thus constituting migratory motion in the sense discussed above. Thus each network is a phase and the *particles within the phase ineract between themselves elastically*. We may thus posit a cross-linked reference network that deforms affinely, relative to which the other phases (networks) suffer migratory motion. It is clear that in this model the (Helmholtz) free energy density ψ of the whole is the sum of the free energy densities ψ^r of

its parts ($r = 0, 1, \ldots, n$), where ψ^0 pertains to the affine phase. The following equations, therefore, are applied

$$\begin{aligned} \psi^0 &= \psi^0(y_{i,\alpha}), \\ \psi^r &= \psi^r(y_{i,K}{}^{(r)}) = \psi^r\{y_{i,\alpha}x^{\alpha}{}_{,K^{(r)}}\}, \\ \psi &= \sum_0^r \psi^r, \end{aligned} \tag{2.3}$$

where, in Eq. $(2.3)_2$ the chain rule of differentiation was used. Implicit in Eqs. (2.3) and (2.4) is the stipulation that the interactive forces among particles are of short range. A general statement of Eq. $(2.3)_3$ is Eq. (2.4):

$$\psi = \psi(y_x, y_p{}^r), \qquad r = 1, 2, \ldots, n. \tag{2.4}$$

Of interest is the case where the phase drifts relative to the initial configuration but maintains an elastic, albeit weak, connection with that configuration. If this connection is modelled by means of an elastic spring, then there will be an additional contribution to ψ by virtue of the term $(p^K - \delta^k{}_{\alpha}x^{\alpha})$, i.e., the difference in position of the phase at time t and at time zero. Thus now:

$$\psi = \psi(y_{i,\alpha}; x^{\alpha}{}_{,K}; p^K - \delta^K{}_{\alpha}x^{\alpha}) \tag{2.4'}$$

or

$$\psi = \psi(y_x; x_p; p - x). \tag{2.4''}$$

MODEL (ii). This model is more complex and it represents a different physical situation. Initially, all the networks are cross-linked and elastically interactive, so that the material consists of one single cross-linked network udergoing affine deformation. Thus, initially,

$$\psi = \psi(y_{i,\alpha}). \tag{2.5}$$

Since, however, the bonds have strength of statistical variability, one may conceive a situation where at some critical free energy level $\psi = \psi_{(1)}$, one phase, say $r = 1$, will become elastically detached, so that subsequently,

$$\psi = \psi^{\star}(y_{i,\alpha}) + \psi^1(y_{i,K}{}^{(1)}) \tag{2.5'}$$

and the domain consists of one affine and one migratory phase. We note parenthetically that $\psi^{\star}$, at the transition point, need not be equal to $\psi_{(1)}$ because of the loss of elastic energy associated with the fracture of cross-links connecting the migratory to the affine phase.

In a similar fashion, when an energy level $\psi_{(2)}$ is reached such that $\psi^* = \psi_{(2)}$, another phase becomes elastically detached so that two migratory phases are operative. Now:

$$\psi = \psi^{**} + \psi^1(y_{i,K}{}^{(1)}) + \psi^2(y_{i,K}{}^{(2)}). \tag{2.5''}$$

Thus, the difference between the first and second models is that, in the latter, the migratory phases are not present *ab initio* and the onset of a migratory phase is delayed until the free energy density of the affine phase has reached a "threshold" value, in a manner reminiscent of a yield surface in plasticity. Other models are, of course, also possible.

3. A variational principle

We begin with an integral form of a principle which is of purely mechanical character, in that it avoids questions of entropy and temperature under conditions of irreversibility (even though the question of existence of entropy was dealt with by VALANIS [11, 12], in an earlier work). Furthermore, it is simple and leads to direct results. The principle is in the form of the global statement that applies to a dissipative continuous medium, in this case one with n migratory phases. If $\dot{\Psi}$ is the (virtual) rate of change of the stored energy Ψ (Helmholtz free enrgy in thermodynamics) of such a medium in its reference configuration x, with domain V and surface S, then

$$\dot{\Psi} = \int_S T_i v_i \, dS + \int_V f_i v_i \, dV - \int_V D \, dV, \tag{3.1}$$

where v_i is a virtual velocity field, T_i are the surface tractions and f_i are the body forces (including inertial forces), and D is the internal dissipation density, which is always non-negative, i.e.,

$$D \leq 0. \tag{3.2}$$

The internal dissipation density D is due to the rate of work of the internal forces Q_L acting on the migratory velocity fields v^L, where:

$$v^L = \dot{p}^L = \partial p^L / \partial t|_x \,. \tag{3.3}$$

Thus

$$D = \sum Q_L v^L \geq 0, \tag{3.4}$$

where

$$\sum Q_L v^L = \sum_r Q_L^{(r)} v_{(r)}^L, \qquad r = 1, 2, \ldots, n.$$

Hence, to summarize,

$$\dot{\Psi} = \int_S T_i v_i \, dS + \int_V f_i v_i \, dV - \int_V Q_L v^L \, dV. \tag{3.5}$$

The physical foundations of this principle are given in Appendix II.

Equation (3.5) is a statement of the fact that, for all *admissible* virtual velocity fields v_i and v^L, at constant T_i, f_i and Q_L, the virtual rate of change of the free energy of a region is equal to the virtual rate of work done by the external body as well as surface forces, minus the virtual dissipation due to the virtual rate of work done by the internal forces Q_L.

With regard to the admissibility of the velocity fields v_i and v^L, we point out that while v_i are completely arbitrary, v^L must satisfy the dissipation inequality:

$$Q_L v^L > 0, \qquad \text{if} \quad \|v^L\| > 0, \quad \|Q_L\| > 0 \tag{3.6}$$

for all r, double bars denoting norms, i.e., $\|v_L\|^2 = v_L v^L$, so that equality (3.5) may be written in terms of the Ineq. (3.7)

$$\dot{\Psi} \leq \int_S T_i v_i \, dS + \int_V f_i v_i \, dV \tag{3.7}$$

for all arbitrary virtual velocities v_i, and v^L, subject to the constraint that in V, $Q_L v^L \geq 0$, with the proviso that the equality sign applies only in the case when $\|Q_L\| = 0$ and/or $\|v^L\| = 0$.

We complete the variational statement by stipulating that for all v_i^*, these being velocity vectors associated with virtual rigid body motion,

$$\dot{\Psi} = 0, \qquad \|v^L\| = 0. \tag{3.8}$$

This is a constitutive statement. The fact, as we shall show, that this is also a statement of (dynamic) equilibrium, raises philosophical questions as to whether equilibrium is an independent law, or a form of constitutive law, (common to all materials whose constitution is determined by the dependence of the free energy density on the displacement and internal field gradients), that rests on the stipulation that, under condition of (virtual) rigid body motion, the free energy is invariant and the dissipation is zero, since in fact $\|v^L\| = 0$.

For the purposes of the analysis we introduce, in the variational principle, the Helmholtz free energy density ψ, per unit undeformed volume, such that:

$$\Psi = \int_V \psi \, dV \tag{3.9}$$

assuming short-range interaction among particles. We thus have a variational principle in terms of the following inequality:

$$\int_V \dot{\psi}\, dV \leq \int_S T_i v_i\, dS + \int_V f_i v_i\, dV, \tag{3.10}$$

where $\dot{\psi} \equiv (\partial\psi/\partial t)_x$.

4. Field equations in the presence of internal fields

We begin with the generic Eq. $(2.4)_1$, i.e.,

$$\psi = \psi(y_{i,\alpha}; p^K{}_{,\alpha}; q^K), \tag{4.1}$$

where $p^K{}_{,\alpha}$ is the inverse of $x^\alpha{}_{,K}$, i.e.,

$$x^\alpha{}_{,K} p^K{}_{,\beta} = \delta^\alpha{}_\beta \tag{4.2}$$

and $q^K = p^K - \delta^K_\alpha$.

Thus

$$\dot{\psi} = (\partial\psi/\partial y_{i,\alpha}) v_{i,\alpha} + (\partial\psi/\partial p^K{}_{,\alpha})(v^K{}_{,\alpha} + \partial\psi/\partial q^K v^K, \tag{4.3}$$

where

$$v^K = \partial q^K/\partial t = \partial p^K/\partial t|_x\,, \tag{4.4}$$

$$v^K{}_{,\alpha} = (\partial p^K{}_{,\alpha}/\partial t)_x\,. \tag{4.5}$$

Hence

$$\dot{\psi} = \psi^\alpha{}_i v_{i,\alpha} + \psi^\alpha{}_K v^K{}_{,\alpha} + \psi_L v^L, \tag{4.6}$$

where

$$\psi^\alpha{}_i = \partial\psi/\partial y_{i,\alpha}\,, \qquad \psi^\alpha{}_K = \partial\psi/\partial p^K{}_{,\alpha}\,, \qquad \psi_L = \partial\psi/\partial q^L. \tag{4.7}$$

We now use Eq. (4.5) in the variational inequality (3.10) to find:

$$\int_V (\psi^\alpha{}_i v_{i,\alpha} + \psi^\beta{}_L v^L{}_{,\beta}) dV \leq \int_S T_i\, v_i\, dS + \int_V f_i\, v_i\, dV. \tag{4.8}$$

The left-hand side of Eq. (4.8) is now recast in surface and volume integrals with the aid of the Green–Gauss theorem, and Eq. (4.9) is thereby obtained:

$$\int_S (\psi^\alpha{}_i n_\alpha - T_i) v_i\, dS - \int_V [(\psi^\alpha{}_{,i})_{,\alpha} + f_i]\, v_i\, dV + \int_S \psi^\beta{}_L n_\beta v^L\, dS - \int_V \left[(\psi^\beta{}_L)_{,\beta} - \psi_L\right] v^L\, dV \leq 0. \tag{4.9}$$

DISCUSSION. Before we proceed with the consequences of Eq. (2.4) we note that, generally, on a part of the surface S, namely S_T, tractions are applied, while on its complement S_Y displacements or velocities V_i are applied instead. Therefore, on S_T the virtual velocities v_i are arbitrary while on S_Y these are zero. With regard to the boundary conditions of the migrating phases (and following the discussion at the end of Appendix II), the surface S is the sum of the sub-surface S_0 on which the velocities of the phases are unknown and thus the virtual velocities are arbitrary, and the sub-surface S_P, which is impenetrable to phase migration, and on which the migratory velocities $V^L = 0$. No other physical situation is possible (see discussion at the end of Appendix II). Thus on S_0 the virtual velocities v^L are arbitrary while on S_P:

$$p^K = \delta^K{}_\alpha x^\alpha \tag{4.10}$$

and the virtual velocities v^L are zero. In the interior both v_i and v^L are arbitrary except that v^L are admissible only if they satisfy the dissipation inequality.

With the above discussion in mind, let a set of admissible v^L in V be prescribed, in the sense of Ineq. (2.1). The virtual velocity fields v_i on S_T, v_i in V and v^L on S_0, can be independently and arbitrarily prescribed. Thus setting these equal to zero, and noting that v_i are zero on S_Y and v^L are zero on S_P, one finds in view of Ineq. (4.9), that

$$\int_V \left[(\psi^\beta{}_L)_{,\beta} - \partial\psi/\partial q^L\right] v^L \, dV \geq 0. \tag{4.11}$$

Now keeping v_i in V and V^l on S null, one may prescribe v_i on S_T in a manner that violates Ineq. (4.9), if the bracket under the surface integral does not vanish. Thus

$$\psi^\alpha{}_i n_\alpha = T_i \quad \text{on } S_T, \tag{4.12}$$

$$v_i = V_i \quad \text{on } S_Y, \tag{4.13}$$

where V_i are known functions of time and the surface coordinates. Repeating the same argument for the other integrals one finds that

$$(\psi^\alpha{}_i)_{,\alpha} + f_i = 0 \quad \text{in } V \tag{4.14}$$

and

$$\psi^\beta_L n_\beta = 0 \quad \text{on } S_0, \qquad v^L = 0 \quad \text{on } S_P. \tag{4.15}$$

DISCUSSION. Equation (4.14) replicates the equation of motion in continuum mechanics when internal fields are absent. Here we show that the equation applies

in the presence of internal fields. Therefore if f_i contain inertia forces, as in the dynamic case, then

$$f_i = g_i - \varrho_0 \partial^2 y_i(x^\alpha, t)/\partial t^2, \tag{4.16}$$

where g_i are body forces other than inertia forces and ϱ_0 is the reference density of the domain. We point out that to obtain Eq. (4.14) in the presence of inertia forces, we choose a virtual velocity field which is accelerationless, i.e. V_i is a function of x^α only and independent of time.

REMARK. As noted above, the physics of the problem is such that tractions are prescribed on S_T ($\leq S$) with full kinematic freedom of the particles on the surface, while the deformation of the surface S_Y ($S_Y \leq S$) is prescribed by means of a relation:

$$y_i{}^S = y_i{}^S(x^\alpha{}_S, t), \tag{4.17}$$

where $y_i{}^S$ and $x^\alpha{}_S$ denote the coordinates of the particles on the deformed and undeformed surface, respectively. In the former case Eq. (4.12) applies. In the latter case v_i are prescribed on the surface since

$$v_i = V_i = (\partial y_i{}^S/\partial t)_x \tag{4.18}$$

and Eq. (4.13) applies. With regard to the migratory boundary conditions, the surface velocities V^L are arbitrary on S_0 while V^L are zero on S_P.

5. Internal equations of motion

We begin by noting that Eqs. (4.11), (4.12) and (4.13) in conjunction with Eqs. (3.5) and (3.9) lead to the following relation for the dissipative forces Q_L

$$\int_V \left\{ (\psi^\beta{}_L)_{,\beta} - \partial\psi/\partial q^L - Q_L \right\} v^L \, dV = 0. \tag{5.1}$$

Since this equation must be true for all arbitrary (including infinitesimal) domains, the local form of Eq. (5.1) results:

$$\left\{ (\psi^\beta{}_L)_{,\beta} - \partial\psi/\partial q^L - Q_L \right\} v^L = 0. \tag{5.2}$$

Equation (5.2), however, cannot be satisfied for all admissible fields v^L (see Appendix I), unless:

$$(\psi^\beta{}_L)_{,\beta} - \partial\psi/\partial q^L - Q_L = 0. \tag{5.3}$$

Equation (5.3) is the equation of internal equilibrium that relates the dissipative force Q_L to the divergence of the bi-vector ψ^β_L.

At this point we recall Ineq. (3.6), i.e., $Q_L v^L \geq 0$, which is a constraint or a requirement of positive dissipation in the presence of non-affine deformation. The constraint demands that Q_L and V^L should be related, otherwise they could be prescribed independently and in a manner that would violate the inequality. The most obvious relation is a linear one of the form:

$$Q_K = b_{KL} v^L, \tag{5.4}$$

where b_{KL} is a covariant "viscosity tensor". Equation (5.4) is a statement to the effect that the dissipative (resistive) force is a linear and homogeneous function of the migratory velocity of a phase.

Equations (5.3) and (5.4) combine to give Eq. (5.5),

$$\psi^{\beta}{}_{K,\beta} - \partial\psi/\partial q^K = b_{KL} v^L \tag{5.5}$$

which is the equation for the motion of the particles in a migratory phase.

The initial conditions

The initial conditions are obtained from the presumption that the material is in a quiescent state at $t = 0$. Thus

$$y_i(x^\alpha, 0) = \delta_{i\alpha} x^\alpha, \qquad q^K(x^\alpha, 0) = 0, \tag{5.6}$$

$$v_i(x^\alpha, 0) = 0. \tag{5.7}$$

At this point we summarize the equations pertinent to the motion of the domain, reference being made to the individual phases $r = 1, 2, \ldots, n$.

Summary of equations

In V

$$\psi = \psi(\partial y_i/\partial x^\alpha; \partial p^K/\partial x_\alpha; g^K), \tag{5.8}$$

$$(\psi^\alpha{}_i)_{,\alpha} + g_i = \varrho_0 \partial^2 y_i(x^\alpha, t)/\partial t^2, \tag{5.9}$$

$$\psi^{\beta}{}_{K,\beta} - \psi_K = b_{KL} v^L. \tag{5.10}$$

On S_T

$$\psi^\alpha{}_i n_\alpha = T_i. \tag{5.11}_1$$

On S_Y

$$y_i{}^S = y_i{}^S(x^\alpha{}_S, t) \quad \text{or} \quad v_i = V_i. \tag{5.11}_2$$

On S_0

$$\psi^{\beta}{}_L n_\beta = 0. \tag{5.11}_3$$

On S_P

$$v^L = 0. \tag{5.11}_4$$

The initial conditions are such as in Eqs. (5.6) and (5.7).

5.1. Invariance under rigid body motion

We restate the two conditions stated previously, to be satisfied under conditions of (virtual) rigid body motion:

$$\dot{\psi} = 0, \qquad \|v^L\| = 0. \tag{5.12}$$

These conditions are fundamental in putting further restrictions on the form of ψ and in identifying physically certain constitutive constraints.

To show this we employ Eq. (3.5), i.e.,

$$\dot{\Psi} = \int_S T_i v_i \, dS + \int_S f_i \, dV - \int_V Q_L v^L \, dV \tag{5.13}$$

which in the presence of rigid body motion then becomes:

$$\int_S T_i v_i \, dS + \int_V f_i v_i \, dV = 0. \tag{5.14}$$

(i) *Rigid body translation*

In this case v_i are constant in V. Thus, in view of Eq. (5.14),

$$v_i \left\{ \int_S T_i \, dS + \int_V f_i \, dV \right\} = 0. \tag{5.15}$$

A set of three linearly independent vectors v_i can be found for which Eq. (5.15) must hold. This is possible iff

$$\int_S T_i \, dS + \int_V f_i \, dV = 0. \tag{5.16}$$

Using the classical argument of applying Eq. (5.16) to a tetrahedron of vanishing dimensions in the undeformed domain, one finds that

$$T^{\alpha}{}_i n_\alpha = T_i, \tag{5.17}$$

where the tractions T_i are calculated in the x-frame and pertain to the undeformed area. We recognize $T^{\alpha}{}_i$ as the First Piola-Kirchhoff stress tensor. Furthermore, in the light of Eqs. (4.13) and (5.17),

$$T^{\alpha}{}_i = \psi^{\alpha}{}_i. \tag{5.18}$$

If we transform the domain of integration in Eq. (5.14) to that of the deformed configuration and apply the same procedures, we find that

$$T_{ij} n_j = T'_i, \tag{5.19}$$

where T_{ij} is the Cauchy stress and the traction T_i', where $T_i = \mathrm{Det}(y_{i,\alpha})T_i'$, are calculated in the y-frame and pertain to the deformed area. The following tangent transformations apply:

$$n_\alpha = y_{i,\alpha} n_i\,, \qquad T^\alpha{}_i = J\,T_{ij} x^\alpha{}_{,j}\,, \qquad J\,T_{ij} = T^\alpha{}_i y_{j,\alpha}\,. \tag{5.20}$$

(ii) *Rigid body rotation*

Here, the virtual velocity v_i is caused by a *virtual* angular velocity Ω_i brought about by rotation of the spatial frame of reference y_i. Therefore there are no induced centrifugal forces as there would be, had Ω_i been actual, i.e., an angular velocity of the domain itself. Thus Ψ does indeed remain invariant in the presence of a virtual angular velocity field Ω_i.

We now begin Eq. (5.21):

$$v_i = e_{ijk}\Omega_j\, y_k\,, \tag{5.21}$$

where e_{ijk} is the permutation tensor and Ω_i is an arbitrary angular velocity vector, brought about by rotation of the frame of reference y_i. Again, transforming the domain of integration in Eq. (5.14) to that of the deformed configuration and applying classical arguments we find that:

$$T_{ij} = T_{ji}\,. \tag{5.22}$$

Thus, in view of Eqs. (5.18), $(5.20)_3$ and (5.22):

$$\psi^\alpha{}_i y_{j,\alpha} = \psi^\alpha{}_j y_{i,\alpha} \tag{5.23}$$

Eq. (5.23) is a restriction on the functional form of ψ.

Further Invariance Considerations. We recall Eq. (5.8):

$$\psi = \psi(y_{i,\alpha}; p^K{}_{,\alpha}). \tag{5.24}$$

Virtual rigid body rotation leaves ψ as well as $x^\alpha{}_{,K}{}^{(r)}$ invariant. However, $y_{i,\alpha}$ is a bi-vector and represents in fact the three vectors: $y_{i,1}$; $y_{i,2}$; $y_{i,3}$. A clasical theorem in continuum mechanics (see for instance ERINGEN [17]), is that a scalar function ψ of three vectors $\mathbf{a}_r$ remains invariant under rotation of the frame of reference iff it is a function of the inner products $\mathbf{a}_r \cdot \mathbf{a}_s$ and the determinant $|a_{ir}|$. Furthermore, if ψ is centro-symmetric, i.e., invariant under reflection of the frame of reference, as it must be since the choice of the spatial reference frame is arbitrary, then ψ must be an even function of $|a_{ir}|$, since $|a_{ir}|$ changes sign upon reflection.

It follows, therefore, that a necessary and sufficient condition that ψ be invariant under rigid body rotation and reflection of the spatial frame of reference y_i is that

$$\psi = \psi(C_{\alpha\beta}; p^K{}_{,\alpha}; q^K), \tag{5.25}$$

where $C_{\alpha\beta}$ is the Right Cauchy-Green tensor ${y_x}^T y_x$. One can verify that condition (5.23) is now trivially satisfied.

5.2. Conditions of material isotropy

In strictly affine deformations, the mathematical definition of material isotropy is invariance of a constitutive equation, or property, under rotation and inversion of the material frame of reference x^α. In the present case, however, the situation is more complex and lends the theory a wider scope for material characterization. For instance, a migratory phase may be isotropic initially but may evolve into an anisotropic state as migration proceeds. We thus distinguish between two distinct possibilities:

(i) *Isotropy in the initial state whereby ψ is invariant under rotation and inversion of the material frame x^α*

(ii) *Isotropy of phase "r" in the migrated state, in which event ψ remains invariant under rotation and inversion of the frame $p^K{}_{(r)}$.*

We note that in (ii) we have introduced a formal, rigorous definition of "strain-induced anisotropy" in phase r, a lack of invariance if ψ under rotation and inversion of the frame $p^K{}_{(r)}$.

Restrictions on ψ

(i) *Isotropy in the initial state*

This means invariance of ψ under rotation (and inversion) of the material frame x^α. We begin with Eq. (5.25) which we write in the form:

$$\psi = \psi(C_{\alpha\beta}; x^\alpha{}_K; q^K). \tag{5.26}$$

In the case ψ is an isotropic function of the tensor $C_{\alpha\beta}$, and the three vectors $x^\alpha{}_{,K} : \alpha = 1, 2, 3$. Thus

$$\psi = \psi(I_\alpha : C_{KL}; G_{KL}; q^K), \tag{5.27}$$

where $C_{KL} = C_{\alpha\beta} x^\alpha{}_{,K} x^\beta{}_{,L}$; $G_{KL} = \delta_{\alpha\beta} x^\alpha{}_{,K} x^\beta{}_{,L}$ and I_α are the three principal invariants of $C_{\alpha\beta}$.

(ii) *Isotropy in the initial state and migratory phase 1*

In this case ψ is an isotropic function of $G^{(1)}_{KL}$, $C_{KL}{}^{(1)}$ and q^k but a general function of the tensors $G_{KL}{}^{(r)}$, $C^{(r)}_{KL}$ and $q^{(r)}$, $r = 2, 3, \ldots, n$. In other words, if a phase remains isotropic during its migratory motion then ψ will be an isotropic function of G_{KL}, C_{KL} and q^K of that particular phase.

Thus, more generally, specific material symmetries in the initial configuration x involve invariance under appropriate rotations of frame x, while evolving symmetries in a specific phase r involve invariance under appropriate rotations of frame $p^K{}_{(r)}$.

5.3. Linearization of the field equations

We complete this section by giving the linearized form of the field equations and boundary conditions (5.8)–(5.11)$_4$. The basis of the linearization scheme is the premise of small deformation in the sense that:

$$y_i = \delta_{i\alpha}x^\alpha + \eta u_i, \tag{5.28}$$

$$p^K = \delta^K{}_\alpha x^\alpha + \eta q^K, \tag{5.29}$$

where η is a small real number. Equations (5.28) and (5.29) are then substituted in Eqs. (5.8)–(5.11)$_4$, terms in η are retained, while terms in η^2 and higher order are neglected. Subsequently η is set equal to unity. Furthrmore since, ultimately, all equations are referred to the reference frame x, following the analysis all indices are replaced by small Latin letters. Note, parenthetically, that since the frame p now collapses onto the frame x, there cannot be any *evolution* of anisotropy of phase, if the phase is initially isotropic.

Thus, beginning with the relations:

$$p^K{}_\alpha = \delta^K{}_\alpha + q^K{}_{,\alpha}, \tag{5.30}$$

$$C_{\alpha\beta} = \delta_{\alpha\beta} + 2\eta\varepsilon_{\alpha\beta}, \tag{5.31}$$

$$C_{KL} = \delta_{KL} + 2\eta\varepsilon_{KL} - 2\eta q_{KL}, \tag{5.32}$$

$$G_{KL} = \delta_{KL} - 2\eta q_{KL}, \tag{5.33}$$

where $\varepsilon_{\alpha\beta}$ is the strain tensor while $2q_{KL} = q_{K,L} + q_{L,K}$, the following equations result for all r:

In V

$$\psi = \psi(\varepsilon_{ij}, q_{i,j}{}^{(r)}, q_i{}^{(r)}) \tag{5.34}$$

or

$$\psi = \psi(\varepsilon_{ij}, q_{ij}{}^{(r)}, q_i{}^{(r)}) \tag{5.35}$$

if the domain is initially isotropic. Also

$$(\partial\psi/\partial u_{i,j})_{,j} + g_i = \partial^2 u_i/\partial t^2, \tag{5.36}$$

$$(\partial\psi/\partial q_i{}^{(r)}{}_{,j})_{,j} - \partial\psi/\partial q_i{}^{(r)} = b_{ij}{}^{(r)}\partial q_i{}^{(r)}/\partial t \quad (r \text{ not summed}). \tag{5.37}$$

On S_T

$$(\partial\psi/\partial u_{i,j})n_j = T_i; \tag{5.38}_1$$

on S_0

$$(\partial\psi/\partial q_{i,j}^{(r)})n_j = 0; \tag{5.38}_2$$

on S_u

$$u_i = U_i\,; \tag{5.39}_1$$

on S_P

$$q_i = 0. \tag{5.39}_2$$

Initial conditions

$$u_i(x,0) = (\dot{u})(x,0) = 0; \qquad q_i{}^{(r)}(x,0) = 0. \tag{5.40}$$

6. A worked example

To illustrate the ramifications of the non-local theory, we present in this section a worked example of simple quasi-static shearing in one dimension. Let a half-space be infinite in directions x and z and semi-infinite in direction y. The material domain is in a quiescent state when, at time $t = 0$, a shearing traction $T_0(t)$ is applied in direction x on the surface $y = 0$. Let

$$\psi = (1/2)Au_y^2 + Bu_y q_y + (1/2)Cq_y^2\,, \tag{6.1}$$

where $u_y \equiv \partial u/\partial_y$, $q_y \equiv \partial q/\partial_y$, i.e., a subscript denotes differentiation. The pertinent boundary conditions then are: At $y = 0$, $T = T_0(t)$; $\partial\psi/\partial q_y = 0$. At $y = \infty$, all variables are bounded. At $t = 0$, $u = q = 0$. The equilibrium condition, Eq. (5.27), gives:

$$(\partial\psi/\partial u_y)_y = 0 \tag{6.2}$$

while the equation of motion for the internal variable q is given by Eq. (6.3):

$$(\partial\psi/\partial q_y)_y = b\,q_t\,. \tag{6.3}$$

In view of Eq. (6.2), the shear stress $T(= \partial\psi/\partial u_y)$ is uniform in the domain as in the local theory. However this is not true of the strain. Eqs. (6.2) and (6.3) combine to give the following (diffusion) equation for q:

$$C_1 q_{yy} = b\,q_t\,, \tag{6.4}$$

where $C_1 = C - B^2/A$. We have solved Eq. (6.4) by the usual Laplace Transform technique and obtained the following expression for the shear strain γ

$$\gamma = \int_0^t J(x; t-\tau)(\partial T_0/\partial\tau)\,d\tau. \tag{6.5}$$

Note that memory function $J(y,t)$ plays the role of a creep function except that now, at variance with local theory, it is a function of x as well as t. Equation (6.6) gives the analytical form of J, found from the solution

$$J(y,t) = A^{-1}\left\{H(t) + (B^2/AC_1)\text{erfc}\left[y/(2at^{1/2})\right]\right\}, \tag{6.6}$$

where $a^2 = b/C_1$. In Fig. 1 we show the dependence of γ on time at various y-stations when T_0 has the form of a Heaviside step function, in which event $\gamma(y,t) = J(y,t)$. Evidently the strain "diffuses" into the half-space as time increases.

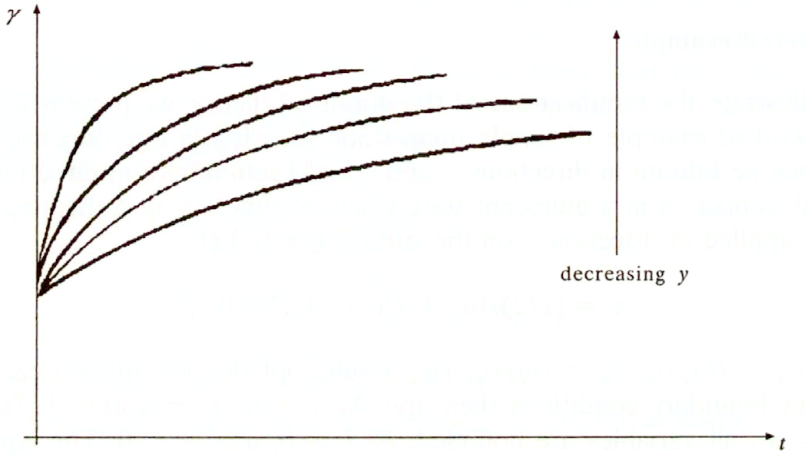

FIG. 1. Shear strain versus time for different values of y.

7. Postscript on plasticity

Previously, VALANIS [15, 16], we have developed the constitutive equations of plasticity and viscoplasticity, in the context of the local theory of thermodynamics of internal variables, by introducing the concept of "intrinsic time" z, and substituting z for t in the equations of evolution of these variables. The theory developed here may be extended to materials that are strain-rate indifferent, or partially indifferent, by the use of a similar procedure, whereby $\dot{z}$ premultiplies the left-hand side of the equations of motion of the internal fields. Eq. (5.10) will now read

$$\dot{z}\left\{\psi^{\beta}{}_{,K^{(r)}} - \psi_{K^{(r)}}\right\} = b^{(r)}_{KL}\, v^{L}_{(r)} \quad (r \text{ not summed}). \tag{7.1}$$

The precise nature of $\dot{z}$ will be discussed in future studies.

Appendix I

The task is to prove that if

$$(Q_L + \psi_L)v^L = 0 \tag{I.1}$$

for all admissible v^L, where $\psi_L \equiv (\psi^{\beta}{}_{,L})_{,\beta}$, then

$$(Q_L + \psi_L) = 0. \tag{I.2}$$

As discussed in Sec. 2, v^L is admissible if

$$Q_L v^L > 0, \qquad \psi_L v^L < 0 \tag{I.3}$$

for all $\|Q_L\| \neq 0$, $\|\psi_L\| \neq 0$, $\|v^L\| \neq 0$. Otherwise v^L are arbitrary.

P r o o f. If Q_L and ψ_L are collinear and either of the same sign or *unequal*, the proof is trivial. Let $Q_L = \alpha\psi_L$, where $\alpha \neq -1$. Then in view of Eq. (I.2) $\psi_i \delta q_i = 0$. However, the constraints $\psi_L v^L = 0$ and $\psi_L v^L < 0$, cannot be satisfied simultaneously if $\|\psi_L\| \neq 0$. Thus, in this case, $\alpha = -1$ and $Q_L + \psi_L = 0$.

If Q_L and ψ_L are not collinear then there exists a vector B_L normal to the plane of the vectors Q_L and ψ_L ($Q_L B^L = 0$, $\psi_L B^L = 0$), such that the scalar product $p = \varepsilon^{LMN} Q_L \psi_M B_N > 0$. The three vectors Q_L, ψ_L and B_L are linearly linearly independent. We now introduce two vectors: R^L, normal to the plane of ψ_L and B_L, and P^L normal to the plane of Q_L and B_L, i.e.,

$$R^L = \varepsilon^{LMN}\psi_{MNk}, \qquad P^L = \varepsilon^{LMN} Q_M B_N . \tag{I.4}$$

It may now be shown that all vectors v^L of the form:

$$v^L = \alpha R^L + \beta P^L + \gamma B^L, \tag{I.5}$$

where α and β are positive scalars and γ in non-negative, are admissible. In fact

$$Q_L v^L = \alpha p, \qquad \psi_L v^L = -\beta p \tag{I.6}$$

thus satisfying inequalities (I.3).

Three vectors ${v^L}_r$ are then constructed as in Eq. (I.7),

$$\delta {v^L}_r = \alpha_r R_i + \beta_r P_i + \gamma_r B_i \tag{I.7}$$

where $\alpha_r > 0$, $\beta_r > 0$, $\gamma_r \geq 0$. These vectors are admissible and, furthermore *linearly independent* if $\gamma_1 = 1$, $\gamma_2 = 0$, $\gamma_3 = 0$, and the determinant condition (I.8) is satisfied

$$\begin{vmatrix} \alpha_1 & \alpha_2 \\ \beta_1 & \beta_2 \end{vmatrix} \neq 0. \tag{I.8}$$

Since one can always find positive scalars such that $\alpha_1\beta_2 - \alpha_2\beta_1 \neq 0$, condition (I.1) now demands that the vector $(Q_L + \psi_L)$ be orthogonal to three linearly independent vectors. This is not possible if the said vector is different from zero. Thus $Q_L = -\psi_L$.

Appendix II

Variational principle

Physical foundations

To derive Eq. (3.1) we begin with the observation that, actually, the rate of (virtual) work $\dot{W}_S$ done by the surface tractions is

$$\dot{W}_S = \int_S \sum T_i^{(r)} v_i^{(r)}\, dS, \tag{II.1}$$

where $\mathbf{T}^{(r)}$ are the surface tractions on the phases of the domain and $\mathbf{v}^{(r)}$ are the corresponding (virtual) velocities of the phases, i.e.,

$$v_i^{(r)} = \partial y_i(p^K{}_{(r)}, t)/\partial t|_x. \tag{II.2}$$

More precisely, and since p^K are migration maps given by the relation

$$P^K = p^K(x^\alpha, t) \tag{II.3}$$

and omitting the index r on the right-hand side of (II.4), for simplicity of notation, the phase velocity $v_i^{(r)}$ is given by Eq. (II.4):

$$v_i^{(r)} = \partial y_i(p^K(x^\alpha, t), t)/\partial t|_x = (\partial y_i/\partial p^K)\partial p^K/\partial t|_x + \partial y_i/\partial t|_p. \tag{II.4}$$

Quite clearly $\partial p^K{}_{(r)}/\partial t|_x (= v^K{}_{(r)}$ is the migratory velocity of phase r while $\partial y_i(p^K{}_{(r)}, t)/\partial t|_p$ $(= v_i{}^{(r)}{}_{(p)})$ is the velocity of the phase relative to the present reference configuration p. Thus:

$$v^{(r)} = \partial y_i/\partial p^K{}_{(r)} v^K{}_{(r)} + v_i{}^{(r)}{}_{(p)}. \tag{II.5}$$

Equation (II.5) is merely the rule of addition of velocities.

In a similar manner the rate of (virtual) work $\dot{W}_V$ done by the body forces is

$$\dot{(W)}_V = \int_V \sum_r f_i^{(r)} v_i^{(r)}\, dV. \tag{II.6}$$

Thus, the statement that the rate of change of the free energy of a domain is equal to the rate of work done by the applied surface and body forces minus the rate of dissipation (all rates being virtual), has the analytical form of Eq. (II.7)

$$\dot{\Psi} = \int_S \sum_r T_i^{(r)} v_i^{(r)}\, dS + \int_V \sum f_i^{(r)} v_i^{(r)}\, dV - \int_V D\, dV. \tag{II.7}$$

It is a posited premise in continuum mechanics that the forces that constitute a surface traction are shared equally by all particles of the neighbourhood. With the above in mind, let $n_0, n_1, \ldots, n_n$, be the particle densities of the phases (at the surface) such that $\sum n_r = 1$. It then follows that

$$\mathbf{T}^{(r)} = n_r \mathbf{T}, \qquad \mathbf{T} = \sum \mathbf{T}^{(r)}. \tag{II.8}$$

In a similar manner,

$$\mathbf{f}^{(r)} = n_r \mathbf{f}, \qquad \mathbf{f} = \sum \mathbf{f}^{(r)}, \tag{II.9}$$

where n_r are now the particle densities in V (if different from S). Substituting equations $(II.8)_1$ and $(II.9)_1$ in Eq. (II.7) we recover Eq. (II.6) of the text, i.e.

$$\dot{\Psi} = \int_S T_i v_i \, dS + \int_V f_i v_i \, dV - \int_V D \, dV, \tag{II.10}$$

where

$$v_i = \sum n_r v_i^{(r)} \tag{II.11}$$

i.e. v_i is the *mean*, number-averaged (virtual) velocity and is equal to the one that would be calculated from the first principles, in the case if the (virtual) velocities of the phase were not equal.

The superscript r of the function $y_i^{(r)}$ on the right-hand side of Eq. (II.2) signifies the fact that the deformation of the phases is not compatible, in the sense that, after deformation, each phase r occupies a point $y_i^{(r)}$ in the spatial system, not necessarily the same as $y_i^{(r+1)}$, say, or any other $y_i^{(m)}$, for that matter.

Thus, to be precise, the free energy density ψ^r in model (i) in the Sec. 2. Physical Foundations, should be given by Eq. (II.12)

$$\psi^{(r)} = \psi^r(\partial y_i^{(r)} / \partial p^K{}_{(r)}), \qquad r \text{ not summed.} \tag{II.12}$$

But then the theory would be too complex, and mathematically and physically intractable. In this simpler physical approach the deformation gradient $\partial y_i^{(r)} / \partial p^K{}_{(r)}$ has been replaced in Eq. (II.12) by the *mean* deformation gradient $\partial y_i / \partial p^K{}_{(r)}$ where

$$y_i = \sum_r n_r \, y_i^{(r)}.$$

Thus

$$v_i = \partial y_i / \partial_t|_x = \sum_r n_r \, v_i^{(r)} \tag{II.13}$$

as in Eq. (II.11), assuming n_r to be constant.

Discussion of boundary conditions

When the boundary conditions were discussed in the text, the question was posed whether a diffusive velocity $v^L{}_{(r)}$, of a phase r, could be prescribed at the boundary. This is experimentally not feasible – since at the boundary, separate motions of the phases cannot be distinguished experimentally – unless, of course, $v^L{}_{(r)} \equiv 0$ for all r. This is achievable physically by making the pertaining part of the boundary impenetrable to particle migration. In this case,

$$p^K{}_{(r)} = \delta_\alpha{}^K x^\alpha \tag{II.14}$$

for all r. Thus

$$v^K{}_{(r)} = \partial p^K{}_{(r)}/\delta t|_x = 0, \tag{II.15}$$

and in view of Eq. (II.5),

$$v_i{}^{(r)} = v_i\,. \tag{II.16}$$

Thus, either the diffusive velocities $v^K{}_{(r)}$ of the migrating phases are not prescribable on the boundary, or if they are, then they all identically vanish.

A footnote on dissipation

In reference to Eq. (II.5), quite clearly the dissipative velocity is the non-affine, migratory velocity v^L. Thus when resistance to such motion exists, through a resistive force Q_L, then the rate of dissipation is the rate of work done by the dissipative forces, i.e., $Q_L v^L$.

We make the statement of "when resistance exists" so as to open the door to the possibility of *elastic* non-affine deformation. This, in principle, could be achieved through breaking of bonds but without resistance to subsequent motion. In this event D would be zero. This case is merely a sub-case of the theory already presented. The relevant equations are obtained by setting the right-hand side of Eq. (5.10) equal to zero.

One thus obtains a theory of non-local elasticity without the need for higher gradients of deformation, by introducing the concept of internal fields.

References

1. R.A. TOUPIN, *Elastic materials with couple stress*, Arch. Rat. Mech. Analysis, **11**, 119–132, 1962.
2. R.A. TOUPIN, *Theories of elasticity with couple stress*, Arch. Rat. Mech. Analysis, **17**, 85–112, 1964.
3. R.D. MINDLIN, *Micro-structure in linear elasticity*, Arch. Rat. Mech. Analysis, **16**, 51–78, 1964.
4. R.D. MINDLIN, *Second gradient of strain and surface tension in linear elasticity*, Int. J. Solids and Structures, **1**, 417–438, 1965.

5. A.E. GREEN and R.S. RIVLIN, *Multipolar continuum mechanics*, Arch. Rat. Mech. Analysis, **17**, 113–1471, 1965.

6. E.C. AIFANTIS, *Remarks on media with microstructure*, Int. J. Eng. Science, **22**, 961–968, 1984.

7. E.G. AIFANTIS, *On the microstructural origin of certain inealastic models*, J. Eng. Mat. Technology, **106**, 326–330, 1984.

8. E.C. AIFANTIS, *On the structure of single slip and its implications for inelasticity: Physical basis and modelling of finite deformations of aggregates*, J. GITTUS *et al.* [Eds.], pp. 283–324, Elsevier, London 1986.

9. I. VARDOULAKIS and E.C. AIFANTIS, *A gradient flow theory of plasticity for granular materials*, Acta Mechanica, **87**, 197–214, 1991.

10. I. VARDOULAKIS and G. FRANTZISKONIS, *Micro-structure in kinematic-hardening plasticity*, European J. Mech., **11**, 467–486, 1992.

11. K.C. VALANIS, *Irreversibility and existence of entropy*, J. Non-linear Mechanics, **6**, 337–360, 1971.

12. K.C. VALANIS, *Partial integrability as a basis of existence of entropy in irreversible systems*, ZAMM, **63**, 73–80, 1993.

13. K.C. VALANIS, *The viscoelastic potential and its thermodynamic foundations*, Iowa State University Report 52, 1967, J. Math. Physics, **47**, 267–276, 1968.

14. B. COLEMAN and M. GURTIN, *Thermodynamics of internal state variables*, J. Chem. Physics, **47**, 599–613, 1967.

15. K.C. VALANIS, *A theory of viscoplasticity without a yield surface*, Arch. Mech., **23**, 517–533, 1971.

16. K.C. VALANIS, *Fundamental consequences of a new intrinsic time measure. Plasticity as a limit of the endochronic theory*, Arch. Mech., **32**, 171–191, 1990.

17. C.A. ERINGEN, *Mechanics of continua*, John Wiley & Sons, New York 1967.

ENDOCHRONICS, VANCOUVER, USA.

Received January 7, 1997.

DIRECTIONS FOR THE AUTHORS

The journal *ARCHIVES OF MECHANICS (ARCHIWUM MECHANIKI STOSOWANEJ)* deals with the printing of original papers which should not appear in other periodicals.

As a rule, the volume of a paper should not exceed 40 000 typographic signs, that is about 20 type-written pages, format: 210 × 297 mm, leaded. The papers should be submitted in two copies. They must be set in accordance with the norms established by the Editorial Office. Special importance is attached to the following directions:

1. The title of the paper should be as short as possible.

2. The text should be preceded by a brief introduction; it is also desirable that a list of notations used in the paper should be given.

3. The formula number consists of two figures: the first represents the section number and the other the formula number in that section. Thus the division into subsections does not influence the numbering of formulae. Only such formulae should be numbered to which the author refers throughout the paper, and also the resulting formulae. The formula number should be written on the left-hand side of the formula; round brackets are necessary to avoid any misunderstanding. For instance, if the author refers to the third formula of the set (2.1), a subscript should be added to denote the formula, viz. $(2.1)_3$.

4. All the notations should be written very distincly. Special care must be taken to write small and capital letters as precisely as possible. Semi-bold type should be underlined in black pencil. Explanations should be given on the margin of the manuscript in case of special type face.

5. It has been established to denote vectors by semi-bold type. Trigonometric functions are denoted by sin, cos, tg and ctg, inverse functions – by arc sin, arc cos, arc tg and arc ctg; hyperbolic functions are denoted by sh, ch, th and cth, inverse functions – by Arsh, Arch, Arth and Arcth.

6. Figures in square brackets denote reference titles. Items appearing in the reference list should include the initials of the first name of the author and his surname, also the full title of the paper (in the language of the original paper); moreover;

a) In the case of books, the publisher's name, the place and year of publication should be given, e.g.,
5. S. Ziemba, *Vibration analysis*, PWN, Warszawa 1970;

b) In the case of a periodical, the full title of the periodical, consecutive volume number, current issue number, pp. from ... to ..., year of publication should be mentioned; the annual volume number must be marked in black pencil so as to distinguish it from the current issue number, e.g.,
6. M. Sokołowski, *A thermoelastic problem for a strip with discontinuous boundary conditions*, Arch. Mech., **13**, 3, 337–354, 1961.

7. The authors should enclose a summary of the paper. The volume of the summary is to be about 100 words.

8. The authors are kindly requested to enclose the figures prepared on diskettes (format PCX, BitMap or PostScript).

Upon receipt of the paper, the Editorial Office forwards it to the reviewer. His opinion is the basis for the Editorial Committee to determine whether the paper can be accepted for publication or not.

The printing of the paper completed, the author receives 10 copies of reprints free of charge. The authors wishing to get more copies should advise the Editorial Office accordingly, not later than the date of obtaining the galley proofs.

The papers submitted for publication in the journal should be written in English. No royalty is paid to the authors.

Please send us, in addition to the typescript, the same text prepared on a diskette (floppy disk) 3 1/2″ or 5 1/4″ as an ASCII file, in Dos or Unix format.

EDITORIAL COMMITTEE
ARCHIVES OF MECHANICS
(ARCHIWUM MECHANIKI STOSOWANEJ)